Three Dimensional Distribution of Cloud Types over the Indian Region and Associated Dynamics

Thesis Submitted to

Cochin University of Science and Technology

In Partial Fulfilment of the Requirements
for the Award of

Doctor of Philosophy
in
Atmospheric Science

Under the Faculty of Marine Sciences

by

Kandula V Subrahmanyam

Space Physics Laboratory

Vikram Sarabhai Space Centre

Indian Space Research Organisation

Thiruvananthapuram – 695022

India

March 2018

Declaration

This is to declare that the work presented in this thesis was carried out at the Space Physics Laboratory (SPL), Vikram Sarabhai Space Centre (VSSC), Thiruvananthapuram for the award of the degree of Doctor of Philosophy in Atmospheric Science from the Cochin University of Science and Technology, Cochin, Kerala State, India. This Thesis is the outcome of the original work done by me and the work did not form part of any dissertation submitted for the award of any degree, diploma, associateship or any other title or recognition from any University/Institution.

March, 2018 **Kandula V Subrahmanyam**

Thiruvananthapuram (Author)

भारत सरकार
अंतरिक्ष विभाग
विक्रम साराभाई अंतरिक्ष केन्द्र
तिरुवनंतपुरम-६९५०२२
केरला, भारत
फोन: ००९१ ४७१ २५६२५६३
फेक्स: ००९१ ४७१ २७०६५३५

Government of India
Department of Space
Vikram Sarabhai Space Centre
Thiruvananthapuram-695 022
Kerala, INDIA
Telephone: (0091-471) 2562563
Fax: (+91-471) 2706535
Email: k_kishorekumar@vssc.gov.in

अन्तरिक्ष भौतिकी प्रयोगशाला
SPACE PHYSICS LABORATORY

डॉ. के किशोर कुमार/ Dr. K. Kishore Kumar
Scientist/Engineer-SF

March 2018

CERTIFICATE

Certified that the thesis entitled "**Three Dimensional Distribution of Cloud Types over the Indian Region and Associated Dynamics**" submitted by **Mr. Kandula V Subrahmanyam** (Ph.D. Reg.No.4436) to Cochin University of Science and Technology, Cochin, embodies the original results of the investigations carried out at the Space Physics Laboratory, Vikram Sarabhai Space Centre, Thiruvananthapuram, under my supervision. The work presented in this thesis has not been submitted for the award of any other degree, diploma or associateship to any other University or Institution.

Dr. K. Kishore Kumar
(Thesis Supervisor)

Countersigned

Dr. Radhika Ramachandran
Director, SPL

भारत सरकार
अंतरिक्ष विभाग
विक्रम साराभाई अंतरिक्ष केन्द्र
तिरुवनंतपुरम-६९५०२२
केरला, भारत
फोन: ००९१ ४७१ २५६२५६३
फेक्स: ००९१ ४७१ २७०६५३५

सत्यमेव जयते

Government of India
Department of Space
Vikram Sarabhai Space Centre
Thiruvananthapuram-695 022
Kerala, INDIA
Telephone: (0091-471) 2562563
Fax: (+91-471) 2706535
Email: k_kishorekumar@vssc.gov.in

अन्तरिक्ष भौतिकी प्रयोगशाला
SPACE PHYSICS LABORATORY

डॉ. के किशोर कुमार / Dr. K. Kishore Kumar
Scientist/Engineer-SF

March 2018

CERTIFICATE

This is to certify that all the relevant corrections and modifications suggested by the audience during the Pre-synopsis Seminar and recommended by the Doctoral Committee of **Mr. Kandula V Subrahmanyam** (Ph.D. Reg.No.4436) have been incorporated in the thesis.

Dr. K. Kishore Kumar
(Thesis Supervisor)

Dedicated

To

My Wife & Daughters

Acknowledgements

Simply listing the names of those who helped me to finally attain this feat over the past five years seems utterly insufficient at Space Physics Laboratory, Vikram Sarabhai Space Centre, Thiruvananthapuram, during 2012-2017. But each played an important role. These contributions seem particularly significant during the course of research work to flourish.

First and foremost, I express my deep sense of gratitude to my thesis supervisor ***Dr. Karanam Kishore Kumar****, for his constant encouragement, valuable suggestions and the intense concern in the progress of my research work. His scientific spirit, vision, clarity, command and in-depth knowledge in the Earth's atmospheric processes helped me to visualize the existing challenges in the realms of cloud research. I am benefited a lot from him and acknowledges greatly for the valuable scientific discussions and the knowledge and experience I have gained from him during the course of this work as well as in my personal life. Further, I am grateful to him for the inexhaustible and extreme patience he showed while dealing with me. In every sense, none of this work would have been possible without him.*

I sincerely thank to Dr. Geetha Ramkumar, who has been always supported and provided the valuable suggestions during the periodic reviews of my work.

I would like to express sincere thanks to Dr. Radhika Ramachandran, Director, SPL for providing necessary space to complete the thesis towards its final phase. Her comments and suggestions during the periodic reviews were highly valuable and inspiring for me. Her keen observation and innate thinking really helped me a lot for making up the mind to have a wider perspective on several scientific aspects.

I also express sincere thanks Prof. R. Sridharan, Dr. K. Kirshnamoorhty and Dr. Anil Bhardwaj, Former Directors, SPL for their constant encouragements.

Special thanks to Dr. N.V.P. Kiran Kumar, who has helped me in learning the program skills at the beginning of my thesis work and his constant support.

I sincerely thank to Shri G. Vishwanathan, Former Director, ISRAD, Bangalore who held my hand into the field of Radar Meteorology and for his constant support.

My sincere thanks to the Academic Research and Doctoral committees (Members: Dr. K. Rajeev, Dr. R. Prabha Nair, Dr. Tarun Kumar Pant, Dr. C. Suresh Raju, Dr. S. Suresh Babu, Dr. Satheesh Thampi, Dr. Raj Kumar Chowdary, Dr. Bala Subrahamanyam, Dr. Vipin Kumar Yadav, Dr.Siddarth Shankar Das, Dr. Sunil Kumar) in monitoring the progress of my research work at SPL. The reviews and seminars have always been helpful for developing confidence, improving presentation skill and refining the research work.

I sincerely acknowledge the CloudSat Team for providing the primacy data for the current thesis through their Web site at http://cloudsat.cira.colostate.edu. I also acknowledge TRMM team for providing the rainfall and latent heating data through http://disc.sci.gsfc.nasa.gov. The ERA-Interim reanalysis data on atmospheric fields were provided by ECMWF from http://www.ecmwf.int/products/data.

I would also like to thank office staffs at SPL for their support and keeping the necessary things for my reviews during the course of my work. Special thanks to R. Sisira at SPL, who has meticulously arranged the all the documents required during the CUSAT Review committees.

My special thanks to the office mates at Cochin University of Science and Technology, Cochin for their support during the thesis period.

I wish to acknowledge the support of my colleagues, Dr. C. Vineeth, Girach Imran, K. Sobhan Kumar and Evening Tea Gang at SPL for their conversations and for providing an endless supply of smiles.

I truly acknowledge my parents, ***Mr. K V. Subba Rao and Mrs. K, V. Subbulu****, who's longing and prayers brought throughout my academic carrier.*

I also acknowledge support of my brother, ***Mr. K, Koteswara Rao****, who has been the cornerstone throughout my academic carrier and he always supported my dreams and aspiration. He is the person, who held my hand into the field of scientific research and for all he has done for me.*

Last but not the least I must thank my dear wife ***Mrs. K, Udaya Lakshmi****, whose love, support and culinary skills kept me happy and healthy throughout my journey. Also she has kept me at sane, balanced and cheerful throughout this whole process.*

My endless love to my daughters, ***K, Ipsitha Hasini*** *and* ***K, Tejashwitha*** *for their sacrifices to make this work possible.*

Kandula V Subrahmanyam

Contents

Publications in Journals

Thesis publications

1. **Subrahmanyam, K.V.** and Karanam Kishore Kumar, CloudSat observations of cloud-type distribution over the Indian summer monsoon region, ***Ann. Geophys.***, 31, 1155-1162, doi: 10.5194/angeo-31-1155-2013, **2013**. (**Chapter 3**)
2. **Subrahmanyam, K.V.** and Karanam Kishore Kumar, Vertical structure of Stratocumulus clouds and associated dynamics over the Arabian Sea during Indian summer monsoon season, ***J. Appl. Remote Sens.*** 12(1), 016018 (2018), doi: 10.1117/1.JRS.12.016018, **2018a.** (**Chapter 3**)
3. **Subrahmanyam, K.V.** and Karanam Kishore Kumar, Cloud type distribution in Tropical Cyclones formed in the North Indian Ocean using CloudSat observations, ***IEEE-Journal of Selected Topics in Applied Earth Observations and Remote Sensing,*** 10.1109/JSTARS.2017.2786666, **2018b**. (**Chapter 4**)
4. **Subrahmanyam, K.V**. and Karanam Kishore Kumar, CloudSat observations of Multi-layered clouds across the globe, ***Climate Dynamics,*** DOI 10.1007/s00382-016-3345-7, **2017**. (**Chapter 5**)
5. **Subrahmanyam, K.V.** and Karanam Kishore Kumar, TRMM observations of Latent heat distribution over the Indian summer monsoon region and associated dynamics, ***Proc. of SPIE*** **Vol**. 9876, 98762W, doi: 10.1117/12.2223905, **2016**. (**Chapter 6**)

Related publications

6. **Subrahmanyam, K.V.** and Karanam Kishore Kumar, Megha-Tropiques/SAPHIR measurements of humidity profiles: validation with AIRS and global radiosonde network, *Atmos. Meas. Tech. Discuss.,* 6, 1–32, 2013.
7. **Subrahmanyam, K.V.**, Karanam Kishore Kumar and Alur Narendra Babu, Phase relation between CAPE and precipitation at diurnal scales over the Indian summer monsoon region, *Atmospheric Science Letters, doi: 10.1002/asl2.566,* 2015.
8. **Subrahmanyam, K.V.**, Karanam Kishore Kumar, N.V.P. Kiran Kumar and G.Viswanathan, Evaluation of Doppler Weather Radar MEGHA-2700 Observations Using Gematronik Doppler Weather Radar and TRMM Precipitation Radar, *Meteorological Applications*, DOI: 10.1002/met.1571, 2016.
9. **Subrahmanyam, K.V.** and Karanam Kishore Kumar, New insights into the convective system characteristics over the Indian summer monsoon region using space based passive and active remote sensing techniques, *IETE Technical Review* (*under review*), 2017.

Conference presentations

International

1. **Subrahmanyam, K.V.**, Karanam Kishore Kumar, Pradeep C, Channabasava B and Shanmuga Sundari J, Monsoon Clouds over Thumba: A C-band Polarimetric Doppler Weather Radar Perspective, 2nd Indian Conference on radar Meteorology (iRAD), Tirupathi, January, 2018.
2. **Subrahmanyam, K.V.**, Karanam Kishore Kumar and Natalie D. Tourville, CloudSat observations of three-dimensional distribution of cloud types in Tropical Cyclones, 2nd Indian Conference on radar Meteorology (iRAD), Tirupathi, January, 2018.
3. **Subrahmanyam, K.V**. and Karanam Kishore Kumar, New insights into the convective system characteristics over the Indian summer monsoon region using space based passive and active remote sensing techniques, 3rd Regional Conference on radio Science, URSI-RCRS 2017, March 1-4, Tirupathi, India, 2017.
4. **Subrahmanyam, K. V.** and Karanam Kishore Kumar, TRMM observations of Latent heat distribution over the Indian summer monsoon region and associated dynamics, SPIE: Remote Sensing of the Atmosphere, Clouds, and Precipitation, Delhi, India, April, 2016.
5. **Subrahmanyam, K.V.**, New insights into the convective system characteristics over the Indian summer monsoon region using space based passive and active remote sensing techniques, URSI Atlantic-RadioScicne Conference, 2015 **(AT-RASC Young Scientist Award)**.
6. **Subrahmanyam, K. V.**, and Karanam Kishore Kumar: Diurnal variation of CAPE and precipitation and their phase relation over Indian Summer Monsoon region, International Tropical Meteorology (INTROMET) - 2014, Chennai, February 21-24, 2014 **(Best paper Award)**.
7. **Subrahmanyam, K. V**. and Karanam Kishore Kumar, Diurnal variation of CAPE and precipitation and their phase relation over Indian Summer Monsoon region, URSI Asia-Pacific Radio Science Conference - 2013,Taipei, Taiwan, September 3-7, 2013. **(AP-RASC Young Scientist Award)**.
8. **Subrahmanyam, K. V.** and Karanam Kishore Kumar, The role of dynamics in distribution of various types of clouds in the Indian Monsoon region: A study using five years of CloudSat observations, COSPAR-2012, Mysoore, India, 2012.
9. **Subrahmanyam, K. V**. and Karanam Kishore Kumar, The role of dynamics in distribution of various types of clouds in the Indian Monsoon region: A study using five years of CloudSat observations, OCHAMP-2012, Pune, India, 2012.

National

1. **Subrahmanyam K.V.,** Karanam Kishore Kumar, Kiran Kumar N.V.P and Thampi, SB., Characterizing the life cycle of Mesoscale Convective Systems using Doppler Weather radar observations, Indian Conference on radar Meteorology (iRAD), Kharagpur, January, 2017.
2. **Subrahmanyam, K. V.**, and Karanam Kishore Kumar: New Insights into the convective charratcertsics over the Indian summer monsoon region, National Space Science Symposium (NSSS)-2016, Trivandrum, India, February, 2016.
3. Siddarth Shankar Das, M. V. Ratnam, K. N. Uma, **K. V. Subrahmanyam**, G. A. Imran, A. K. Patra, K. K. Kumar, K.V. Suneeth, G. Ramkumar, Influence of tropical cyclone NILAM in transporting stratospheric air masses : Observation based on MST radar, ozone profiling and Megha-Tropiques, National Space Science Symposium (NSSS)-2014, Dibrugarh, India, 2014.
4. **Subrahmanyam, K. V.** and Karanam Kishore Kumar, Distribution of cloud types in inner and outer rainbands of Tropical Cyclones, National Space Science Symposium (NSSS)-2014, Dibrugarh, India, 2014.
5. **Subrahmanyam, K. V.** and Karanam Kishore Kumar, CloudSat observations of multilayered Clouds across the Globe, National Space Science Symposium (NSSS), Tirupathi, India, 2012.

List of Acronyms

Ac	Altocumulus
ARB	Arabian Sea
As	Altostratus
BoB	Bay of Bengal
CALISPO	Cloud-Aerosol Lidar and Infrared Pathfinder Satellite Observation
Cb	Cumulonimbus
Cc	Cirrocumulus
CCN	Cloud Condensation Nuclei
CEN	CloudSat Educational Network
CI	Central India
Ci	Cirrus
CPR	Cloud Profiling Radar
CRM	Cloud Resolving Model
Cs	Cirrostratus
CSH	Convective Stratiform Heating
Cu	Cumulus
DC	Deep Convective
DJF	December–January– February
DO-OP	Daylight Only Operations
ECMWF	European Centre for Medium-Range Weather Forecasts
FOC	Frequency of Occurrence
GCM	General Circulation Models
HDF	Hierarchical Data Format
HH	Hydrometeor Heating
HPA	High Power Amplifiers
INSAT	Indian Satellite
IR	Infrared
ISCCP	International Satellite Cloud Climatology Project
ISM	Indian summer monsoon
ITCZ	Inter Tropical Convergence Zone

IWC	Ice Water Content
JJA	June– July–August
JJAS	June-July-August-September
LH	Latent Heating
LLJ	Low Level Jet
LTS	Lower Tropospheric Stability
LWC	Liquid Water Content
MAM	March–April–May
MSF	Mean Stream Function
NH	Northern Hemisphere
Ns	Nimbostratus
PR	Precipitation Radar
PRF	Pule Repetition Frequency
PRH	Precipitation Radar Heating
QOTL	Quasi Optical Transmission Line
RFES	Radio Frequency Electronics Subsystem
Sc	Stratocumulus
SEM	Significant Echo Mask
SH	Southern Hemisphere
SLH	Spectral Latent Heating
SON	September–October–November
St	Stratus
TEJ	Tropical Easterly Jet
TIROS	Television and Infrared Observation Satellite
TRMM	Tropical Rainfall Measuring Mission
WG	Western Ghats
WMO	World Meteorological Organization

PREFACE

Owing to the importance of cloud in hydrological cycle, general circulation and radiative forcing, any aspect of it is a cynosure to meteorologists as well as common men across the globe. As the accurate representation of cloud processes and their feedback in the general circulation models are the need of the hour, cloud studies have been placed at a high pedestal by the meteorological community. By now, it is well established that the cloud properties remain the largest uncertainty in climate model forecasts. By interacting with both short- and long-wave radiation, clouds play crucial role in the radiative budget at the surface, within and at the top of the atmosphere. Understanding of the atmospheric radiative heating and latent heat release associated with clouds are central to any study dealing with general circulation as well as precipitation. Realizing the importance of clouds and their role in predicting the climate changes, a host of studies were carried out in the past to divulge this ubiquitous feature of the earth's atmosphere. Most of these studies emphasized the importance of cloud vertical structure on atmospheric circulations, including the effects of variations of cloud top and base heights, cloud-layer thicknesses, and the vertical distribution of multilayered clouds as they significantly modify vertical and horizontal gradients in radiative and latent heat fluxes. The unanimous view of many of the atmospheric researchers is that the detection of multi layered clouds is important from climate standpoint and any attempt to quantify the global warming should include the radiative impacts of clouds, which is severely hampered by ignoring the multi layered cloud parameters in models. Thus it is important to have quantitative measurements of the geographic distribution and variations of cloud vertical layers to accurately predict the climate change.

Apart from the total cloud amount and its vertical distribution, one more important aspect of clouds is the cloud type. It is known that depending upon the cloud type, the radiative properties, the latent heat released and microphysical properties of clouds largely differ. Earlier studies investigated the radiative flux changes induced by the occurrence of different cloud types using International Satellite Cloud Climatology Project cloud data and a radiative transfer model. These studies emphatically showed that the cloud-type variations are as important as cloud cover in modifying the radiation field of the earth–atmosphere system. Thus it becomes clear that apart from the three-dimensional distribution of cloud cover, it is important to have cloud type distribution to quantify the feedback provided by the clouds in totality.

The Indian summer monsoon (ISM) is one of the most investigated topics in the realms of meteorology. This synoptic system serves as natural laboratory for cloud studies. Many studies on the ISM by several researchers across the globe contributed

constructively to the present understanding of this enigmatic large-scale system. Generally, it is believed that the continental-scale land-sea thermal contrast drives the large-scale Monsoon circulation. However, once the monsoon is set, its advancement, maintenance and withdrawal depends not only on the large-scale dynamics but also on the internal dynamics initiated by the cloud systems embedded within the monsoon system. These cloud systems over the ISM region modify the thermal structure and moisture budget of the troposphere by releasing latent heat, modifying the radiative heating and through precipitation. Thus the clouds are an important integral part of the monsoon system and any attempt to understand the latter should include the detailed investigations on the former. Even though there are studies on cloud distribution over the ISM region, there are no studies focusing on vertical structure of cloud type distribution. Sufficient knowledge of the spatial distribution of individual cloud types would aid the accurate radiation and latent heat calculations, which in turn will help in accessing the role of clouds in maintaining and advancement of the ISM. So it becomes important to know, which types of clouds occur over which region of ISM.

The major gap areas in the realms of cloud studies are the vertical distribution of various cloud types, multi-layered clouds and the associated dynamics. In this regard, the present thesis focuses on understanding the three-dimensional distribution of various cloud types and the role background dynamics in their distribution over the ISM region. The vertically resolved multi-layered cloud distributions as well as vertical structure of latent heating are also addressed in the present thesis. The principal data used for the present work is the five years of CloudSat observations during 2006 to 2011. Using CloudSat observations, role of dynamics in three dimensional distributions of various cloud types over the ISM region is investigated for the first time. Further, the formation mechanism in terms of background dynamics for various cloud types is also examined. Using the CloudSat observations over several tropical cyclones formed in the North Indian Ocean surrounding Indian subcontinent during 2006 to 2014, a composite distribution of cloud types is constructed for the first time. This study revealed what type of clouds present in which part of tropical cyclone. As clouds in tropical cyclones are interconnected with cyclones dynamics and play a very important role in its sustenance and intensification, the results obtained in the present study assumes their importance. The distribution of multi-layered clouds in connection with general circulation of the atmosphere is also investigated using CloudSat observations and re-analysis fields. Apart from these, the vertical structure of latent heating of precipitation clouds as observed by Precipitation Radar on board Tropical Rainfall Measuring Mission over ISM region and their association with various cloud types are also investigated.

List of Figures

List of Tables

Chapter 1

Introduction to Clouds

"Clouds are pictures in the sky
They stir the soul, they please the eye
They bless the thirsty earth with rain,
which nurtures life from cell to brain-
But no! They're demons, dark and dire,
hurling hail, wind, flood, and fire
Killing, scarring, cruel masters
Of destruction and disasters
Clouds have such diversity-
Now blessed, now cursed,
the best, the worst
But where would life without them be?"

-Vollie Cotton

1.1 Introduction

The earth's atmosphere is twitchy fluid rotating around the earth and constantly driven by the heat from the Sun. The atmospheric processes influence the other parts of the earth's environment, namely biosphere, hydrosphere and lithosphere. The atmosphere seems to be a very thin layer and consist of gases, which provides an indispensible shield from the harmful radiation from the Sun. Based on vertical structure of temperature, the Earth's atmosphere is divided into five different layers, viz, Exosphere, Thermosphere, Mesosphere, Stratosphere and Troposphere. Out of the five layers, Troposphere is the lowest layer of earth's atmosphere, where all the weather phenomena occur and the present thesis work is mainly focused on this part of the atmosphere. Troposphere means the realm of mixing, because air is vigorously mixed and stirred by storms, convection and wind systems. The troposphere, whose thickness varies with location and season, has an average height of ~16 km in tropics. In this region, the temperature decreases with a lapse rate of about 6.5 K/km of altitude. The height where the temperature stops decreasing is referred to as tropopause, a thin zone of transition between the troposphere and the

stratosphere. The uneven heating of the regions of the troposphere by the Sun causes convection currents, large-scale patterns of winds that move heat and moisture around the globe. The presence of the large amount of water vapour in this layer is responsible for formation of clouds and precipitation. A cloud is a visible aggregate of tiny water droplets or ice crystal suspended in the air. The clouds are the main focus of the present thesis.

The clouds formed in the Earth's atmosphere play a key role in modulating the radiation budget of the planet, in hydrological cycle and in driving the large-scale as well as mesoscale atmospheric circulations. Being a one of the sources for fresh water, the clouds are of fundamental importance to common men. Studies of clouds are cynosure for many atmospheric researchers as they play myriad role in many processes taking place in the Earth's atmosphere, especially precipitation and latent heating. Analyses from the International Satellite Cloud Climatology Project (ISCCP) reveal that the global mean cloud coverage fraction is 68.6%. Thus, from space, the earth appears as a planet semi-enshrouded by these visible aggregates of water drops and ice crystals. These masses of clouds are an integral part of global climate and water cycle and also an integral part of weather forecasting analysis. In addition, clouds aid in redistributing extra heat from the equator towards the poles and are required for precipitation to occur and hence, are an essential part of hydrological cycle. The balance between incoming and outgoing energy determines the Earth's temperature and ultimately climate. Even small changes in the abundance or location of cloud could change the climate more than the anticipated changes caused by greenhouse gases, anthropogenic aerosols, or the factors associated with global change. There is no dispute on the importance of clouds in controlling both weather and climate of a given location.

Clouds exhibit a wide variety of sizes and shapes, which reflect variations in the atmospheric processes leading to their formation. Individual cloud for example, small cumulus clouds cover a few hundred meters in the horizontal and vertical and

normally have a lifetime of less than an hour. Clouds are also directly linked to several weather phenomena. Rain and snow are obviously produced in clouds, as are thunder and lightning. The latent heat released in the atmosphere due to condensation and freezing processes is known to be one of the most important processes, which helps in maintaining the tropical storms as well as driving the tropical circulation. The clouds nuance the radiative fluxes emitted both by the sun and the earth that we experience every day. If clouds form on a sunny day the maximum temperature near the surface will be lower than without them, a direct consequence of the reflection of sunlight by clouds. Like that, if the sky is enclosed by low clouds at night the near-surface temperature will not drop as low as beneath clear sky conditions due to the trapping of terrestrial radiation by the clouds. Because of these reasons, it is obvious that it is desirable for any form of weather forecast to include a prediction of the occurrence and type of clouds and precipitation.

Depending on their characteristics and height in the atmosphere, clouds can influence the energy balance in different ways. The way in which clouds interact with the environment and affects the Earth's radiative energy balance is one of the primary uncertainties in global circulation models. The observations of clouds are more important for improving and validating the numerical models of Earth's climate and for seasonal and longer term climate predictions. The role of clouds remains a major uncertainty in current day climate change simulations. Long back, it has been realized that Global Circulation Models should include the accurate representation of the clouds in their models. Since then considerable amount of work has been devoted towards the exploration of clouds. Most of these studies gave emphasis on cloud amount and its vertical distribution. Apart from the total cloud amount and its vertical distribution, one more important aspect of clouds is the cloud type, which will be discussed later in this chapter. It is known that depending upon the cloud type, the radiative properties, the latent heat released and microphysical properties of clouds largely differ. Earlier studies investigated the

radiative flux changes induced by the occurrence of different cloud types using ISCCP data and a radiative transfer model. These studies emphatically showed that the cloud-type variations are as important as cloud cover in modifying the radiation field of the earth–atmosphere system. Thus it becomes clear that apart from the three-dimensional distribution of cloud cover, it is important to have cloud type distribution to quantify the feedback provided by the clouds in totality.

1.2 Formation of clouds in the Earth's atmosphere

Besides Nitrogen (78% by volume) and oxygen (21% by volume), atmospheric air contains the water vapour, which has very high spatio-temporal variability in the lower troposphere. Typically, the water vapour varies in the range of 0-4% in the atmosphere. The capacity of the air to hold the water vapour decreases with temperature. The air can hold a certain amount of water vapour and when it can take no more it is said to be 'saturated'. When a parcel of air rises, it expands and cools adiabatically. Eventually, the air becomes saturated, that is, its vapour pressure is the same as the saturation vapour pressure at that temperature. Further rising of the air parcel leads to condensation, i.e. the formation of liquid water. If the temperature is below zero degrees Celsius, super cooled water droplets form, otherwise water droplet freezes and becomes ice crystal, where the temperature is too low. Rising unsaturated air (i.e., air that does not contain the water droplets) cools at 9.8 degree centigrade per kilometre, adiabatically. Once cloud has begun to form, the latent heat of condensation is released inside the rising air parcel, as a result of which the ascending air cools at less than 9.8 degree centigrade per km (between 4 and 7 degree centigrade per km). For any cloud droplet to form there must be condensation nuclei present. These cloud condensation nuclei (CCN) are tiny particles suspended in the air, for example sea salt or dust. Fortunately, there are plenty of CCNs in the air. Therefore, no water droplets are ever made up of only pure water but will have impurities. One of the important processes in the formation of clouds is the lifting mechanism, i.e. lifting the air parcel from the surface to higher altitudes, where temperature is relatively low so that water vapour condenses to

form clouds. There are four main lifting mechanisms such as orographic lifting, frontal lifting, convergence and convective heating.

Orographic Lifting: In this mechanism, the air lifted over a barrier, like a mountain. As the air flow across the barrier or the mountain, it has to rise up because it nowhere to go further. Air parcel cools and expands, when it ascend over the mountain. Maximum moisture in the air parcel condenses and forms a cloud over the side of the mountain, which is known as the windward side. The cloud formed in this mechanism is called as 'orographic cloud'.

Frontal Lifting: Another mechanism for cloud formation is the frontal lifting. Where the two air masses of different densities meet, a front will be formed at the interface. In a frontal lifting, an air mass is lifted up over the other air mass and a vertical motion is induced in the atmosphere. There are two fronts that occur in the atmosphere known as cold front and warm fort. A cold front happens when the cold air mass advances into a warm air mass; whilst a warm air mass advances onto a cold air mass, warm front will occur. Cold fronts can develop in vertical direction and form the thunderstorms. Therefore, a cold front brings vibrant changes in weather.

Convergence is when the air converges around the centre of a low pressure area. As the air flows from one place to another place horizontally and meets the low pressure area along the surface of the earth, then it is forced to ascend and form the clouds. The Inter Tropical Convergence Zone (ITCZ), where trade winds from both the hemispheres meet, is one of the cloudiest regimes in the Earth's atmosphere.

Convective Lifting: When the sun heats the ground, the air which in turn heats at the surface through conduction. The warm air at the ground will eventually rise. The rising air will expand and cool thus leads to formation of the clouds. If the atmosphere is stable, fair weather cumulus clouds form. If the atmosphere is unstable, then the cloud can develop vertically and forms the deep convective clouds

or thunderstorms. The higher the surface temperature, the more convection occurs and vigorous thunder storms may occur with the availability of moisture in the atmosphere. The uneven surface heating by the solar radiation plays an important role in convective lifting.

1.2.1 Stability of the atmosphere

When a parcel of air rises in the atmosphere adiabatically, it expands and cools. When the air parcel is unsaturated (i.e. relative humidity is less than 100%) the rate at which the temperature of the air parcel decreases is called the dry adiabatic rate. As the raising air cools, relative humidity increases as air temperature approaches to dew point temperature. The dew point temperature is the temperature to which air must be cooled at constant pressure to get it saturated. If the air cools to dew point temperature, the relative humidity becomes 100%, on further lifting, condensation happens and cloud formation takes place. Latent heat is released into the raising air due to the phase changes in the water molecules. This heat added due to condensation, offsets the cooling due to expansion of the air parcel. So, the air now cools at a lower rate than the dry adiabatic rate called the moist adiabatic rate. When saturated air parcel sinks it is compressed and warmed at moist adiabatic rate since the warming causes evaporation, which in turn decreases the rate of warming to moist adiabatic rate.

Stability of the atmosphere can be determined by comparing the temperature of a rising parcel to that of its surroundings. If the rising air is colder than its environment, it will be denser (heavier) and tend to sink back to its original level. In this case, the air is said to be stable because it resists upward movement. If the rising air is warmer and, therefore, less dense (lighter) than the surrounding air, it will continue to rise until it reaches the same temperature as its environment. This is an example of unstable air. The rate at which the air temperature changes with elevation is called the lapse rate. Since this is the rate at which the air temperature surrounding us will be changing if we start climbing upward into the atmosphere, we

can call it the environmental lapse rate. The atmosphere is always absolutely stable when the environmental lapse rate is less than the adiabatic lapse rate, in the case of unsaturated parcel. Since air in an absolutely stable atmosphere strongly resists upward vertical motion, it will tend to spread out horizontally if forced to rise. The atmosphere is said to be unstable when the environmental lapse rate is more than the adiabatic lapse rate. In the unstable atmosphere, there is more chances for the formation of deep convective systems reaching as high as tropopause. The atmosphere is said to be neutral when the environmental lapse rate is equal to the adiabatic lapse rate. In the case of saturated parcel, the environmental lapse rate will be compared with moist adiabatic lapse rate to determine the stability of the atmosphere. The stability of the atmosphere is thus very important component for the formation of clouds and their vertical development.

1.3 Classification of Cloud Types

Before 18th century, a complete description about cloud characteristics was not available. Valuable information on the meteorological history, in general, can be found in the text books by *Frisinger* (1977), *Middleton* (1965), *Khrgian* (1970) and *Schneider-Carius* (1955). *Lamarck* (1744-1829) is the one who realized the various forms of clouds and first to give a simple classification of clouds in the year 1802. Even though, his cloud classification received a little attention during that time. *Howard* (1772-1864), an English naturalist, lived almost contemporaneously with *Lamarck* and developed a cloud classification system, which was well received and got general acceptance by the meteorological community. Howard employed Latin words to describe clouds as they appear to a ground observer. He named a sheet like cloud stratus (Latin for “layer”); a puffy cloud cumulus (“heap”); a wispy cloud cirrus (“curl of hair”); and a rain cloud nimbus (“violent rain”). In Howard’s system, these were the four basic cloud forms. Other clouds could be described by combining the basic types. In 1887, Abercromby and Hildebrandsson expanded Howard’s original system and published a classification system with only slight modification, which is still in use today. In fact, several scientists [*Scorer*, 1963; *Howell*, 1951] have

attempted to design a classification scheme based on cloud motions. However, meteorologists wish to label the various cloud forms, which generally adhere to the classifications given in the International Cloud Atlas [*World Meteorological Society*, 1956]. Ten principal cloud forms are divided into four primary cloud groups. Each group is identified by the height of the cloud's base above the surface: high clouds, middle clouds, and low clouds as given in Table 1.1. The fourth group contains clouds showing more vertical than horizontal development. Within each group, cloud types are identified by their appearance. Figure 1.1 shows the classification of clouds according to height and form. This figure corresponds to midlatitude region .

Table 1.1 Cloud classifications

High level Clouds	**Middle level clouds**	**Low level clouds**	**Clouds with vertical development**
Cirrus(Ci)	Altostratus(As)	Stratus(St)	Cumulus(Cu)
Cirrostratus (Cs)	Altocumulus(Ac)	Stratocumulus(Sc)	Cumulonimbus(Cb)
Cirrocumulus (Cc)		Nimbostratus(Ns)	

1.3.1 High level Clouds

High level clouds in middle and low latitudes generally form above 6000 m (20,000 ft). Because the air at these elevations is quite cold and "dry," high clouds are composed almost exclusively of ice crystals and are also rather thin.

***Cirrus*:** The most common high clouds are the cirrus (Ci), which are thin, wispy clouds blown by high winds into long streamers called mares' tails. They look like a white, feathery patch with a faint wisp of a tail at one end. These clouds generally moves along the background wind. Usually the presence of cirrus cloud in the atmosphere indicates the pleasant weather conditions.

Cirrocumulus: These clouds seen less frequently than cirrus, appear as small, rounded, white puffs that may occur individually or in long rows. When in rows or

small wave shape, the cirrocumulus cloud has a rippling appearance that distinguishes it from the silky look of the cirrus and the sheet like cirrostratus. Cirrocumulus seldom cover more than a small portion of the sky. The rounded patches or the marked with spots of cirrocumulus cloud reflects the sunlight in red and yellow color and thus looks one of the most beautiful clouds.

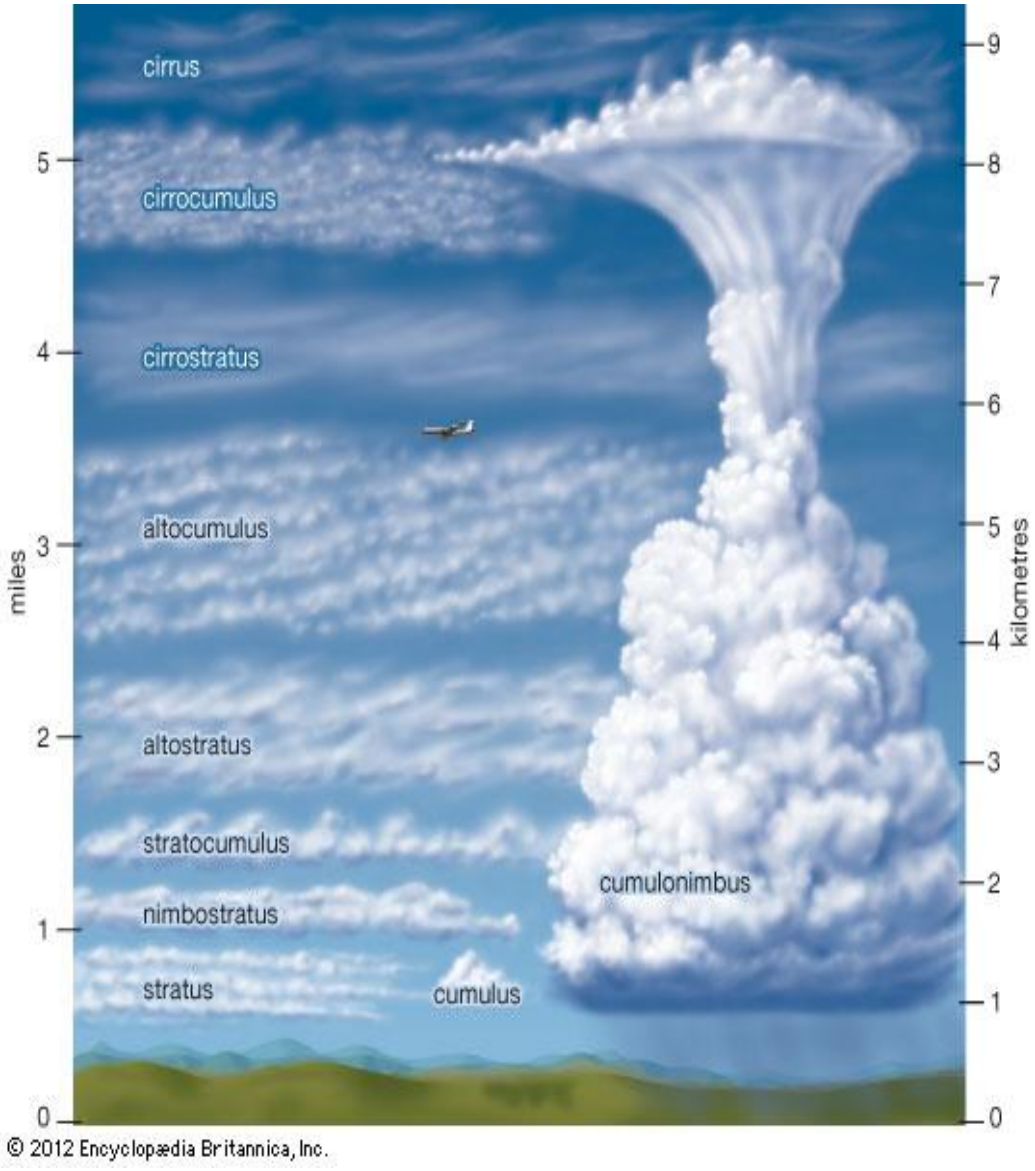

Figure 1.1: Cloud classification (Figure courtesy: Encyclopaedia Britannica, Inc., 2012)

***Cirrostratus*:** The thin, sheet like, high clouds that often cover the entire sky are cirrostratus (Cs). They are so thin that the sun and moon can be clearly seen through them. The ice crystals in these clouds bend the light passing through them and will often produce a halo, a ring of light that encircles the sun or moon. These clouds cover the entire sky with white appearance. Cirrostratus and altocumulus clouds are frequently forms with prior to the advancement storms. Thus these kinds of clouds generally used to predict the precipitation within 12 to 24 hours.

1.3.2 Middle level Clouds

The middle clouds have bases between 2000 and 6000 m (6500 to 20,000 ft)altitude region.. These clouds are composed of water droplets and when the temperature becomes low enough, some ice crystals will be formed.

***Altocumulus*:** These clouds are middle level clouds that are composed mostly of water droplets and are rarely more than 1 km thick. They appear as gray, puffy masses, sometimes rolled out in parallel waves. Generally, one portion of altocumulus cloud is darker than the portion of these cloud. This will help to identify the altocumulus clouds from the high level clouds such as cirrocumulus clouds. By the appearance of individual altocumulus cloud in puffy shapes are larger than he higher cloud of cirrocumulus. Sometimes these clouds looks like a castellated appearance in the sky, that is their upper parts looks like castle turrets. Sometimes these turrets are small cumulus clouds growing from the altocumulus and their presence shows that the atmosphere is unstable at middle levels in the atmosphere. Further, these turrets clouds can become tall enough for precipitation to form and this precipitation will soon evaporates , but it may reach the ground occasionally.

***Altostratus*:** It is a gray or blue-gray cloud composed of ice crystals and water droplets. Altostratus clouds often cover the entire sky across an area that extends over many hundreds of square kilometers. The clouds around the sun having the

gray color and dimness of the sunlight are the indication of occurrence of an altostratus cloud. The fact that halos only occur with cirriform clouds also helps one to distinguish them. Another way to separate the two is to look at the ground for shadows. If shadow is not seen, the cloud is altostratus because cirrostratus are usually transparent enough to produce them. Altostratus clouds often form ahead of storms having widespread and relatively continuous precipitation.

1.3.3 Low level Clouds

Low level clouds have base lying below 2000 m (6500 ft). They are almost composed of water droplets; however, in cold weather, they may contain ice particles and snow.

***Stratus*:** Stratus cloud is a uniform grayish cloud that often covers the entire sky. It resembles a fog that does not reach the ground. Normally, no precipitation falls from the stratus, but sometimes it is accompanied by a light mist or drizzle. A thick layer of stratus might be confused with nimbostratus, but the distinction between them can be made by observing the low base of the stratus cloud and that light to moderate precipitation occurs with nimbostratus. Moreover, stratus often has a more uniform base than does nimbostratus. Also, a deck of stratus may be confused with a layer of altostratus. However stratus are lower and darker gray and that the sun normally appears "watery" through altostratus.

Nimbostratus: It is a dark gray, "wet"-looking cloudy layer associated with more or less continuously falling rain or snow. The base of the nimbostratus cloud is normally impossible to identify clearly and its top may be over 3 km (10,000 ft) higher. Nimbostratus is easily confused with the altostratus. Thin nimbostratus is usually darker gray than thick altostratus, and normally cannot see the sun or moon through a layer of nimbostratus. When the nimbostratus cloud is present, the visibility underneath of this cloud is very poor because precipitation will evaporate

and mix with the air in this region. If this air becomes saturated air, then the fog forms below the nimbostratus cloud base.

***Stratocumulus*:** They are low lumpy clouds that appear in rows, in patches, or as rounded masses with blue sky visible between the individual cloud elements. Often they appear near sunset as the spreading remains of a much larger cumulus cloud. Occasionally, the sun will shine through the cloud breaks producing bands of light (called crepuscular rays) that appear to reach down to the ground. The color of stratocumulus ranges from light to dark gray. It differs from altocumulus in that it has a lower base and larger individual cloud elements.

1.3.4 Clouds with vertical development

Cumulus: Cumulus is a puffy cloud takes on a variety of shapes, but most often it looks like a piece of floating cotton with sharp outlines and a flat base .The base appears white to light gray, and on a humid day, may be only 1000 m (3300 ft) above the ground and a kilometer or so wide. The top of the cloud often in the form of rounded towers denotes the limit of rising air and is usually not very high. These clouds can be distinguished from stratocumulus by the fact that cumulus clouds are detached (usually a great deal of blue sky can be seen between each cloud) while stratocumulus usually occur in groups or patches. Also, the cumulus has a dome or tower-shaped top as opposed to the generally flat tops of the stratocumulus. Cumulus clouds are associated with fair weather because their vertical development is small; therefore, these clouds are called "*fair weather cumulus*."

Cumulonimbus or deep convective clouds: If a cumulus cloud continues to grow vertically, it develops into a massive cumulonimbus (Cb) , a thunderstorm cloud. While its dark base may be no more than 600 m (2000 ft) above the earth's surface, its top may extend upward to the tropopause, over 12,000 m (39,000 ft) higher in the midlatitude and 16,000 m in tropics. Tremendous amounts of energy released by the condensation of water vapor within a cumulonimbus result in the development

of violent up and downdrafts, which may exceed ~3 m/s. The lower (warmer) part of the cloud is usually composed of only water droplets. Higher up in the cloud, water droplets and ice crystals both abound, while, toward the cold top, there are only ice crystals. The great thunderheads may contain all forms of precipitation ,large raindrops, snow- flakes, snow pellets, and sometimes hailstones ,which can fall to earth in the form of heavy showers. Lightning, thunder, and even tornadoes are associated with the cumulonimbus.

1.4 Microphysical properties of clouds

Apart from the physical properties of clouds such as their appearance, height and its fraction, clouds can be characterized by their microphysical properties. The microphysical properties of clouds are cloud droplet size, liquid water content (LWC) and ice water content (IWC), which can controls the hydrological cycle of earth. The LWC and IWC are the amount of water or the amount of ice per cubic meter of air in gm^{-3}. The formation of precipitation and the amount of rainfall depends on cloud liquid water content and also on the droplet size. These microphysical properties of clouds play an important role in radiative budget of the earth's atmosphere, i.e. by reflecting the considerable fraction of solar radiation that the cloud reflects back to space. The amount of reflected sunlight depends on the type of cloud and the amount of liquid/ice water content within the cloud. Besides this reflectance, emissivity and optical depths are the radiative properties of clouds. The cloud droplets occur in wide range of sizes for different type of clouds.

Figure 1.2 depicts the droplet diameter versus droplet number for some of individual cloud types, which show a broad range of droplet sizes. It can be noted from figure 1.2 that some types of cloud contain small droplets while other cloud types show a broad range of droplet sizes. The drop size distribution peaks at ~ 7 μm for fair weather cumulus and stratocumulus cloud with droplet concentration of ~ 170 cm^3 and ~80 cm^3, respectively. The lower level clouds such as the nimbostratus and stratus cloud has the broad distribution of droplet diameter

ranging from ~ 5-20 μm with droplet concentration of ~40 cm^3. The cumulus congests with considerable vertical development has the large droplet diameter of around 10-20 μm with droplet concentration of ~80 cm^3. Also, the mid-level cloud, altostratus has considerably large droplet diameter (~10 μm) and concentration (~140 cm^3). The sum of all masses of the droplets with in each type of clouds defines its amount of liquid water content or ice water content. The typical values of microphysical properties of various clouds are given in Table 1.2. The droplets of water in a typical cloud range in size from two hundredths of millimetre in diameter to about twenty times this size. The range of liquid water content for Cumulus cloud is 0.05 to 0.2 gm^{-3}, but it may reach up to 0.6 gm^{-3} during its development stage. The highest value of liquid water content (~ 5gm^{-3}) is found in the deep convective clouds. High level clouds such as cirrus clouds are having the lowest number of droplets with large dynamic range. The number of cloud droplets depends on the number of Cloud Condensation Nuclei (CCN), which in turn depends on the aerosol concentration in cubic meter of air where the clouds form. The number of aerosols will decrease with height and very few aerosols serve as CCN at mid-levels, which results in smaller concentration of cloud droplets as compared to clouds formed at lower level such as St/Sc cloud.

1.5 Experimental techniques for cloud observations

a. Ground based observations of clouds

A detailed understanding of the variability of cloud distribution with time and space is essential for accounting the feedback processes among clouds, radiation and the circulation of the atmosphere on both the regional as well as global scale. Observations of the space time variability of clouds which are blanket around the globe are imperative for understanding how it affects the global energy, hydrological cycle and the climate change. Meteorologist have been observing the day-to-day weather and keeping the records about clouds properties for generations. The surface based weather records have made significant contributions to our present

understanding of clouds.

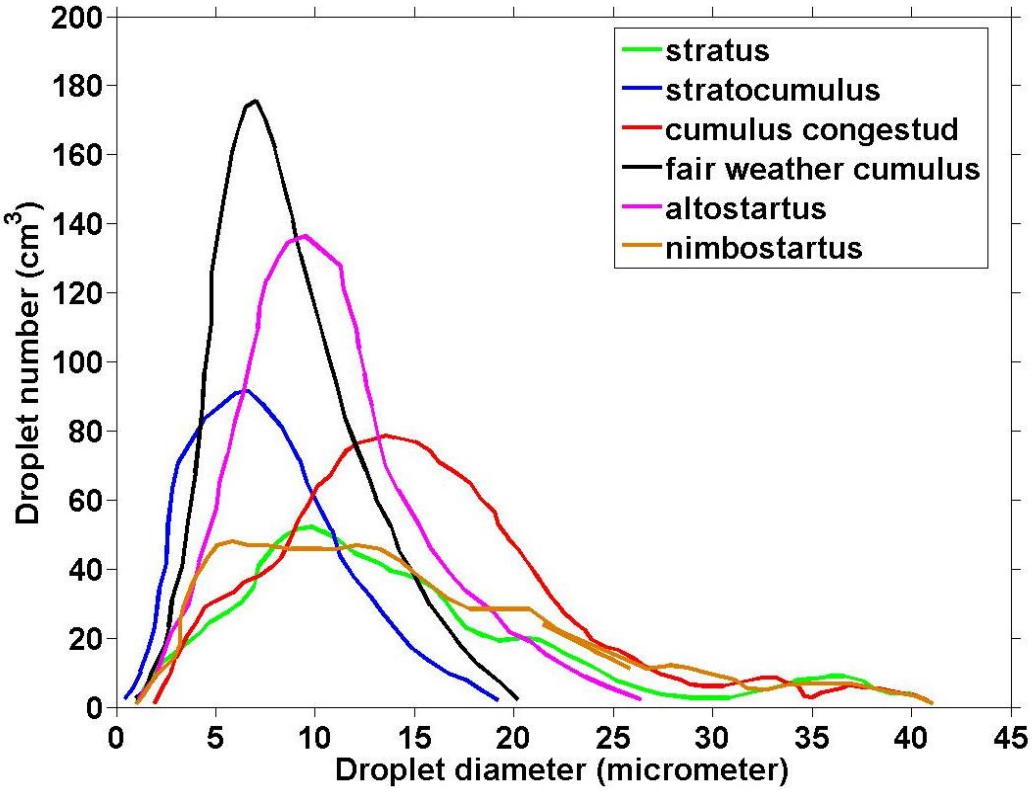

Figure 1.2: Typical droplet size spectra for different types of clouds (redrawn from *Quante [2004]*).

Table 1.2 Typical values of microphysical properties of various clouds formed in the earth's atmosphere (Quante [2004] and Pruppacher and Klett [1997, 1978]).

S.No.	**Cloud Type**	**Parameter**	**Typical value**	**Range of values**
1	Marine Sc	Cloud particle concentration (cm^{-3})	150	45-300
		LWC (gm^{-3})	0.4	0.1-0.6
2	Continent Sc	Cloud particle concentration (cm^{-3})	250	40-500
		LWC (gm^{-3})	0.3	0.03-0.45
3	Cu	LWC (gm^{-3})	-	0.05-0.2

4	Cu congest	LWC (gm^{-3})	-	0.5-2.5
5	DC	LWC (gm^{-3})	-	1.5-5
6	Nimbostratus	LWC (gm^{-3})	-	0.2-0.5
7	Ac/As	Cloud particle concentration (cm^{-3})	100	30-1000
		LWC (gm^{-3})	0.03	0.01-0.75
8	Cirrus	Cloud particle concentration	30	10^{-4}-10^{4}
		IWC (gm^{-3})	0.02	10^{-4}-0.5

These ground based cloud observations are very useful in studying the climate variability, which are constructed from synoptic weather observations. These surface based observations and measurements make important contributions to the climatic data record for a particular location by providing the very high temporal coverage. But these are limited mostly over the continents [*Kidd and Barret*, 1990; *Norris*, 1998; *Norris*, 2000; *Kidd*, 2001]. To the date meteorologists observe visually in the sky and measure the total cloudiness in terms of eights or tenths of sky cover. Further, they identify the low, mid, and high level cloud types by following the synoptic code given by WMO (*WMO*, 1974). One should keep in mind that the measured fraction of cloud covering over the sky may not be the same as the fraction of cloud covering the entire earth. The main advantages of ground based observations are that they provide the regular identification of cloud type, multi decadal time records of cloud history and unobstructed view of low level clouds. However, if sky cloud cover is homogenous they can obstruct the view of high level clouds, where the space based observations are immensely important.

b. Space based observations of clouds

With the limited weather station networks over the continents and the impracticality of making the observation over the oceans, a comprehensive description of the space and time variability of global cloud distribution can only be achieved from the vantage point of space. Space based observations can provide the

certain type of cloud measurements at high spatial and temporal scales. These space based observations complement the surface based observations. These observations are foremost important to the comprehensive data base of earth's cloud ever obtained. The space based observations also provide inputs to design the future satellite missions with greater observing capabilities. These measurements are very important as they provide the new insights into the cloud dynamics and their feedback to general circulation. Further, it is very useful for evaluating the prediction capabilities of climate models. The space based remote sensing of clouds can be broadly classified into passive and active remote sensing techniques [e.g., *Stephen and Kummerow*, 2007].

i. Passive remote sensing of clouds from space

Space based observations of clouds in the visible, near- IR and thermal IR bands have enormously contributed to the current understanding of the global distribution of clouds and their properties [e.g., *Rossow,* 1989; *Roca et al*., 2002]. Passive remote sensing instruments receive the sunlight reflected/emitted from the surface of the earth and clouds and deduce the properties of clouds by using suitable techniques. The passive remote sensing instruments onboard satellites operate in the visible and near-IR channel in the wavelength range of 0.55-1.05 μm, IR channel in 10.5-12.5 μm and the water vapour channel in the range of 6.2-7.6 μm. Most of the space based techniques are centred on the passive remote sensing and provides the two dimensional properties of clouds. Many of the passive remote sensing measurements are limited to the uppermost layer of the cloud and vertically integrated properties of cloud. The synoptic scale distribution of cloud is important because regional anomalies of radiative cooling and latent heating have a major influence upon the energetics of the atmospheric circulation. This type of information cannot be obtained from sun-synchronous polar-orbiting satellites since they sample a location at a fixed local time. Observations by geostationary satellites, which constantly observe a particular region of the globe, are ideal for this purpose. During 1979, five geostationary satellites were launched that carried the spin scan imaging systems

that provide continuous observation of the entire globe, apart from the Polar Regions (*Houghton*, 1979a; 1979b). These observations are very useful for studying the diurnal properties of clouds at regional scales. The first images of the cloud in connection to meteorological processes were provided by the Television and Infrared Observation Satellite (TIROS-1), which was launched in April 1960. The geostationary meteorological satellite provides the information about the cloud movement around the earth at every 30 seconds, but more typically every 30 minutes. Even though, the resolution of those satellite images is coarser than that of the polar-orbiting satellites, but their ability to provide the continuous monitoring of the atmosphere is very crucial for short-range weather forecast. Such short time interval observations are very essential for investigating the lifecycle of convective cloud systems and its diurnal evolution. But the geostationary satellites are placed at very high altitudes and the observations made by them are very poor compared to polar orbiting satellites. However, high temporal resolution measurements provided by geostationary satellites cannot be achieved by the polar orbiting satellites. The geostationary satellites data are extensively used in the global analysis of clouds, carried out by the ISCCP. There are several countries having the geostationary meteorological satellites for weather monitoring, which includes USA (GOES), Europe (Meteosat), Russia (GOMS), Japan (GMS), China (FY) and India (INSAT). India has launched several geostationary satellites to provide the continuous weather information in the visible and IR bands since 1983. These satellites are referred as INSAT series (INSAT-1 (A-D), 2 (A, B, E) and Kalpana-1, INSAT3A, INSAT-3D, 3DR) and observations of these satellites are also used in ISCCP [e.g., *Rajeev et al*., 2008]. The Nimbus-E Microwave Sounder (NEMS) and the Scanning Microwave Sounder (SCAMS), flown on the Nimbus-5 and 6 satellites respectively, demonstrated the potential applications of microwave remote sensing in satellite applications to retrieve the atmospheric parameters such as amount of water vapour and temperature profile (*Waters et al*., 1975, *Kunzi et al*., 2011). Later on, the microwave limb scanning sensors designed to measure the atmospheric composition have become prominent with the launch of Upper Atmosphere Research Satellite (UARS)

by NASA. Passive microwave radiometers also provide the three-dimensional perspective of clouds by sensing the radiation reflected from clouds and the atmosphere at multiple frequencies around the absorption line [*Simpson et al*., 1988].

ii. Active remote sensing of clouds

A passive satellite sensor measures the natural thermal radiation and depends on the day light also. Whilst the active satellite sensors emits its own radiation and detects the radiation reflected/scattered from the clouds in the atmosphere, thereby provides the three-dimensional distribution of cloud properties without depending on the day light conditions. Active sensors, for example RADAR (Radio Detection and Ranging), sends the electromagnetic wave pulse into the atmosphere from satellite and receives the reflected radiation from the hydrometeors with elapsed time interval between emission and return. Thus radar is able to provide the vertical structure of cloud properties. The main advantages of active sensors include the ability to measure anytime regardless of day and time of the season. Tropical Rainfall Measuring Mission –Precipitation Radar (TRMM–PR) is the first space borne radar launched jointly by USA and Japan in 1997 with operating frequency of 13.8 GHz. It provides the vertical distribution of precipitation over the tropical regions with a vertical resolution of 250 m over the ocean and land. The swath width of TRMM-PR is 220 km and it can detect the light rain rates to heavy rain rates [*Simpson et al*., 1996; *Kummerow et al*., 1998; *Iguchi et al.*, 2000, *Anagnostou*, 2004]. TRMM-PR has filled many gap areas in the understanding of cloud dynamics and its connection with the circulation patterns. It provided the first space based quantitative estimation of precipitation and classification of convective and stratiform cloud systems. In line with this, the CloudSat and CALIPSO launched in 2006 have immensely contributed to the present understating of the vertical structure of cloud distribution over the globe [e.g., *Stephens et al.*, 2002; *Cetrone and Houze*, 2009]. CloudSat operates at millimetre wavelength frequency (94 GHz) and CALIPSO is a lidar. CloudSat is able to detect the non-precipitating clouds to very light drizzle

clouds, but it cannot detect the very thin high level clouds. On the other hand, CALISPO is able to detect thin high level clouds which are not detected by CloudSat. At the same time, CALIPSO cannot detect very thick cloud where CloudSat can detect them. Thus the combination of CloudSat and CALIPSO measurements has been tremendously contributed to the understanding of the vertical distribution of clouds on a global scale.

1.6 A brief note on Indian Summer Monsoon

Tropical belt is the source region for the energy that drives the general circulation of the atmosphere as it has the maximum influx of solar radiation and thus plays a very important role in transporting the heat and moisture along the meridional direction. Tropical region having the warmer and humid atmosphere is conducive for the formation clouds, frequently. Of the various phenomena that characterize the tropical region, the most visible feature is the ITCZ, where the moisture laden winds from both the hemispheres converge to form a zone of large convection, cloudiness and precipitation. This constitutes the ascending branch of the Hadley circulation to mark the meteorological equator. The convective cloud system of ITCZ is critical in terms of latent heat release and its contribution to planetary albedo in the atmosphere. The ITCZ has a periodic movement in the north-south direction in tune with the apparent annual migration of the Sun [e.g., *Webster et al*., 1998]. Associated with periodic moment of ITCZ, there are long periods or seasons of wet weather, called the monsoons. Over Indian region, during June to September, the winds are south-westerly to westerly on the equatorward side and easterly on the other side of ITCZ and the monsoon is referred to as South-West monsoon and also Indian summer monsoon (ISM). Generally, it is believed that the continental-scale land-sea thermal contrast drives the large-scale Monsoon circulation. The ISM is one of the most investigated topics in the realms of meteorology. This synoptic system serves as natural laboratory for cloud studies. The following rough estimation illustrates the importance of ISM in terms of its contribution in energy budget over the Indian

region. The average radiation received over the Earth' surface is ~ 170 Watt/m^2. The radiation received over the Indian region (i.e., from 5-30^{0}N; 71-95^{0}E) is 1.06x10^{15} Watts. The average amount of rainfall for 120 days during the ISM over the Indian region is ~ 4 x 10^{15} Kg. Therefore, the heat liberated by the monsoon rains over the Indian region is 0.96 x 10^{15} Watts. Thus, the latent heat liberated by monsoon rains in the atmosphere over the Indian region is almost equal to the shortwave radiation received by the same area [*Subbaramayya and Ramanadham*, 1981].

1.7 Studies on global distribution of clouds

Investigations on global distribution of clouds using space based measurements have been greatly contributing to the present understanding of clouds and their properties over the variety of geographical locations. Analyses from the ISCCP reveal that the global mean cloud coverage fraction is 68.6%. [*Rossow*, 1989; *Hemsfiled and Fulton*, 1994; *Rossow and Schiffer*, 1999; *Wang and Rossow*, 1998; *Hartmann et al*., 2001; *Gambheer and Bhat*, 2001; *Sathiyamoorthy et al*., 2004; *Roca et al*., 2005; *Meenu et al*., 2010; *Rajeevan et al*., 2012; *Nair et al*., 2011; *Hazra et al*., 2015]. Clouds play a pivotal role in modulating the weather and climate of the earth's atmosphere by changing the radiation balance through vertical and horizontal transfer of energy, atmospheric thermo-dynamical structure and hydrological cycle. Clouds are principal factors in governing radiation energy balance regionally as well as globally. By interacting with both short- and long-wave radiation, clouds play crucial role in the radiative budget at the surface, within and at the top of the atmosphere [*Trenberth et al*., 2014; *L'Ecuyer, et al*., 2015; *Stephens and L'Ecuyer*, 2015]. The temporal and spatial distribution of cloud systems determine the time and place of the heat release. Tropical cloud clusters modify the vertical heating adequately to amend the large-scale circulation and deep convection [*Houze*, 2010]. Cloud vertical structure, including its top and base altitudes and cloud thickness affects the large-scale circulation by altering the gradients of total diabatic heating/cooling [*Webster and Stephens,* 1984]. *Wang et al*. (2000) reported the climatology of cloud vertical structure using global rawinsonde observations of humidity profiles and provided

the much needed information about single and multi-layer clouds [*Wang and Rossow*, 1995; *Wang et al*., 2000; *Huang et al*., 2005].

Many attempts have been made in the past to include the cloud feedback processes in weather as well as climate models. Figure 1.3 shows the cloud feedback parameter for all the models tested in 1990 and again in 1996. It is evident that the different numerical models used or developed in the year 1990 and models used in the year 1996 are not even in the consistence of the sign of the cloud feedback parameter [*Cess et al*., 1996]. This can be considered as the one of the evidence for the uncertainty in the representation of clouds in current models and they need improvement continuously. Apart from their importance in earth's climate, role of clouds in precipitation is very important in day-to-day weather forecasts.

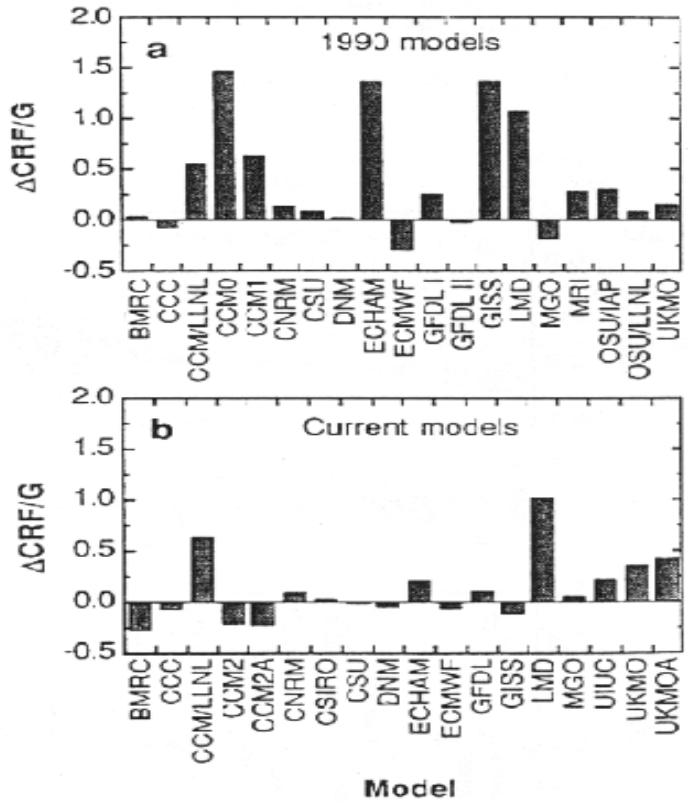

Figure 1.3: The cloud feedback parameter (see text for explanation) as produced by a number of GCMs in 1990 (top panel) and 1996 (bottom panel). [Figure courtesy: *Cess et al*., (1996). The x-axis represents the acronym of various climate models.

The correct representation of clouds and their associated processes and feedback in the General Circulation Models (GCMs) are the need of the hour [*Stephens*, 2005; *Randall et al*., 2007]. Due to these reasons, the cloud studies are of paramount importance to the meteorological community. Understanding of the latent heat released by clouds in the atmosphere and cloud radiative heating are the central objectives to any study which deals with atmospheric circulation and clouds. Most of these studies emphasized the importance of cloud vertical structure on general circulations, including their top and bottom altitude variations with respect to various geographical locations. Apart from these, multi-layered cloud distributions which are significantly alter the vertical and horizontal distribution of latent heat and radiative heat fluxes [*Webster and Stephens*, 1984].

Studies focusing on the spatial and vertical distribution of clouds over Indian region and its surrounding oceanic areas are rather limited, especially the vertical distribution [e.g., *Gambheer and Bhat*, 2000; *Roca and Ramanathan*, 2000; *Roca et al*., 2002; *Zuidema*, 2003; *Sathiyamoorthy et al*., 2004; *Meenu et al*., 2010, 2011; *Nair et al*., 2011; *Rajeevan et al*., 2012]. The unanimous view of many of the atmospheric researchers is that the identification and distribution of multi-layered clouds is important from climate standpoint and any attempt to quantify the global warming should include the radiative impacts of clouds, which is severely hampered by ignoring the multi layered cloud parameters in models [*Gupta et al*., 1992; *Wielicki et al*., 1995; *Wang et al*. 2000; *Chen et al*. 2000a, 200b]. To determine the importance of cloud feedback mechanism, one has to quantify the distribution of cloud vertical structure to diagnose the processes involved. Changes in cloud vertical structure depends on the locations of cloud top and base, number of cloud layers and thickness, which affects the circulation pattern in atmospheric GCMs by modifying the distribution of atmospheric latent heating rates [*Wang and Rossow*, 1998]. Thus it is important to have quantitative measurements of the geographic distribution and variations of cloud vertical layers to accurately predict the climate change. Numerous studies have reported the effects of clouds on the general circulation in

the past [*Slingo and Slingo*, 1988; *Randall et al*. 1989; *Wang and Rossow*, 1998]. *Randall et al.* [1989] studied the effect of vertical structure of clouds on the general circulation by using numerical models and found that the general circulation strength is sensitive to the distribution of cloud vertical structure. Further, importantly it modifies the radiative heating of the atmosphere. *Wang and Rossow* [1998] carried out a series of trails using NASA Goddard Institute for Space Studies GCM to study the effects of vertical distribution of clouds on atmospheric circulations. They also found that the effect of cloud vertical structure in GCMs. One of the important findings of the above study was that the strength of the circulation is sensitive to the gradients in the cloud vertical distribution rather than horizontal distribution. All these studies pointed out that the cloud vertical structure is the one of the key elements in understanding the cloud feedback mechanism [*Rossow et al*., 2005]. So, it becomes inevitable to establish the vertical distribution of clouds and to study their role in modifying the atmospheric circulation for better understanding of cloud feedback mechanisms.

Apart from the total cloud amount and its vertical distribution, one more important aspect of clouds is the cloud type. It is known that depending upon the cloud type, the radiative properties, the latent heat released and microphysical properties of clouds largely differ. *Chen et al*., [2000a] investigated the radiative flux changes induced by the occurrence of different cloud types using ISCCP cloud data and a radiative transfer model. These authors emphatically showed that the cloud-type variations are as important as cloud cover in modifying the radiation field of the earth–atmosphere system and further showed that the largest annual mean changes of the global top-of-atmosphere and surface shortwave radiative fluxes are produced by stratocumulus, altostratus, and cirrostratus clouds whereas cirrus, cirrostratus, and deep convective clouds cause most of the annual mean changes in the global top-of atmosphere long-wave radiative fluxes. Thus it becomes clear that apart from the three-dimensional distribution of cloud cover, it is important to have cloud type distribution to quantify the feedback provided by the clouds in totality.

1.7.1 Field experiments/campaigns to investigate the cloud characteristics

With the fast developments in the information technology and electronics, the remote sensing, data processing, display and transmission of weather data reaching a new facet and increasing computational power in weather numerical modelling studies have been contributed greatly to the present understating of cloud dynamics and its evolution during its life time. There have been several field campaigns conducted around the globe to investigate the detailed structure and dynamics of precipitating cloud systems. Most of the experiments are conducted on cloud systems to keep the records of data collected by those campaigns during 1940s-1990s and for better documentation for generations. Understanding the cloud characteristics and its interactions with the background dynamics had been took place in 1990s-2000s and made significant contributions to the present understating of cloud systems. Data derived from those field experiments and campaigns can be used to fine tune cloud resolving models. From the year 2000 onwards, studies on the parameterization of cloud systems and their interactions with the environment have been given priority. Table 1.3 gives the various field campaigns and experiments that took place in connection with investigation of cloud systems across the globe. Figure 1.5 shows the geographical locations along with the campaigns carried out to explore the cloud systems and associated dynamics over various part of the globe.

Table 1.3 Field campaigns and experiments in connection with cloud systems over the globe

S.No	Name of Experiment	Duration	Goal/Focus/Objectives
1	TRIP- The Thunderstorm Research International Program	Summer of 1946-1947	Large-scale investigations of thunderstorms
2	IIOE-International Indian Ocean Expedition	1960-1965	To study Monsoon
3	ISMEX- Indian Summer Monsoon Experiment	Summer -1973	To study Indian summer monsoon

4	GATE – Global Atmospheric Research Program (GARP) Atlantic Tropical Experiment	15 June – 23 Sept., 1974	To understand the tropical atmosphere and its role in driving the global circulation
5	MONSOON-77	1977	To study the monsoon onset, depression, etc.
6	W-MONEX-Winter Monsoon Experiment	1978/1979	A campaign under GARP to study the winter monsoon
7	MONEX- Monsoon Experiment	Summer 1979	To study the Indian summer Monsoon
8	CCOPE- Cooperative Convective Precipitation Experiment	22 May-7Aug, 1981	Program on convective clouds and storms to elucidate how the microphysical processes and the air motions interact in the formation and development of precipitation
9	JAWS- Joint Airport Weather Study	15May-13 Aug, 1982	To study the convective microbursts
10	EMEX-The Equatorial Mesoscale EXperiment	Jan – Feb 1987	To investigate the mesoscale convective systems in the monsoon flow
11	CINDE-The Convection Initiation and Downbursts	22 June-7 Aug,1987	To study the processes leading the formation of deep convection and the physics of downburst
12	AMEX-The Australian Monsoon EXperiment	Oct-1986 Jan-Feb 1987	Aimed at better documentation of large-scale weather patterns over Australia that are associated with monsoon flow
13	TAMEX-The Taiwan Area Mesoscale EXperiment	1 May- 29 June, 1987	To study the mesoscale circulation associated with the Mei-Yu front and to study the evolution of MCSs
14	DUNDEE- The Down Under Doppler and Electrical Experiment	Nov,1988-Feb 1989	To study the dynamical and electrical properties of MCSs

15	CaPE- The Convection and Precipitation /Electrification Experiment	8 July- 18 Aug, 1991	To study the development of mesoscale convective systems with numerical forecast of winds
16	TOGA-COARE - Tropical Ocean Global Atmosphere-The Coupled Ocean Atmosphere Response Experiment	Nov- Feb 1993	To understand the principal atmospheric processes that organize convection in the warm pool region
17	MCTEX-The Monsoon Continent Thunderstorm EXperiment	Nov-Dec 1995	To investigate the life cycle of island- initiated MCSs within the Maritime continent
18	INDOEX-The Indian Ocean Experiment	18 Feb-31 March, 1998	To study the role of ITCZ in the transport of species and their resulting radiative forcing
19	JASMINE - Joint Air-Sea Monsoon Coast of India Experiment	1999	To study the convection during pre to onset of monsoon over Indian Ocean
20	BOBMEX- Bay of Bengal Monsoon Experiment	1999	To study the Indian Monsoon
21	STEPS-The Severe Thunderstorm Electrification and Precipitation Study	May-July 2000	For better understanding the interactions between kinematics, precipitation, electrification in severe thunderstorms
22	ARMEX – Arabian Sea Monsoon Experiment	2002-2005	To study the monsoon over the Arabian Sea and west coast of India
23	BAMEX- The Bow Echo and MCV Experiment	20 May-6 July, 2003	To examine the life cycle of MCSs
24	AMMA- African Monsoon Multidisciplinary Analysis	EOP 2005-2007	To improve knowledge and understanding of the West African monsoon
25	RAINEX-Hurricane Rainband and Intensity change Experiment	15 Aug-30 Sept, 2005	To document hurricane rainbands and inner-core structures to gain insight into how they interact and, ultimately, affect

			hurricane intensity changes
26	TWP-ICE- Tropical Warm Pool-International Cloud Experiment	Jan-Feb, 2006	To study the tropical warm pool region
27	MISMO- The Mirai Ocean Cruise for the Study of the Madden Julian Oscillation-convection Onset	Oct-Dec, 2006	To study the onset mechanism of convection in the MJO
28	CTCZ- Continental Trough Convergence Zone	2008-2012	To study the continental convective cloud systems over India
29	MC3E- Midlatitude Continental Convection Clouds Experiment	April-May 2011	To provide the most complete characterization dataset for convective cloud systems, precipitation, and their environment
30	DC3- Deep Convective Clouds & Chemistry Experiment	1 May-30 June, 2012	To investigate the importance of deep convective clouds including their dynamics, physical and lightning process on upper tropospheric composition
31	DYNAMO-Dynamics of the MJO	1 October- 31 March, 2012	To understand the MJO initiation processes and to improve simulation and characterize the ensembles of convection associated with each stage of MJO

1.8 Studies on the distribution of clouds over Indian Summer Monsoon region

Owing to its socio-economic impacts, the ISM is one of the most investigated topics in the realms of meteorology. Many studies on the ISM by several researchers across the globe contributed constructively to the current understanding of this enigmatic large-scale system [*Webster et al*., 1998]. The distribution of clouds and the fraction

of occurrence on regional as well as global scale are made possible with the launch of geostationary meteorological satellites since 1979. There have been numerous studies on the fraction of cloud, distribution of clouds and its diurnal variation over the ISM region [e.g., *Gambheer and Bhat*, 2001; *Sathiyamoorthy et al*., 2004; *Roca et al*., 2005; *Meenu et al*., 2010; *Rajeevan et al*., 2012; *Nair et al*., 2011]. Further, by using the passive bands of visible and IR channels onboard geostationary platforms, the observed clouds are classified into low-, mid- and high-level cloud based on cloud top brightness temperature by using different threshold conditions [*Nakazawa*, 1988; *Roca et al*., 2002; *Zuidema*, 2003; *Rajeev et al*., 2008; *Devasthale and Grassal*, 2009; *Meenu et al*., 2010; *Sathiyamoorthy et al*., 2013; *Ahn et al*., 2015]. The Spatial and vertical distribution of clouds over the Indian region are also studied by using space based active sensors such as TRMM and CloudSat [*Yuan and Houze*, 2011; *Nair et al*., 2011; *Rajeevan et al*., 2012; *Li et al*., 2014; *Peng et al*., 2014; *Zhang et al*., 2014; *Yan et al*., 2016]. TRMM has filled many gaps in the understanding of the tropical precipitating clouds and their variations, including the vertical structure of tropical deep convective systems. On the other hand the CloudSat provided the three-dimension structure of non-precipitating clouds [*Iguchi et al*., 2000; *Simpson et al*., 1988; *Stephens et al*., 2002; *Hence and Houze*, 2011, 2012; *Pokhrel and Sikka*, 2013; *Kumar et al*., 2014; *Yang et al*., 2015]. Figure 1.5 shows the phenomenological description of cloud studies over the Indian region using various space based observations of clouds. *Gambheer and Bhat* (2000; 2001) examined the distribution of deep convective system over the Indian region using INSAT data and found the bimonthly modulation in the in the areal extent of convective systems over the Indian region and also reported the mean speed of deep convective system, which is around 7 to 9 m/s. Further, *Zuidema* (2003) examined the life cycle of convective clouds over the Bay of Bengal using 3-hourlyinfrared satellite data. It was found that the time of maximum occurrence of convective cloud is around early morning over the bay and the cloud systems dissipates after the sunrise. Another important aspect of convective clouds over the Bay of Bengal is that they propagate in the southwest direction. *Meenu et al*. (2010) studied the long-term regional

distribution of clouds over the Indian region using Advanced Very High Resolution Radiometer (AVHRR) data. It was found that the deepest clouds are formed over the northern BoB during the summer monsoon months. *Roca et al*. (2002) studied the deep convective cloudiness and their relation with the upper tropospheric humidity over the Indian region by using multi-satellite observations. The influence of the Tropical Easterly Jet (TEJ) on spreading the cloud tops over the Indian monsoon region was studied by *Sathiyamoorthy et al*. (2004). It was observed that the upper level wind shear sweeps the cloud tops and a significant correlation is found between the strength of TEJ and high cloud amount. *Nair et al*. (2011) studied the vertical distribution of clouds using CloudSat observations over the Indian region and found that the presence of 'pool of inhibited cloudiness' over the Sri Lanka during ISM season. The mean vertical distribution of clouds during active and break spells associated with ISM region was examined by *Rajeevan et al*. (2012) using CloudSat observations. Further they studied the intra-seasonal variability of vertical structure of clouds over the Indian region. The spatial and temporal distribution of deep convective clouds was analysed by *Peng et al*. (2014) using CloudSat and CALIPSO observations. It was found that the highest vertical extent of deep convective clouds are occurred over the Asian monsoon region and their vertical structure in mesoscale convective systems were analysed by *Yuan et al*., (2011). While the interaction between the dynamics and cloud microphysics over the Western Ghats during summer monsoon was studied by *Kumar et al*. (2014).

Generally, it is believed that the continental-scale land-sea thermal contrast is the origin of large-scale Monsoon circulation [*Wallace and Hobbs,* 1977]. However once the monsoon is set, its advancement, maintenance and withdrawal depends not only on the large-scale dynamics but also on the internal dynamics initiated by the cloud systems embedded within the monsoon system. Even though there are studies on cloud distribution over the ISM region, there are no studies focusing on cloud type distribution. Sufficient knowledge of the spatial distribution of individual cloud types would aid the accurate radiation and latent heat calculations, which in turn will help

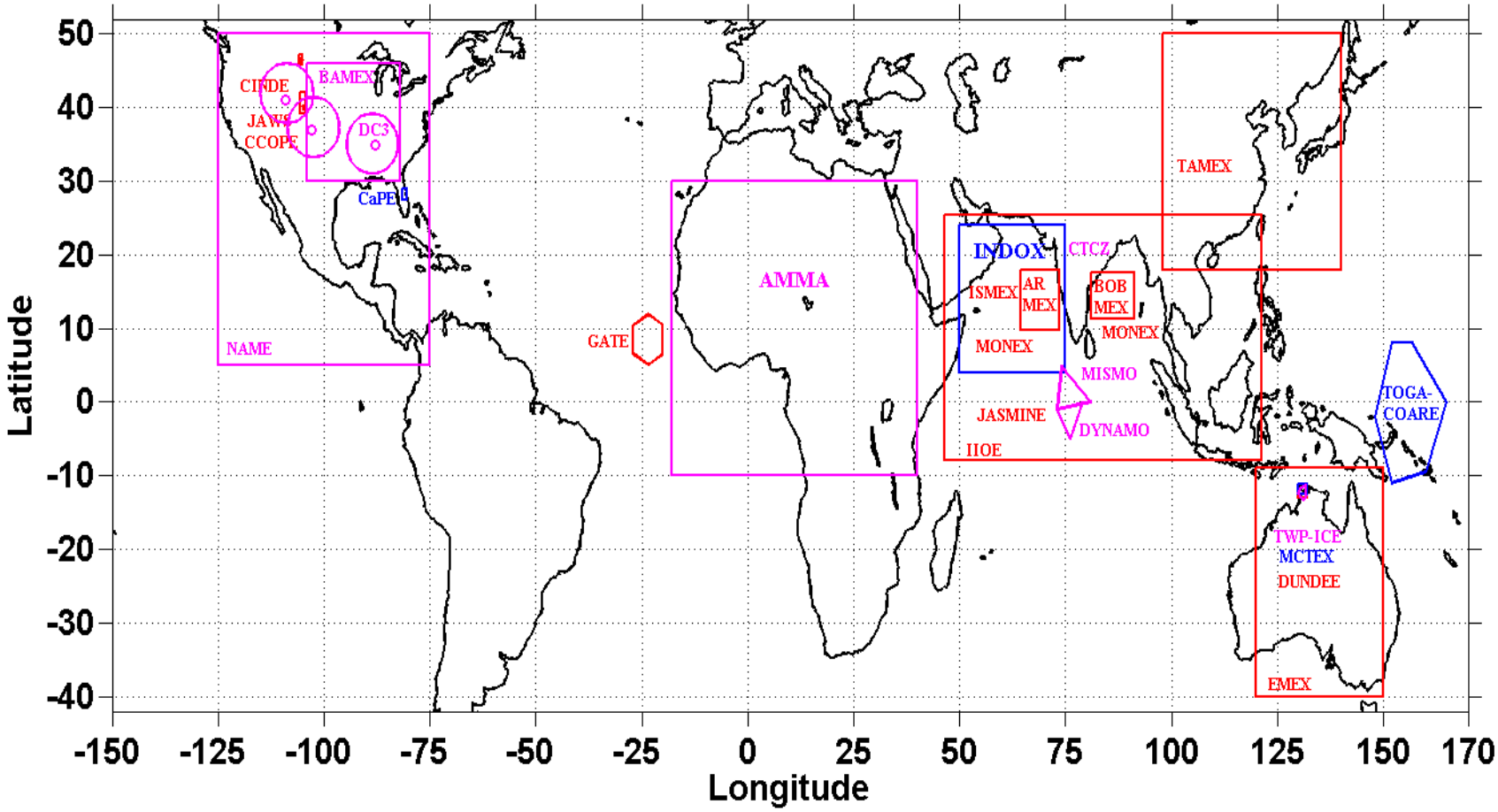

Figure 1.4: Geographical locations of various filed campaigns conducted to study the cloud systems over the globe, since 1940. Acronyms of respective campaigns are given in Table (1.3).

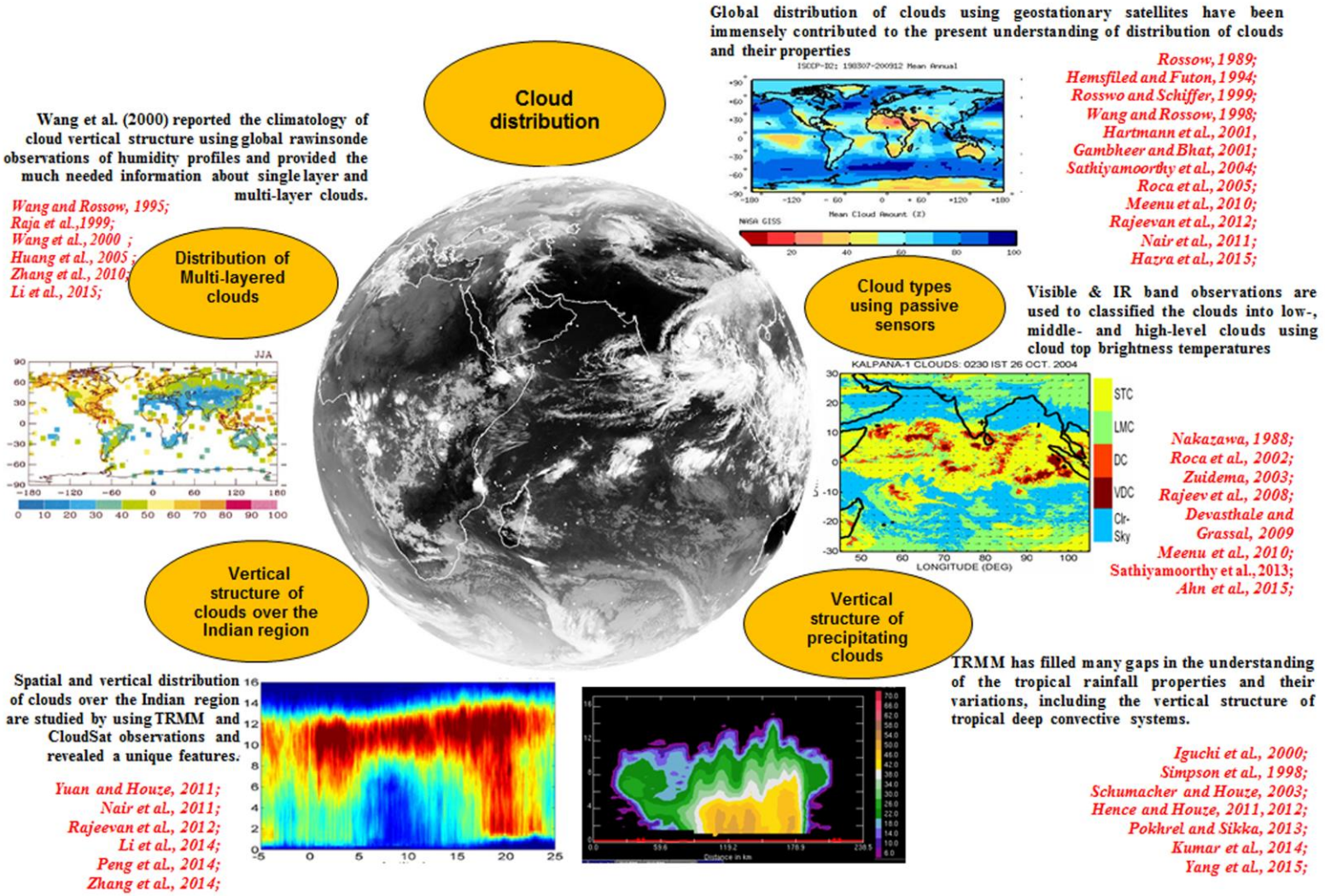

Figure 1.5: Phenomenological description of cloud studies over the Indian region.

in accessing the role of clouds in maintaining and advancement of the ISM. So it becomes important to know, which types of clouds occur over which region.

1.9 Motivation and Scope of the present thesis

The above discussion emphasizes the importance of cloud vertical structure as well as cloud types for climate related studies. Till now, cloud types and associated dynamics during monsoon season are not yet understood fully. The seasonal, spatial and climatological distributions of individual cloud types are very important to understand the cloud physical processes and their effects on climate system. Despite the considerable improvement of the physical realism of cloud and type of cloud representation in GCMs and their feedbacks are still the weakest component of current GCM [e.g., *Senior and Mitchell,* 1993; *Cess et al*., 1996]. Sufficient knowledge of the distribution of individual cloud types would therefore aid the radiation calculations of future climate prediction models and also helps to evaluate the schemes for generating clouds in GCMs. The major gaps areas are in the knowledge of the vertical distribution of various cloud types and the distribution of multi-layered clouds and associated dynamics. In this regard, the present doctorial work focuses on the three dimensional distribution of cloud types and multi-layered clouds and examines their formation mechanism in terms of background dynamics over the study region.

The main objectives of the present thesis are:

1. To investigate the role of dynamics in three dimensional distribution of cloud types during the Indian summer monsoon
2. To construct the composite distribution of cloud types in Tropical Cyclones formed in the North Indian Ocean surrounding the Indian region.
3. To examine the role of large scale dynamics in formation of multi-layered clouds and their distribution.

4. To study the spatial distribution of vertical structure of latent heating in precipitating clouds and their association with various cloud types during the Indian summer monsoon.

Chapter 2 describes the data used for the present study along with their limitations, quality checks of each data set, methodology used for the analysis and the possible errors associated with each data set. The principal data used for the present study is the CloudSat observations. **Chapter 3** presents three dimensional distributions of various types of cloud over ISM region and provides the preferential regions of occurrence of each type of cloud over the study region for the first time. The prevailing dynamics responsible for the preferential formations of cloud types are also discussed in this chapter. The composite distribution of cloud types in tropical cyclones is presented in **Chapter 4**. This chapter discusses what type of clouds present in which part of tropical cyclones that are formed over the North Indian Ocean surrounding the Indian subcontinent. **Chapter 5** discusses the distribution of vertically resolved multi-layered clouds and the role of large scale dynamics in controlling the formation of multi-layered cloud for the first time. The cloud base and top altitudes for multi-layered clouds are also discussed. The results on spatial and temporal variability of vertical structure of latent heating during ISM region are presented in **Chapter 6**. The vertical structures of LH of individual cloud types such as Sc and Deep convective clouds are investigated. It is envisaged that the results from the present study will advance our understanding of the vertical and horizontal distribution of cloud types over ISM and associated dynamics, which in turn will help to improve the representation of cloud types in numerical models. Finally, **Chapter 7** provides the summary and major conclusions from the present thesis work and the scope for future investigations in the light of present results.

Chapter 2

Instruments and Data

"Errors using inadequate
data are much less than
those using no data at all"
-Charles Babbage, circa 1850

Present thesis focuses on the three dimensional distribution of cloud types and associated dynamics over the ISM region. The principal dataset used in the present study is that of the CloudSat having 94 GHZ cloud radar onboard. Cloudsat is part of a constellation of satellites known as A-train. Apart from Cloudsat, the observations from CALIPSO and TRMM are also used in the thesis. For the background winds, the reanalysis datasets are used. The following subsections provide the details of each instrument and dataset used in the thesis.

2.1 A-Train Constellation

The A-train is a constellation of satellites, which is known by other names such as P.M. constellation and A.M. constellation. The P.M. constellation refers for post meridiem with respect to the mean local time of the ascending orbit of satellite occurring after the noon meridian, which is contrasted with A. M. constellation. The A.M. constellation stands for the Afternoon Meridiem constellation and most often called by "The A-Train". The A-Train has a group of six satellites from three countries and all moving nearly in the same orbit to provide the unprecedented observations of the earth science measurements. It starts with Orbiting Carbon Observatory (OCO), Aqua, CloudSat, Cloud-Aerosol Lidar with Orthogonal Polarization (CALIOP), Polarization and Anisotropy of Reflectances for Atmospheric Science coupled with Observations from a Lidar (PARASOL) and Aura satellites. All these satellites are lined up on orbit, one after another and 'Aqua' is considered the A-Train anchor. The A-Train constellation begun with

Aqua launch in May 2002 followed by Aura in July 2004, PARASOL in December 2004 and the Joint CALIPSO/CloudSat launch in April 2006. OCO and Glory failed due to launch vehicle fairing problems in 2010 and 2011 respectively. Later, OCO-2 and GCOM launched in July 2014 respectively. The main purpose of the A-Train constellation is to measure near simultaneous observations of the earth. Figure 2.1 shows the A-Train constellation. The equator crossing time of each satellite is listed in the figure 2.1. Aura starts to crosses the equator at ~1:15 local time (LT), CloudSat at ~ 1:31 LT. After 15 seconds, CALIPSO crosses the equator at ~ 1:31:15 LT and provide the near simultaneous observations clouds. While PARASOL crosses at ~ 1:33 LT and the tail ender Aqua crosses the equator at ~ 1:38 LT. This A-Train formation enables the CloudSat to track CALIPSO in a very precise way. Overall string of all satellites stretches across the 3000 kilometres with a speed of 7 km per seconds. CloudSat orbits approximately 460 km behind Aqua and much closer in front of CALIPSO-only around 93.8 km away, which corresponds to 12.5 seconds average delay between radar and lidar measurements [e.g., *Stephens et al*., 2002; 2008].

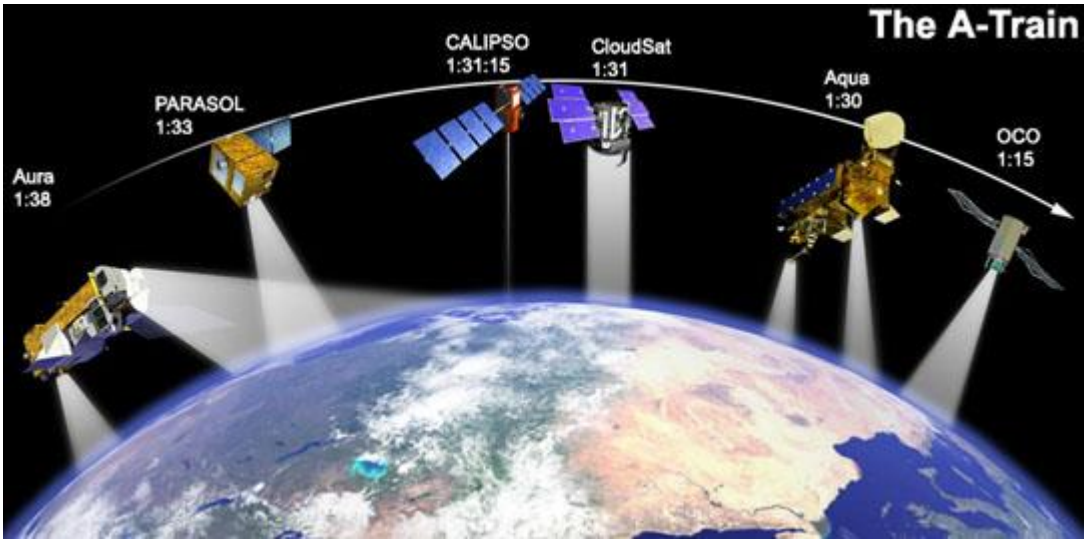

Figure 2.1: CloudSat placed in the A-Train constellation (Courtesy from CloudSat web page: http://www.cloudsat.cira.colostate.edu/dataHome.php).

2.2 CloudSat-Cloud Profiling Radar (CPR)

CloudSat is part of A-Train constellations that was launched in 2006 along with CALIPSO satellite to study the clouds in detail to better characterize the role they

play in regulating the earth's climate. With the launch of CPR on-board CloudSat and Cloud-Aerosol Lidar with Orthogonal Polarization (CALIOP) on-board CALIPSO in late April 2006, unprecedented information on vertical distribution of hydrometeors are available for the atmospheric research community. CloudSat and CALIPSO observations have been extensively used in the recent past to study the cloud vertical structure. The major science objectives for CloudSat are to better understand the vertical structure and the micro physical properties of clouds such as 1) the measurements of the vertical structure of clouds, which are fundamentally important for improving our understanding of how clouds affect both local- and large-scale environments 2) the vertical structure of cloud liquid water content and ice water content and 3) the vertical structure of cloud optical properties.

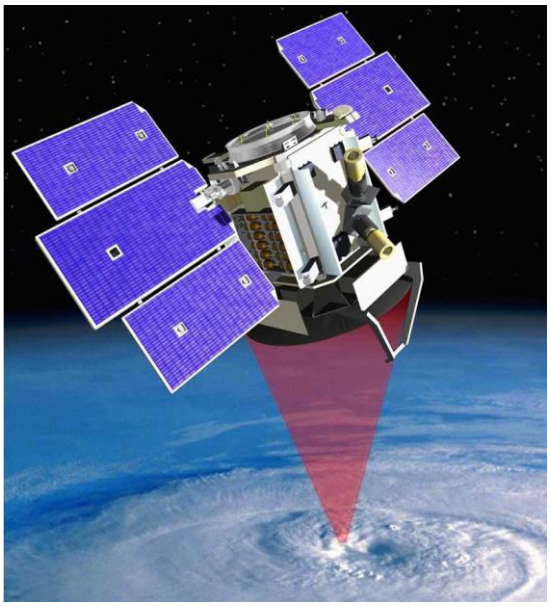

Figure 2.2: Artist view of Cloud Profiling Radar (CPR) in flight mode (image credit: NASA/JPL).

2.3 Design of CPR instrument

Figure 2.2 depicts the graphical representation of CloudSat satellite. The primary goal of the CPR is to achieve a minimum detectable reflectivity of -28 dBZ at the end of the mission and it is required, since the scattering from cloud particles are very weak [*Im et al*., 2005]. For maximizing the cloud detection sensitivity, the CPR design consists of following subsystems: Radio Frequency Electronics

Subsystem (RFES), High Power Amplifiers (HPA), Antenna Subsystems and Digital Subsystems (DSS). The RFES consist of an up-converter which can generates a pulsed signal for 94 GHz and the signal is amplified to around 200 mW by a state-of-the-art MMIC power amplifier. The received signal of REFS down-converts into Intermediate Frequency (IF) and IF signal is detected using a high dynamic range of logarithmic amplifier. Figure 2.3 shows the simplified version of block diagram of CPR [*Im et al.*, 2005; 2006; 2007].

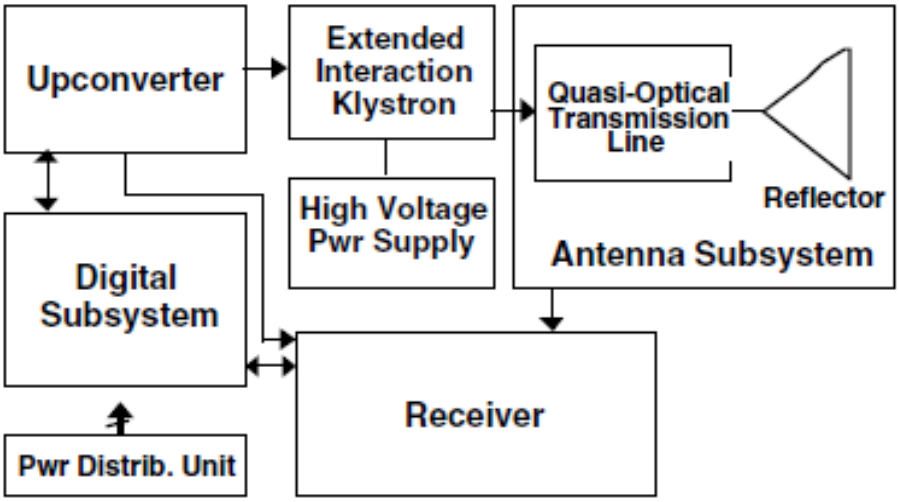

Figure 2.3: Simplified version of CPR block diagram (Adapted from *Im et al.*, 2005).

The HPA amplifies the transmitted radar pulse to a nominal power range of 1.7 kW. The HPA consists of Extended Interaction Klystron (EIK) and a high-voltage power supply. The HPA provides a 20 kV power needed to operate the EIK and further provides telemetry data to subsystems. The 94-GHz EIK and the 20-kV HVPS on-board CloudSat are the first of their kinds being flown in space. The CPR antenna diameter is 1.85 meter reflector of composite graphite material to reduce the mass (Fig 2.4). The gain of the antenna is greater than 63.1 dBi and the half-beam width is < 12 degree. The side lobes of CPR antenna is < ~ -50 dB for angles ≥ 7 degrees from boresight. Figure 2.5 shows the assembly of CPR subsystems of HPA and antenna. The quasi-optical transmission line (QOTL) replaces the conventional waveguide and circulator for sending power from the HPA to the reflector and sending received power to the receiver subsystem. The advantage of the QOTL over conventional waveguide and circulator is reduced

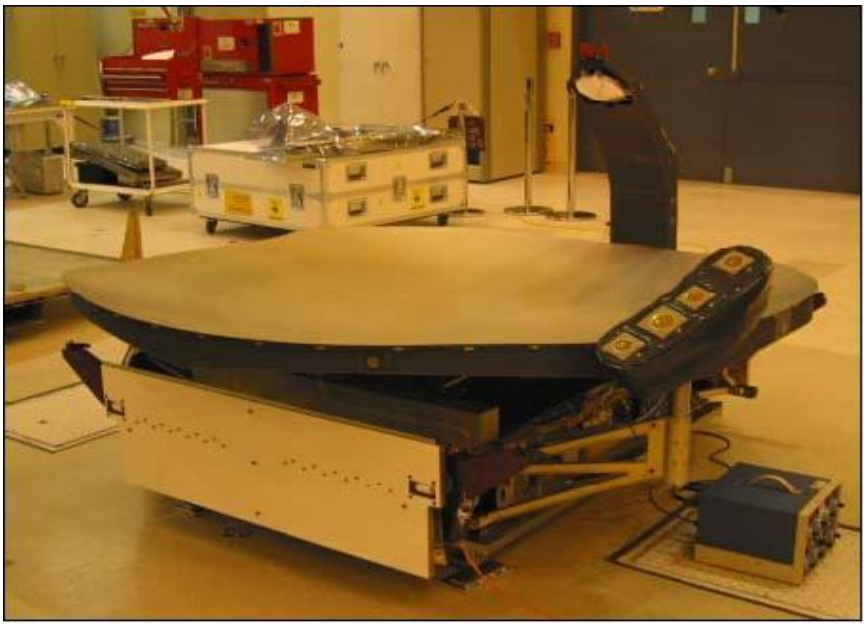

Figure 2.4: CPR Antenna Subsystem flight model (Adapted from *Im et al*., 2005).

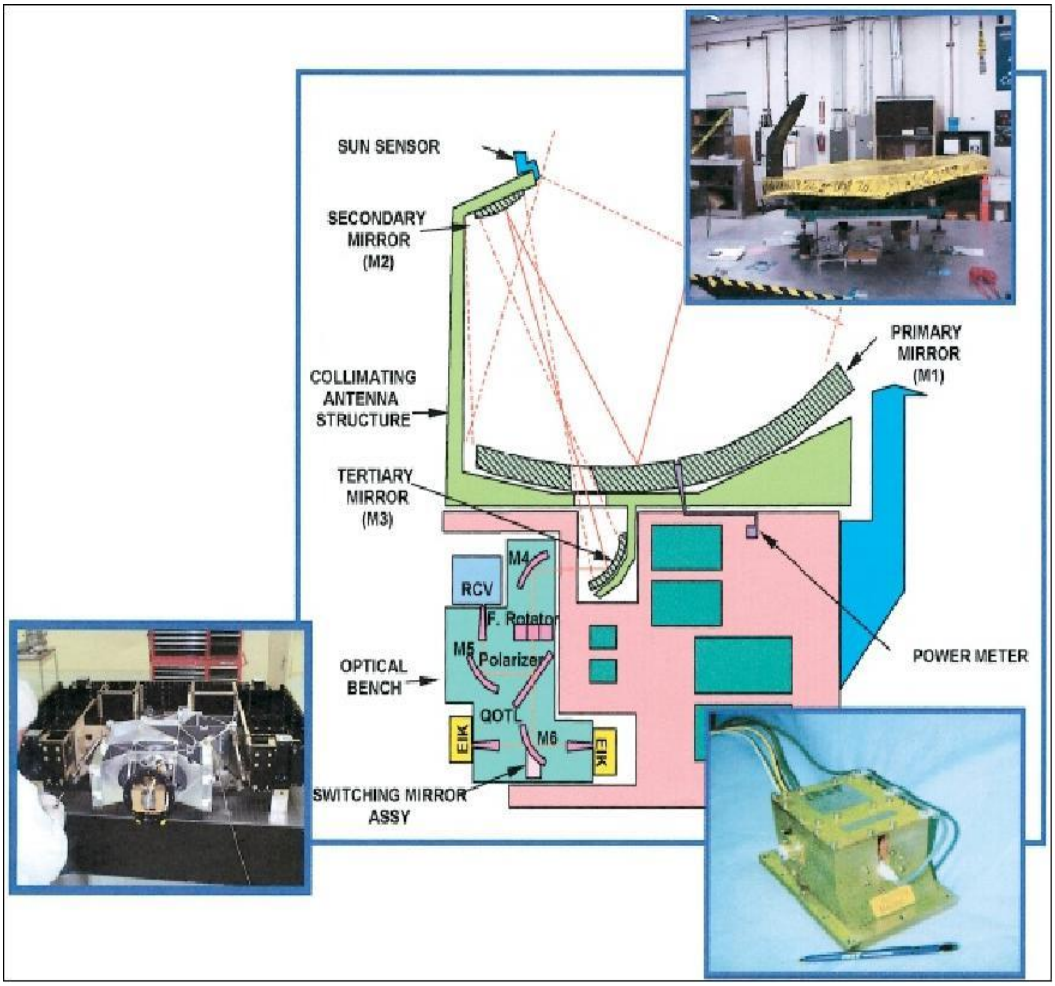

Figure 2.5: The CPR assembly with a schematic of the antenna and HPA subsystems (Image credit: NASA)

reduced loss, important for meeting sensitivity requirements. The DSS provides the command, control, and telemetry interface to the S/C. It includes a Control and Timing Unit and a data handling unit that accepts the analog signal from the RFES logarithmic detector. It digitizes it and performs the required sample averaging of 0.16 s. The received power of many samples of CPR is averaged and the estimated noise is subtracted to detect the low reflectivity of clouds. The number of samples can be increased by increasing the PRF (Pule Repetition Frequency) of CPR but the maximum PRF is dependant by the unambiguous range. The CPR is permitting to detect the surface return and cloud return up to an altitude of 25 km and the nominal range window size is set to 30 km. The system noise is estimated using the clear air radar returns from 25 km to 30 km attitude [*Im et al*., 2006; 2007].

The CPR on board CloudSat operates at 94 GHz with cross- and along-track resolution of 1.4 km and 1.7 km respectively [*Im et al*., 2005]. The vertical resolution of CPR is 480 meters, but the backscatter signal is oversampled to 240 meter resolution. The minimum detectable reflectivity of hydrometeors is ~ -28 dBZ and it was found to be -30 to -31 dBZ from the CloudSat initial results [*Haynes and Stephens*, 2007]. CloudSat makes about 14 orbits per day with two times equator crossing at 0130 and 1330 LT. The CloudSat orbital path repeats around every 16 days to revisit the same geographic location at same local time. The horizontal separation distance between the each ascending (descending) orbit of CloudSat is around 180 km. CloudSat is a Sun-Synchronous orbit (705 km equatorial altitude) with 98.2 degree inclination. Unlike the other traditional satellites such as TRMM, which have a large field of view and observe the most part of the globe, CloudSat smear the earth's atmosphere by cross- and along-track resolution of 1.4 km and 1.7 km respectively and provides exactly 233 diamonds in the longitudes over the globe. Figure 2.6 shows the schematic picture of CPR operation onboard CloudSat. CPR sends 3.3 μs pulses with a PRF of 4300 Hz. The radar pulses cover 1.3 km x 1.3 km instantaneous footprint on the ground, but the effective footprint is around 1.3 km x 1.7 km. Each individual profiles are sampled to 1.1 km apart by averaging 688 pulses within a integration

time of 0.16 seconds. The radar vertical bin resolution is 480 m and is oversampled to 240 m. All CloudSat derived products are generated for the lowest 30 km height range.

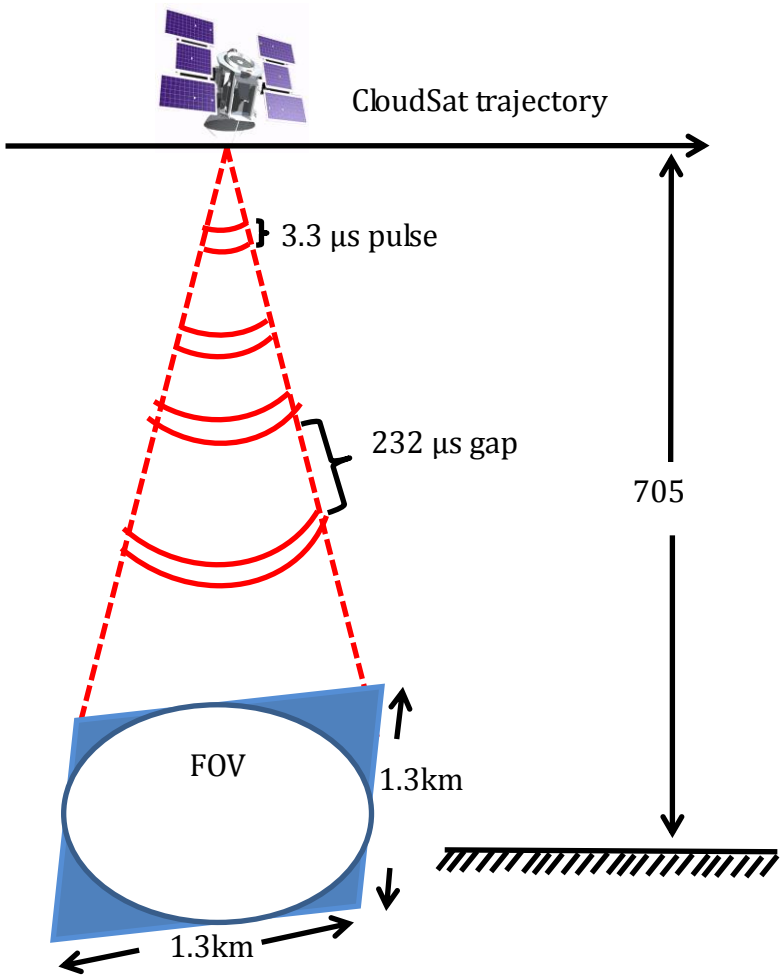

Figure 2.6: Schematic representation of operation of CPR in flight.

Figure 2.7 depicts the CloudSat orbits over the Indian region during 16 day cycle. Red colour line indicates the CloudSat ascending nodes and descending nodes are represented by the blue colour line. Since CPR transmits the signal in the upper part of microwave region, where the radar signal is not significantly attenuated by clouds, enables it to detect the 80% of water cloud and 90% of all ice clouds. CloudSat will allow us to study the interior structure of non-precipitating clouds to light drizzle clouds. Figure 2.8 shows an example of radar reflectivity from a segment of CloudSat orbit. It shows the vertical structure of deep convective cloud, whose cloud top extends above 12 km and further shows the convective

outflows as cirrus anvils. Table 2.1 provides the important specifications of CPR system. With ~240 m vertical resolution, this radar can probe optically thick large- hydrometeor layers. However, CloudSat is not sensitive to optically thin clouds. On the other hand, the Lidar on board CALIPSO owing to its shorter operating wavelength (532 nm) has ability to sense optically thin layers and tenuous cloud tops with vertical resolution as high as 30 m. More details of CloudSat and CALIPSO can be found in *Stephens et al*., (2008) and *Winker et al*., (2007) respectively. The synergy between these two instruments can nearly provide a complete picture of cloud distribution across the globe. *Mace et al*., (2009) suggest that greater than 90% of cloud layers are correctly identified as cloud, by making use of the combination of the CloudSat and CALIPSO observations.

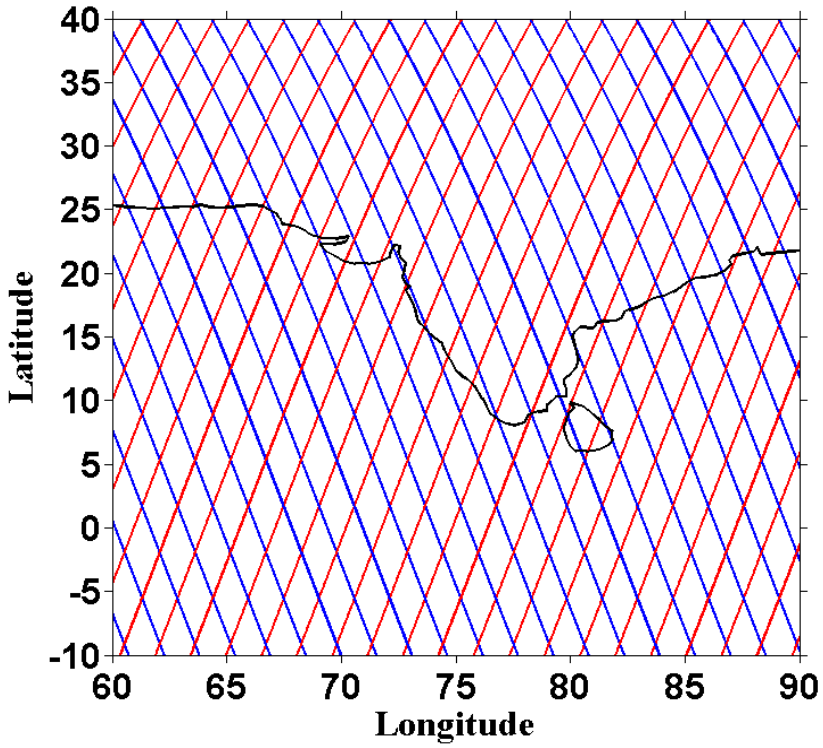

Figure 2.7: CloudSat passages over the Indian region.

The CloudSat CPR is experienced a severe battery anomaly in late 2011. In April 2011, CPR is encountered a battery problem and caused the satellite to depart from the A-Train for one year. CloudSat CPR is successfully resumed for science operation in 27th October 2011 and it re-joined the A-Train in 15th May 2012. After battery rectification, CloudSat operates in Daylight Only Operations (DO-

OP). DOOP mode would require the CPR to cycle into a standby mode sequence when overpassing the Earth while in eclipse (non-daylight portions of the orbit). CloudSat and CALIPSO were maintained in a close orbital management so that they both effectively imaged similar volumes of the cloud systems within 15 seconds of one another to enable the amalgamation of their respective observations.

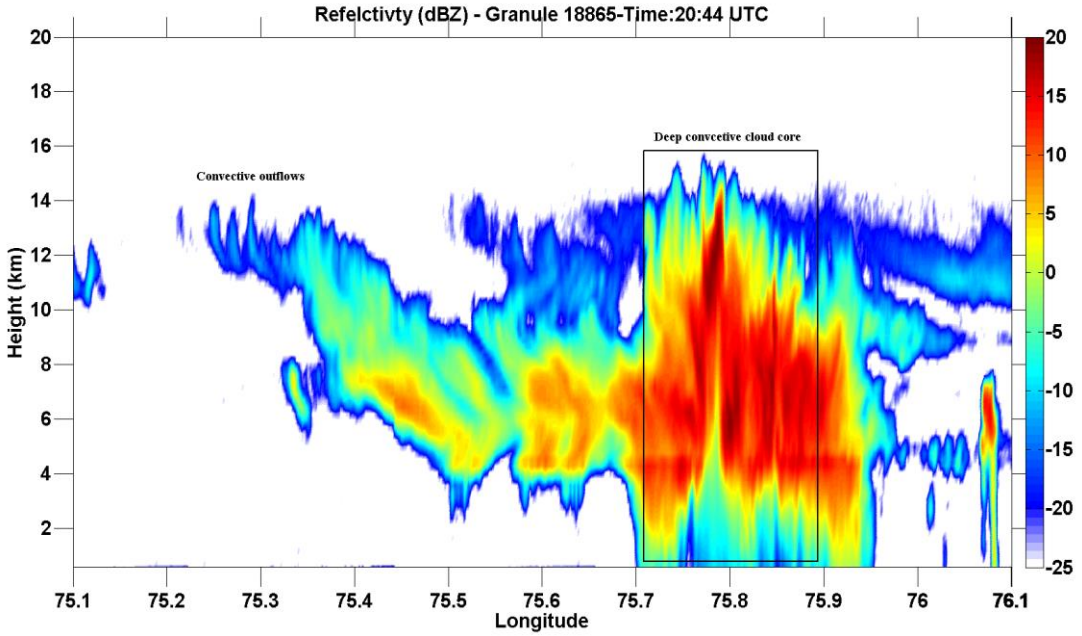

Figure 2.8: Vertical structure of deep convective cloud as observed by CloudSat CPR.

Table 2.1 CloudSat specifications

S.No.	Parameter	Value
1	Nominal Frequency	94 GHz
2	Pulse Width	3.3 μs
3	PRF	4300 Hz
4	Minimum detectable signal	-30 dBZ
5	Data window	Up to 25 km
6	Antenna size	1.85 meter
7	Dynamic Range	70 dB
8	Integration time	0.16 seconds
9	Nadir angle	0.16 degree
10	Vertical resolution	480 m (oversampled to 240 m)
11	Cross-track resolution	1.4 km
12	Along –track resolution	1.7 km

2.4 Scattering of microwave radiation

The main operating principle of CPR is scattering of microwave radiation by molecules and cloud particles. When an electromagnetic radiation interacts with the particles, the part of the energy is absorbed, scattered and re-emitted. For a monochromatic radiation attenuation for absorption and scattering is represented by the equation

$$dI_\lambda = -I_\lambda \sigma_\lambda ds$$

Where I_λ is monochromatic radiance at wavelength λ

σ_λ is the volume extinction coefficient due to scattering and absorption in m^{-1}

ds is a path length through the medium (air).

By integrating above equation from height h_0 to h, we get

$$I_\lambda = I_\lambda \exp(\int_{h0}^{h} \sigma_\lambda (h')dh')$$

Above equation cane be formulated as

$$I_\lambda = I_{\lambda 0} T$$

Where T is the transmission of radiation that passes through the slab of the atmosphere

$$T = \exp(\int_{h0}^{h} \sigma_\lambda (h')dh')$$

The complex refractive index of spherical particle of homogeneous composition is m=n ± ik. The scattering efficiency of ideal spherical particles can be expressed as a function of size parameter x:

$$x = \frac{2\pi r}{\lambda}$$

Where r is the radius of the particle, and λ is the wavelength of the incoming monochromatic plane wave.

Figure 2.9 shows the scattering efficiency of a spherical particle as a function of size parameter for various indices of refraction. From this figure, it is evident that

for smaller values of x (for $x \leq 1$), the scattering efficiency is very low and is inversely proportional to the fourth power of wavelength and is called as Rayleigh scattering regime. For $0.1 \leq x \leq 50$, the scattering efficiency exhibits an oscillatory behaviour and is referred to as Mie scattering regime. While for the values of $x \geq 50$, the scattering efficiency approaches to 2 and is called as geometric optics regime. The parameter x can give us an idea of how strongly CPR radiation interacts and scattered from various particles of the atmosphere. The CPR operating wavelength (3.2 mm) is weakly scattered by molecules and aerosols in the Rayleigh regime with more strong scattering from the particles whose diameter is larger than 50 micrometre such as cloud droplet, rain drops, hail and large ice particles (Figure 2.10).

2.5 Cloud Radar measuring principle and sampling characteristics

The CPR on-board CloudSat is similar to ground based cloud radar but provides the rich information about spatial distribution of vertical structure of cloud systems. The CPR measures the backscattered power, that is radiated by the clouds as a function of distance from the spacecraft i.e., CloudSat. The received backscattered signal from the CloudSat CPR is found from the radar equation

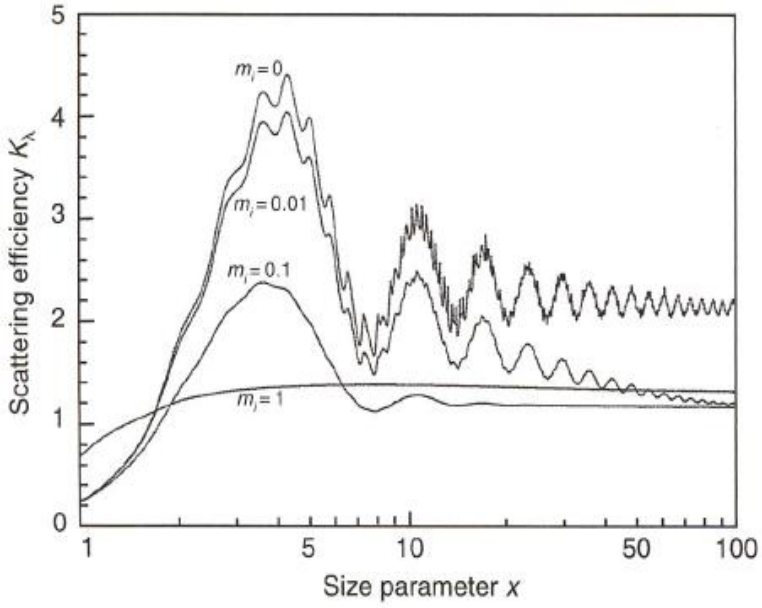

Figure 2.9: Scattering efficiency as a function of the size parameter x for four different indices of refraction with m=0, 0.01, 0.1 and 1[Adapted from *Wallace and Hobbs* (2006)].

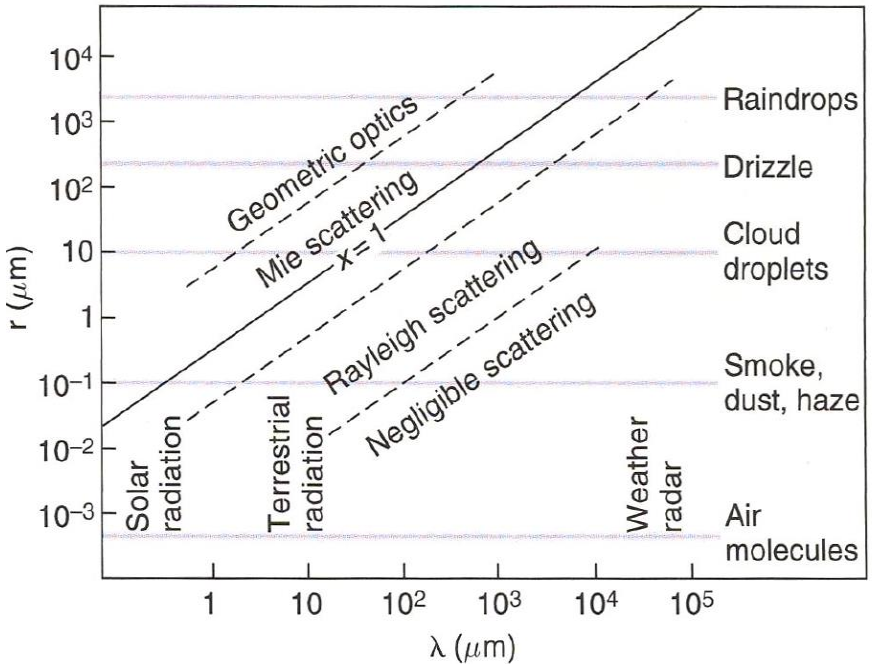

Figure 2.10: Size parameter x as a function of wavelength of the incident radiation and particle radius r [Adapted from *Wallace and Hobbs* (2006)].

$$P_r = \frac{P_t.\lambda^2.G^2.\Delta.\Omega.\eta}{4\pi^3.r^2}$$

Where P_r is the received power at the antenna

Δ is the range resolution,

Ω is the integral of the normalized two-way antenna pattern

η is the backscatter cross section per unit volume (reflectivity)

$$\eta = \frac{P_r.C.r^2}{P_t}$$

Where $C=4\pi^3/[\lambda^2.G^2.\Delta]$ is the radar constant

$$Z = \frac{\lambda^4.\eta.1018}{\pi^5.|K|^2}$$

Where Z is the reflectivity in $mm^6.m^{-3}$

K is the dielectric constant ~0.75 for 94 GHz

Z is converted to dBZ by taking 10 times the base 10 logarithm

The CloudSat radar samples at 625 kHz. At this frequency, the burst rate is 0.16 sec/bursts and the CloudSat PRF is 4300 Hz. From this we can compute the number of pulses per burst is 4300 pulses/sec x 0.16 sec/burst=688 pulses/bursts. The pulses are averaged to produce a single reflectivity value for each profile. The CloudSat antenna produces an instantaneous footprint of approximately 1.3 km (at mean se level). The velocity along track is ~ 7km/sec. Using this velocity and the sample rate of 0.16 sec/profile, one can compute approximately the time taken for generating a CPR profile at every 1.1 km along track. Each profile has 125 vertical bins. Each bin is 240 m thick. The CloudSat data Granule is defined as one orbit. The time stamp that is assigned to the granule is the time that corresponds to the centre of profile. Data window is 30 km height by 37,088 profiles wide and there are ~ 36,383 profiles per granule.

2.6 CloudSat Significant Echo Mask (SEM) algorithm

The CPR records range resolved profiles of backscattered power form hydrometeors. These measurements as enclosed in the level 1B input data denotes a 0.16 seconds average returned power that correspond nominally to a horizontal resolution of 1.7 km along track by 1.3 across track. The range resolution is 0.48 km and it is oversampled to generate a range gate spacing of 0.24 km. The main purpose of the Significant Echo Mack (SEM) algorithm is to identify the hydrometeors echo, who's returned power is significantly different from noise and to establish the probability that such echoes contains the hydrometeor information only in the GeoProf algorithm. The goal of SEM algorithm is to increase the identification of hydrometer echoes while minimizing the occurrence of false detections in the CloudSat CPR. Since the minimum reflectivity detection is -28 dBZ and some hydrometeors may have the backscatter signal below the detection of threshold of the CPR. The level 1B data contains the power return $P_{r,ij}$ in each resolution volume, where i defines the along the track dimension and j is the vertical dimension. The measured backscattered power is composed of a sum of power return from the atmosphere

($P_{n,ij}$) and the system noise power ($P_{n,ij}$) assumed to be due primarily to the mixer noise. Initial criteria for a significant return is

$$P_{r,ij} > P_{n,ij} + (3\sigma_n)$$

Where σ_n is the standard deviation of $P_{n,ij}$ estimates by examining P_n in nearby regions above the tropopause, where no atmospheric return will be measured in the reported value $P_{r,ij}$**.** While there will be very few occurrences where the noise will be identified as significant echo and hydrometeors returns where the noise power is less than the 3-singma level as given below.

$$P_{n,ij} < P_{n,ij} + (3\sigma_n)$$

The Gaussian probability that the pixel is noise can be expressed as

$$P_z = \frac{1}{\sigma n\sqrt{2\pi}} \exp\left(\frac{-1}{2\sigma n^2} \left(P_r - \bar{P}_{n,ij} \right)^2 \right)$$

Where P_r is the mean signal in the data window and the effective value of P (P_{eff}) for that volume is taken as

$$P_{eff} = \sum_i \log(P_i)$$

In summary, if the received power of CPR is greater than the sum of noise power and 3σ**,** the echo is considered as a hydrometeor.

2.7 Limitations of CloudSat observations

The main limitations of the CloudSat CPR and CALIPSO are listed below:

1. The CloudSat CPR is primarily insensitive to hydrometeor echoes near to the surface i.e., up to 1 km above the surface due to ground clutter [Marchand et al., 2008].
2. The horizontal resolution of CPR is ~ 1.7 km along track and 1.3 across track and its vertical resolution is 0.24 km. It means that the small scale cloud with the spatial and vertical dimensions are cannot be resolved by CPR.
3. The minimum detectable reflectivity is ~-28 dBZ, which corresponds to non-precipitating cloud system. For the clouds whose reflectivity below this threshold cannot detected by CPR.

2.8 CloudSat Data Structure

The CloudSat data format is the HDF (Hierarchical Data Format version) – EOS (Earth Observing System) 2. HDF-EOS2 is the extension of HDF4 and it is the primary format for storage and distribution of scientific and other ancillary data for user community. The data format is self-explanatory and independent of binary format in a single file. The objects in HDF-EOS2 file includes multi-dimensional array and defines the three new data types based on regular structure of HDF4. It mainly containing the following three data types 1) Swath, it is a time series of scan lines along and across the satellite track as shown in figure 2.11) Grid, it is the geolocated data on rectilinear grid and 3) Point is the sparsely geolocated data. Further fields in the HDF-EOS2 are separated into Geolocation Fields and Data filed groups. According HDF-EOVs metadata, the fields, dimensions and their relation between geolocation and data files are described.

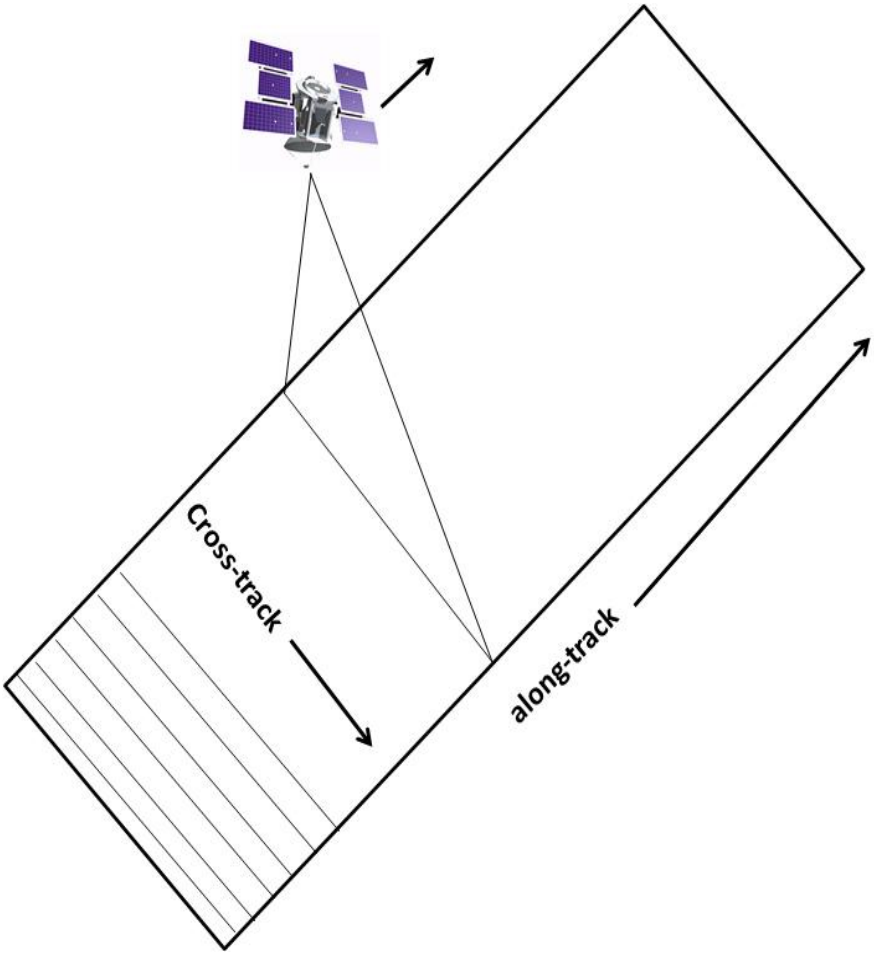

Figure 2.11: CloudSat-CPR swath.

2.9 CloudSat Data Products

There are two types of CloudSat data products; Standard data products and Auxiliary data products. Auxiliary data products are produced from ancillary data that are mapped in the horizontal to the centre of the CloudSat profile footprint and vertical to the centre of each CloudSat profile bin. The CloudSat data products used in the present thesis are (1) 2B-CLDCLASS product for cloud classification developed by *Sassen and Wang*, 2008. (2) 2B-GEOPROOF-LIDAR product for detecting the multi-layered clouds by combing the CALIPSO-lidar observations developed by *Mace et al.*, 2007.

2.9.1 2B- CLDCLASS Product

Wang and Sassen [2001] developed an algorithm to classify clouds by combining the measurements of ground-based multiple remote sensors. *Sassen and Wang* [2008] described the cloud cluster analysis for classifying clouds by using vertical and horizontal cloud properties, the presence or absence of precipitation from both CloudSat and MODIS observations along with temperature profiles from ECMWF reanalyses data. The first step in the cloud cluster analysis involves conversion of the vertical profiles of reflectivity derived from CloudSat observations into meaningful microphysical quantities and then identification of the clouds based on cloud mask algorithm is performed. The cloud clustering analysis provides cloud horizontal and vertical extent features along with cloud layer structures, which are determined by using CloudSat bins with significant CPR cloud mask values (≥30). The cloud cluster algorithm considers only the significant CPR cloud mask values 30 and above, which is provided by cloud mask algorithm. Further, classification of the cloud type is done based on microphysical properties, maximum reflectivity and corresponding temperature at that level, cloud vertical and horizontal extent and the precipitating properties. Complete details on the cloud classification algorithm can be found in 2B-CLDCLASS product description document at http://www.cloudsat.cira.colostate.edu/dataHome.php. The 2B-CLDCLASS data product provides the cloud information as a function of latitude, longitude and altitude with the same resolution that of CPR observations. The main advantage

of CloudSat is that it provides the vertical structure of hydrometeors over the foot-print of CPR along its path. However, CPR is not sensitive to optically thin clouds such as high-altitude thin cirrus clouds. The limitations of 2B-CLDCLASS product are (1) surface contaminations in the lower 3 to 4 range bins of CPR vertical reflectivity profiles, which will have implications in classifying St and Sc clouds and (2) the CPR is not sensitive to high altitude thin clouds, which will have implications in detecting the Ci clouds [*Marchand et al*., 2008; *Behrangi et al*., 2012; *Subrahmanyam and Kumar*, 2013]. Both these limitations will result in fewer detection of St, Sc and Ci clouds than actually present. One should keep these limitations in view while interpreting the observations. Despite these limitations, cloud type classification are derived using the CPR reflectivities along with auxiliary data from ECMWF reanalysis fields along its path, which is very useful for assessing the role of clouds in energetics and dynamics of the atmosphere as a function of cloud type. This product is not validated with any other observational measurements and we have found that there is a preliminary comparison study using CloudSat Educational Network (CEN)-collected observations of cloud type during the period from 2007-2008. The comparison of the observed cloud types and those retrieved using the CloudSat 2B-CLDCLASS product was carried out. There were 227 coincidental measurements between CEN schools and CloudSat overpasses within ~ 100 km radius and results have shown that approximately 66% agreement between the surface observers and CloudSat observations (*Rogers and Vane*, 2010). The maximum number of cloud types provided by this product is eight and they are Cirrus (Ci), Altostratus (As), Altocumulus (Ac), Stratus (St), Stratocumulus (Sc), Cumulus (Cu), NimboStratus (Ns) and Deep Convective (DC) clouds (i.e., Cumulonimbus). Out of eight clouds Ns, St, Sc, Cu, Ac and Dc are categorized as precipitating clouds and remaining clouds are non-precipitating clouds. Further these clouds are classified into high-, middle- and low-level clouds. The CloudSat cloud type algorithm follows the different threshold conditions for various cloud type identification, which are listed in Table 2.2.

Table 2.2 CloudSat cloud type algorithm.

Type	**Z_{max}**	**Precip itation**	**Length (km)**	**Highest Z_{max} frequency**	**Other**
Cirrus	<-3dBZ T<-22.5^{0}C	No	2→>1000	-25dBZ@ -40^{0}C	
Altostratus	<10dBZ -20^0<T<-5^{0}C =-30dBZ@ -45^{0}C	No	50→>1000	-10dBZ@ -25^{0}C	
Altocumulus	<0dBZ -20^0<T<-5^{0}C =-30dBZ@ -35^{0}C	No	2→>1000	-25dBZ@ -10^{0}C	T_{top}> -35^{0}C
Stratus Stratocumulus	<-5dBZ -15^0<T<25^{0}C	Yes/No	2→>1000 50→>1000	-25dBZ@ 10^{0}C (Bright band)	Altitude of Zmax<2 km AGL
Cumulus	<0dBZ -5^0<T<25^{0}C	Yes/No	2-25	-25dBZ@ 15^{0}C	ΔZ>2km
Deep (cb)	>-5dBZ -20^0<T<25^{0}C	Yes	10-50	10dBZ@ 5^{0}C	ΔZ>6km
Ns	-10<Z<15dBZ -25^0<T<10^{0}C	Yes	>100	+5dBZ@ 0^{0}C	ΔZ>4km

2.9.2 2B- GEOPROF-LIDAR Product

The 2B-GEOPROF-LIDAR product contains the combined cloud mask information derived from CPR and CALIPSO, which indicates the confidence level in detection of clouds, ranging from 0 to 40. A cloud mask of 30-40 indicates the high-confidence detections and less false detections (i.e., less than 2% for 30 and less than 0.2 % for values of 40). This algorithm developed by combining the CPR and lidar observations and to provide the geometrical hydrometeor or vertical profile. It further identifies the layer base and layer top of hydrometeor in each vertical profiles of CPR. The CPR is able to penetrate optically thick clouds, where lidar signals attenuates. On the other hand, the lidar can detect the tenuous hydrometeor layer which falls below the CPR detection threshold. Thus by combining the radar and lidar observations can provide complimentary information about the occurrence of hydrometeor layers and their vertical structure. This product's algorithm is designed to extract the maximum information about the multi-layered cloud structures. Since the two sensors have

different spatial and vertical resolutions, GEOPROFF-LIDAR algorithm adopts the spatial and vertical resolution of CPR. Figure 2.12 depicts the view of CPR footprints (blue colour) with coincident lidar footprints (red colour). The solid circle around the lidar and radar footprints represents the 1 and 2 sigma of standard deviation of pointing measurements. The left panel shows the vertical slice of CPR. Red colour boxes represent the CALIPSO cloud mask features which correspond to below 8.2 km. Above 8.2 km; the lidar foot print will be 1x0.333x0.075 km along track, across track and vertical, respectively. This product provides maximum up to five layers of hydrometeor information from the combined observations of radar and lidar sensors.

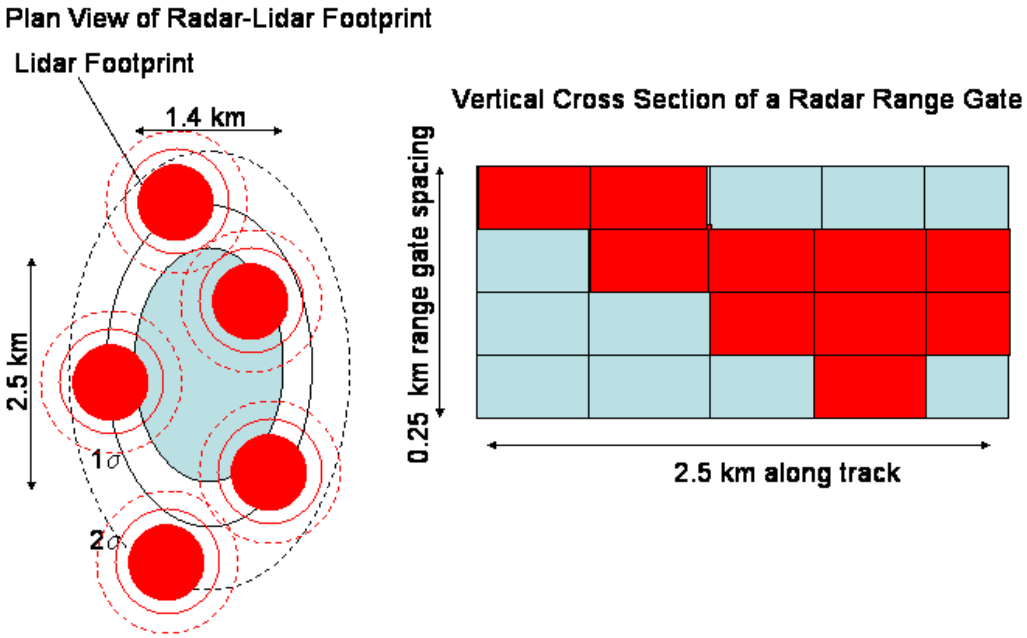

Figure 2.12: Conceptual view of CPR-lidar overlap [Figure courtesy: 2B-GEOPROOF-LIDAR product document].

More details on CloudSat products can be found in the CloudSat Data Products Handbook (http://www.cloudsat.cira.colostate.edu). Overall, the geoproof-lidar algorithm performs fairly well but there some data quality issues, which are listed below. The most mis-classification is the labelling of aerosol layer as a cloud layer by CALIPSO profile. Thus a small portion of aerosol layer can be misidentified as a cloud layer. Apart from that, portions of some base of cirrus

cloud also mislabelled as aerosol layers and some tropospheric polar cloud are erroneously labelled as aerosol layers in CALIPSO observations. There are few issues in In the CPR observation also, which are to be kept in mind while analysing the data (*Mace et al*., 2007, *Marchand et al*., 2008).

As mentioned earlier, the minimum detectable signal of CPR is about -30 dBZ. Therefore, some fraction of non-precipitating liquid water clouds such as altocumulus and stratus cloud over the continents cannot be detected by CPR, which are beyond detection limit of CPR. Another possibility is the reflection from the ground surface. The first few range bins in the CPR measurements are contaminated by ground clutter. Below 500 meters, CPR contains no hydrometeor information and between ~ 500 meter and 1 km, it can identify the hydrometeor layer with reduced ground clutter. For any research analysis, it is advised to consider CPR signals above 1km altitude, which is free from the surface reflections, particularly over the ground. With these limitations this product provides valuable information on the distribution of multi layered clouds. Additional information on this product can be found at http://www.cloudsat.cira.colostate.edu/dataHome.php

2.10 TRMM Spectral Latent Heating (SLH) data

Tropical rainfall Measuring Mission (TRMM) was the first space rain gauge launched in 1997 sweeping the latitudes between 38^0S and 38^0N and was located above the Earth's surface at an altitude of 402.5 km with an inclination of 35 degree to earth's equatorial plane. There are several payloads onboard TRMM such are, Precipitation Radar (PR), TRMM Microwave Imager (TMI), Visible and Infrared Scanner (VIRS), Clouds and Earth's Radiant Energy Sensor (CERES) and Lighting Imaging Sensor (LIS). The swath width of TRMM-PR is 215 km and a horizontal footprint of 4.3 km at nadir. The prime objective of TRMM is to study the variability in tropical precipitation in both space and time. In fact, understanding the nature of variability in precipitation has been increased tremendously with TRMM measurements. Another prime objective of this mission is to study the vertical structure of latent heating released in the earth's

atmosphere. Previous studies estimated the latent heating using satellite based measurements mainly using passive microwave radiometer observations [e.g, *Adler and Rodgers*, 1977]. They estimated the total column latent heating within the tropical cyclone. Latent Heating (LH) is the energy associated with the phase changes of water molecule in the atmosphere. Energy is released in the atmosphere during the process of condensation, freezing and deposition, while it is absorbed during evaporation, melting and sublimation. The LH release is dominent during the condensation process, which is ~ 7 times larger as compared to freezing. The process associated with phase transition of water molecule cannot be directly detectable with the present remote sensing instruments. That is the reason why the satellite retrievals are heavily depends on the cloud resoling models (CRM).

LH estimations used in this study is derived from TRMM based retrievals along with Goddard Cumulus Ensemble (GCE) - Cloud Resolving Model (CRM) simulations (e.g., *Tao et al*., 2006; 2016). TRMM measurements provided the rain rate estimates over the tropics since 1997 and are the main basis for the estimation of LH data products. The main basis for the estimating LH is the relationships between latent heating and the vertical distribution of hydrometeors, surface rainfall characteristics and the dynamics among the cloud layers. There are few algorithms such as Convective Stratiform Heating [CSH- *Tao et al*., 1993], Goddard Profiling [GPROF-*Olson et al*., 1999, 2006] heating, Hydrometeor Heating [HH- *Yang and Smith*, 1999; *Yang et al*., 2006], Precipitation Radar Heating [PRH- *Satoh and Noda*, 2001] and Spectral Latent Heating **[**SLH- *Shige et al*., 2004, 2007] algorithms for retrieving the latent heating from TRMM observations. These algorithms are briefly discussed here.

2.10.1 CSH algorithm

The CSH algorithm utilizes the TRMM's precipitation radar measured surface precipitation rates, the percentage of its stratiform and convective precipitation, and the location of the observed cloud system. It mainly uses the pre-estimated information on the relationship between the rain arte characteristics and latent

heating generated from CRM look up tables. The CSH algorithm applied on life time of precipitating cloud systems ranging from 3 hours to 1 month and its spatial scales ranging from 50 to 500 km. This algorithm has been used extensively for comparison with various filed campaigns such as GATE, TOGA-COARE, SCSMEX, TRMM-LBA and KWAJEX programs [*Tao et al*., 1993].

2.10.2 GPROF Heating algorithm

The Goddard Profiling (GPROF) Heating algorithm developed especially for the applications of TRMM-TMI passive microwave radiometer radiance measurements. A large range of hydrometeors and their heating profiles were generated by GCE-CRM along with passive microwave radiometer radiances values. Thus a look up table is generated for a range of TMI-radiances for estimating latent heating. *Yang et al*. (2004) verified the vertical structure of latent heating using this algorithm with other independent estimates from Kwajalein dual-Doppler radar data and SCSMEX rawinsonde analyses and found that GPROF heating rates were fairly consistent with other estimates [*Olson et al*., 1999, 2006].

2.10.3 HH algorithm

Estimation of LH is also possible without prior information of LH look up tables by treating each layer of the atmosphere independlty. The HH algorithm follows the same. Firstly, the net flux of water is estimated in or out of the layer under steady state conditions. Then these fluxes of water are compared with the mean value over a given location. Primarily, a decrease in flux of water is associated with evaporation, melting and sublimation, while the increase is associated with condensation, freezing and deposition. Thus the basis for the HH algorithm is the hydrometeor mass flux [*Yang and Smith*, 1999].

2.10.4 PRH algorithm

The PRH algorithm uses rain rate profiles and fraction of convective and startiform to estimate the vertical structure of LH. Firstly, an initial guess of

vertical velocity profile is estimated based upon the vertical rain rate structure. The vertical velocity information used to estimate the LH profile under steady state condition, similar to HH algorithm. An iterative method is applied to correct the original vertical motion profile to ensure that vertically integrated net heating and surface rain rates are consistent [*Satoh and Noda*, 2001].

2.10.5 SLH algorithm

SLH algorithm, similar to CSH, employes a set of three look up tables for estimation of LH generated using CRM model data. These are associated with three types of rainfall characteristics such as convective, stratiform and anvil part of deep convective system. The look up tables is separated with respect to the vertical precipitation profiles. Along with the look up tables, the precipitation top height (PTH) for convective and stratiform part and melting level also used in this algorithm. The naming 'spectral' comes from this spectrally indexed table, and it is designed so in order to reduce the dependency of tables on the CRM simulations of specific field campaigns. The main advantage of this algorithm is the fundamental differences between shallow convective rain and deep convective rain classification based on the PTH information. Further it also generates the vertical structure of LH associated with anvil region of decaying deep convective precipitation [*Shige et al.*, 2004, 2007].

2.10.6 Errors associated with LH data sets

Since all the five algorithms utilizes the CRM generated look up tables and are subjected to systematic errors associated with model deficiencies. Also CRM look up tables are generated for given set of environmental conditions based on the field campaigns. These tables may not completely represent the total spectrum of real atmospheric conditions. The algorithm such as CSH, GPROF and SLH are estimated mainly using CRM information and model simulations are considered only a limited range of atmospheric conditions. Previous modelling studies suggest that instantaneous LH profiles derived from TRMM are somewhat ambiguous. It advised to take space-time averages of LH estimates over s specific

region in order to minimise the random errors associated with estimation of LH structure. *Shige et al*. [2004] found that the spatial average of LH estimates reduces the random errors in SLH data reasonably.

In the present study, 16 years of (1998 to 2013) Spectral Latent Heating (SLH) data (SLH-L3-V2) are used to investigative the vertical structure of latent heating and its association with various types of clouds. This dataset has a spatial resolution of 0.5 x 0.5 degree. It provides the LH information over the region between 37 degree south to 37 degree north. The units of latent heat conditional means are K/hour multiplied with 100. Time-mean spatial distribution and zonally averaged latitudinal height distribution of latent heating is estimated over the ISM region for the present study. Further, the latent heating associated with precipitating cloud types are studied over the regions of, Arabian Sea, Western Ghats, Bay of Bengal and Central India where Sc, Cu and deep convective clouds are predominantly formed.

2.11 Reanalysis data

Reanalysis is a systematic approach to produce three-dimensional meteorological fields by using a modern data assimilation scheme to reprocess the past observations. Reanalyses are blended with data assimilation schemes which ingest all the available atmospheric observations at every 6-12 hours being analysed. This rigid scheme provides a dynamically consistent assessment of the state of the atmosphere at each time step. Reanalysis uses the widest variety of observations for data assimilation which includes the measurements from a single station to global coverage of satellite observations. It is performed with a single data assimilation scheme, which ensures that the reanalysed data fields are not affected by the up gradation of model, changes in spatial and vertical resolution or any other modifications introduced in the operational forecasting system. This robust approach produces detailed description of the state of the atmosphere consisting of gridded fields of pressure, temperature, winds, humidity and ozone as well as other forecast parameters such as rainfall, cloud fraction, etc. Several reanalysis datasets are available to the user community such

as ECMWF Reanalysis (ERA), NCEP (National Centre for Environmental Prediction) reanalysis, MERRA (Modern-Era Retrospective analysis for Research and Applications) and Japanese Reanalysis (JRA55). All of these datasets, generally, yield consistent results. In the present thesis, ERA-Interim reanalysis used to study the background atmospheric conditions. ERA-Interim is one of the recent reanalysis datasets on global scales produced by European Centre for Medium-Range Weather Forecasts (ECMWF). It provides the reanalysed atmospheric fields on temporal and spatial scales starting from the 1 January 1979 onwards [*Dee et al*., 2011]. It assimilates the atmospheric fields with 12 hourly cycles in a forward mode. In each cycle, all the available observations from satellite and ground based measurements are merged with prior information from model to predict the state of the atmosphere on global scales. Then these are used to initialise the model for next run [*Dee et al.*, 2011]. The gridded ERA-Interim data set provides the 3-hourly temporal resolution for various surface parameters and 6-hourly interval for three dimensional atmospheric fields covering from troposphere to stratosphere [*Dee et al.*, 2011]. The ERA-Interim reanalysis data during 2006-2013 are used to study the background dynamics in the present thesis.

Chapter 3

The role of dynamics in three dimensional distribution of cloud types during the Indian summer monsoon

"I am the daughter of Earth and Water,
And the nursling of the Sky;
I pass through the pores of the ocean and shores;
I change, but I cannot die.
For after the rain when with never a stain,
And out of the caverns of rain,
Like a child from the womb, like a ghost from the tomb,
I arise and unbuild it again."
- P. B. Shelley

3.1 Introduction

Owing to its socioeconomic impacts, the ISM is one of the most investigated topics in the realms of meteorology. Many studies on the ISM by several researchers across the globe contributed constructively to the present understanding of this enigmatic large-scale system [*Webster et al*., 1998; *Gadgil,* 2003]. Generally, it is believed that the continental-scale land–sea thermal contrast is the origin of largescale monsoon circulation [*Wallace and Hobbs*, 1977]. However, once the monsoon is set, its advancement, maintenance and withdrawal depends not only on the largescale dynamics but also on the internal dynamics initiated by the cloud systems embedded within the monsoon system. These cloud systems over the ISM region

modify the thermal structure and moisture budget of the troposphere by releasing latent heat, modifying the radiative heat, and through precipitation. Thus the clouds are an important integral part of the monsoon system, and any attempt to understand the latter should include the detailed investigations on the former. Realizing its importance, many attempts were made in the past to study the cloud distribution over the ISM region [*Grossman and Garcia*, 1990; *Laing and Fritch*, 1993]. Most of these studies used passive remote sensing techniques and are thus limited to fraction of cloud cover over the ISM region. However, *Wonsick et al*. [2009] focused on detailed study on cloud variability over the monsoon region in terms of total, low, high and convective cloud amounts throughout the different phases of the monsoon. Very recently, *Li et al*. [2011] accessed the radiative impacts of single- and multi-layered clouds using A-Train observations. These results indicated that the multi-layer clouds have a significant impact on radiation budget and differ with that of single-layered clouds. Thus it is important to know not only the amount of cloud cover but also its vertical distribution. For example, high level clouds tend to warm the climate, while low-level clouds lead to a cooling effect [*Ramananthan et al*., 1989]. Recently, *Tang and Chen* [2006], using the MODIS/Terra measured cloud properties dataset, investigated the characteristics of clouds associated with the Asian summer monsoon. These authors emphasized the distribution of low-, mid- and high-level clouds and found that a large amount of high clouds exist in the Indian monsoon region. Thus it becomes important to know the three-dimensional distribution of the clouds.

Apart from the total cloud amount and its vertical distribution, one more important aspect of clouds is the cloud type. It is known that depending upon the cloud type, the radiative properties, the latent heat released and microphysical properties of clouds largely differ. *Chen et al.* [2000a] investigated the radiative flux changes induced by the occurrence of different cloud types using International Satellite Cloud Climatology Project cloud data and a radiative transfer model. These authors emphatically showed that the cloud-type variations are as important as cloud cover

in modifying the radiation field of the earth–atmosphere system and further showed that the largest annual mean changes of the global top-of-atmosphere and surface shortwave radiative fluxes are produced by stratocumulus, altostratus, and cirrostratus clouds; whereas cirrus, cirrostratus, and deep convective clouds cause most of the annual mean changes in the global top-of atmosphere longwave radiative fluxes. Thus it becomes clear that, apart from the three-dimensional distribution of cloud cover, it is important to have cloud type distribution to quantify the feedback provided by the clouds in totality. Even though there are studies on cloud distribution over the ISM region, there are no studies focusing on cloud type distribution. Sufficient knowledge of the spatial distribution of individual cloud types would aid the accurate radiation and latent heat calculations, which in turn would help in accessing the role of clouds in the maintenance and advancement of the ISM. So it becomes important to know which types of clouds occur over which region. In this regard, a study is carried out using five years [2006–2010] of CloudSat observations during June-July-August-September [JJAS] months to establish the three-dimensional distribution of individual cloud types over the ISM region for the first time.

3.2 Data and methodology

Five years of CloudSat observations during June-July-August-September months over the ISM region form the basis for the present study. The cloud profiling radar [CPR] onboard CloudSat operates at 94 GHz with cross- and alongtrack resolution of 1.4 and 1.7 km respectively, which is a part of the A-Train constellation. With ~240m vertical resolution, CPR can probe optically thick large-particle layers. However, CPR is not sensitive to optically thin clouds such as high-altitude cirrus clouds. More details on CloudSat can be found in chapter 2. For the present study, 2B-CLDCLASS data product of version 5 was used over the ISM region [10^0 S to 30^0 N, 50^0 to 100^0 E]. In the following section, briefly discuss the cloud classification algorithm, which was implemented in deriving the 2BCLDCLASS product.

Wang and Sassen [2001] developed an algorithm to classify clouds by combining the measurements of ground-based multiple remote sensors. Further, *Sassen and Wang* [2008] described the cloud cluster analysis for classifying clouds by using vertical and horizontal cloud properties, the presence or absence of precipitation from both CloudSat and MODIS observations along with ECMWF temperature profiles. The present data product uses this algorithm for cloud type classification. The cloud cluster analysis converts the vertical profiles of reflectivity from CloudSat into meaningful microphysical data quantities and identifies the clouds based on the cloud mask algorithm. The cloud clustering analysis provides cloud horizontal and vertical extent features and cloud layer structure with significant CPR cloud mask values [>=30]. Further, classification of the cloud type is done based on microphysical properties, maximum reflectivity and corresponding temperature at that level, cloud vertical and horizontal extent and the precipitating properties. Complete details on the cloud classification algorithm can be found in the 2B-CLDCLASS product description document at http: //www.cloudsat.cira.colostate.edu/dataHome.php. The maximum number of cloud types provided by this product is eight: cirrus [Ci], altostratus [As], altocumulus [Ac], stratus [St], stratocumulus [Sc], cumulus [Cu], nimbostratus [Ns] and deep convective [DC] clouds [i.e., cumulonimbus]. Out of the eight clouds, Ns, St, Sc, Cu, Ac and Dc are categorized as precipitating clouds, and remaining clouds are no precipitating clouds. Further these clouds are classified into high-, middle- and low-level clouds. This product is available as a function of latitude, longitude and altitude with the same resolution as that of CPR. There have been attempts in the recent past to validate this product. The CloudSat Educational Network [CEN], a primary education and public outreach component of the CloudSat mission, collected visual observations of cloud type during the period of 2007– 2008 and compared the observed cloud types to those retrieved using the CloudSat 2B-CLDCLASS product. There were 227 coincidental measurements of CEN and CloudSat within 100 km radius. The preliminary comparison has shown 66% agreement between the surface observers and CloudSat observations [Rogers and Vane, 2010]. Very recently,

Behrangi et al. [2012] used the 2B-CLDCLASS product to study the vertical and horizontal distributions of the cloud types across different seasons over the contiguous USA and surrounding areas. In this study, the authors describe the 2B-CLDCLASS product in detail including their limitations: [1] surface contaminations in the lower 3 to 4 range bins of CPR vertical reflectivity profiles will have implications in classifying St and Sc clouds, and [2] the CPR is not sensitive to high-altitude thin clouds, which will have implications in detecting the Ci clouds. Thus both these limitations will result in fewer detections of St, Sc and Ci clouds than actually present. One should keep these things in mind while interpreting the observations. The second limitation can be overcome by combining the CALIPSO observations. However, it will be done in near future. We have followed the following procedure to calculate the frequency of occurrence of each cloud type. [1] The observations over the study region are grouped into 2.5×2.5 grid boxes. [2] The number of occurrences of each cloud type as a function of altitude is estimated in each grid box. [3] The number of occurrences of each cloud type is then divided by the number of occurrences of all cloud types at each altitude. [4] The height profile of frequency of occurrence of each cloud type within each grid box is estimated. [5] From these height profiles, the altitude at which the maximum frequency of occurrence takes place is found for each cloud type for a given grid box. [6] The maximum frequency of occurrence at the altitude [provided by step [5] is then used to create the maps over the ISM region, which will be discussed in the next section. The height profiles of frequency of occurrence in each grid box provided the 3-D distribution of cloud types over the ISM region [*Subrahmanyam and Kumar,* 2013].

3.3 Spatial distribution of cloud types over the ISM region

By adopting the method described in Section 3.2, quantified the frequency of occurrence of various cloud types, and Figure 3.1 (a–h) show the five-year [2006–2010] mean distribution of frequency of occurrence of Ci, As, Ac, St, Sc, Cu, Ns and DC clouds over the ISM region during JJAS. Figure 3.1 contains both daytime and nighttime observations of CloudSat. It has to be remembered that we have estimated

the frequency of occurrence at each altitude bin and Figure 3.1 corresponds to the altitude where maximum frequency of occurrence of corresponding cloud is observed. As the altitude at which maximum frequency of occurrence takes place differs from one grid box to another, we have taken the mean of these altitudes over the study region, and the same is provided in Figure 3.1 as mean altitude. From Figure 3.1 (a) it is evident that the distribution of Ci is highly concentrated over south Bay of Bengal (BoB), Indian peninsula and Indian Ocean. During the ISM, the convective storms over most northern parts of BoB (known as the Head BoB) produce copious amounts of Ci clouds [formed from the anvil of deep convective clouds], which are spread over the ISM region by the strong Tropical Easterly Jet [TEJ] [*Sathiyamoorthy et al*., 2004]. The maximum percentage of occurrence of Ci cloud is ~30–35 %. As discussed in Section 3.2, the CloudSat underestimates the occurrence of Ci clouds as it is not sensitive to optically thin cirrus clouds. CloudSat observations over the ISM region are limited to two local times per day. If there are any diurnal variations in particular cloud occurrence, it may bias the frequency of occurrence estimations discussed here. However, an attempt is made to bring out the differences between the frequencies of occurrence of each cloud during day- and nighttime over the ISM region, which will be discussed later in this section. The Ci clouds are known for their role in radiative forcing, and thus their unambiguous spatial distribution assumes its importance. Figure 3.1 (b) shows the distribution of frequency of occurrence of As clouds, which seem to occur preferentially over BoB compared to over the Arabian Sea. Interestingly, occurrence frequency of As cloud is higher over oceans than over land in contrast to Ac cloud distribution shown in Figure 3.1 (c), which frequently occur over land. The frequency of occurrence of Ac is found to be high over Bangladesh, Tibetan Plateau region and uniformly distributed over the Indian landmass. The preferential occurrence of Ac over land is a relatively new observation and needs to be further investigated in terms of microphysical processes associated with Ac clouds. Frequency of occurrence of St and Ns clouds is shown in Figure 3.1 (e) and (g), respectively. From these maps it is evident that occurrence of these two clouds is very low compared to other cloud

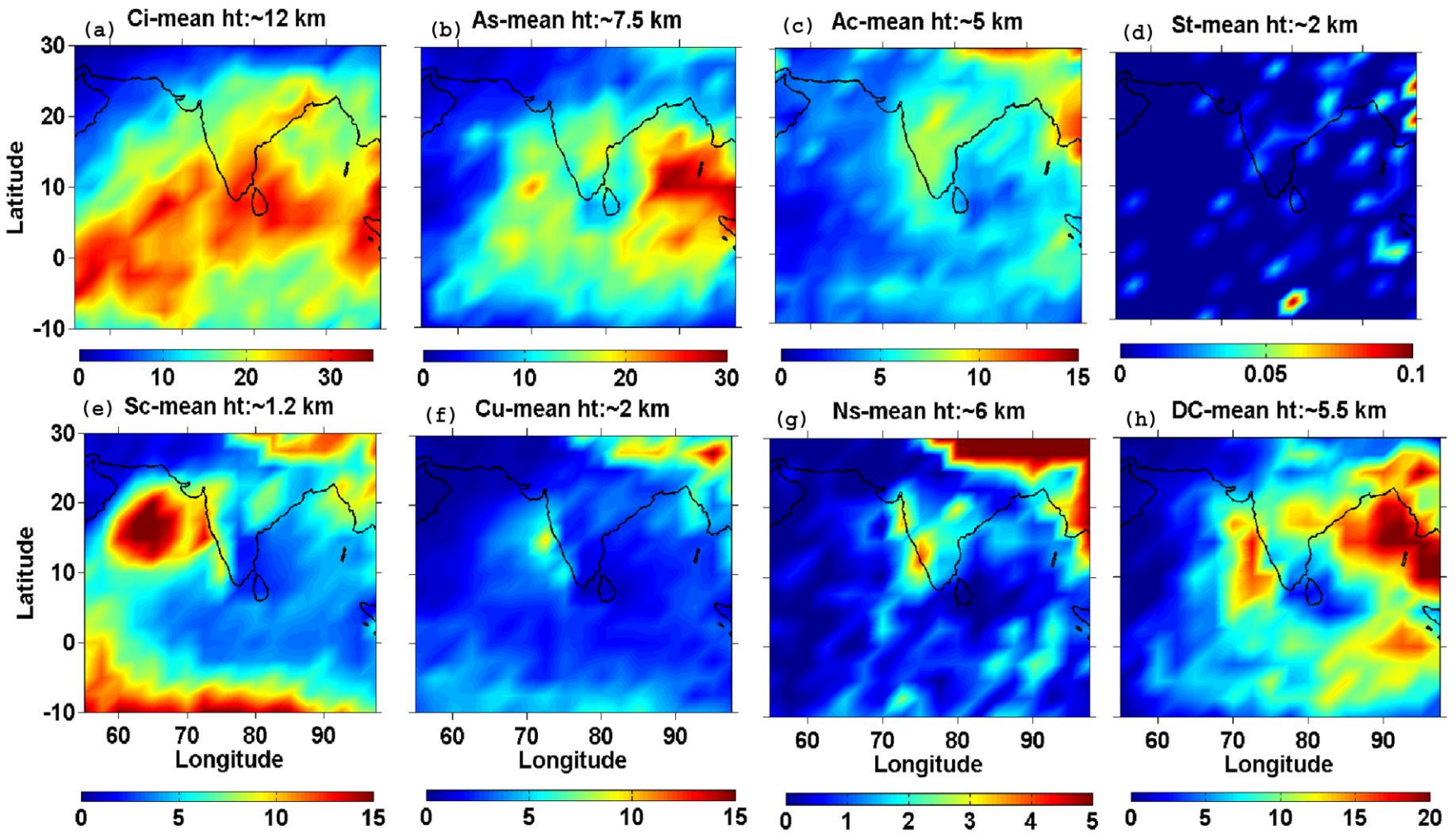

Figure 3.1: Five-year [2006–2010] mean distribution of frequency of occurrence during JJAS of (a) Ci, (b) As, (c) Ac, (d) St, (e) Sc, (f) Cu, (g) Ns and (h) DC clouds over the ISM region. The mean altitude provided at the top of the maps corresponds to the average of peak altitudes at which maximum frequency of occurrence is observed over the study region.

types over the study region. Especially the occurrence of St clouds is almost non-existent over the ISM region. This can be to some extent attributed to the surface contamination of CPR in the lower heights up to ~1 km. But, in the case of Ns cloud distribution, there is considerable amount of occurrences over the Tibetan Plateau region. Frequency of occurrence of Sc cloud is shown in Figure 3.1 (e), which readily reveals its maximum occurrence over the Arabian Sea region and also over equatorial Indian Ocean. It is interesting to note that the Sc clouds form scarcely over the BoB. The spatial distribution of Sc clouds is also very crucial as it plays an important role in shortwave radiative forcing resulting in cooling of the surface. The confinement of Sc clouds over the Arabian Sea can be attributed to the descending motion from monsoon convection apart from lower tropospheric thermal inversion that occurs during the ISM period over this region [*Sathiyamoorthy et al*., 2011]. The weak descending motions over the Arabian Sea during the ISM period can suppress the vertical development of clouds. The strong winds over the Arabian Sea during the ISM period can cool the sea surface by upwelling, which also can play a role in suppressing the convection. Besides these reasons, there is a strong mixing of dry air from Arabian Desert at around 650–500 hpa, which further dilutes the vertical development of the convection over the Arabian Sea [*Subrahmanyam and Kumar,* 2013]. Thus there are strong dynamical processes that prevail over the Arabian Sea, which results in limiting the convection growth and seems to be the prime reason for formation of Sc clouds as observed in the present study. These aspects will be further discussed later in this section.

Figure 3.1 (f) shows the frequency of occurrence of Cu clouds, which are relatively high over Tibetan Plateau region and the western coast of southern India. A secondary peak can also be observed in Cu occurrence over equatorial Indian Ocean. Other than these regions, Cu occurrence frequency is very low over the study region. The distribution of DC clouds, which are very important in both radiative and latent heat estimations as well as in precipitation over the ISM region, is shown in Figure 3.1h. Compared to other cloud types, the distribution of DC clouds has been well

documented over the ISM region [*Grossman and Garcia*, 1990; *Laing and Fritsch*, 1993; *Houze et al*., 2007]. From Figure 3.1 (h), it can be noted that the DC clouds are highly concentrated in the northeast of BoB, a consistent feature reported by earlier studies [*Zuidema*, 2003]. A secondary peak in frequency of occurrence of DC can be noted over the western coast of India and central India. These DC clouds produce large amounts of precipitation, and good or bad monsoon mostly depends on the distribution and frequency of occurrence of these clouds. It is also known that the highest mean precipitation over the ISM region takes place over BoB, and thus the distribution of DC clouds becomes very important not only from a hydrological standpoint but also from a dynamical standpoint as large amounts of latent heat released in these system maintain the monsoon circulation [*Zuidema*, 2003]. The continental tropical convergence zone, which extends from the Indo-Gangetic Plain into the BoB, plays a key role in the development of DC clouds by pumping the sufficient moisture into the atmosphere over the north BoB. Thus Figure 3.1 (a–h) depicts the five-year mean distribution of various cloud types associated with the ISM, and it is observed that dynamics plays a vital role in this distribution [*Subrahmanyam and Kumar, 2013*]. As mentioned earlier, it is important to know what type of cloud forms over which region to assess the feedback provided by the clouds to the large-scale ISM. Figure 3.1 provides these details for the first time.

3.4 Diurnal variation of cloud type distributions

It is important to know the diurnal variation in occurrence of cloud types, if any, as CloudSat observations cover only two local times over the ISM region. These satellites cross the Equator at approximately 13:30 and 01:30 local times. Over the ISM region CloudSat observations are made at ~06:00–09:00UTC [local day] and 18:00–21:00UTC [local night]. The results depicted in Figure 3.1 correspond to the mean of all the observations regardless of day or night. As the observations from CloudSat are available during both day and night, an attempt is made to evaluate the difference between the day and night distribution of frequency of occurrence of various cloud types, and the same is shown in Figure 3.2. We have generated the

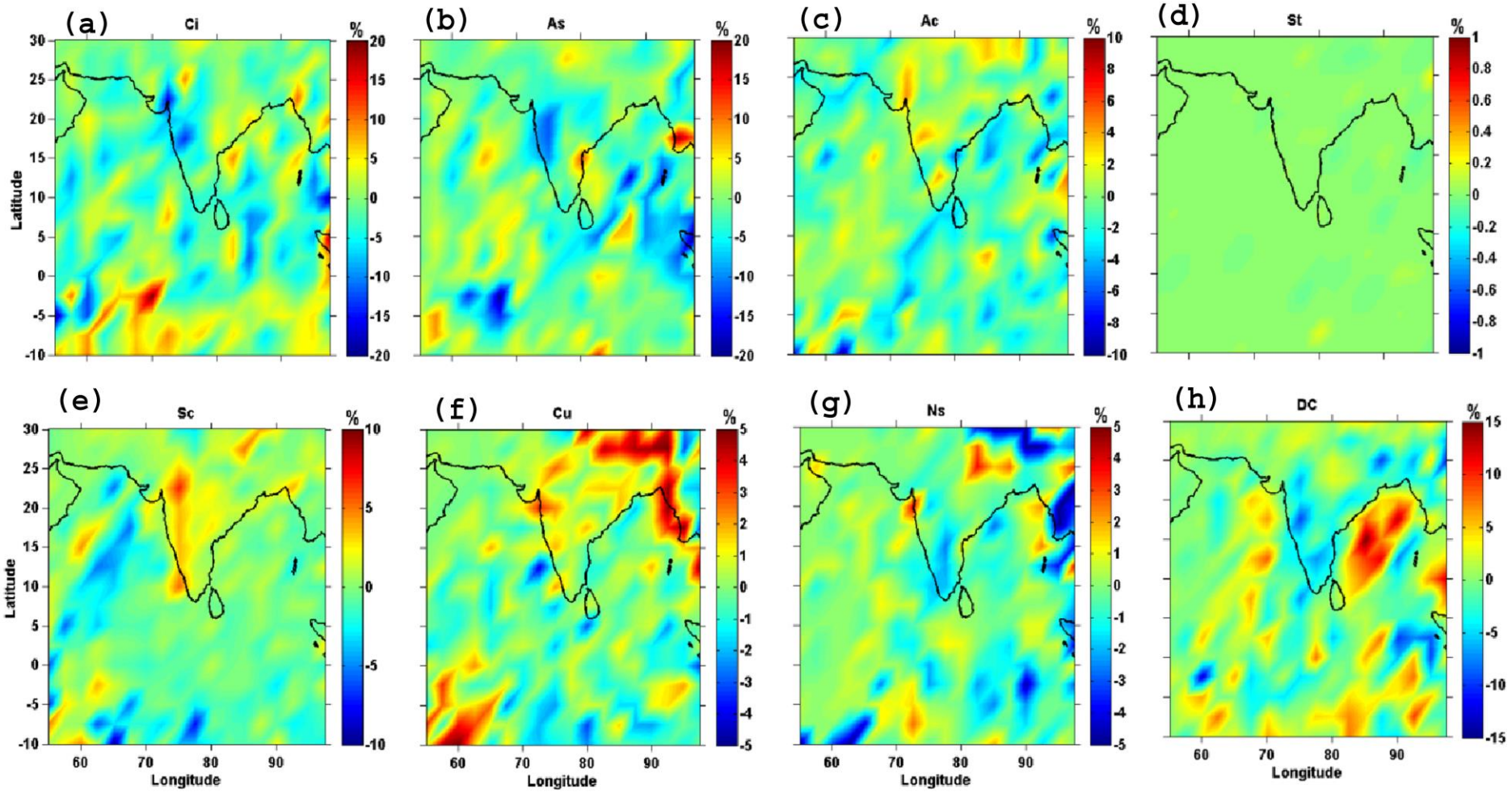

Figure 3.2: Same as figure 3.1 but for differences in frequency of occurrence during day- and night-time.

distribution maps similar to Figure 3.1 for both day- and night-time, separately. The night-time maps are then subtracted from the daytime maps to obtain the difference between the two. The positive values in Figure 3.2 indicate that the particular cloud type occurrence is higher during the daytime than during the night-time. The first impression from this figure is that there is no coherent diurnal variation in occurrence of various cloud type except for DC clouds over BoB. Again, the St cloud is underrepresented here. Most of the clouds show a diurnal variation of ~5% in their occurrence. However, there are pockets of isolated highs in diurnal variations as in the case of Ci clouds over the Indian Ocean, which show diurnal variation as high as 20 %. The DC clouds show ~15% diurnal variations especially over BoB. With these few exceptions, there is no notable diurnal variation in the occurrence of particular cloud types over the ISM region [*Subrahmanyam and Kumar,* 2013]. Thus the five-year JJAS mean distribution of frequency of occurrence of cloud types shown in Figure 3.1 is not much affected by the diurnal variations in cloud occurrence frequency as CloudSat observations are available during both local day and night-time as confirmed from Figure 3.2.

3.5 Interannual variability of cloud type distributions

One of the most complex problems associated with the ISM is its interannual variability [*Goswami and Xavier*, 2005]. A part of the interannual variability of the ISM can be attributed to the interannual variability of the various cloud distribution and the feedback provided by these clouds. In order to investigate the interannual variability of the frequency of occurrence of various cloud types, we have established the same for individual years from 2006 to 2010. Figure 3.3 (a–f) show the interannual variations in frequency of occurrence of the various cloud types Ci, As, Ac, Sc, Cu and DC clouds respectively from 2006 to 2010. The interannual variability of St and Ns is not included here as their frequency of occurrence is lower than other cloud types, as mentioned earlier. The frequency of occurrence of Ci clouds is relatively higher over the south Arabian Sea and equatorial Indian Ocean in 2006, 2007 and 2010, whereas the distribution of Ci is higher over south BoB in 2008 and 2009. However, during all

the years, one can notice the signature of TEJ in the distribution of Ci clouds. Further, the distribution of Ci clouds depends on the distribution of DC clouds over head BoB, as a majority of Ci clouds over the ISM are formed from the outflow of DC clouds. The interannual variation of As clouds is shown in Figure 3.3 (b), which readily reveals that the distribution of these clouds is limited to BoB during the years 2006, 2008 and 2009, whereas it is observed over the Arabian Sea also during the years 2007 and 2010. With an exception during the year 2009, the distribution of As over the Arabian Sea seems to exhibit the biennial oscillation. Figure 3.3 (c) depicts the interannual variation of Ac clouds; as discussed earlier, these clouds preferentially form over land. There is a little interannual variation in the Ac cloud distribution over the ISM region. The interannual variation of Sc clouds is shown in Figure 3.3 (d). It is very interesting to note the consistency of these cloud occurrences over the Arabian Sea as well as over the equatorial Indian Ocean during all the years. Except during the 2009, the frequency of occurrence of these clouds over the Arabian Sea is coherent and limited to a narrow region, and the interannual variation is not very prominent. Figure 3.3 (e) shows the interannual variation of Cu clouds. There are two prominent peaks in the occurrence of these clouds: one over the Tibetan Plateau and the other over the west coast of India. There is a little interannual variation in their occurrence over these regions. Finally, the interannual variation of DC cloud occurrence is shown in Figure 3.3 (f). From this figure, it is evident that the DC clouds spread over the entire BoB and the Arabian Sea region in 2007 and 2010, whereas in 2006, 2008 and 2009 they are highly concentrated in the northeast BoB. One more noteworthy observation is the lack of DC clouds over the Indian landmass during the year 2009 as compared to other years. The year 2009 was a drought year with 22% deficiency in all India monsoon rainfall as compared to the long-term monsoon rainfall over the region. Thus Figure 3.3 (a–f) describes the interannual variation in distribution of frequency of various cloud types occurring over the ISM region. The dynamical, thermal and moisture structure of the background atmosphere during these years could be the principal reason for the observed interannual variability of these clouds, which have to be further investigated. As mentioned earlier, the distributions shown in Figures 3.1 and 3.3 correspond to the

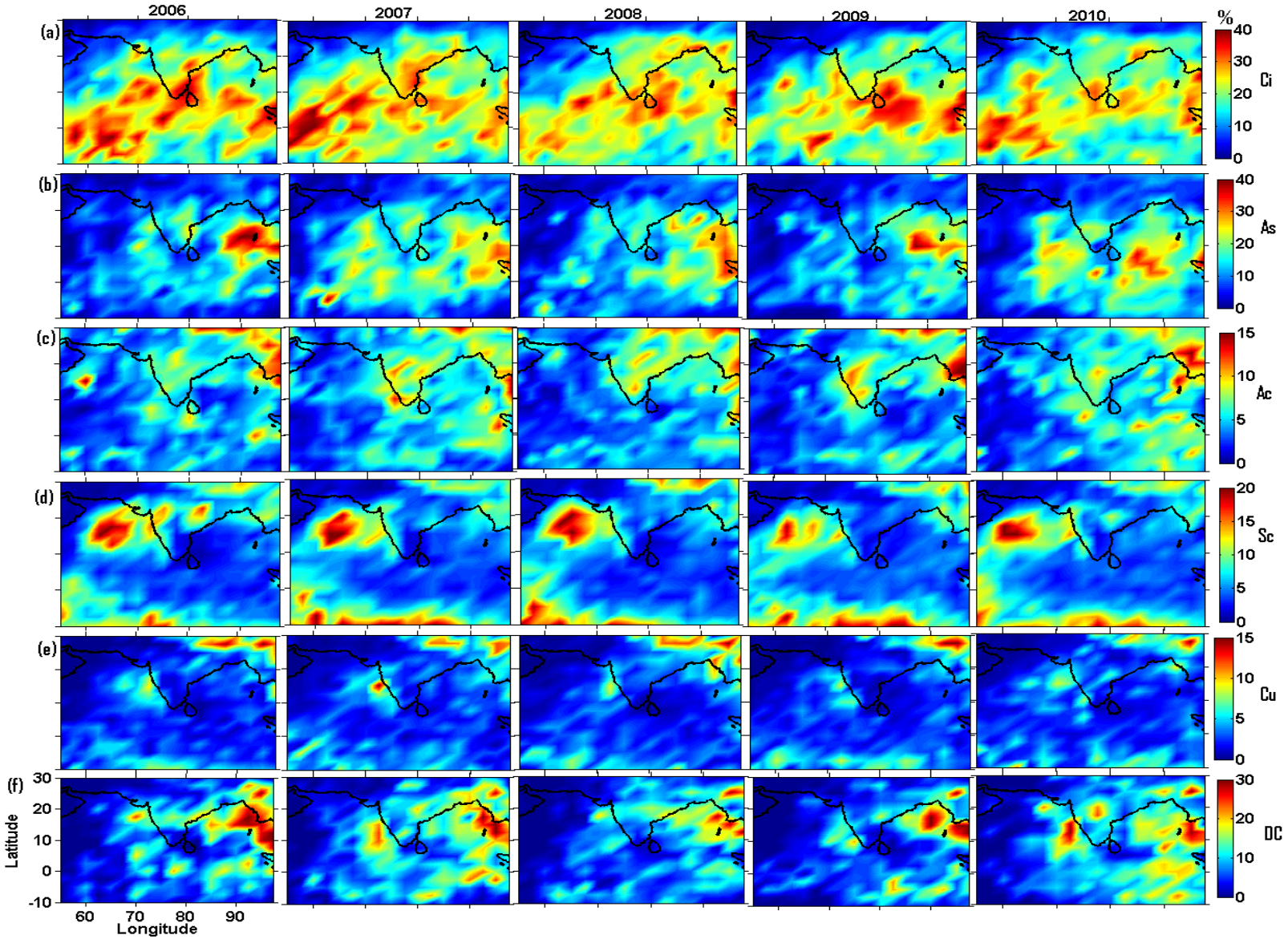

Figure 3.3: Distribution of frequency of occurrence of (a) Ci, (b) As, (c)] Ac, (d) Sc, (e) Cu and (f) DC clouds during the years 2006 - 2010.

height at which maximum occurrence of that particular cloud is found [*Subrahmanyam and Kumar, 2013*]. However, it will be useful to have the height distribution of various cloud types over the ISM region.

3.6 Vertical distribution of cloud types

The frequency of occurrence of individual cloud types are averaged in each range bin over the entire ISM region, and Figure 3.4 (a–f) show the vertical distribution of frequency of occurrence of Ci, As, Ac, Sc, Cu and DC clouds, respectively. The vertical distribution of Ci, As, Ac, Sc, Cu and DC clouds peaks at 12, 7.5, 6, 1.1, 2 and 5 km height, respectively. The vertical distribution of these clouds in terms of cloud type is very important from radiative forcing stand point. The vertical extent of various cloud types shown in figure 3.4 is consistent with the present understanding. The vertical limit of the DC clouds is as high as 16 km. The deviations of all India monsoon rainfall from the long-term mean during the individual years 2006–2010 are given in Figure 3.4 (f). This information has been taken from the India Meteorological Department. From these rainfall deviations, it can be noted that the year 2009 is a drought, and all other years are near-normal [2006 and 2008] to excess year [2007 and 2010]. During the drought year of 2009, it can be noticed that the frequencies of occurrence of all cloud types are reduced compared to other years, and it is very interesting to note that the vertical distribution of DC clouds reflects the monsoon rainfall [i.e., their frequency of occurrence is higher in excess years than in near-normal and drought years]. Thus the present study established the three-dimensional distribution of various cloud types occurring over the ISM region for the first time, which are very vital for understanding the feedback provided by the clouds to the monsoon system. The present study also opens up the possibility to assess the role of individual cloud types in modifying the background thermal structure of the troposphere through radiative and latent heating [*Subrahmanyam and Kumar,* 2013].

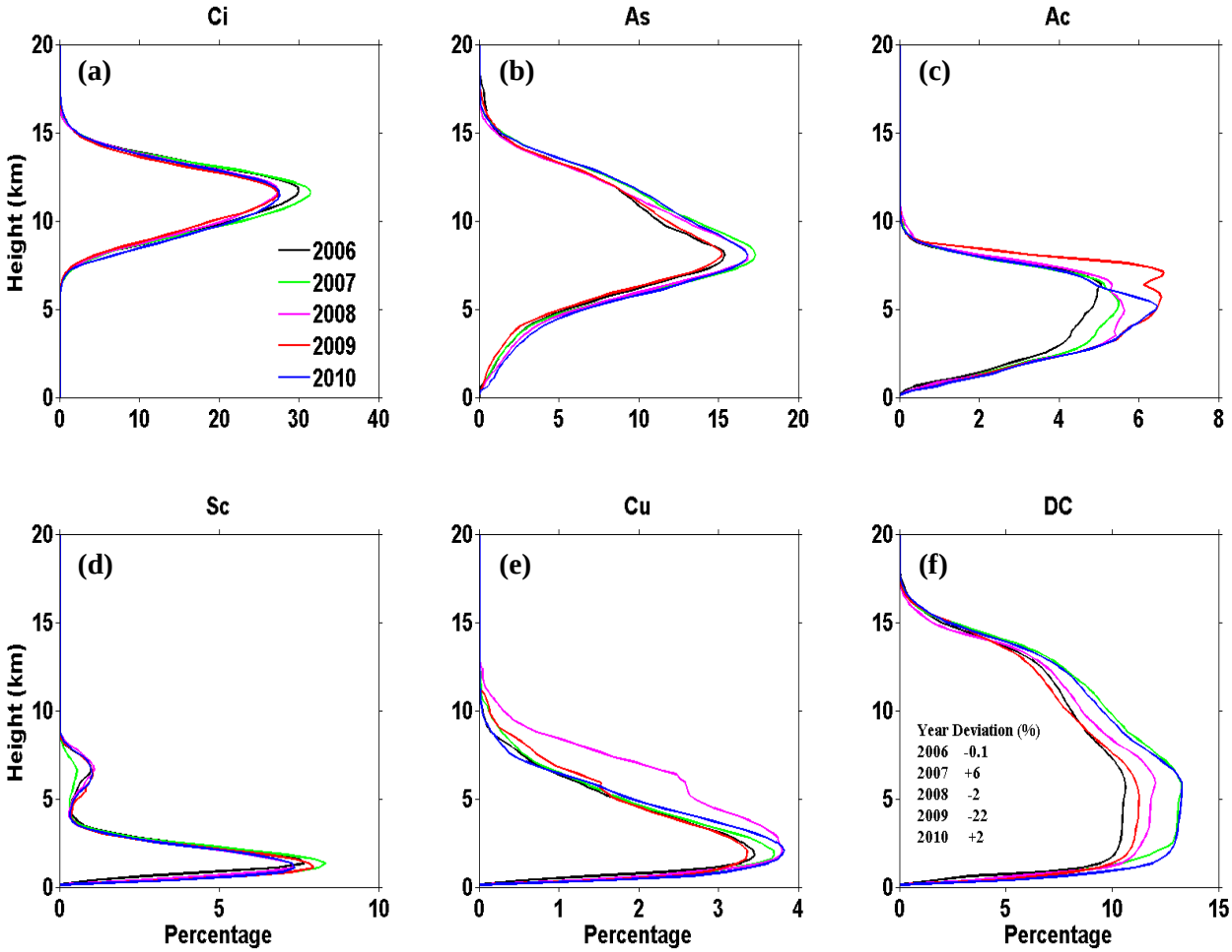

Figure 3.4: Vertical distribution of frequency of occurrence of (a) Ci, (b) As, (c) Ac, (d) Sc, (e) Cu and (f) DC clouds averaged over the ISM region during 2006 -2010

3.7 The role of prevailing dynamics in the formation of cloud types during ISM region

From the above discussion, it is evident that the maximum frequency of occurrence of Sc clouds take place during ISM over the Arabian Sea, Cu clouds over the Western Ghats, As clouds over land and Ac clouds over oceanic region and DC clouds over the north east BoB regions. This section discusses the prevailing dynamics and thermal structure aiding in the formation of various clouds such as Ci, Cu, DC and Sc clouds over the ISM region. The TEJ plays an important role in the distribution of Ci clouds

over the Indian region during summer monsoon period. The vigorous convective activity over BoB produces a large fraction of DC clouds over this region as shown in figure 3.1 (h). The anvils of these Dc clouds are detached and smeared away by strong TEJ at 100 hpa level thus aiding in distribution of cirrus over the Indian region as seen in figure 3.1(a) [*Sathiyamoorthy et al*., 2004]. Besides this, DC clouds transport the large amount of water vapour into the upper troposphere, which also facilitates the formation of cirrus clouds.

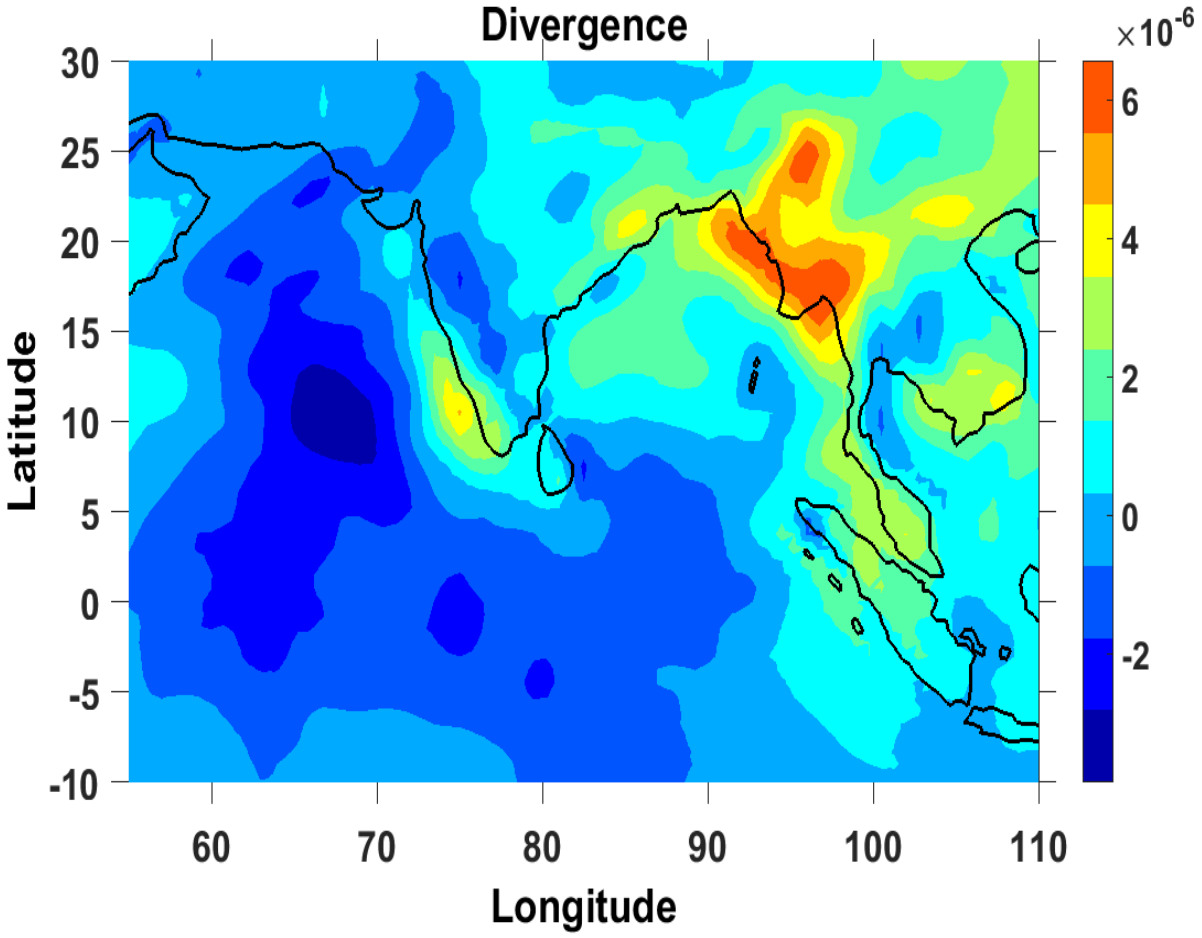

Figure 3.5: Five (2006-2010) year mean divergence at 100 hPa level during the ISM period.

The maximum occurrence of Cu is found to be over Western Ghats region (3.1(f)). The formation of Cu clouds over the Western Ghats is mainly due to orographic features present at this region. The interaction of moisture laden Low Level Jet (LLJ) with

Western Ghats aids in formation of Cu as well as Dc clouds over this region. Figure 3.5 show the five (2006-2010) mean spatial distribution of divergence at 100 hPa level derived from ERA-Interim reanalysis data during the ISM period. A positive value indicates divergence, while negative for convergence. From this figure, it is evident that relatively large upper level divergence exists over the BOB and Western Ghats. It is known that the upper level divergence is associated with low level convergence and the convergence of moisture form low level leads to the formation of deep convective clouds during the ISM period as seen in figure 3.1 (h). Thus lower level convergence plays a major role in formation of DC clouds over the Head BoB [*Subrahmanyam and Kumar,* 2018a].

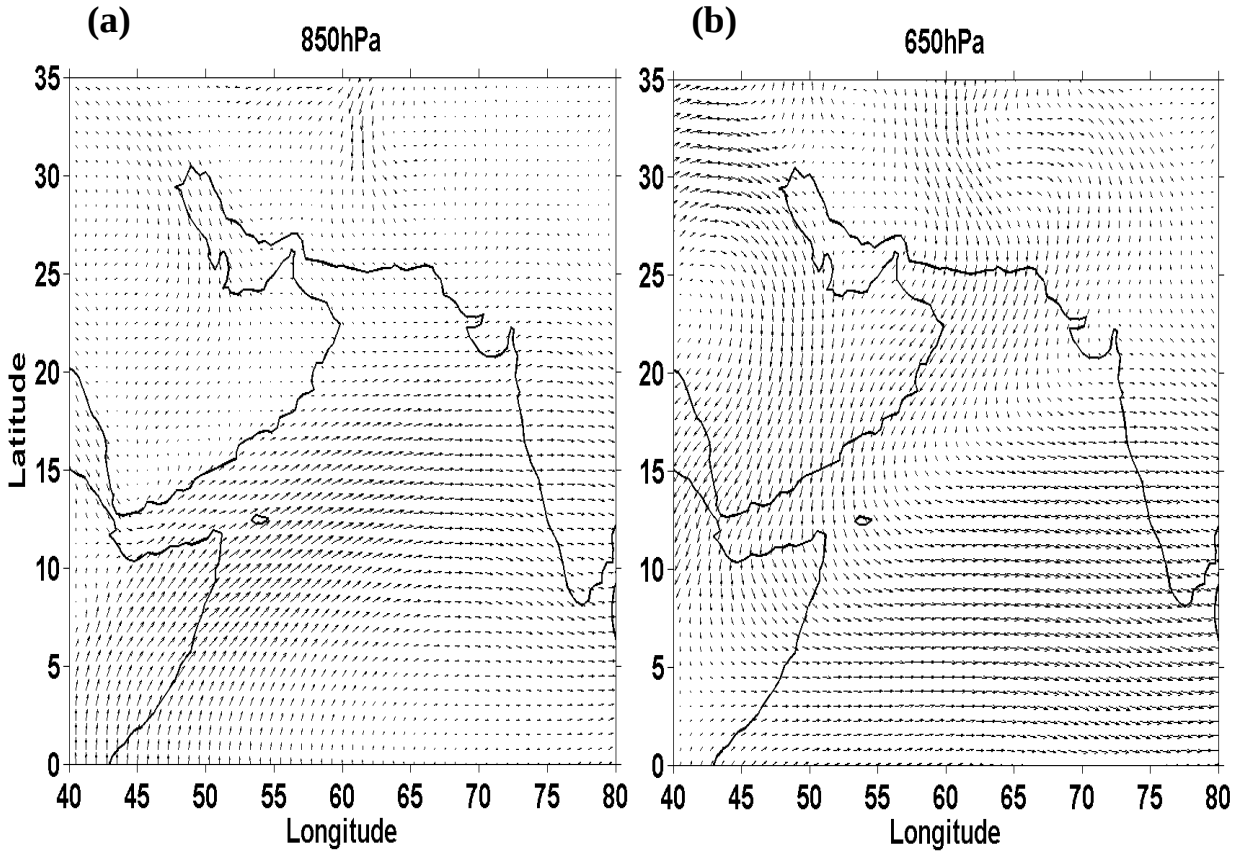

Figure 3.6: Five year mean winds during the ISM period at (a) 850 hPa and (b) 650 hPa derived from ERA-Interim reanalysis datasets.

Now, we investigate the formation of Sc cloud over the Arabian Sea, which is very consistent year-after year. Figures 3.6 (a) and (b) show the mean winds at 850 hPa and

650 hPa level respectively during ISM period constructed using ERA-Interim reanalysis winds. Among many atmospheric circulation features during ISM, the LLJ occurring at 850 hPa is one of the prominent factors, which is depicted in figure 3.6(a). The thermal gradient between the Indian Ocean and Asian landmass is the primary driver for the LLJ. The core of the ISM LLJ lies around 850 hPa level and play a vital role in transporting the moisture from oceanic to land region resulting in widespread rainfall over the Indian Subcontinent [*Joseph and Sijikumar*, 2004]. From figure 3.6(a), it can be noted that the winds accelerate in the 5-10^0 N region (Entrance) and decelerate in the 15-20^0 N region (Exit). Thus the moisture carried by the LLJ from the entrance region with accelerating winds converge at the exit region with decelerating winds and this low level convergence may be conducive for moisture convergence to form clouds over this region [*Sathiyamoorthy et al*., 2013]. However, the upper level winds, sea surface temperature and the background thermal structure dictate the vertical development of the clouds. Figure 3.6(b) shows the vector winds over the ISM region at 650 hPa level. From this figure it is evident that there are strong southward winds from the Arabian land mass towards the Arabian Sea during this season. These winds are supposed to be very dry as they pass through the desert region and thus can affect the vertical development of the clouds through entrainment [*Subrahmanyam and Kumar,* 2018a]. Thus from figure 3.6 it can be noticed that the lower tropospheric winds by transporting moist air are conducive for formation of the clouds whereas mid-tropospheric winds by transporting dry air inhibits their vertical development over the study region.

Further, as mentioned earlier the background thermal structure also plays a vital role in the vertical development of the clouds. To investigate this aspect, the temperature profiles from ERA-Interim reanalysis datasets are examined over the study region. Figure 3.7 shows the monthly mean profiles of temperature over the study region for June, July, August and September months. The mean temperature profile is obtained by averaging all the profiles in 10-20^0 N latitudinal and 60^0-75^0 E longitudinal belt. From this figure, it can be noted that there exists a strong thermal inversion in the 950-850

hPa level over the Arabian Sea. As mentioned earlier, the thermal inversions inhibit the vertical development of clouds and thus these regions are favourable for formation of low level clouds such as Sc clouds. These thermal inversions together with advection of dry air at 650 hPa level from the Arabian desert leads to inhibition of vertical development of clouds over west Arabian Sea. The formations of thermal inversions over Arabian Sea were reported in the past [*Narayanan and Rao*, 1981].

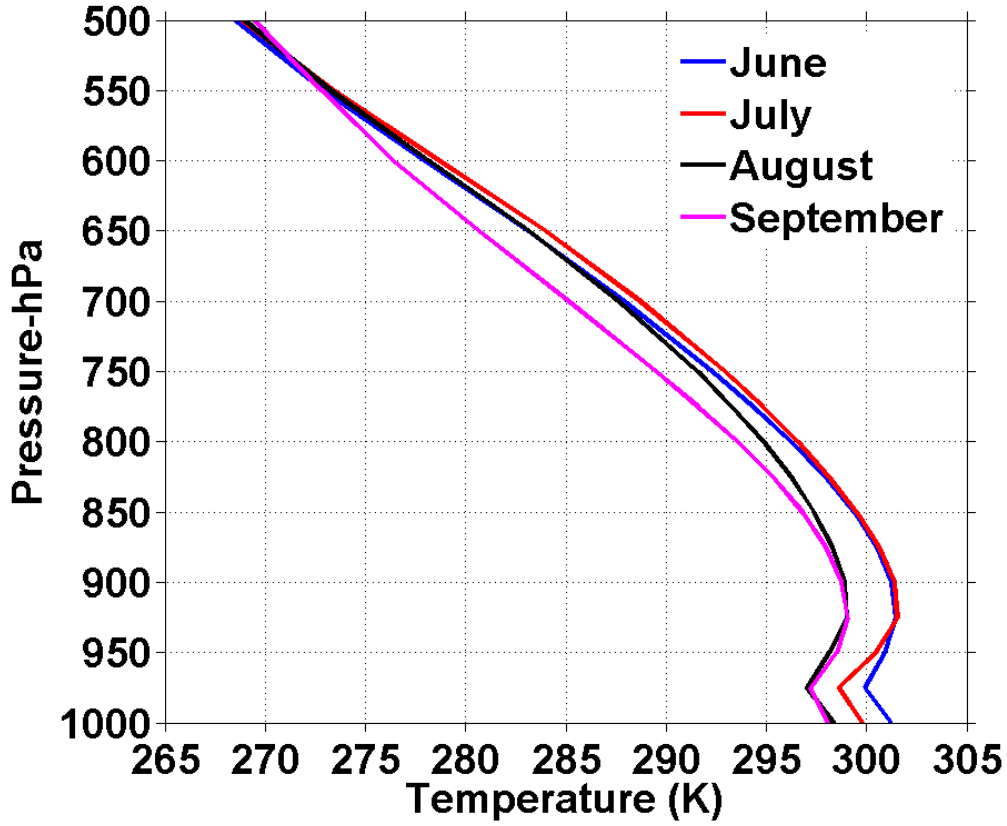

Figure 3.7: Monthly mean temperature profiles observed over the Arabian Sea during ISM period and averaged in the 60-70^{0}E and 15-25^{0}N region.

One of the important factors contributing to the formation of these inversion layers is the subsidence associated with monsoon convection over the Indian land mass and the Bay of Bengal. To examine, whether such subsidence is present over the study region, the vertical velocity dataset from ERA-Interim reanalysis data is used. Figure 3.8 shows the mean pressure-longitude section of Omeag and winds at 15^0 N (where frequency of occurrence of Sc clouds are maximum) during the month of August over

the study region. The negative velocity shows the upward motion and positive velocities show the downward motions. It is known that the magnitudes of vertical velocities provided by reanalysis are not validated. However the reanalysis datasets are able to identify the large-scale up and down drafts, for example, the Walker Circulation can be readily identified by using the vertical velocities derived from reanalysis datasets [*Subrahmanyam and Kumar*, 2017].

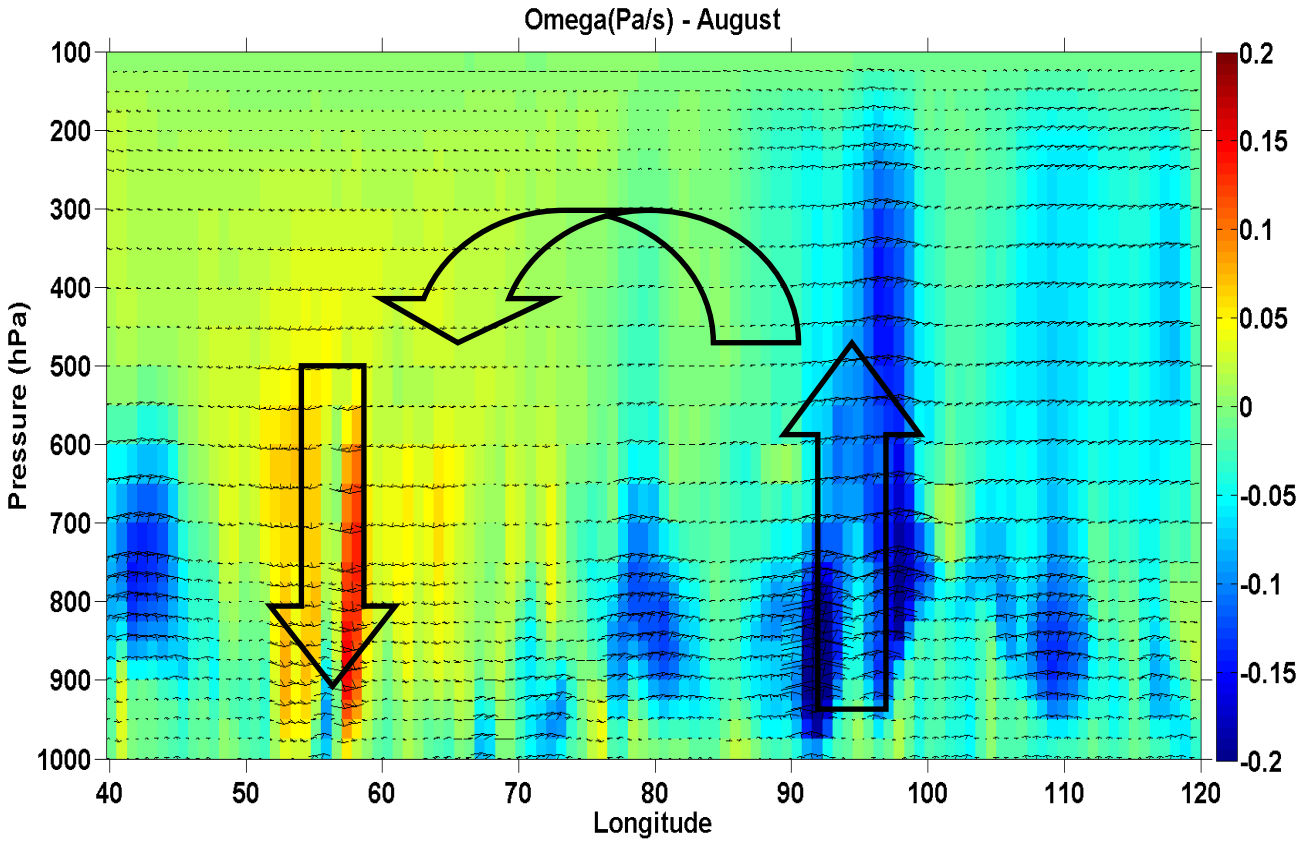

Figure 3.8: Five year mean climatology of pressure-longitude section of Omega and winds derived from ERA-Interim reanalysis datasets for the month of August.

From the figure 3.8, it is evident that the strong subsidence takes place over the study region, which can result in thermal inversion through adiabatic compression. The dry and hot air advected from the Arabian Desert also may play a role in development of the observed inversion layers. Also, the downdrafts over the study region can directly suppress the vertical development of clouds as shown in figure 3.8. Descending motion of monsoon circulation can be seen in figure 3.8 during the month of August in which

the deep convective activity is high over Indian region as well as over the BoB. The negative (positive) Omega values indicate the upward (downward) motion of monsoon convection shown by solid arrow symbol in figure 3.8 over the longitude sector around 90-100 E. The associated downward motion can be found around the 55-60 E, where the maximum frequency of occurrence of Sc cloud forms (fig 3.1(e)). Thus the thermal inversions formed over the Arabian Sea due to descending motion induced by monsoon convection play a key role in the formation of observed Sc clouds. A strong convection can overcome the thermal inversion layers and can develop into deep convection. However, the strength of the convection has dependency on the sea surface temperature. The strong winds over the Arabian Sea during the ISM period can cause upwelling of the sea thus cooling the sea surface, which in turn weakens the convection [*Subrahmanyam and Kumar,* 2018a].

In general, Sc clouds tend to form under large scale subsidence associated with the Hadley as well as Walker circulations. One of the important parameters used in the earlier studies to identity the potential locations for the formation of Sc clouds, is the lower tropospheric stability (LTS). The LTS is an indicator of the atmospheric stability at lower levels, which is defined as the difference of potential temperature at 700 hPa and 1000 hPa levels [*Klein et al.*, 1995]. If the observed LTS is higher then there is less chance for the vertical development of clouds. Figure 3.9 shows the mean distribution of Sc clouds in terms of frequency of occurrence along with LTS in contours during the month of August. From this figure it is evident that the region of maximum in frequency of occurrence coincides with the regions of larger LTS. This observation suggests that the areas of high LTS are not favourable for development of clouds vertically as discussed earlier. However, the larger LTS magnitudes are consequence of the thermal inversion as shown in figure 3.7. Thus there are three factors, viz., low sea surface temperature, large scale subsidence induced thermal inversion, and dry air intrusion in mid troposphere, which influence the vertical development of clouds over the Arabian Sea and favours the formation of Sc clouds [*Subrahmanyam and Kumar, 2018a*].

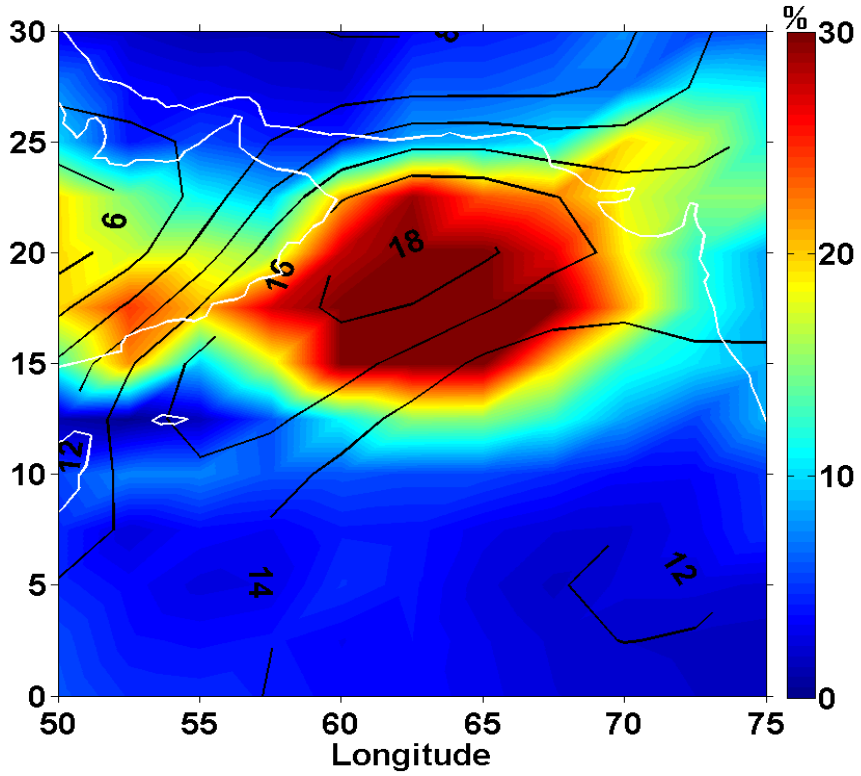

Figure 3.9: Five year mean spatial distribution of FOC of Sc clouds along with contours of LTS over the study region observed during the month of August.

3.8 Summary

Five years [2006–2010] of CloudSat observations over the ISM region are used to establish the three-dimensional distribution of various cloud types in terms of their frequency of occurrence for the first time. The mean distribution of Ci clouds emphatically showed the role of TEJ in spreading the anvils of DC clouds forming over the head BoB. These clouds are most frequently observed over the Indian peninsula, south BoB and Indian Ocean. It is observed that the Sc clouds form most frequently over the north Arabian Sea and are confined to a narrow region. The prevailing dynamical features during the ISM period seem to be responsible for the formation of these clouds over the Arabian Sea. It is also observed that Ac clouds form preferentially over land and As clouds over BoB. The mean distribution of Cu clouds showed three distinct peaks over the Tibetan Plateau, western coast and equatorial Indian Ocean. The distribution of DC clouds, which are very important from a

hydrological standpoint, showed a pronounced peak in their occurrence frequency overhead BoB and secondary peaks over western coast, south BoB and central India. The frequencies of occurrence of St and Ns clouds are found to be much lower than other cloud types over study region. The diurnal variations in frequency of occurrence of all these clouds are also established using day- and nighttime observations of CloudSat. The interannual variations of all these clouds are discussed, and it is observed that the region over which a particular cloud occurs is consistent from one year to another. The mean vertical distribution of all the cloud types over the ISM region is also established. The vertical structure of DC showed year-to-year variations, which is consistent with the India summer monsoon rainfall observations during that study period. The role of prevailing dynamics in the formation of various cloud types is also investigated. It is envisaged that the present study will be helpful in quantifying the feedback of an individual cloud type to the ISM.

Chapter 4

Cloud type distribution in Tropical Cyclones formed in the North Indian Ocean surrounding the Indian region

"You carry both lighting and thunder in that
Space between your bones and sour
Become the storm you are hiding from
A hurricane does not run from the rain"
-**Nikita Gill**

4.1 Introduction

The devastation caused by tropical cyclones makes them one of the important topics of research in the realms of meteorology. The prediction of intensity and movement of tropical cyclones are the two important topics addressed by several researchers across the globe to understand these complex atmospheric-oceanic systems. Among many atmospheric processes associated with tropical cyclones, the clouds embedded in these systems play an important role in precipitation as well as modulating the energy budget of the earth's atmosphere [e.g., *Bergman and Salby*, 1997]. Once formed, further intensification and movement of the tropical cyclones, among other factors; depend on the latent heat released in the clouds embedded in them [e.g., *Houze*, 2010]. The latent heat released in clouds modifies the internal dynamics of

cyclone and the dynamics in turn dictate the cloud distribution within in the cyclone. However, the amount of latent heat released by various cloud types is different. By knowing the cloud type, it may be possible to infer the latent heat released indirectly. In recent times, climate models are able to simulate the development of tropical cyclones [e.g., *Fudeyasu et al*., 2010, *Bu et al*., 2014]. However, most of the climate models are not able to simulate vertical structure of clouds in tropical cyclones [*Su et al.*, 2011; *Su et al*., 2008; *Masunaga et al*., 2008]. So it becomes important to study the vertical distribution of clouds within a cyclone for having better insights into its internal dynamics and vice versa. Doppler radars, dropsondes, aircraft measurements and satellite based passive and active remote sensing techniques have been employed in the past to better understand the cloud systems within tropical cyclones. In the past, observations of tropical cyclones have progressively improved using satellite based measurements with more advanced instruments over the years [e.g., *Rappaport et al*., 2009]. However, early days' satellite observations of tropical cyclones are relied upon infrared and visible images from geostationary satellites to estimate cyclone position and intensity [e.g., *Dvorak*, 1984]. Subsequent satellite measurements were improved by adding passive microwave sensors with the ability to penetrate into cirrus cloud decks and disclose cyclone structures [*Kidder et al*., 1978; *Velden and Smith*, 1983]. The passive remote sensing measurements have their own advantages and disadvantages. Infrared radiometer onboard geostationary satellites provide continuous observations of evolution and movement of cyclones, but they cannot provide the vertical distribution of clouds in cyclones. Especially, infrared radiometers cannot provide the information below the high altitude clouds such as thick cirrus. Consequent satellite missions added additional microwave sensors with channels at more frequencies [TMI, AMSR-E, AMSU, SSM/I], which have yielded relatively more accurate cyclone forecasts [*Fudeyasu et al*., 2010]. Precipitation radar [PR] on board Tropical rainfall

Measuring Mission [TRMM] provided vertical structure of convective clouds [Simpson et al., 1998], however- TRMM- PR is not very sensitive to non-precipitating clouds and cannot provide continuous observations of cyclone. Understanding about the structure and dynamics of tropical cyclones is improved tremendously with the TRMM-PR observations [*Hence and Houze*, 2008; *Houze*, 2010]. Further, concerns about the possible effects of global warming on tropical cyclone activity have motivated a number of theoretical and modelling studies [*Emanuel*, 2001].

Information on three dimensional distribution of cloud types were very limited until the launch of CloudSat [*Stephens et al*., 2002] and CALIPSO [*Winker et al*., 2007] satellites, which are part of A-Train constellation. A-train provides the unique opportunity to combine the observations of precipitation, radiation and clouds. The combined observations from CloudSat/CALIPSO provide three-dimensional distributions of various cloud types and vertically resolved radiative heating structure [*Mace*, 2010; *Behrangi et al*., 2012; *Subrahmanyam and Kumar*, 2013; 2017; *L'Ecuyer et al*., 2008; *Haynes et al*., 2013]. The central objective of the present study is to construct the composite cloud type distribution embedded in tropical cyclones and cloud radiative heating rates as a function of radial distance from the eye of the cyclones formed in the North Indian Ocean using CloudSat observations. *Durden et al*. [2009] studied the seventeen tropical cyclones passes of CloudSat and found that the reflectivity is relatively higher in the eye-wall region compared other regions of tropical cyclones and oriented more vertically. While *L'Ecyer et al*. [2015] showed the composite structure of tropical cyclone observed by CloudSat in connection with background wind shear and further showed that environment wind shear play a vital role in the dynamics and formation of tropical cyclone. The present study attempts to bring out the composite vertical structure of cloud type distribution within tropical cyclone which is envisaged to shed light on which type of clouds form

in which part of a cyclone.

4.2 Data and Methodology

For the present study, observations of Cloud Profiling Radar [CPR] [onboard CloudSat] over tropical cyclones formed in Arabian Sea and Bay of Bengal surrounding the Indian subcontinent during the years 2006-2014 are used. The operating frequency of CPR is 94 GHz and it provides observations with 240 m vertical resolution and 1.4 and 1.7 km cross- and along-track resolution, respectively [*Stephens et al*., 2002]. Recently, *Tourville et al*., [2015] compiled A-Train observations over Tropical cyclones, which is a unique dataset to investigate the different aspects of clouds embedded in tropical cyclones. This dataset provides information on vertical structure of clouds, precipitation, cloud properties, environmental storm conditions and tracks of the cyclone [*Tourville et al*., 2015]. Among these datasets, the 2B-CLDCLASS product of CloudSat, which provides the cloud type information, is used for the present study [*Sassen and Wang*, 2008]. CloudSat algorithm classifies clouds into eight types, viz., cirrus [Ci], Altostratus [As], Altocumulus [Ac], Stratus [St], Stratocumulus [Sc], cumulus [Cu], Nimbostratus [Ns] and Deep Convective [DC]. The classification is based on different aspects of hydrometeors' vertical and horizontal scales using CPR measured reflectivity and ancillary data including ECMWF temperature profiles and surface topography [*Sassen and Wang*, 2008]. The 2B-CLDCLASS data product employs cloud cluster algorithm for cloud type classification using CloudSat observations. The cloud cluster algorithm derives various cloud types using the reflectivities from CPR along with other additional information from ECMWF reanalysis data. The cloud cluster algorithm considers only the significant CPR cloud mask values 30 and above, which is provided by cloud mask algorithm. Further, classification of the cloud type is done based on microphysical properties, maximum reflectivity and corresponding

temperature at that level, cloud vertical and horizontal extent and the precipitating properties. Complete details on the cloud classification algorithm can be found in 2B-CLDCLASS product description document at *http.//www.cloudsat.cira.colostate.edu/dataHome.php*. The 2B-CLDCLASS data product provides the cloud information as a function of latitude, longitude and altitude with the same resolution that of CPR observations. The main advantage of CloudSat is that it provides the vertical structure of hydrometeors over the foot-print of CPR along its path. However, CPR is not sensitive to optically thin clouds such as high-altitude thin cirrus clouds. More details on CloudSat can be found in *Marchand et al*. [2008]. The limitations of 2B-CLDCLASS product are [1] surface contaminations in the lower 3 to 4 range bins of CPR vertical reflectivity profiles, which will have implications in classifying St and Sc clouds and [2] the CPR is not sensitive to high altitude thin clouds, which will have implications in detecting the Ci clouds [*Marchand et al.*, 2008; *Behrangi et al*., 2012; *Subrahmanyam and Kumar*, 2013, *Subrahmanyam and Kumar*, 2018b]. Both these limitations will result in fewer detection of St, Sc and Ci clouds than actually present. A detailed description of cloudSat and its data products are provided in chapter 2.

One should keep these limitations in view while interpreting the observations. Despite these limitations, cloud type classification are derived using the CPR reflectivities along with auxiliary data from ECMWF reanalysis fields along its path, which is very useful for assessing the role of clouds in energetics and dynamics of the atmosphere as a function of cloud type. The following steps are adopted to calculate the frequency of occurrence of each cloud type as a function of distance from the eye of cyclone. Step 1: The CloudSat observations are gridded with respect to the distance from the center of tropical cyclone. Step 2: The number of each cloud type is estimated as a function of height. Step 3: The number of occurrence of each cloud

type is divided by the number of occurrence of all cloud types at each height and the same is used to construct the composite cloud type distribution in a tropical cyclone as a function of distance from the eye of the cyclone [*Subrahmanyam and Kumar*, 2018b].

Table 4.1 List of Tropical Cyclones occurred in North Indian Ocean during 2006 to 2014.

S. No.	Cyclone Name	Period	Basin
1	MUKDA	21 Sept - 24 Sept, 2006	ARB
2	AKASH	12 May - 15 May,2007	BoB
3	GONU	1 June - 7 June, 2007	ARB
4	SIDR	11 Nov - 16 Nov, 2007	BoB
5	NARGIS	27 Apr - 7 May, 2008	BoB
6	RASHMI	25 Oct - 27 Oct, 2008	BoB
7	KHAIMUK	13 Nov - 16 Nov, 2008	BoB
8	NISHA	25 Nov - 29 Nov, 2008	BoB
9	BIJILI	14 Apr- 17 Apr, 2009	BoB
10	AILA	23 May - 26 May, 2009	BoB
11	PHYAN	4 Nov - 11 Nov, 2009	ARB
12	LAILA	17 May - 21 May, 2010	BoB
13	BANDU	19 May - 23 May, 2010	ARB
14	PHET	30 May - 7 June, 2010	ARB
15	GIRI	20 Oct - 23 Oct, 2010	BoB
16	JAL	1 Nov - 8 Nov, 2010	BoB
17	THANE	25 Dec - 30 Dec, 2011	BoB
18	MURJAN	22 Oct - 26 Oct, 2012	ARB
19	NILAM	28 Oct - 1 Nov, 2012	BoB
20	MAHASEN	10 May - 17 May, 2013	BoB
21	LEHAR	23 Nov - 28 Nov, 2013	BoB
22	MADI	6 Dec - 13 Dec, 2013	BoB
23	NANAUK	10 June - 14 June, 2014	ARB
24	HUDHUD	7 Oct - 14 Oct, 2014	BoB
25	NILOFAR	25 Oct - 31 Oct, 2014	ARB

Table 4.1 lists the number of cyclone events formed in the North Indian Ocean surrounding the Indian subcontinent during 2006-2014, which were used in the present study. The table also provides the period of the cyclone. Figure 4.1 (a) shows the number of CloudSat observations over the tropical cyclone as a function of radial distance from the eye of the cyclone. From this figure, it is clear that there are relatively few observations over the eye of a cyclone as compared to other parts of the system. However, the cloud type distribution is normalized with the total number of observations to estimate the frequency of occurrence of each cloud as a function of radial distance from the eye of the cyclone. Figure 4.1 (b) shows the number of CloudSat observations in each cyclone from 2006 to 2014. The information on regions of their formation is also given in the figure. On an average each cyclone has about 1500 CloudSat profiles in and around them. From this figure, it is evident that the present observations are not dominated by any particular cyclone. Further, these observations are separated into two subsets, one set having observations during developing stage and other during mature stage. The developing and mature stages are identified using the formation of well-defined eye and the information provided by the India Meteorological Department. However, identifying the eye during formative and dissipating stage is very difficult and thus focused on mature stage of the cyclone alone in the present study.

Figure 4.2 depicts the schematic of vertical cross section of tropical cyclone [redrawn from *Frank*, 1973] highlighting the vertical cloud distribution and internal circulation. The basic anatomy of the cyclone consists of an eye, eye-wall, moat, inner and outer rain-bands. However, the nomenclature slightly differs among the meteorologists. From this illustration, it is clear that the eye-wall, the inner and the outer rain bands of cyclones consist of deep convective systems reaching up to the tropopause and the presence of cirrus clouds resulting from outflows of these deep

convective systems. This is a simplified cloud distribution of a tropical cyclone and there are other clouds embedded within these systems. From this schematic, it can be observed that the top of the deep convective clouds decreases with distance from

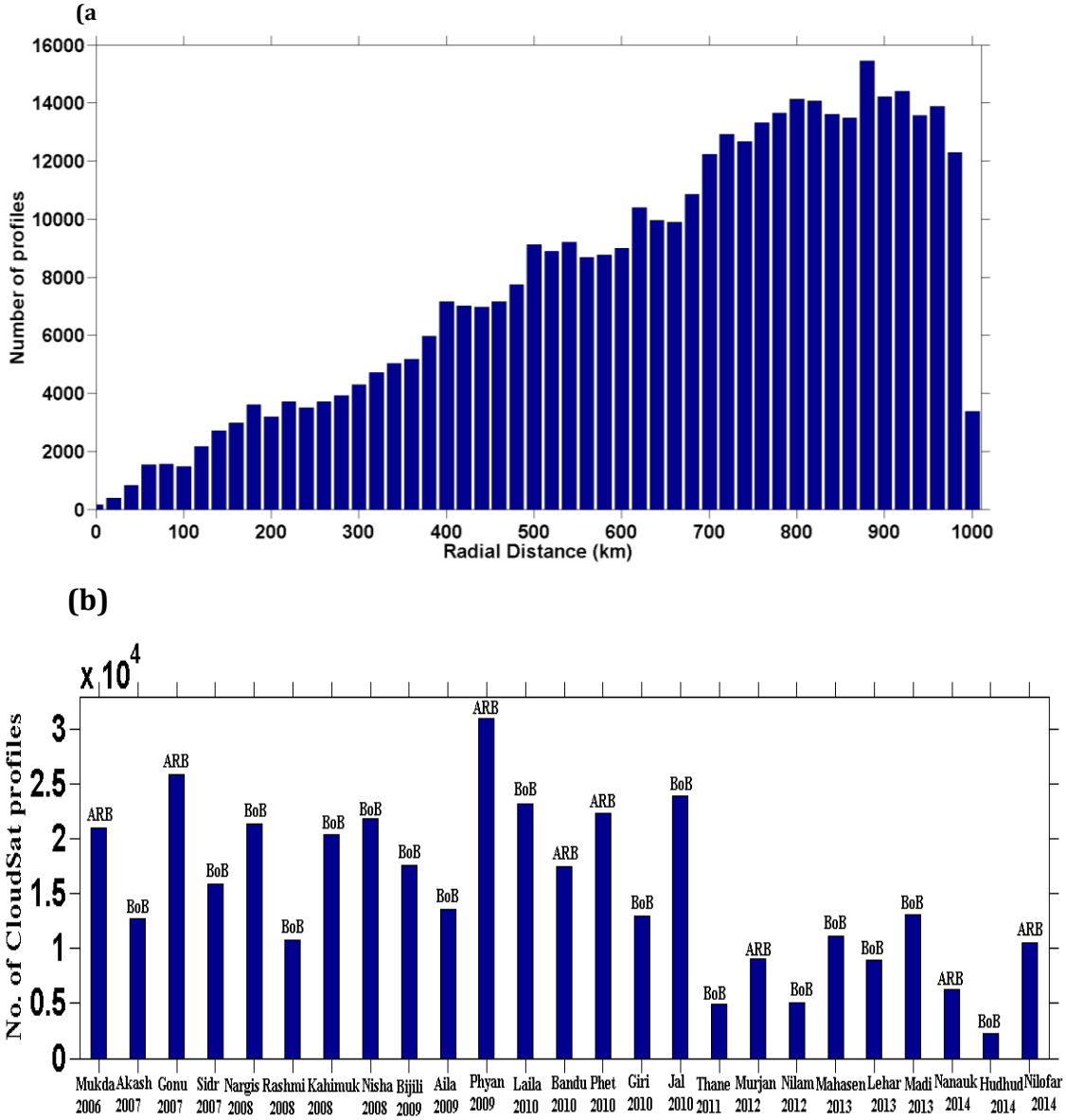

Figure 4.1: (a) The number of CPR profiles as a function of radial distance from eye of the cyclone and (b) the number of CPR profiles in each cyclone.

the eye. This is attributed to the inhibition of vertical development of clouds by the out flows of deep convection from eye-wall region of a cyclone. The dynamics responsible for the formation of deep convective clouds as well as cirrus clouds in various regions of the tropical cyclone is reported by *Houze et al.* [2010]. A complete description of cloud distribution, especially cloud types in tropical cyclones is yet to be generalized and the present study is an attempt towards this end using CPR on board CloudSat.

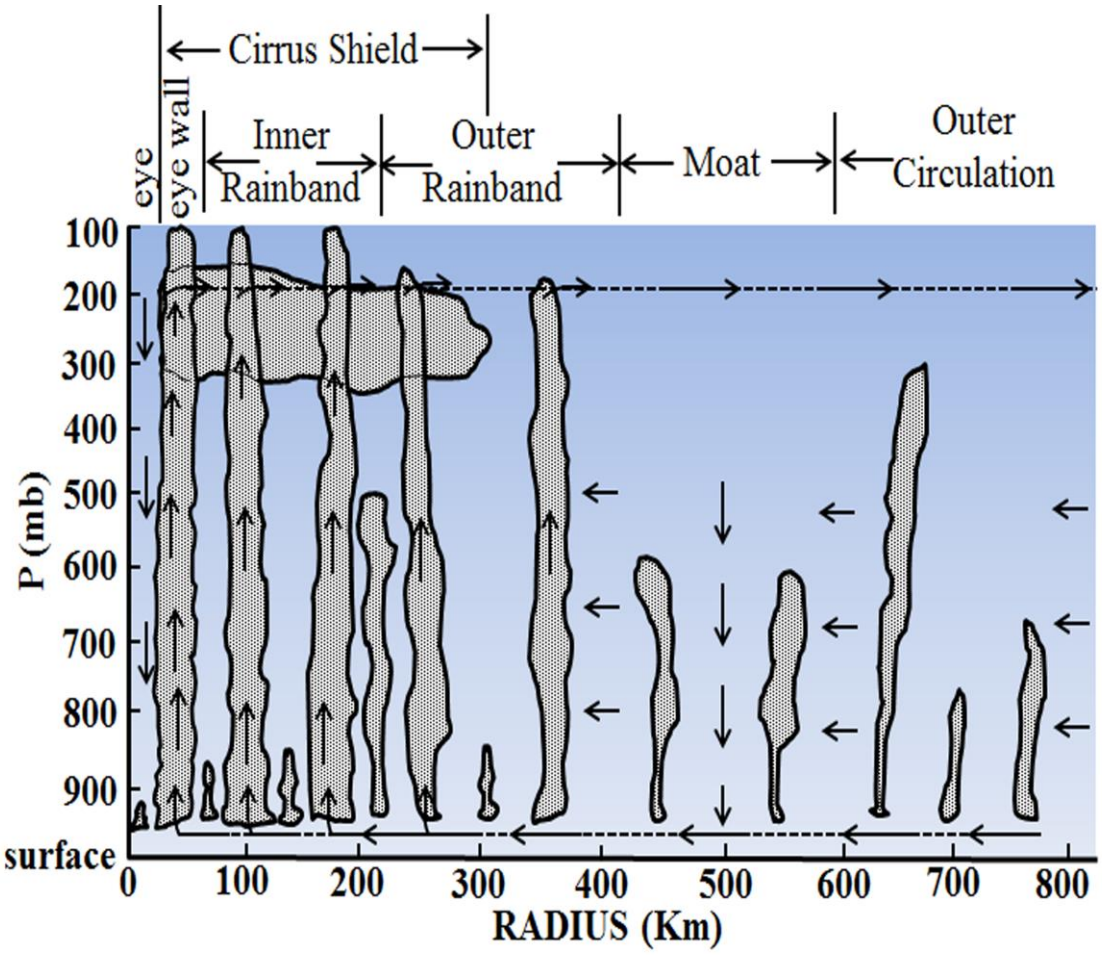

Figure 4.2: Schematic view of vertical cross section of tropical cyclone [adopted from *Frank*, 1973].

4.3 Cloud type distribution in 'GONU' cyclone observed by CloudSat

Figures 4.3 (a) and (b) show CloudSat track through the GONU cyclone's eye and its inner rainband respectively on 2 June 2007 at two different times. GONU cyclone was developed on 1st June 2007 in the eastern Arabian Sea and it developed into matured stage on 4th June. It started weakening on 6th June and then dissipated on 7th June after making the landfall. The CloudSat reflectivity observations along its track over the GONU cyclone provided valuable information on the vertical structure of clouds and are shown in Figure 4.3 (c) and (d), which correspond to the CloudSat ground tracks indicated by red lines in Figures 4.3 (a) and (b) respectively. These figures depict the vertical cross section of cloud reflectivity as observed by the CPR along the CloudSat track. The radar reflectivity derived from backscatter signal from the cloud droplets forms the basis for deriving cloud microphysical information including its type. From these two figures, echo tops reaching as high as 15-16 km corresponding to deep convective clouds can be observed. In conventional geostationary satellite observations, it is difficult to discern the high cloud and deep clouds and the active remote sensing observations used in the present study resolve this paradox [*Subrahmanyam and Kumar*, 2018b]. The horizontal distribution of radar reflectivity along the CloudSat track also reflects the circulation pattern with in tropical cyclone. The regions which are void of clouds represents the regions of down drafts, regions with reflectivity spread through ~2-15 km represents the updraft region and the regions where the reflectivity is confined in 10-15 km region represents the convective outflow regions. Thus using the reflectivity structure one can infer some of the dynamical aspects of the cyclone structure. Further, the cloud type distributions are constructed and are depicted in Figures 4.3 (e) and (f) corresponding to CloudSat tracks shown in Figure 4.3 (a) and (b) respectively. In Figure 4.3 (e), the various sectors of tropical cyclone viz., eye, eye wall, rainbands and anvils are labelled. Only small portion of the eye of the GONU cyclone is captured

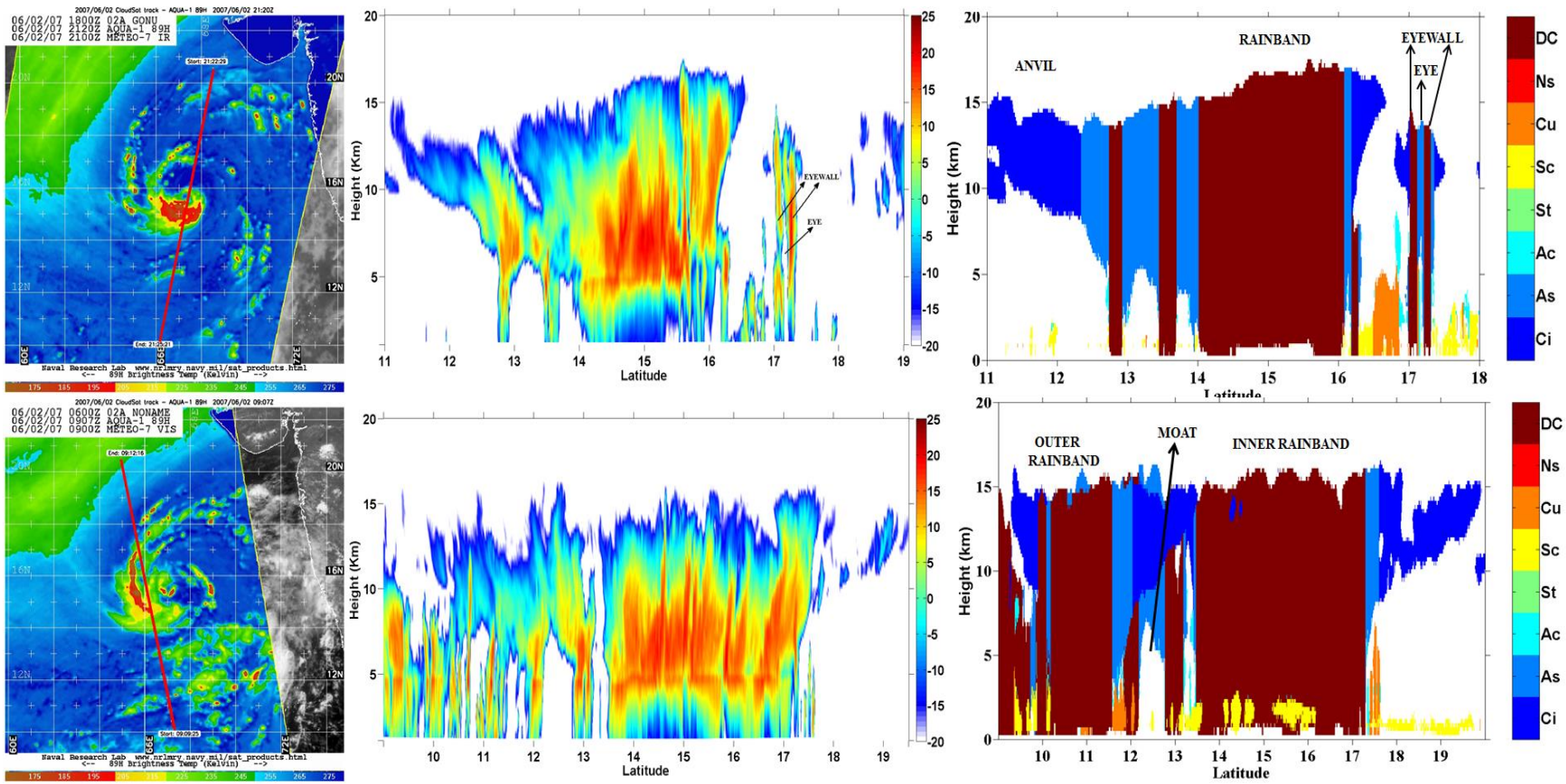

Figures 4.3: The CloudSat track through the GONU cyclone's (a) eye and (b) inner rainband on 2 June 2007. (c) and (d) The CloudSat reflectivity corresponding to CloudSat tracks shown in (a) and (b), respectively. (e) and (f) The cloud type distribution corresponding to CloudSat tracks shown in (a) and (b), respectively.

by the CPR in one direction. However, it provides valuable information on the vertical structure of cloud types embedded in the observed cyclone. One can observe the clouds such as stratocumulus, altocumulus and altostratus with in the eye. This region is void of any deep convective clouds as this region is dominated by the downdrafts from surrounding deep convective systems [*Houze*, 2010]. On either side of the eye, deep convective systems representing the eye wall can be noticed in Figure 4.3 (e). The outflows from the eye walls can be noticed in the form of cirrus clouds below which there are cumulus and stratocumulus clouds. The rainband is dominated by the deep convective clouds, which occupy the latitude band between 14 and 16 degrees followed by the thick altostratus and cirrus clouds. It has to be remembered that this cross section represent a small portion of a tropical cyclone and a comprehensive description may require several observations along many parts of the systems. However, the vertical cross section shown in Figure 4.3 (e) along the cyclone eye represents the typical cloud type distribution, which is consistent with the present understanding. In Figure 4.3 (f), the CPR observations of cloud types over the inner and the out rainbands are depicted. In the inner rainband, the deep convective cloud occupies the latitude band 13.5 to 17^0 N degrees followed by cirrus and altostratus clouds on either side. At low-levels of inner rainbands, there are little amount of stratocumulus clouds. A clear signature of moat can be noticed in the 12-13^0 N latitude regions. The moat is a cloud-free region representing the regions of intense down drafts and separating inner and outer rainbands. However, in many cyclones the moat region is found between an old and new eye walls. The outer rain bands shown in figure 4.3[f] are also dominated by the deep convective systems followed by cirrus and altostratus clouds. Thus Figures 4.3 (e) and (f) depict the typical cloud type distribution in the regions adjacent to the cyclone's eye and in the inner/outer rainbands, respectively. The cloud type distribution depicted in figure 4.3 is from instantaneous observations of CloudSat

over the GONU cyclone and as mentioned in section 4.2, a total number of 25 cyclone observations are used to construct a composite cloud type distribution. It is known that the cloud distribution varies largely from one cyclone system to another and also depends on the category and stage of a cyclone. Any attempt to construct the composite cloud distribution in cyclones should consider these aspects. However, previous studies based on decades of observations on the tropical cyclone proposed a generalized pattern of clouds around the eye, inner and outer rainbands of the cyclone [*Houze*, 2010]. So, by making use of multiple observations of CloudSat over different parts of tropical cyclones, a composite cloud type distribution is constructed as a function of height and the radial distance from the cyclone's eye.

4.4 Composite cloud type distribution in Tropical cyclones

Figure 4.4 (a-g) shows the frequency of occurrence of Deep Convective clouds [DC], Cirrus [Ci], Altostratus [As], Nimbostratus [Ns], Altocumulus [Ac], Stratocumulus [Sc], Cumulus [Cu], respectively as a function of height and radial distance from the eye of cyclones. To obtain the frequency of occurrence, the number of occurrences of each cloud type as a function of altitude is estimated and the same is divided by the number of occurrences of all cloud types at each altitude. The DC clouds distribution depicted in Figure 4.4 (a) shows its peak frequency of occurrence of 50% at ~50-100 km radial distance from the eye with a vertical extent of ~16 km. The tallest DC clouds form very near the eye of a cyclone and the tops of these clouds gradually decrease thereafter as a function of radial distance [*Subrahmanyam and Kumar*, 2018b]. Most of the previous studies have shown the DC clouds very near to the eye of the cyclones and the present results show that even though these clouds are present near to the eye, the maximum frequency of their occurrence is slightly away from the eye as shown in the Figure 4.4 (a). From this figure, it is also evident that

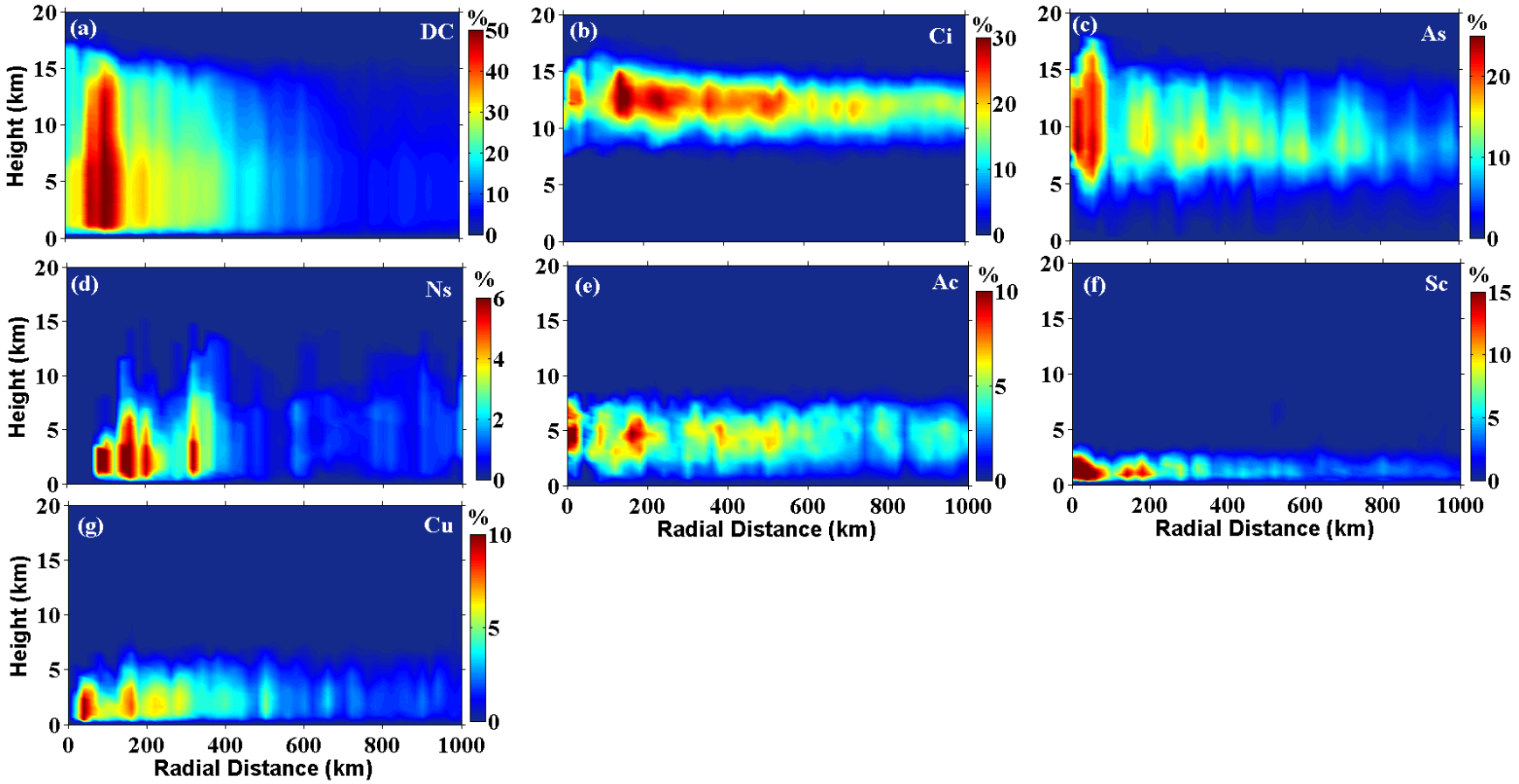

Figure 4.4: (a-g) The frequency of occurrence of Deep Convective clouds [DC], Cirrus [Ci], Altostratus [As], Nimbostratus [Ns], Altocumulus [Ac], Stratocumulus [Sc], Cumulus [Cu], respectively as a function of height and radial distance from the eye of the cyclone.

the DC clouds distribution shows band structures representing their preferential regions for formations such as the inner and the outer rainbands. The frequency of occurrence of DC clouds drastically decreases beyond 500 km from the eye. The warm sea surface temperature and low level convergence of moisture are the prime driving force for the DC cloud formation in cyclones. The latent heat released in theses clouds forms the basis for further intensification of cyclone. Both the latent heating of condensation and freezing contributes to the heating apart from cloud radiating heating. The DC clouds formed in the cyclones are different from the DC clouds that form in another convective system. The main difference between these two types of DC clouds being the swirling updrafts and cloud bases in the cyclones [*Houze*, 2010]. By now, it is well known that the outflows in the DC clouds in cyclones are responsible for the generation of Ci clouds. The Ci cloud distribution in tropical cyclones are depicted in Figure 4.4 (b), which shows that these clouds occur at around 13-15 km height region with a maximum frequency of 30% (at 14-15 km altitude) at around ~200 km radially from the eye of the cyclones. This frequency of occurrence is at a particular altitude where it peaks. It is interesting to note that the peak in Ci clouds are observed just after the peak in the DC clouds shown in Figure 4.4 (a), which further strengthens the assertion that the principal source for Ci clouds is the outflows from the DC clouds. This observation also vouches for the present approach for constructing the composite cloud distributions using multiple cyclone observations. Significant amounts of Ci clouds are observed up to 1000 km radial distance from the eye, which is well known from earlier observations. From this figure, it is also clear that the Ci cloud tops are gradually decreasing as a function of radial distance as in the case of DC clouds. The outflow from the DC clouds, which forms the Ci clouds, plays a vital role in radiative forcing as well as in limiting the vertical growth of the DC clouds. Apart from the outflows of the DC clouds, there is a possibility of *in situ* generated Ci clouds. However, in cyclones the majority of Ci clouds are formed from the DC cloud outflows. With time,

Ci clouds transform into the large and deeper stratus and cirrostratus clouds. Further, the cirrostratus clouds can seed the As cloud formation. Figure 4.4 (c) shows the distribution of As clouds in tropical cyclones. The As cloud distribution shown in this figure is not consistent with the present understanding of characteristics of these clouds. In general, As clouds occur in the height region of ~3-10 km in the tropics and are classified as mid-level clouds. But Figure 4.4 (c) shows tops of As clouds as high as 16 km near the eye of cyclone with a peak frequency of occurrence of ~25%. There seems to be an issue in distinguishing DC and As clouds in the cloud classification algorithm, especially in cyclones. It can be explained on the basis of the tilted DC clouds in tropical cyclones.

As mentioned earlier, the DC clouds in the tropical cyclones swirls and thus will be titled with respect to its base. The CPR, which observes the clouds in nadir view, may be classifying the upper portion of the tilted DC as As cloud. This scenario is illustrated in figure 4.5, which shows the possibility of CPR classifying the upper portion of the DC clouds as As. The rectangular box shown in figure 4.5, which is a part of eye-wall DC clouds may be classified as As cloud in the present algorithm. This type of slanting eye-wall clouds are discussed by *Houze* [2010]. One more possibility is that the transition region between the DC clouds and their outflows may also be classified as As clouds. This assertion is substantiated by the cloud classification observations depicted in Figures 4.3 (e) and (f), which show that the DC clouds are accompanied by As clouds in most of the cases. Further, from Figure 4.4 (a), it can be noted that near to the eye of cyclone, the frequency of occurrence of DC clouds are limited to ~7 km. Above this altitude, a peak in the frequency of occurrence of As clouds is observed over this region. Thus it seems that the cloud classification algorithm identifies the upper portions of the DC clouds and the transition region between these clouds and their outflows as As clouds. So while estimating the frequency of occurrence DC clouds and

As clouds in the tropical cyclones, these aspects have to be considered. However, this will not have any consequence on the overall frequency of occurrence of the DC clouds as it will only affect the vertical distribution as shown in Figure 4.4 (a). In the present study, not implemented any corrections to existing cloud type identification and retained the original classification provided by the CloudSat product.

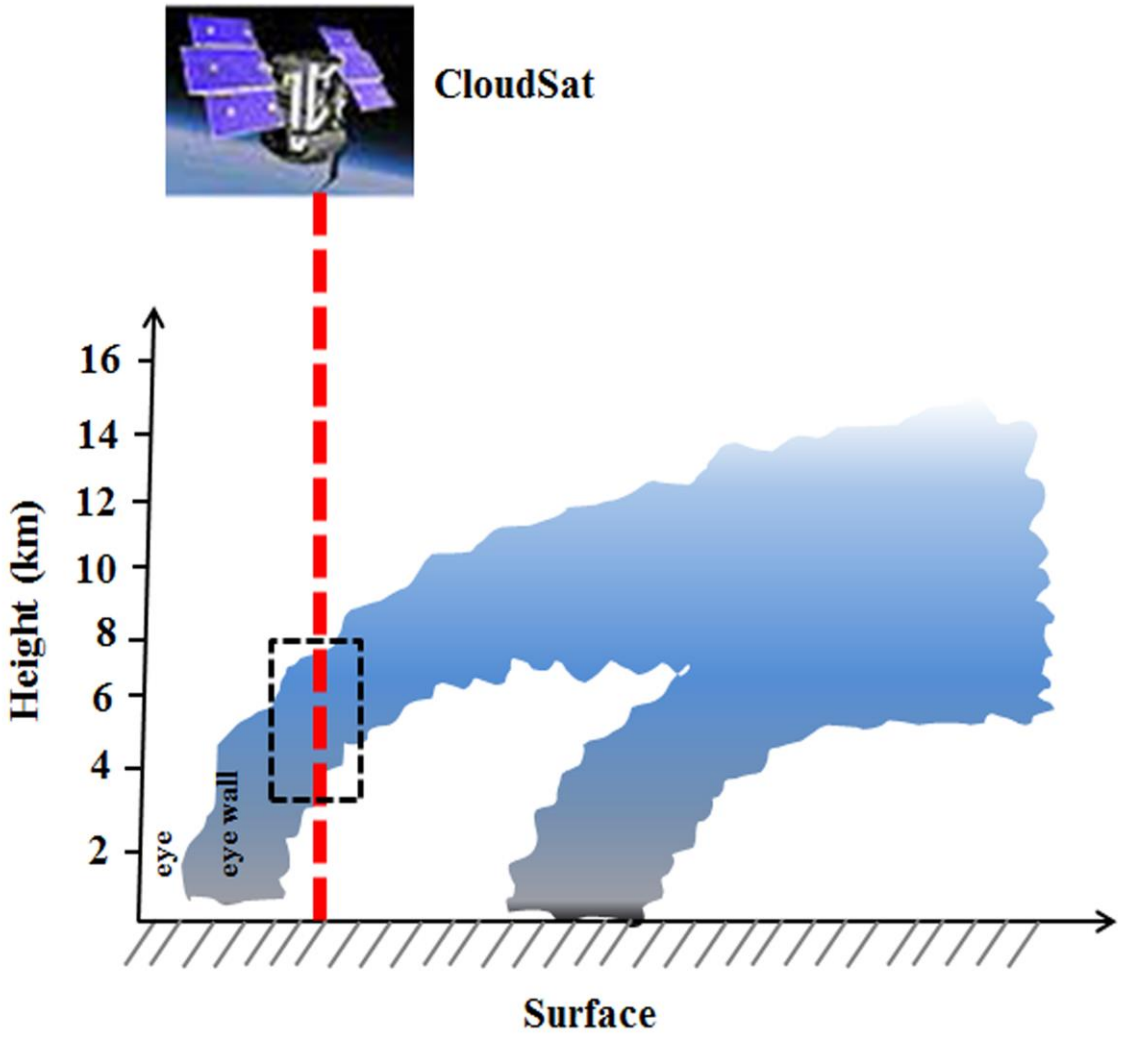

Figure 4.5: Illustration of CloudSat nadir view over the upper portion of the tilted DC cloud.

The As clouds descend to lower heights with time and can evolve as Ns clouds. However, apart from As clouds, Ns clouds can form directly also. Figure 4.4 (d) shows the composite height distribution of Ns clouds as a function of the radial distance from the cyclone's eye. From this figure, it can be noted that the frequency of occurrence of Ns clouds is relatively low [~6%] as compared to the other clouds discussed so far. Ns are rain bearing clouds and dominate in contributing to the precipitation production. These clouds are limited in their occurrence within ~400 km from the eye of the cyclones with their tops reaching ~10 km. Thus the outflows from the DC clouds can trigger the formation of Ci, As and Ns clouds and influence their frequency of occurrence in tropical cyclones [*Subrahmanyam and Kumar*, 2018b].

Figure 4.4 (e) shows the composite height distribution of frequency of occurrence of Ac clouds as a function of the radial distance from the eye of cyclone. It shows a peak frequency of occurrence of 10% near to the eye. The horizontal extent of these clouds is very large and comparable to that of Ci clouds. Even though the Ac clouds are not important for their contribution to the precipitation production, these clouds play a significant role in radiative forcing. The low-level clouds such as Sc are most common in the center of the cyclone. Figure 4.4 (f) shows the composite distribution of frequency of occurrence of Sc clouds as a function of the radial distance from the eye of cyclone. From this figure, it evident that the Sc clouds most frequently occurs near the eye of cyclone with a peak frequency of occurrence of ~15%. The tops of Sc clouds are confined to ~2.5 km and these clouds can form up to a horizontal distance of 600 km region around the cyclone. It is well known that the dynamical response of ascending air in the DC clouds near the eye wall of cyclone will induce descending motion in the eye of cyclone and the descending air is responsible for the cloud-free zone in the eye. However, the low level convergence of moisture in the eye results in the formation of

Sc clouds, whose vertical development is inhibited by the downdrafts initiated by the adjacent DC clouds. The downdrafts in the eye give rise to an inversion layer in the lower troposphere that act as a lid to the raising air thus limiting the vertical development of the clouds. Apart from Sc clouds, it is also common to observe the Cu clouds in the eye. Figure 4.4 (g) shows the composite height distribution of frequency of occurrence of Cu clouds as a function of radial distance from the eye. The frequency of occurrence of these clouds shows a peak of ~10% with their tops reaching up to ~5 km. Reasonable amount of these clouds can be seen as far as ~600 km from the eye. Most of these clouds are formed in the shadows of the DC cloud outflows and under the downdraft regions of cyclones. Most often Sc and Cu clouds are formed adjacent to each other in cyclones. Thus Figure 4.4 depicts the composite height distributions of various clouds as a function of radial distance from the eye of a cyclone, which is consistent with the conceptual models of tropical cyclones. Furthermore, to have a comprehensive view of the cloud type distribution embedded in tropical cyclones, a contour map of frequency of occurrence of all clouds as a function of radial distance from the eye of the cyclone is generated as shown in Figure 4.6. This type of representation aids in visualizing what type of clouds dominates in which part of cyclone. The contour intervals are not same for all the clouds. The decrease of cloud tops as a function of the radial distance from the eye is more clearly seen in this figure. The peak in frequency of occurrence of the DC clouds is followed by Ci cloud peak. It is also noted that there are distant regions showing peak in the frequency of occurrence of various clouds embedded in cyclone. For example, the Ns clouds show their frequency of occurrence at five distant bands from the cyclone's eye in Figure 4.6 (at 100, 300, 600, 800 and 900 km) with decreasing frequency of occurrence from one band to another. Overall, the mean cloud type distribution [mean over 0-1000 km horizontal extent of cyclones] is investigated. Apart from the biases discussed in previous sections, the composite cloud distribution discussed in the present study may also be affected by the asymmetry of cloud distribution with respect to the eye of a cyclone. However, the consistency of the cloud distribution discussed in the present study with that of the conceptual models is very encouraging.

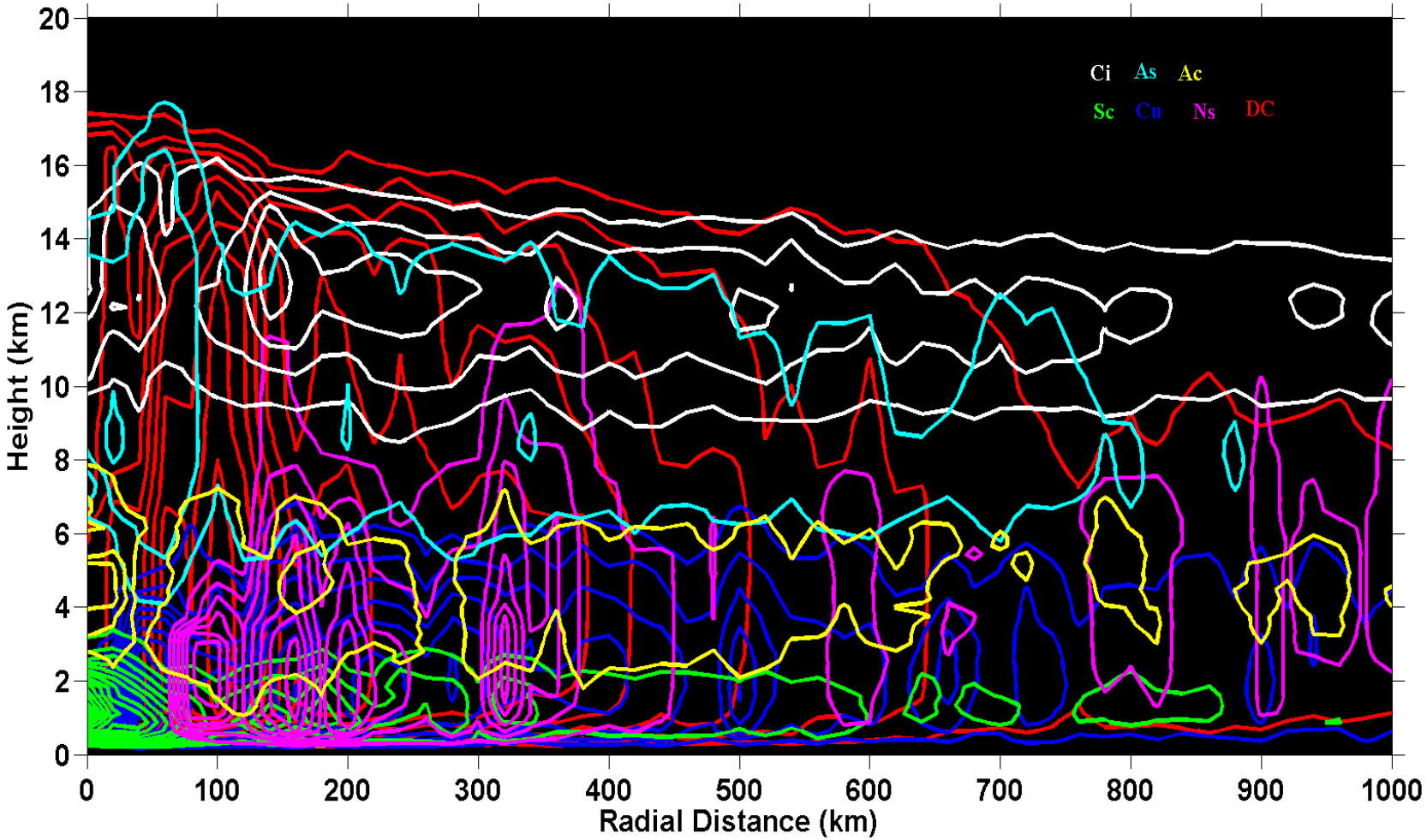

Figure 4.6: Comprehensive view of the frequency of occurrence of various clouds embedded in the tropical cyclones. The contour intervals are not same for all the clouds. White, cyan, yellow, green, blue, magenta and red colors for Ci, As, Ac, Sc, Cu, Ns and DC clouds respectively.

4.5 Summary

CloudSat observations of tropical cyclones formed in the North Indian Ocean surrounding the Indian subcontinent during the years 2006 to 2014 are investigated to study the three dimensional cloud type distribution over the tropical cyclones. A total number of 25 tropical cyclones (8 in Arabian Sea and 17 in Bay of Bengal) observed by CloudSat are analyzed to construct the composite vertical structure of cloud type distribution. The cloud type distribution reproduced many of the known tropical cyclone features such as the DC clouds at the eye walls, Ci cloud anvils and cloud free zones between the inner and the outer rainbands known as Moat in the lower troposphere. It is found that the DC clouds are always accompanied by As and Ci clouds and their peak frequency of occurrence is ~ 50 % at ~50-100 km radial distance from the cyclone's eye. It is also observed that the DC clouds extend up to ~ 16 km near to the eye and their top altitudes decrease gradually as a function of radial distance from the eye of cyclone. The Ci cloud distribution showed a peak frequency of occurrence of 30% (at ~14-15 km altitude) at around ~200 km radially from the eye. The peak in Ci clouds is observed right next to the peak in the DC clouds indicating that Ci clouds form from the outflows of the DC clouds. However, the distribution of As clouds showed some discrepancy with respect to the present understanding of these clouds. This is probably due to CloudSat classifying the upper portion of the slanted DC cloud as As clouds. One more envisaged possibility is that the transition region between the DC and their outflows may also be classified as As clouds by the CloudSat algorithm. The Sc clouds are observed in the center of cyclone as their vertical growth is inhibited by the downdrafts induced by the adjacent DC clouds, which limit their cloud top height to ~ 2.5 km. The Cu clouds are observed in the shadows of the DC cloud outflows and the significant amounts of these clouds are seen as far as ~ 600 km radially from the center of the eye. Most frequently, the Sc and Cu clouds are observed adjacent to each other in the present study. It is found that there are distant regions showing the peak in frequency of occurrence of various clouds embedded in the cyclone. Thus the present study brought out the three-dimensional distribution of cloud types and associated dynamics in and around tropical cyclones along with their radiative impacts. It is now

known that the clouds around tropical cyclones are strongly connected by their internal circulation and play an important role in their development as well as motion. There is a need to assess the ability of present numerical models to simulate the cloud processes in tropical cyclones. It is useful to know the three-dimensional distribution of cloud types and associated dynamics around tropical cyclones. In this context, the present chapter by bringing out the three-dimensional distribution of cloud types and associated dynamics in and around tropical cyclones has important implications in understanding the cloud processes in tropical cyclones.

Chapter 5

Multi-layered cloud distribution and associated dynamics

"We drift apart clouds on different wind
Long we fought to hold our misty grips
But in the end we were again
Clouds on different winds"
-Atticus

5.1 Introduction

Owing to its importance in hydrological cycle, general circulation and radiative forcing, any aspect of clouds is a cynosure to meteorologists as well as common men across the globe. As the accurate representation of cloud processes and their feedback in the general circulation models are the need of the hour, cloud studies have been placed at a high pedestal by the meteorological community. By now, it is well established that the clouds remain the largest uncertainty in climate model forecasts [*Stephens*, 2005; *Randall et al*., 2007]. By interacting with both short and longwave radiation, clouds play crucial role in the radiative budget at the surface, within and at the top of the atmosphere. Understanding of the atmospheric radiative heating and latent heat release associated with clouds are central to any study dealing with general circulation as well as precipitation. Realizing the importance of clouds in Earth's radiation budget and hydrological cycle, a host of studies carried out in the past to divulge this ubiquitous feature of the earth's atmosphere. Most of these studies emphasized the importance of cloud vertical structure on atmospheric circulations, including the effects of variations of cloud top and base heights, cloud

layer thicknesses, and the vertical distribution of multilayered clouds as they significantly modify vertical and horizontal gradients in radiative and latent heat fluxes [*Webster and Stephens*, 1984]. The unanimous view of many of the atmospheric researchers is that the detection of multilayered clouds is important from climate standpoint and any attempt to quantify the global warming should include the radiative impacts of clouds [*Gupta et al*., 1992; *Wielicki et al*., 1995; *Wang et al.,* 2000; *Chen et al*., 2000a]. Thus it is important to have quantitative measurements of the geographic distribution and variations of cloud vertical layers. There were studies in the past, which emphatically showed the cloud effects on the general circulation [*Slingo and Slingo*, 1988 ; *Randall et al.,* 1989; *Wang and Rossow,* 1998]. Especially, *Randall et al*. [1989] examined the response of the atmospheric circulation by varying the cloud vertical distributions in the models. These authors confirmed that the circulation is sensitive to the vertical distribution of clouds, which modifies the vertical radiative heating of the atmosphere. *Wang and Rossow* [1998] performed a series of experiments using the NASA Goddard Institute for Space Studies GCM to study the effects of vertical distribution of clouds on atmospheric circulations. These authors focused on the importance of the vertical structure by exploring quantitatively the different effects between single and multilayered clouds. One of the important findings of this study was that the vertical gradients in the cloud distribution were more important to the circulation strength than horizontal gradients. *Rossow et al.* [2005] pointed out that the key to understand the cloud–dynamical feedback is determining the nature of the relation of radiative and latent heating rate profiles induced by cloud vertical structure. *Mace et al.* [2007] reported that the vertical distribution of zonally averaged hydrometeor occurrence and showed the relationship of clouds with components of the atmospheric general circulation. So, it becomes inevitable to establish the vertical distribution of clouds and to study their role in modifying the atmospheric circulation for better understanding of cloud feedback mechanisms in totality.

The ground based observations using Radars, Lidars and radiosondes provided much needed microphysical properties of clouds, which lead to better understanding of precipitation and radiative properties of the clouds. Even though the ground based techniques provide a wealth of information on clouds, they are not capable of providing the spatial distribution of clouds and their properties on large scale. On the other hand, the regional as well as global distribution of clouds is provided by space based observations. Most of the space based passive remote sensing techniques provide the twodimensional distribution/properties of clouds. Most available satellite measurements from nadir pointing passive remote sensing instruments are limited to retrieval of information about the uppermost cloud layer or column integrated properties whereas active remote sensing techniques provide the vertically resolved cloud properties thus providing three-dimensional perspective of the clouds [Simpson et al. 1988]. The spaced based active remote sensing instruments are providing extensive observations on vertical distribution of clouds. The importance of having multilayer cloud information has been realized very early and many attempts were made in the past to retrieve the same. *Baum et al*. [1995] proposed a method to retrieve the multilayer cloud properties from AVHRR observations using a modified multispectral, multi resolution method. Using this method these authors discriminated the single and multilayer clouds. *Wang and Rossow* [1995] established a method that uses the rawinsonde observations to determine cloud vertical structure. In a seminal study, *Wang et al.* [2000] reported climatology of cloud vertical structure using 20 years of global rawinsonde observations of humidity profiles. This climatology provided much needed information about single layer and multilayer clouds including top and base heights along with thickness of each layer. However, this study was limited to the rawinsonde stations spread over the globe and could not provide the complete picture of multilayer cloud distribution across the globe. Later, *Huang et al*. [2005] proposed a multilayer cloud retrieval system by combining satellite visible and infrared radiances and surface microwave radiometer measurements. However, this

detection method works only in non precipitating conditions. On the other hand, recent cloud radar and lidar observations onboard CloudSat and CALIPSO respectively as a part of the A-Train mission providing a wealth of information on the three dimensional distribution of clouds on a global scale [*Stephens et al*., 2002].

The combination of passive and active remote sensing instruments operating in the A-Train mission providing unprecedented information on cloud vertical structure, aerosol climate effects, and more accurate estimates of surface longwave fluxes and atmospheric heating rate profiles. *Luo et al*. [2009] documented the seasonal variations in occurrence frequency and location of single and multilayer hydrometeors. *Wu et al*. [2009] investigated the differences/similarities of vertical distributions of cloud occurrence frequency from various passive and active sensors. Recently, *Li et al*. [2011] accessed the radiative impacts of single and multilayered clouds using A-Train observations. The results indicated that the multilayer clouds have a significant impact on radiation budget due to their high frequency of occurrence globally and obvious radiative effect differences with that of single layered clouds. However, this study didn't distinguish how many layers are there in the multilayer clouds. The above discussion thus emphasizes the importance of cloud vertical structure for climate related studies. However, there are very few studies in the past focusing on this issue, especially using satellite based active remote sensing techniques. Thus the present chapter studied the multilayer cloud structures across the globe using 4 years of [2007–2010] CloudSat and CALIPSO observations. This chapter describes the geographical distribution and frequency of occurrence of multilayered clouds, which are resolved into one, two, three, four and five layer clouds across the globe. As most of the earlier studies did not further classify the multilayered clouds into two, three, four and five layer clouds, the present study focus on this issue, which is a relatively new component in the ongoing studies of vertical structure of clouds. An attempt is also made to discuss the manifestation of large circulations in geographical distribution of multilayer clouds.

5.2 Data and methodology

With the launch of CPR onboard CloudSat in early June 2006 and CALIOP onboard CALIPSO in late April 2006, unprecedented information on vertical distribution of hydrometeors are available for the atmospheric research community. CloudSat and CALIPSO observations have been extensively used in the recent past to study the cloud vertical structure. For the present study, 2B GEOPROF-LIDAR, a combined auxiliary product of CloudSat and CALIPSO observations are used. This product is produced by extracting the maximum information from the combined potentially spatial overlap region by radar and lidar sensors. This product provides information on the parameters related to vertical structure of clouds, which includes the location of cloud layers in the vertical column, cloud base, cloud top and number of cloud layers. Details of CloudSat and CALIPSO can be found in *Stephens et al*. [2008] and *Winker et al.* [2007] respectively. The synergy between these two instruments can nearly provide a complete picture of cloud distribution across the globe. *Mace et al*. [2009] suggest that greater than 90 % of cloud layers are correctly identified as cloud, by making use of the combination of the CloudSat and CALIPSO observations. The 2B GEOPROF-LIDAR product contains the combined cloud mask information, which indicates the confidence level in detection of clouds, ranging from 0 to 40. A cloud mask of 30–40 indicates the high confidence detections and less false detections (i.e., less than 2 % for 30 and less than 0.2 % for values of 40). More details on CloudSat products can be found in the CloudSat Data Products Handbook [http://www.cloudsat.cira.colostate.edu]. Four years [2007–2010] of 2B GEOPROF-LIDAR data product have been used for the present study with cloud mask of 30–40. The maximum number of cloud layers provided by this product is five. From this product, seasonal variations in frequency of occurrence of one, two, three, four, and five layered hydrometeors are determined over the globe. First, the observations are gridded into 2.5° × 2.5° [longitude × latitude] for each season and then frequencies of occurrence of each cloud layer are determined within the grid. Table 5.1 illustrates the method followed to determine the frequency of occurrence of each layer. In each

grid, the number of occurrence of each layer is counted and the same is normalized by the total number of CloudSat observations in each grid [*Subrahmanyam and Kumar,* 2017]. Following this procedure, the seasonal variation in frequency of occurrence of each cloud layer is determined across the globe. For interpreting the observed geographical distribution of multilayered clouds in terms of largescale circulation, Modern Era Retrospective analysis for Research Application [MERRA] data during the present observational period are used to estimate the meridional mass stream function [MSF] and vertical velocities. The details of MERRA reanalysis can be found in *Rienecker et al*. [2011].

Table 5.1 Illustration of the method followed to determine the frequency of occurrence of multi-layer clouds.

1	1	1	1	2	2	2	3	4	4
1	1	1	1	2	2	2	3	4	4
1	1	1	1	1	2	3	3	4	4
1	1	2	2	2	2	3	3	4	5
1	1	0	2	2	2	3	3	4	5
1	1	1	2	2	3	3	3	4	5
1	0	1	2	2	3	3	4	4	5
0	0	1	2	0	3	3	4	5	0
1	1	0	0	2	3	3	4	5	5
1	1	1	2	2	3	3	4	5	5

2.5 degree

2.5 degree

One- layer cloud Occurrence - 28; Two- 22; Three- 19; Four- 14; Five- 9;
Total no. of observations – 100
Percentage for One-layer clouds = (28/100)*100=28 %

5.3 Spatial distribution of frequency occurrence of one layered clouds

The frequency of occurrence of various cloud layers ranging from one to five layers is quantified by using the above method discussed in section 5.2. The observations are categorized into four seasons viz., December–January– February [DJF], March–April–May [MAM], June– July–August [JJA] and September–October–November [SON]. For each season, 4 years of observations during 2007–2010 are averaged to obtain the mean global distribution of each cloud layer. Figure 5.1 (a–d) shows the mean seasonal variation of frequency of occurrence of single layer clouds during DJF, MAM, JJA and SON over the globe respectively. The striking feature of this figure is, the high frequency of occurrence of single layer clouds during all the seasons over the Southern Ocean. The single layer clouds more or less uniformly distributed over the entire longitudinal belt over 60°–70°S. The frequency of occurrence of single layer clouds over this region ranges from 60 to 70 % with minimal seasonal variations. However, a close look at Figure 5.1 (a) and (c) reveals that the frequency of occurrence of single layered clouds over the Southern ocean is relatively high during Austral summer as compared to winter. From ISCCP, it is known that the mean cloud fraction over the Southern Ocean is about ~0.79 [*Rossow and Schiffer*, 1999]. *Trenberth and Fasullo* [2010] reported that the climate model errors in simulating top of atmosphere fluxes over the Southern ocean are among the largest anywhere in the world. In this regard, any information on these cloud regimes becomes very important to accurately represent them in climate models. These recent model simulations emphasized the importance of having quantitative information on these cloud regimes. Recently, *Haynes et al.* [2011] using multiple datasets of ISCCP and CloudSat–CALIPSO observations investigated the characteristics of the Southern ocean cloud regimes and their effects on the energy

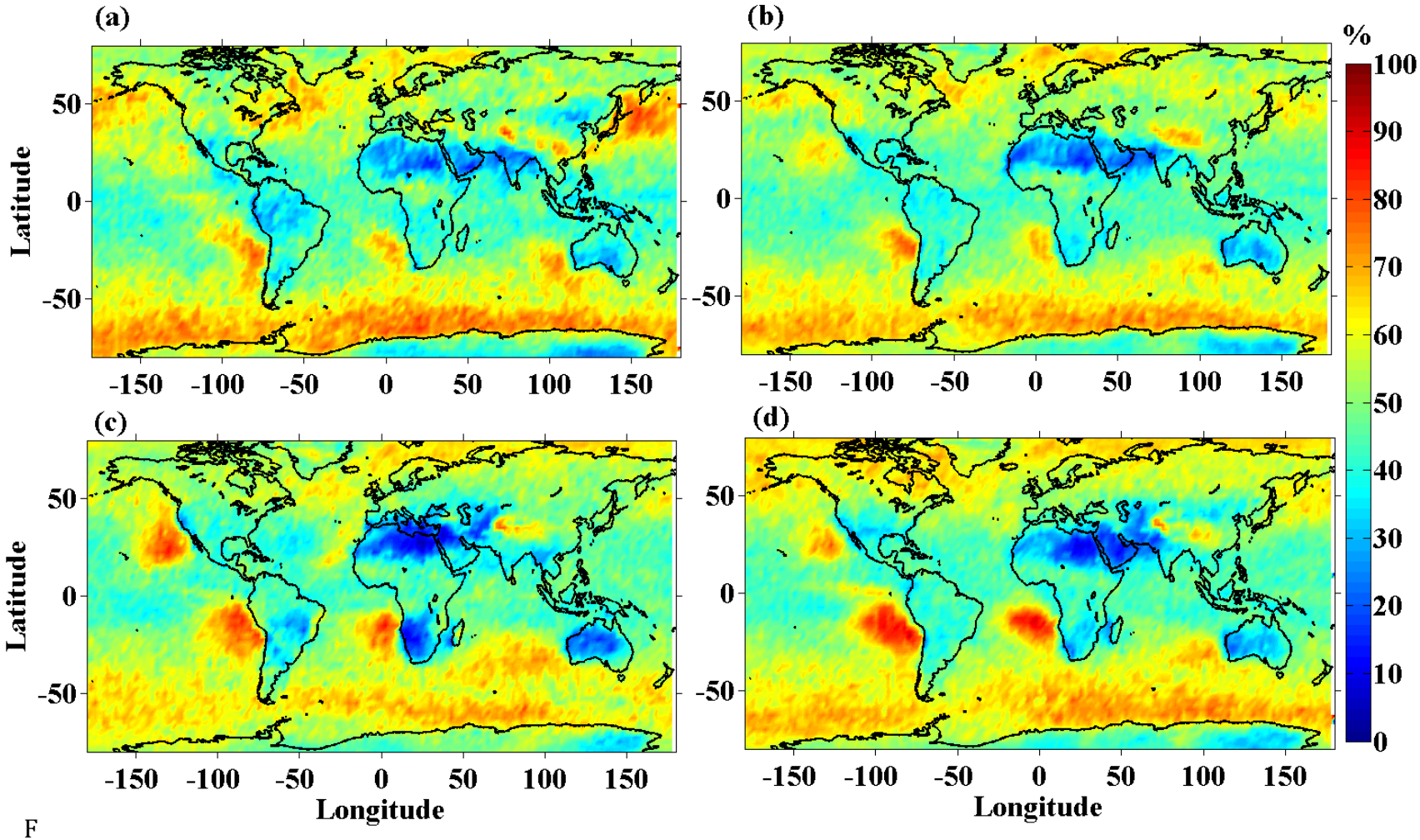

Figure 5.1: Four years mean seasonal variation of frequency of occurrence of single layer clouds during (a) DJF, (b) MAM, (c) JJA and (d) SON across the globe.

budget. These authors reported the vertical structure of the clouds as well as the occurrence of precipitation over the Southern oceanic region. The present study also emphatically brings out the seasonal variations in distribution of single layered cloud over the Southern Ocean and further discussion on vertically resolved multilayer clouds over this region, which is relatively new compared to earlier studies, are discussed in this chapter.

Apart from Southern and Northern hemispheric high latitudes, high fraction of single layer clouds also occur over the South Pacific Ocean near west coast of the South America [~ at 20°–30°S latitudinal belt] and over the South Atlantic Ocean near west coast of South Africa. These two cloud regimes show pronounced seasonal variation with maximum occurrence during SON [~80 %] and minimum during MAM [~60 %]. An additional patch of high fraction of single layered clouds occurs over the North Pacific Ocean near west coast of the North America [~ at 20°–30°N latitudinal belt], which shows maximum during JJA and minimum during DJF. On the other hand, very low frequency of occurrence of one layered clouds can be noticed from Figure 5.1 (a–d) over the North and South Africa, the Middle East and Australia over the 20°–30° latitude belt in both the NH and SH. Even though the low frequency of occurrence of one layered clouds is observed over the same geographical locations during all the seasons, they exhibit pronounced seasonal variation in magnitude with very low fractions during JJA in both the hemispheres. However, it is very interesting to note the couplet of low and high fraction of one layer clouds over the descending branch of the Hadley cell, which is more prominently seen during JJA over the west coast of South Africa and South America [*Subrahmanyam and Kumar,* 2017]. It is expected to be cloud free zone over the descending branch of the Hadley cell. Over the land, the driest regions are found over the descending branches of Hadley Cell. However, over the oceanic regions of Hadley Cell descending branch, due to availability of moisture in the lower levels, single layer clouds can form as observed in Figure 5.1. A detailed discussion on Hadley cell circulation and their relation to single layer clouds will be

discussed in section 5.6.

Apart from abovementioned regions, relatively high fraction of single layer clouds are observed over the Himalayan mounts in the 30°–35°N latitudes. The occurrences of single layered clouds are observed during all most all the seasons with occurrence frequency of 50–60 %. During the DJF i.e. boreal winter, the weather over these regions is dominated by Western disturbances [*Dimri et al.*, 2015] and during JJA i.e., boreal summer by Asian summer monsoon. The topographical features of this region plays vital role in observed cloudiness over these regions during winter and summer seasons. One more striking feature of Figure 5.1 (a–d) is the high occurrence [~60 %] of single layer cloud over Northern Hemisphere high latitudes. Over this region, the frequency of occurrence of one layered clouds is high over the oceans compared to land. One can notice the strong seasonal variation with winter maximum in single layered cloud occurrence over Pacific and Atlantic Ocean at latitudinal belt of 40°–60°N. It is also interesting to note the band of propagating clouds over the Atlantic Ocean sandwiched between Europe and Green Land, coinciding with the midlatitude storm tracks [*Hoskins and Hodges*, 2005; *Bengtsson et al*., 2006 ; *Yuan et al*., 2009; *Dong et al*., 2013]. Unlike over Southern ocean where single layered clouds uniformly distributed along the longitude, over Northern high latitudes, single layered clouds are not uniformly distributed [*Subrahmanyam and Kumar,* 2017]. Thus the seasonal variations in frequency of occurrence of single layered clouds are brought out using the 4 years of combined observations of CloudSat and CALIPSO. The distribution of single layered cloud occurrence and their association with largescale circulations are discussed in section 5.6.

5.4 Spatial distribution of frequency occurrence of two and three layered clouds

Figure 5.2 (a–d) shows the distribution of two layered clouds during the DJF, MAM, JJA and SON seasons. Most of the earlier studies, distinguished the single and

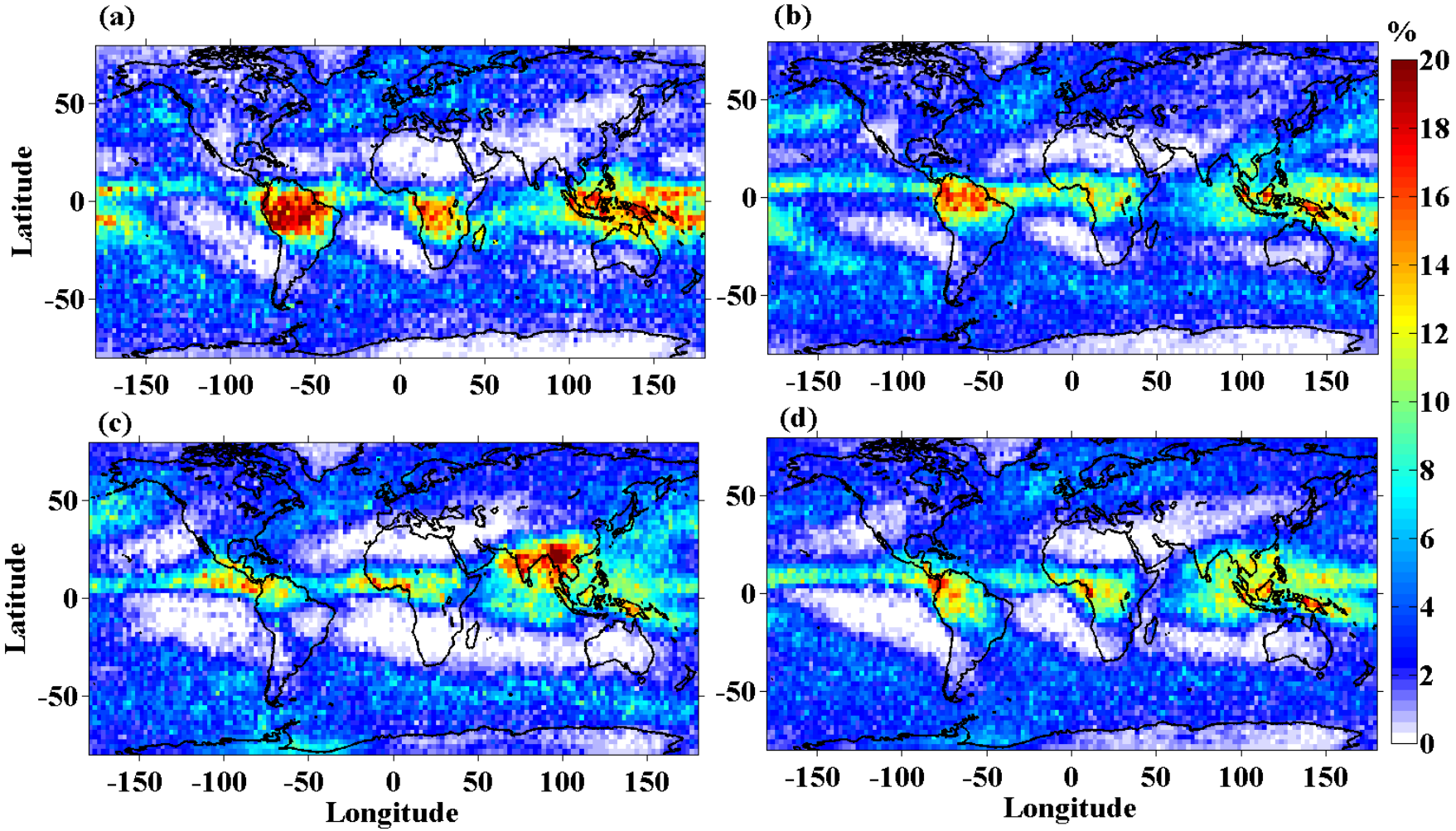

Figure 5.2: Same as figure 5.1 but for two-layer clouds.

multilayer clouds. However, the multilayer clouds were not further classified into two, three, four and five layered clouds. In the present study, the multilayer clouds are further classified into different layers as mentioned earlier, which is relatively a new component of the present study. One interesting inference that can be drawn from Figures 5.1 and 5.2 is the frequency of occurrence of single layered cloud is high over oceans, whereas in the case of two layered cloud it is high over land, especially over the low latitude and equatorial belt. One can notice the migration of ITCZ from South to North and back during DJF to SON. Over the equatorial region, the high frequency of occurrence of two–layer clouds [~40 %] is observed over South America, Central Africa and Indonesian regions during all the seasons with maximum during DJF and minimum during JJA over the 5°S– 5°N latitudes. The locations of relatively high frequency of occurrence of two layered clouds over the equatorial regions more or less coincide with the ascending limbs of the Walker circulation. Walker circulation and its association with multilayer clouds will be discussed later in this section 5.6. During the JJA, there is an increase in the frequency of occurrence of two layered clouds over Indian subcontinent and surrounding oceans, which persist during SON also. This observation can be readily attributed to the presence of Indian summer monsoon circulation over this region, which is dominated by the formation of various kinds of clouds such as cumulus, stratocumulus, cirrus etc. [*Subrahmanyam and Kumar*, 2013]. Over the Southern Ocean also, there is relatively high frequency of occurrence of two layered clouds, which are spread across the longitudes similar to single layer clouds shown in Figure 5.1. However, two layered clouds are relatively discrete as compared to one layered clouds over this region. Apart from these regions, over Arctic and North Pacific oceanic regions also one can notice the relatively high frequency of occurrence of two layered clouds. Thus the global distribution of two layered clouds is quantified and the regions with high frequency of occurrence of these clouds are identified. Figure 5.3 (a–d) depicts the three layered cloud distribution over the globe during the abovementioned four seasons. The three layered cloud distribution is more or

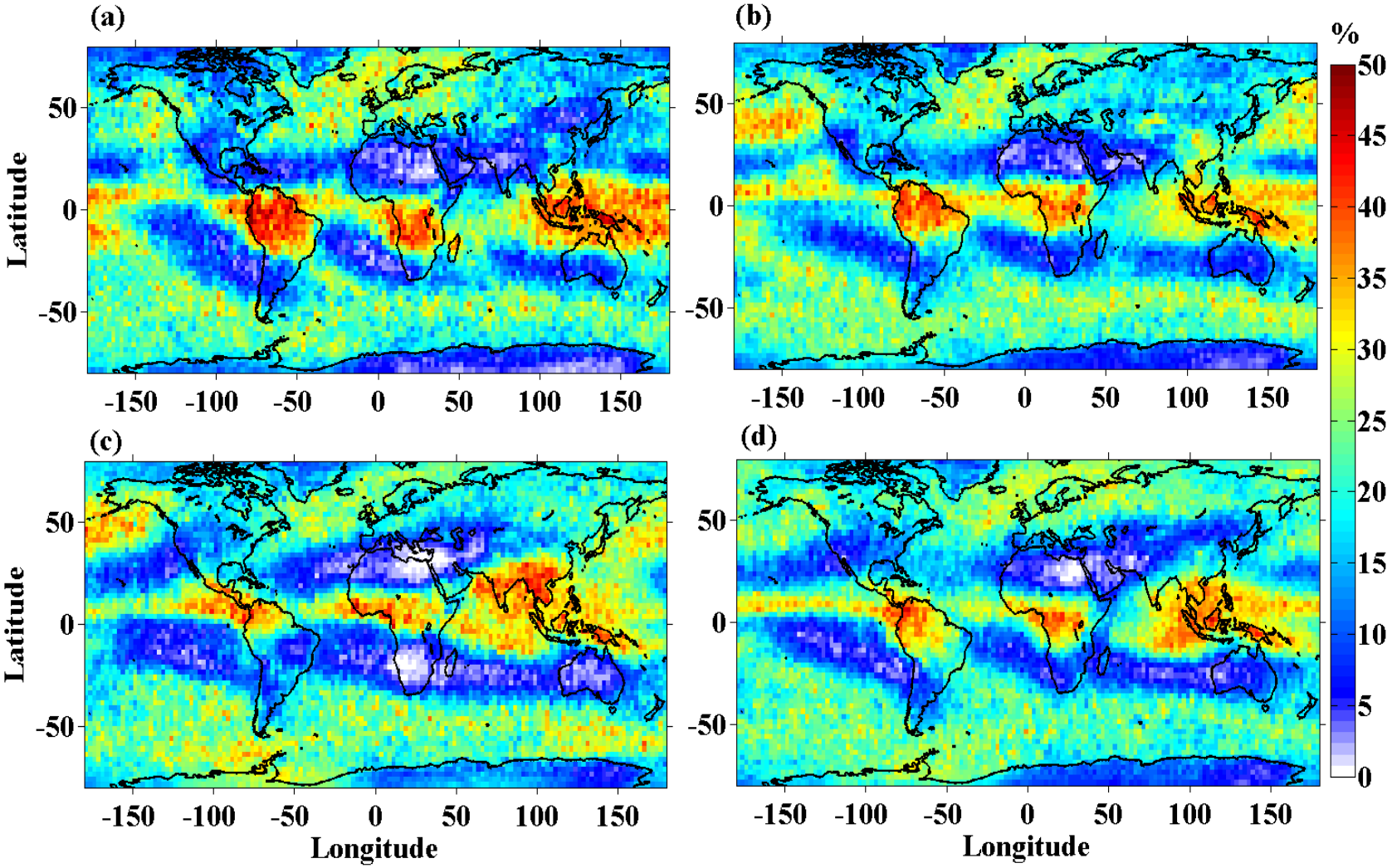

Figure 5.3: Same as figure 5.1 but for three-layer clouds.

less similar to two layered cloud distribution shown in Figure 5.2. The low frequency of occurrence of three layered clouds is again observed over the descending branch of Hadley cell. The signature of descending branch of Hadley cell is more pronounced in three layered clouds and the white patches in the Figure 5.3 indicate that there were no three layered clouds at all over that particular region during the observational period. Over the Southern Ocean, three layered clouds are observed but very discrete in nature. Over this region, there is a seasonal variation in the occurrence of three layered clouds with maximum occurrence during Austral winter. Apart from the Southern oceanic regions, a frequency of occurrence of 15–20 % in three layered cloud formation can be noticed over the Indian subcontinent and surrounding oceanic regions during boreal summer season, which can be directly attributed to the Indian summer monsoon. Abundance of deep convective clouds during the Indian summer monsoon period produce a copious amount of cirrus clouds, which are formed form the anvil of deep convective clouds and spread by the tropical easterly jet. Moreover, during this season, the monsoon low level jet brings moisture from the adjacent oceans to the Indian subcontinent thus aiding the formation of clouds. The prevailing dynamics during this season over ISM region is dominated by low level jet in the lower troposphere and tropical easterly jet in the upper troposphere. It is believed that the shears associated with these jets play a vital role in the formation of multilayered clouds by smearing the clouds. During the Austral summer also relatively high frequency of occurrence in these clouds are observed over ITCZ, especially over land regions viz., South America, Central Africa and Indonesia. These regions again coincide with the ascending limbs of walker circulation as discussed in the case of two layered clouds. Overall, many of the features of three layered cloud distribution are similar to that of two layered cloud distribution.

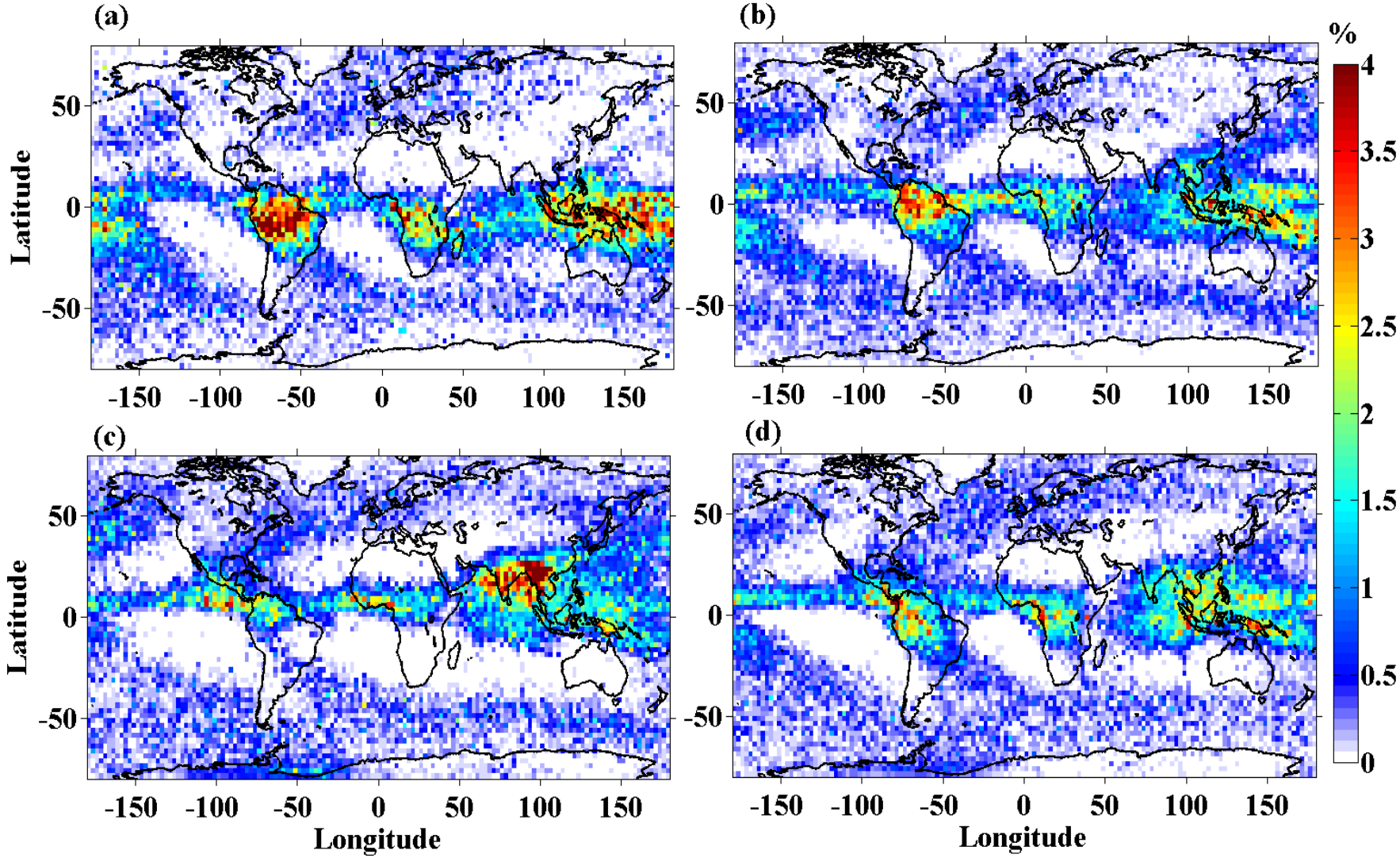

Figure 5.4: Same as figure 5.1 but for four-layer clouds.

5.5 Spatial distribution of frequency occurrence of four and five layered clouds

Figure 5.4 (a–d) shows the frequency of occurrence of four layered clouds over the globe during DJF, MAM, JJA and SON seasons. Even though the frequency of occurrence is very low compared to two and three layered clouds, the geographical locations, where the maximum occurrence of four layered clouds is found, are the same. The notable features very similar to Figures 5.2 and 5.3 are the equatorial maxima during almost all the seasons and pronounced maxima during JJA over the Indian subcontinent. However, one can note ~5 % of four layered clouds over isolated pockets over the Southern Oceanic region, especially during Austral Summer. The distribution of five layered clouds for all the four seasons is shown in Figure. 5.5(a–d). From this Figure, it is evident that the frequency of occurrence of five layered clouds is very low and limited to few geographical locations over the globe. The equatorial belt has the maximum occurrence of five layered clouds during all the seasons compared to all other latitudinal belts, except during JJA, where maximum occurrence shifts to Indian subcontinent as in the case of other multilayer clouds. During the JJA, as discussed earlier, Indian summer monsoon sets over the Indian subcontinent and the winds over this region is dominated by low level westerly jet in the 1–2 km region and tropical easterly jet in the 14–16 km region. The wind shears generated by these two jets in the lower and upper troposphere may play a crucial role in formation of multilayer clouds [*Sathiyamoorthy et al*., 2004]. Further, the latent heat released in the monsoon clouds over this region modifies the tropospheric thermal structure thus altering the vertical structure of static stability, which is important for the cloud formations and its vertical development [*Houze,* 1982; *Bhat et al*., 2002].

One more important observation from Figure 5.5 is the occurrence of five layered clouds over the midlatitude storm tracks, which are very prominently seen over the Southern Pacific and Atlantic Oceans during all the seasons. In the Northern Hemisphere also one can notice the occurrence of five layered clouds over the

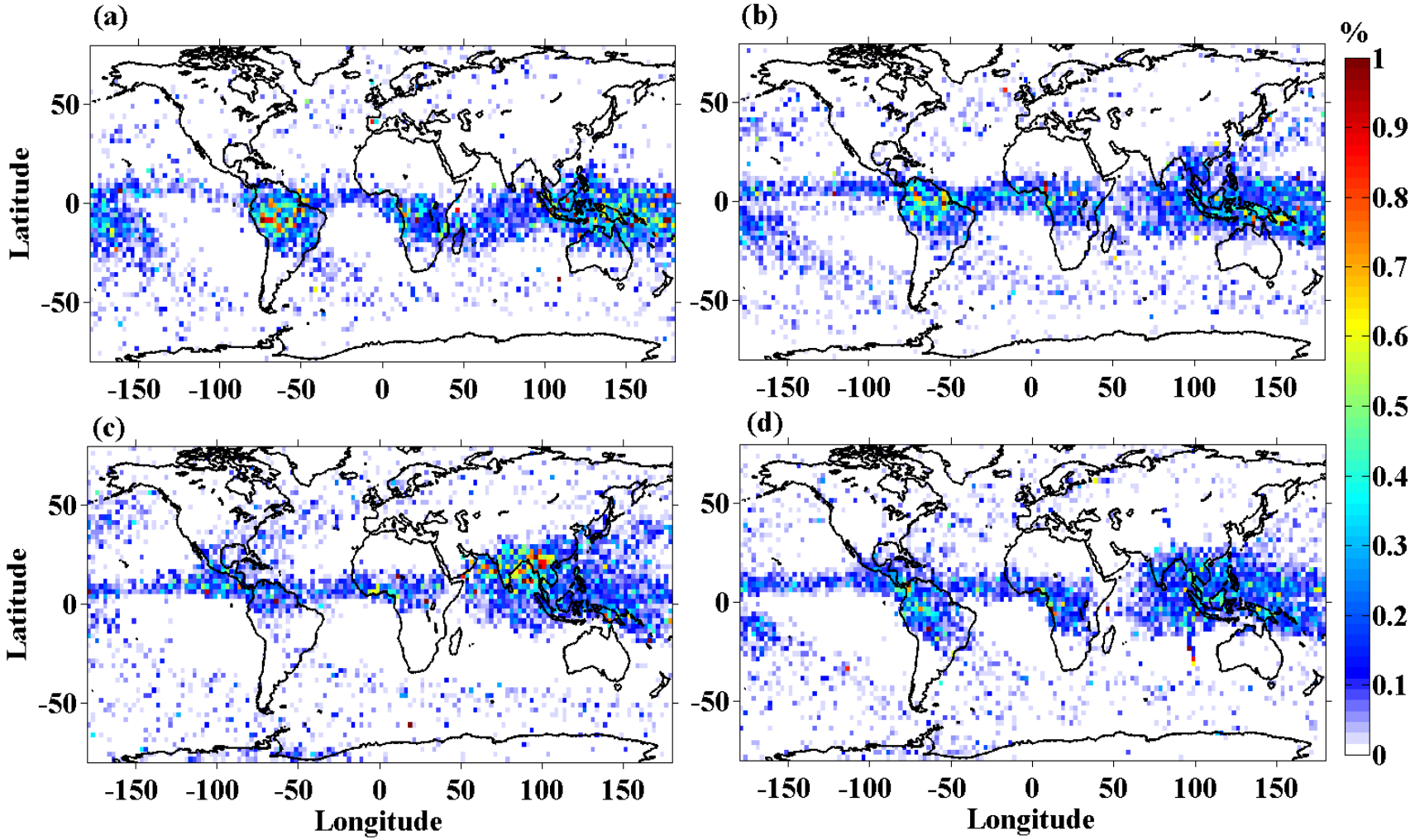

Figure 5.5: Same as figure 5.1 but for five-layer clouds.

Atlantic Ocean storm track. These observations of multilayer cloud distribution over storm track assumes their importance as there are reports, which suggest that these storm tracks are shifting towards the poles and becoming narrower [*Bender et al*. 2011]. To assess the consequence of this storm track shifting towards the poles and their effect on clouds and radiation budget, it becomes obvious to characterize the vertical structure of clouds over these regions.

5.6 Role of large-scale circulation in the formation multi layered clouds

In order to study the role of largescale circulation in the formation of one to five layered clouds depicted in Figures 5.1, 5.2, 5.3, 5.4 and 5.5, the global circulations viz., Hadley and Walker circulation along with the lower tropospheric stability [LTS] are analyzed. To examine the role of largescale circulation in formation of persistent clouds over Southern Ocean, the annual mean meridional mass stream function [MSF] is estimated using MERRA reanalysis data. The MSF can be used to delineate the largescale meridional circulation of the atmosphere. Figure 5.6 shows the annual mean MSF derived using monthly mean meridional winds during the observational period. The positive values of MSF indicate the clockwise circulation and negative values the anticlockwise circulations. From this Figure 5.6 it can be noted that the annual mean ascending limb of the Hadley Cell is located slightly off the equator into the NH. However, the location of ascending limb of Hadley Cell show pronounced seasonal variation, which migrates from SH to NH during Austral Summer to boreal summer [Figure not shown]. From Figure 5.6, it can be noted that at around 60°S there exists a rising limb of Polar cell. The vertical motions over these latitudes aid in transporting water vapor up in the atmosphere thus resulting in formation of clouds. The rising limb of Northern hemispheric Polar cell over 60°N as shown in Figure 5.6 , plays a key role in the formation of clouds observed over Northern Hemisphere [NH] high latitudes as in the case of their Southern Hemispheric [SH] counter parts. However, over NH the maximum cloudiness is confined to oceans, which can be attributed to the availability of water vapor in the ascending limbs of Polar Cell. The

high fraction of single layered cloud regimes observed over west coast of the South America, South Africa and North America [~ at 20°–30° latitudinal belt in respective hemisphere] coincide with the descending branches of Hadley cell as shown in Figure 5.6 on either side of the equator. At the same time, the spatial distribution of multi layered clouds depicted in Figures 5.2, 5.3, 5.4 and 5.5 shows very low cloud amounts over above mentioned regions consistent with the descending branch of Hadley cell. Thus it is clear from Figure 5. 2 that unambiguous Hadley cell signature

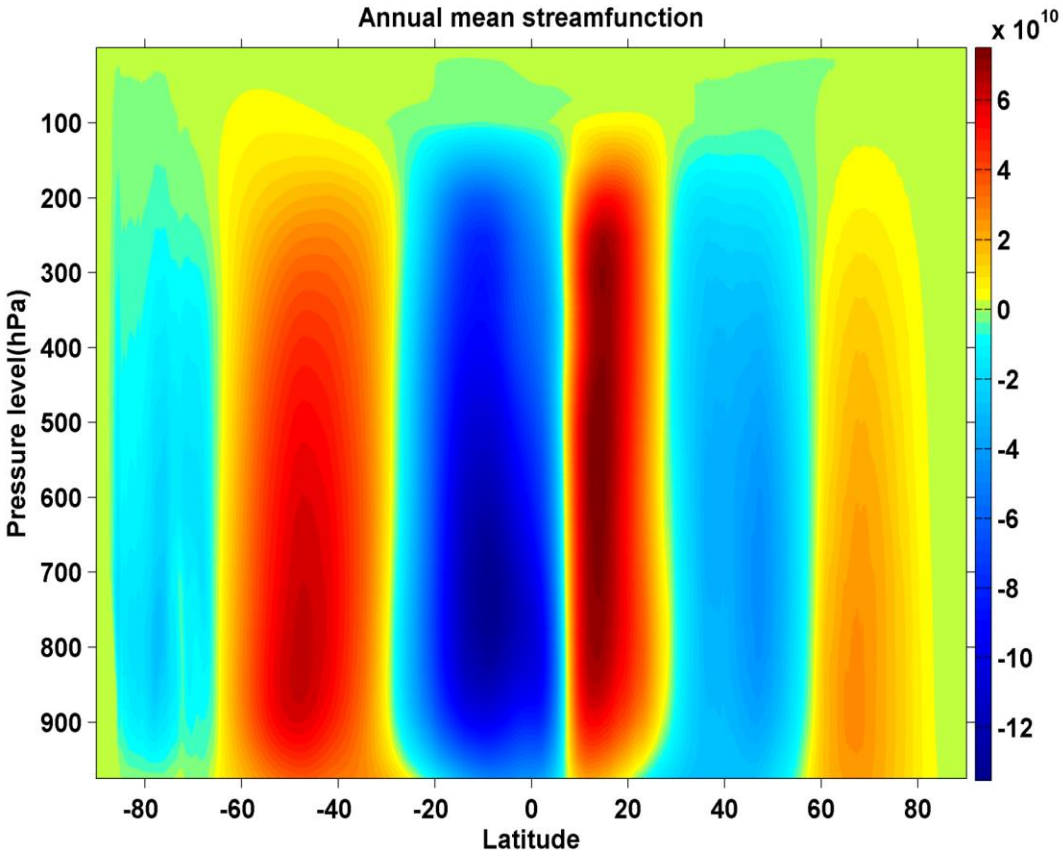

Figure 5.6: Annual mean meridional mass stream function (Kg/s) calculated using MERRA re-analysis data during observational period

can be found in multilayer cloud distribution rather than single layered cloud distribution shown in Figure 5.1. However, the pressure–latitude section of MSF shown in Figure 5.6 is a zonal mean representation of Hadley cell where as the multi

layered cloud distribution shown in Figures 5.1, 5.2, 5.3, 5.4 and 5.5 is zonally resolved. To investigate the zonally resolved Hadley cell, the vertical velocity data from MERRA reanalysis is examined at 500 hPa level [Figure not shown]. This analysis clearly shown the subsidence over the regions of high fraction of single layered clouds observed in the 20°–30° latitude belt of both the hemisphere as shown in Figure 5.1. Figure 5.7 (a–d) shows the 4 year [2007–2010] average LTS derived from monthly reanalysis data during DJF, MAM, JJA and SON respectively. LTS is derived using potential temperature difference between 700 and 1000 hPa levels [*Klein et al*., 1995]. The physical significance of LTS is that it indicates the vertical growth of clouds. Cloud may not vertically grow, if LTS is high and thus they may be confined to the lower levels of the atmosphere. From Figure 5.7, it is evident that LTS is high over the regions where the occurrence of single layered cloud is more especially over descending branches of Hadley cell. The seasonal variation of CAPE using COSMIC observations and their relation to occurrence of multilayered clouds are also investigated. The seasonal evolution of CAPE using COSMIC was reported by *Narendra Babu et al*. [2010]. It is observed that the locations of high CAPE magnitude are coincident with the region of multilayered cloud during all seasons.

Figure 5.8 shows the annual mean pressure–longitude section of vertical velocities [in Pa/s] averaged over 10°S–10°N latitudinal belt, which are obtained from MERRA reanalysis data. The positive values indicate the ascending motion and negative values the descending motion. From this Figure, it is evident that there are three distinct regions of ascending motion over the South America, Central Africa and Indonesia reaching up to 200 hPa level [~14 km]. The ascending limb over Indonesia is wide spread as compared to that of other two regions. These ascending limbs show pronounced seasonal variability in both, locations and intensities of ascending limbs. These ascending limbs play a vital role in formation of clouds and the background horizontal winds and thermal structure are also important in formation

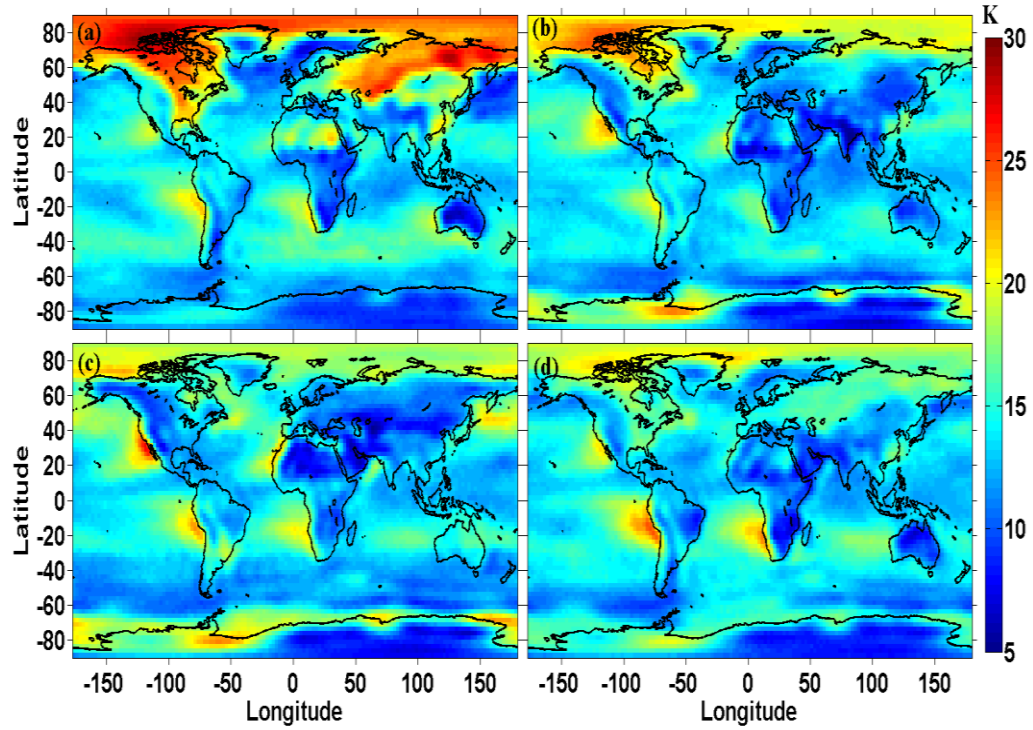

Figure 5.7: The four year (2007–2010) mean lower tropospheric stability for (a) DJF, (b) MAM, (c) JJA and (d) SON.

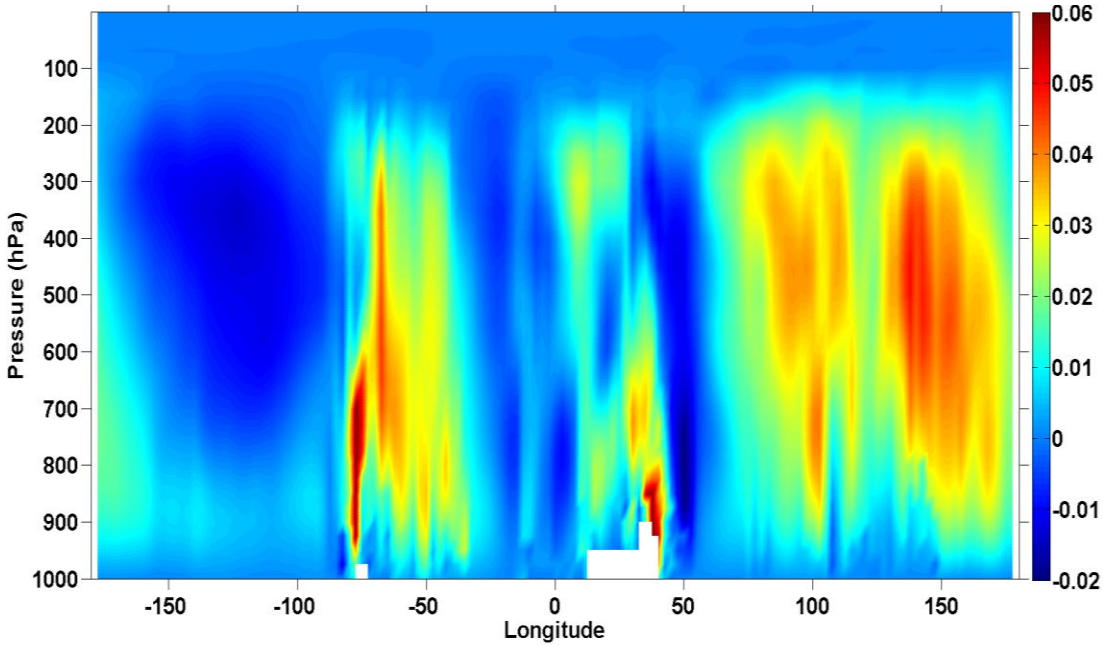

Figure 5.8: Pressure-longitudinal section of climatological mean vertical velocities (Pa/s) averaged over 10^0S-10^0N latitudinal belts.

of multilayered clouds. The studies on the formation of multilayered clouds associated with ascending limbs of Hadley cell and Walker cell are not readily available in the literature. However, there are studies on occurrence of deep convective systems over these regions [*Zipser et al*., 2006]. Deep convective clouds over these regions transport the moisture into the upper troposphere there by facilitating the formation of cirrus clouds. The detachment of anvils from the deep convective systems also contributes to the formation of cirrus clouds. Thus the geographical location of ascending limbs of Walker circulation coincides with the peaks of frequency of occurrence of multi layered clouds over low latitude and equatorial regions. After constructing the climatology of one, two, three, four and five layered clouds across the globe, an effort is made to further quantify the occurrence of multilayer clouds in terms zonal mean frequency of occurrence.

5.7 Zonal mean frequency of occurrence of multi layered clouds

Figure 5.9 (a–d) shows the zonal mean frequency of occurrence of one, two, three and four layered clouds respectively. The each latitudinal distribution curve shown in Figure 5.9 is the 4 years mean. Form this Figure, it can be noted that the single layer cloud distribution exhibits two peaks, one over Southern Hemispheric high latitudes and another over Northern Hemispheric high latitude coinciding with the ascending limb of Polar Cell. The minimum in frequency of occurrence of one layered clouds is observed over the Tropics as shown in Figure 5.9 during all the seasons. As mentioned earlier, there is very little seasonal variation in frequency of occurrence of single layered clouds. However, over the Southern Oceanic region occurrence of single layer clouds are relatively more during Austral summer as compared to Austral winter. The zonal mean latitudinal distribution of two layered clouds depicted in Figure 5.9 (b) show three peaks. Two peaks are found over the same region as in the case of single layered cloud distribution shown in Figure 5.9 (a). However, there is an additional peak over the equator in the two layered cloud

distribution, which can be attributed to the presence of ascending limbs of Walker circulation over these regions. Over the ascending limb of Walker circulation, the moist air is pumped up into the atmosphere resulting in the formation of clouds [*Liu and Zipser*, 2005; *Zipser et al*., 2006]. Depending on the stability of the atmosphere cumulus or deep convective systems form over these regions. Further the anvils of

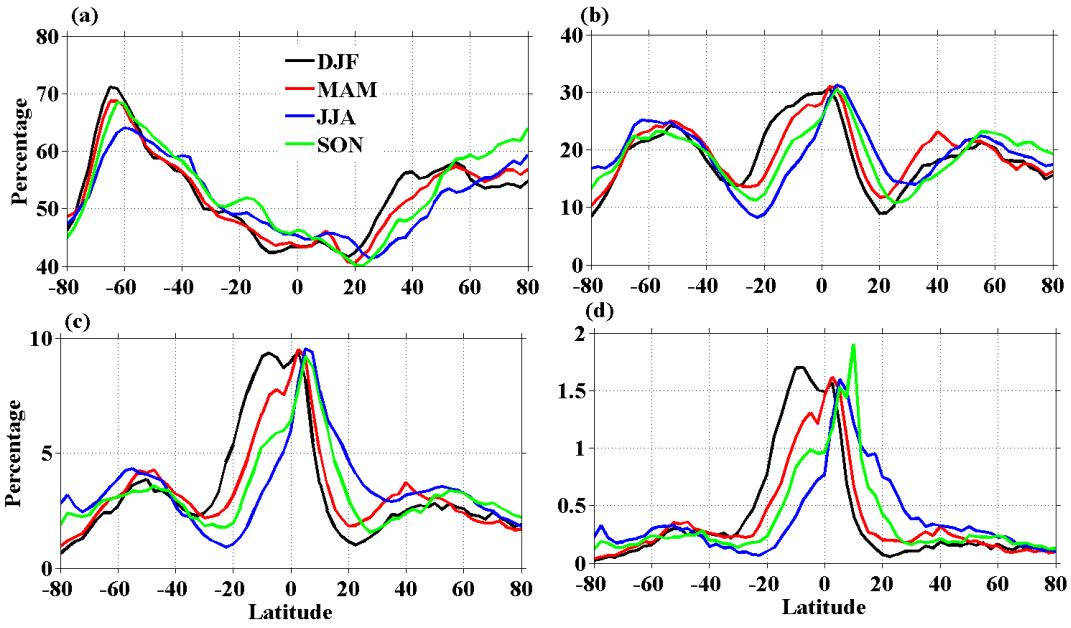

Figure 5.9: The latitudinal and seasonal distribution of zonal mean frequency of occurrence of (a) single, (b) double, (c) triple and (d) four-layer clouds.

deep convective systems may detach to form cirrus clouds, which on descending to lower heights can form midlevel clouds such as alto stratus clouds. So it is envisaged that the regions over the ascending limbs of Walker circulation are conducive for formation of multilayered clouds. The minimum in frequency of occurrence of two layered clouds observed over 20°–30° latitude belt over both the hemispheres in Figure 5.9 (b) correspond to the descending branch of Hadley cell. The presence of downdrafts over these regions will not be favorable for formations of multilayered clouds. It can also be noticed from the Figure 5.9 (b) that during JJA two layered cloud occurrence is maximum over tropical latitudes, where the occurrence of single layered cloud is less. It can be also noted that the Southern Hemispheric high

latitudes show maximum two layered cloud occurrence during winter and minimum during summer whereas the low latitudes show the exactly the opposite i.e., maximum during summer and minimum during winter. There is no systematic seasonal variation over Northern Hemispheric high latitude in the occurrence of two layered clouds, which show maximum during SON. However, the Northern Hemispheric low latitude follows the expected pattern showing maximum during summer and minimum during winter. The 4-year zonal mean latitudinal distributions of three layered clouds are shown in Figure 5.9 (c), which is very similar to Figure 5.9 (b) except for magnitudes. The SH exhibits pronounced seasonal variation in three layered cloud distribution as compared to the NH. Figure 5.9 (d) depicts the zonal mean four layered cloud distribution, which also exhibits similar variations as two and three cloud layers. The zonal mean five layered cloud distribution was also estimated [not shown], which shows preferential peak over the tropical latitude. The occurrence of five layered cloud is more over 0°–20°S latitude during DJF and MAM seasons, while it is more over 0°–20°N latitudes during JJA and SON periods. Thus Figure 5.9 shows the zonal mean latitudinal distribution of various cloud layers. The interannual variation of all the cloud layers shows that there is no significant variation except for maximum occurrence of all the cloud layers. From this Figure, it is evident that the occurrences of three and four layered clouds are more over the tropical latitudes compared to other latitudes. Over all, it is observed that on an average over the globe one, two, three, four and five layered clouds occur at 53, 20, 3.5, 0.4 and 0.04 % frequency respectively. Thus the present study brought out the preferential locations for multilayered cloud formations and the role of largescale dynamics in controlling their distribution.

5.8 Vertical and latitudinal distribution of zonal mean frequency of occurrence of multi layered clouds

After establishing the distribution of multilayer clouds, an attempt is made to establish the vertical distribution of cloud top and base of single as well as multilayer

clouds across globe. However, it is difficult task to present the abovementioned parameters across the globe as it is not practical to average the cloud parameters in a grid. For example, in a given grid of 2.5° × 2.5°, if we estimate the mean cloud base or top of one layer cloud, it can be misleading as there can be a cirrus cloud with high base/top or a cumulus cloud with low base/top. By averaging these two different cloud bases one can end up with misleading values. Thus the mean cloud top and base height in a grid cannot be representative of a given region. The alternative is to have a number of occurrences of various cloud top and bases ranging from 0.25 to 18 km height with 0.25 km interval. Considering the volume of the data to be processed and the number of illustrations to be made, the analysis is restricted to the summer and winter of the year 2007. First, the number of occurrences are estimated over the entire globe in 2.5° × 2.5° and the same is averaged across the longitudinal belt to provide zonal mean occurrences of particular cloud base and top as function of latitude as shown in Figures 5.10 (a–j) and 5.11 (a–j) for winter and summer, respectively. It is to be remembered that only the number of occurrences is averaged but not the cloud base and top. Left panel of Figure 5.10 depicts the latitudinal distribution of zonal mean occurrences of cloud bases of one, two, three, four and five layered clouds and the right panel shows the respective tops for the winter season of 2007. The striking feature of the one layered cloud base latitudinal distribution shown in Figure 5. 10 is the high occurrence of very low level clouds with base ranging from 0.25 to 1 km over both Southern and Northern mid and polar latitudes. However, the high occurrence of low level cloud base is spread over several latitudes in the Southern hemisphere as compared to its Northern counterpart. Over the Northern hemisphere midlatitude region around 40°–50°N, one can notice the secondary maximum in the occurrence of cloud base altitudes ranging from 3 to 6 km, which is not observed in the Southern hemisphere. Over the tropics, the maximum occurrence of single layer cloud base takes place primarily in three bands, 0.5–2, 4–5 and 10–15 km in the Southern hemisphere, where ITCZ prevails during boreal winter and in the Northern hemisphere it is in the 0.5–2 and

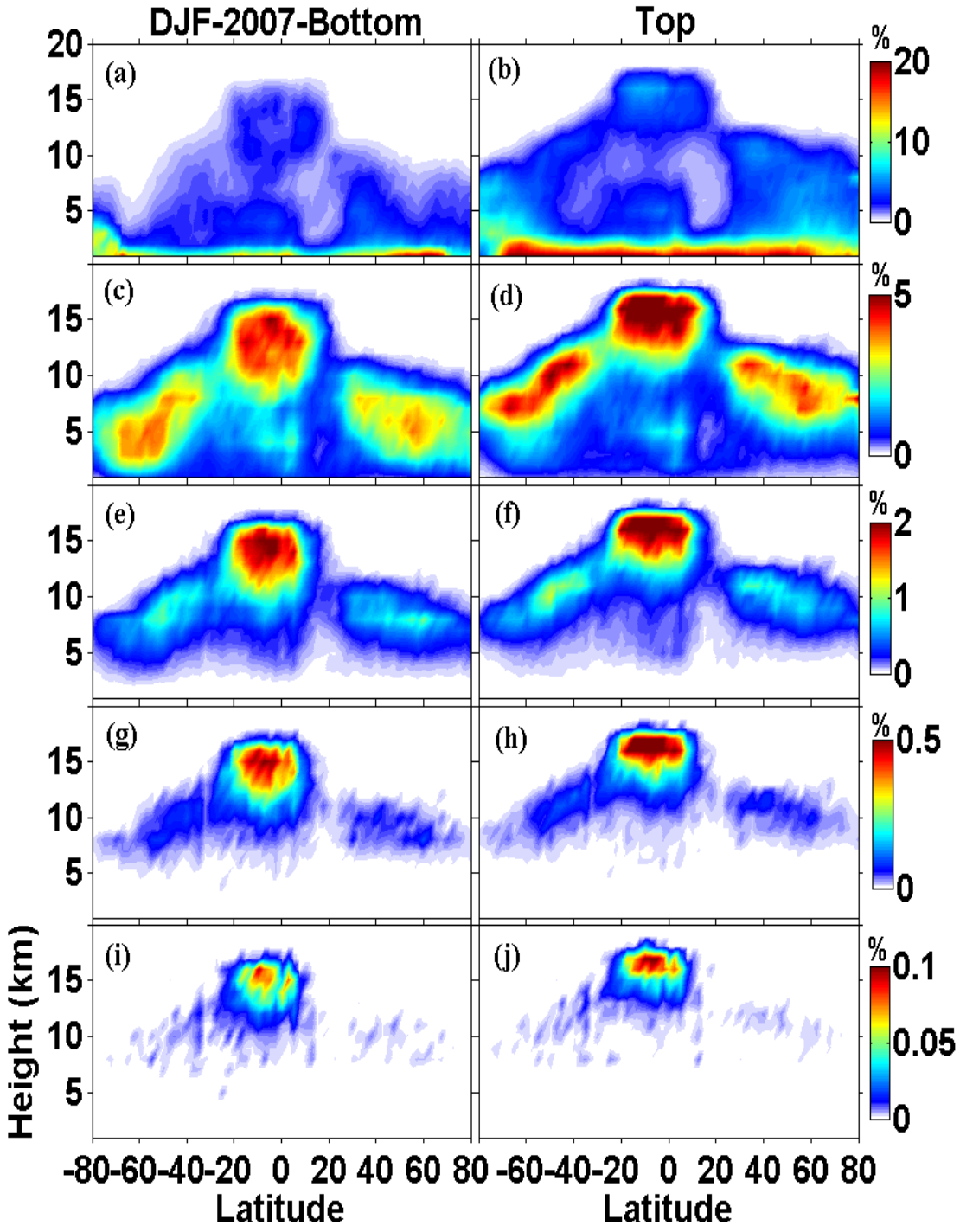

Figure 5.10: Left panel: The latitudinal distribution of zonal mean occurrences of cloud base altitudes of one-, two-, three-, four- and five-layered clouds for the winter season of 2007. Right panel: Same as left panel but for cloud top altitudes.

12–15 km range. The cloud top occurrence corresponding to the single layered clouds is shown in the Figure 5.10 b, which confirms that the most of the clouds observed over southern ocean and North Atlantic are indeed shallow clouds. However, over Northern mid and polar latitudes the cloud tops occur over a very wide band ranging from 1 to 10 km as compared to their southern hemispheric counterparts. One can notice the latitudinal structure of the tropopause, which limits the cloud top altitudes. The cloud tops occur in two bands [3–7 and 14–17 km] over the tropics in Southern hemisphere and in one band in the Northern hemisphere [14–17 km]. Even though, we can roughly infer the cloud type using their base and top altitudes, we restrict our discussion to their base and top altitudes.

Figure 5.10 (c) and (d) shows the latitudinal distribution of zonal mean occurrence of base and top altitude of two layered cloud for the boreal winter of 2007. It is to be remembered that the base and top of all the two layered clouds, which is present in all the multilayer cloud regimes namely two, three, four and five layered clouds are considered here. From this Figure, it can be noted that the two layered cloud bases exhibit similar distribution over mid and polar latitudes of both the hemispheres, which ranges from ~3 to 10 km. Over the tropical latitudes, the Southern hemisphere shows relatively more number of occurrence of two layered cloud base in the 9– 15 km band and spread over 0°–20°S latitudinal band whereas in Northern hemisphere it is limited to 0°–5°N. The latitudinal distribution of cloud top altitude shown in Figure 5.10 (d) also exhibit similar features as cloud base altitudes except that their altitudes are higher. It is interesting to note that the cloud top altitudes reach as high as 17 km in the tropics. Again, one can notice the latitudinal structure of tropopause pronounced in the latitudinal distribution of cloud top altitudes. The latitudinal distribution of base and top altitudes of three, four and five layered clouds also shows the similar structure of two layered cloud and are shown in the Figure 5.10 (e–j). The base altitudes of three layered cloud are in the range of 5–12 km over the mid and polar latitude of both the hemisphere and it is in the range of 12–16 km

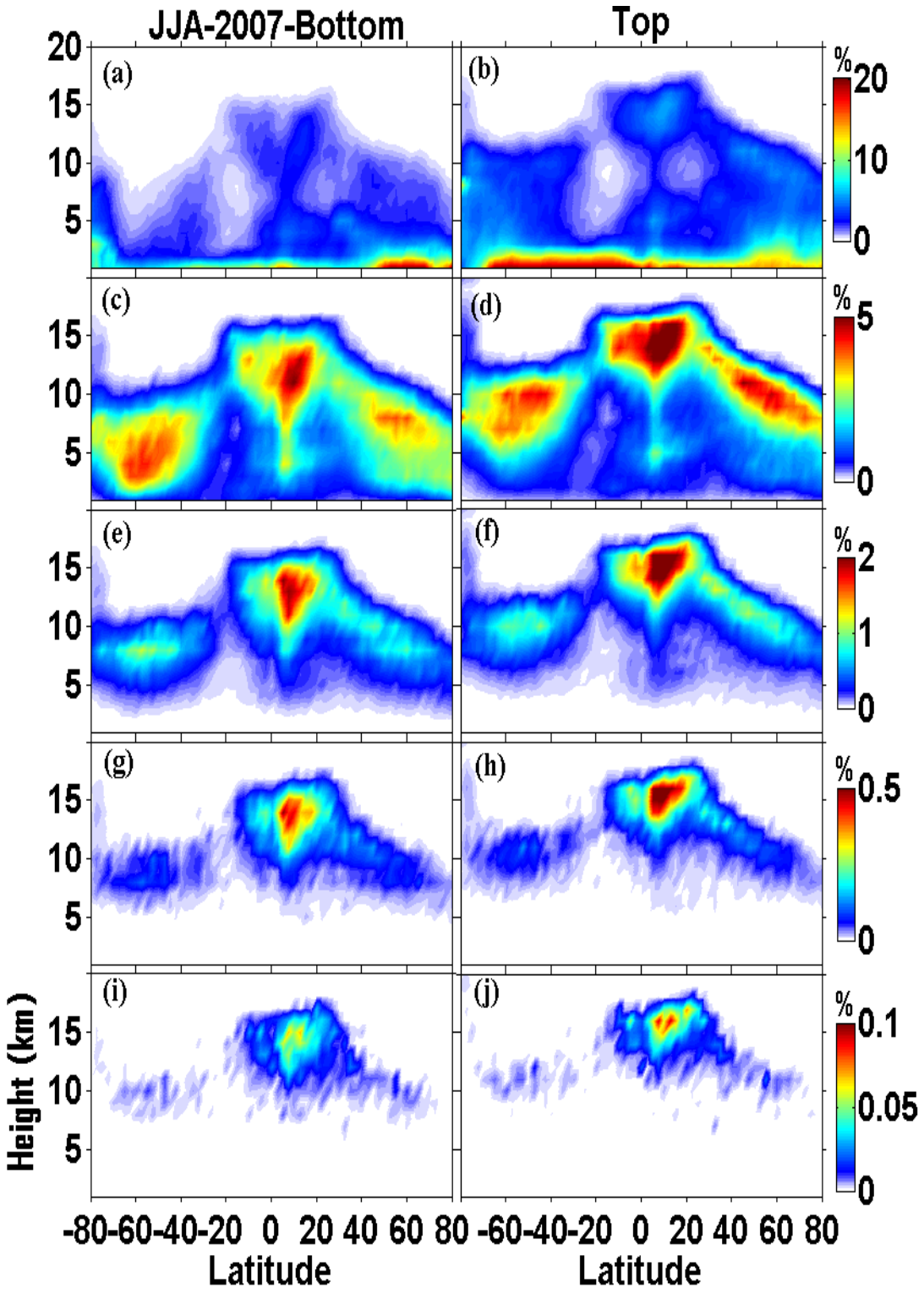

Figure 5.11: Same as figure 10 but for boreal summer of 2007.

in the Tropics. The cloud top altitudes of three layer clouds is also in slightly higher range as compared to their bottoms as shown in Figure 5.10 f as expected. However, the four layered cloud occurrences are limited to tropical and midlatitudes and the five layered cloud occurrence is limited to tropical latitudes only. As mentioned earlier the occurrence of multilayer clouds are relatively more and spread over wider latitudinal band in the southern hemispheric tropical latitudes as compared to the Northern hemisphere, which can be attributed to the position of ITCZ during the boreal winter. Similar latitudinal distributions during the boreal summer of 2007 were carried out and are shown in Figure 5.11 (a–j). The summer time latitudinal distribution of base and top altitudes of various clouds exhibit similar features as that of winter time distribution except that the maximum occurrence shifts to Northern hemisphere from Southern hemisphere along with the position of ITCZ. Thus for the first time, the cloud base and top altitudes of multilayer clouds segregated into different layers are brought out using CloudSat and CALIPSO observations. The frequency distribution of vertically resolved multilayered clouds and their base and top altitudes discussed in the present study will have profound implications in investigating the role of clouds in radiative forcing of the atmosphere as well as in the general circulation. At this juncture, where one of the largest uncertainties in the present day climate models is thought to be the representation of vertically resolved clouds and their feedback, the results presented here assumes its significance.

5.9 Summary

For the first time, the frequency of occurrence vertically resolved multilayer clouds across the globe has been established using 4 years of CloudSat Auxiliary product 2BGEPOROFLIDAR. This merged CloudSat and CALIPSO product can resolve cloud layers up to five. After gridding the observations into 2.5° × 2.5°, they were segregated into four seasons. Four years mean global distribution of one, two, three, four and five layered clouds are constructed and discussed in details. Interesting

features such as very high frequency of occurrence of single layer clouds over Southern Ocean, midlatitude storm tracks, west coast of South America and South Africa and their association with largescale circulations are discussed. The signature of descending branches of Hadley cell is very clear in multilayered cloud distribution maps as compared to that of single layered cloud distribution. Three regions over the equator [South America, Central Africa and Indonesia] are identified where more frequently multilayer clouds occurs. These regions coincide with the ascending limbs of Walker circulation. It is also observed that the maximum occurrence of multilayer clouds migrates along with the movement of ITCZ. Apart from the equatorial region, multilayer clouds are observed more frequently over Indian summer monsoon region and midlatitude storm tracks. On an average over the globe it is observed that one, two, three, four and five layered cloud occur at 53, 20, 3.5, 0.4 and 0.04 % frequency respectively. These global maps of frequency distribution of various cloud layers provide much needed information on where and when the multilayer clouds are observed more frequently including the number of layers. After constructing the frequency distribution, further the occurrence of multilayered clouds is quantified in terms of zonal mean frequency of occurrence. It is noted that the zonal mean latitudinal distribution of single layer cloud exhibits two peaks, whereas two, three and four layered clouds show three peaks. Thus, for the first time the global distribution of multilayered clouds and their association with largescales circulation are brought out using 4 years of CloudSat and CALIPSO observations. Further zonal mean frequency of occurrence of cloud as and top is constructed. The cloud top altitude distribution of various clouds exhibited the signature of latitudinal structure of tropopause as expected. These are the first latitudinal distribution of vertically resolved multilayer cloud base and top altitudes estimated using space based active remote sensing observations, which can be used to verify the outputs of climate models as well as can be used to quantify the role of vertically resolved clouds in earth's radiation budget and global circulation.

Chapter 6

Spatial distribution of latent heating and their association with cloud types over the Indian Summer Monsoon region

"Clouds brings thunder and rain,
And also leaves its hidden energy,
To do work as Sun's do"

6.1 Introduction

The latent heating (LH) is the energy liberated or absorbed in the atmosphere by the phase transition from water molecule via vapour to liquid; vapour to solid and vice versa and it plays a pivotal role in controlling the Earth's atmospheric dynamics. Also, it accounts for three fourth of total heating in the Erath's atmosphere (e.g., *Riehl and Malkus*, 1958). Latent heat plays a major role in driving and modulating atmospheric circulation on various temporal and spatial scales that is from mesoscale to synoptic and planetary scales (e.g., *Nigam et al*., 2000). It is now well established that the latent heat released in clouds is the secondary source of energy for driving the atmosphere, the Sun being the primary. The vertical distribution of latent heating in the atmosphere is also associated with vertical energy transport throughout the troposphere [*Houze,* 1982]. The dynamics of the tropical atmosphere strongly depends on the both vertical and horizontal distribution of latent heating [e.g., *Yanai et al*., 1973]. Variations in the height of the heating peak have significant implications for large-scale circulations in the atmosphere [e.g, *Nigam et al*., 2000]. For example,

Schumacher et al. [2004] show that geographical and temporal variability in convective and stratiform rain fractions, both of which have different vertical heating distributions, plays an important role in shaping the structure of the large-scale tropical circulation response, thus stressing the importance of accurate estimates of the temporal and three-dimensional variability of latent heating. Studies have shown that improved vertical distribution of latent heating allow a better representation of tropical east-west circulation (e.g., the walker circulation) by models other than those using simple heating functions, such as *Webster* [1972] and *Gill* [1980]. Thus, correct assessment of the vertical distribution of heating will lead to better simulations of the large-scale circulation structures. Determining this latent heating distribution is difficult because heating cannot be directly measured. *Yanai et al.* [1973] described atmospheric heating and the latent heating contribution involving Q_1 and Q_2, which are residuals of heat and moisture budgets of the resolvable motion, respectively. However, TRMM observations provide the distribution of latent heating in the tropical regions. It is well known that the different cloud types shows a different radiative properties and LH, which differs largely. Individual cloud types have the different microphysical properties such as liquid water contents and releases different LH forcing to the atmosphere, which will further modifies the background environment. This heating further associated with vertical energy transport with respect to various horizontal scales of precipitating cloud systems and their types (*Houze*, 1982).

There have been a large number of seminal studies in the past focusing on the LH distribution using TRMM measurements [e.g., *Tao et al*., 2006 and *reference therein]*. These studies were mainly investigated the nature of LH with respect different geographical regions and their interaction with the large-scale background environment [e.g., *Hartmann et al*., 1984; *Schumacher et al*., 2004]. But there were not much studies especially on the LH associated with various cloud types over the ISM region. Establishing an accurate horizontal and altitudinal structure of LH is utmost important to better understanding and forecasting climate variability in general circulation models. Therefore, the

information on the LH of various cloud types is important to simulate the different dynamical response in atmospheric climate models at regional and global-scales. It is understood that the spatial and diurnal variation of vertical distribution of LH is an important thermal forcing, especially with respect to ISM region, where the deepest convective clouds occur and releases a large amount of LH into the atmosphere. To understand the cloud feedback mechanism in totality, the LH of various cloud types would be useful along with other cloud properties. As the ISM serves as natural laboratory for studying the clouds and their microphysics, an attempt is made to explore the latent heat distribution over this region using 16 years of TRMM observations. The main focus of the present chapter is the vertical structure of latent heating derived from TRMM and its spatial and temporal distribution over the ISM region. Further, an attempt is made to associate the observed vertical structure of LH to the individual cloud types during the ISM season.

6.2 Data and methodology

As discussed in the chapter 2, the TRMM measures the vertical profiles of latent heat by employing the vertical profile of rain rate and a cloud resolving model. There are few algorithms (such as CSH, GPROFH, HH, PRH and SLH) for retrieving the latent heating from TRMM observations. In the present study, we use 16 years of (1998 to 2013) Spectral Latent Heating (SLH) data (SLH-L3-V2) to investigative the vertical structure of latent heating. This dataset uses the TRMM-precipitation radar measurements and a cloud resolving model (CRM) generated look-up table for both land and oceanic regions over the tropics [*Shige et al*., 2004]. The information taken from TRMM include convective and startiform classification, cloud height, surface rain rate and more. In addition, there are separate look-up tables for convective and shallow startiform regimes based on precipitation cloud top height. Time-mean spatial distribution of vertically integrated latent heating is estimated over the ISM region for the present study. Further, zonally averaged latitudinal height distribution of LH is also estimated.

6.3 Spatial distribution of latent heating over the Indian summer monsoon region

Figure 6.1 (a & b) shows the sixteen years(1998-2013) mean climatological distribution of rainfall over India during winter [December, January, February (DJF)] and summer [June, July, August(JJA)], respectively derived from the TRMM observations. From figure 6.1(a) it is evident that the Indian region is very dry during DJF and relatively more rain fall is observed over equatorial Indian Ocean, especially at 10^0S latitude. However, owing to the presence of ISM, large amount of rainfall occurs during JJA over Western Ghats, Foot hills of the Himalayas and the Eastern Bay of Bengal. Thus, figure 6.1(a & b) depicts the typical climatological mean rainfall over the ISM region and shows its major features. Figure 6.1(c) & (d) shows the vertically integrated latent heating (K/hr) over the ISM region for the period 1998-2010 during DJF and JJA, respectively. The most noticeable feature during JJA is higher LH values over the BoB, the equatorial Indian Ocean and over Indo-Gangetic Plane (IGP) regions. Another interesting feature is the LH pattern over monsoon trough region, which show relatively large magnitudes as shown in figure 6.1(d). During DJF, the higher LH values found to be over eastern Equatorial Indian Ocean, which is the location of ITCZ, where the deep convection prevails during that season. The major difference in spatial distribution of LH during DJF and JJA is due to the migration of ITCZ. The ITCZ migrates northward from January to September and drifts back to equator ward between October and January. Thus primarily, movement of ITCZ is responsible for the observed latitudinal pattern in the intergraded LH distribution over the ISM region. The LH released within this zone drives large-scale circulation in the atmosphere as well as modulates the monsoon circulation. Four regions are identified from figure 6.1 (d), where large amount of latent heat is released during the ISM. These regions are BoB, Arabian Sea (ARB), Central India (CI) and Western Ghats (WG). Figure 6.2 shows the 16 year mean vertical profiles of LH over the BoB, ARB, CI and WG, respectively. The observed vertical structure of LH is very similar over BoB and CI, which peaks at ~ 7km. But, the LH magnitudes are slightly larger over BoB than CI region, because BoB experience a strong presence of deep convection which releases large amount of latent heating

in the atmosphere. Over the ARB and WG regions, the LH vertical structure is mainly associated with shallow convective clouds and thus LH profiles peaks at ~ 2 km height over both the regions. It is also interesting to note that the vertical structure of LH exhibits a bi-modal distribution over BoB and CI regions. The latent heating associated with deep convection is positive thought out the troposphere and it peaks around mid-tropospheric level (~ 6-7 km height) as seen over the BoB and CI regions. The heating associated with shallow convection is positive and peaks at lower tropospheric heights as observed over the ARB and WG regions [*Subrahmanyam and Kumar*, 206].

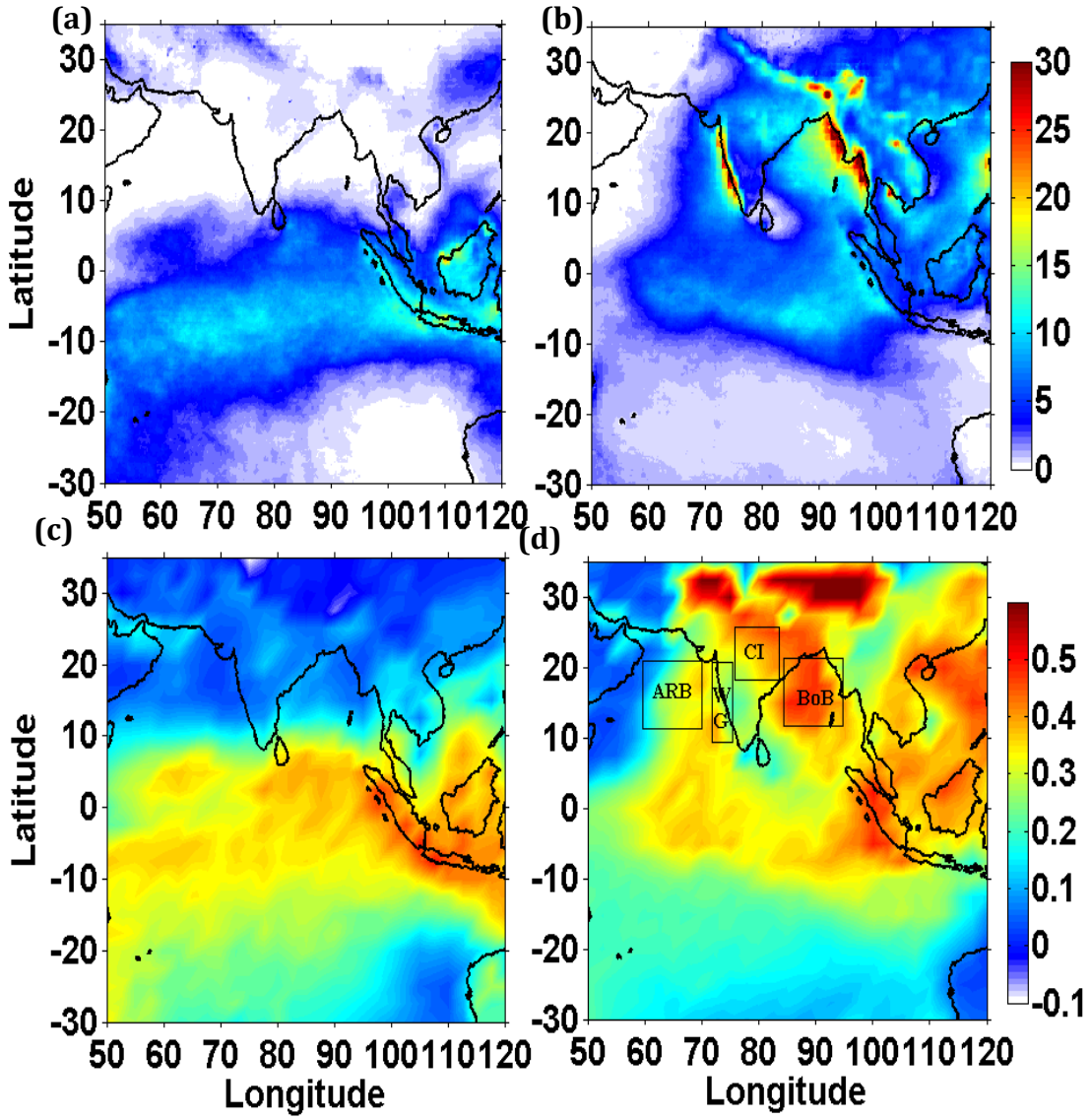

Figure 6.1: Thirteen year mean rainfall (mm/day) during (a) DJF and (b) JJA and vertically integrated LH (K/hr) for (c) DJF and (d) JJA over ISM region.

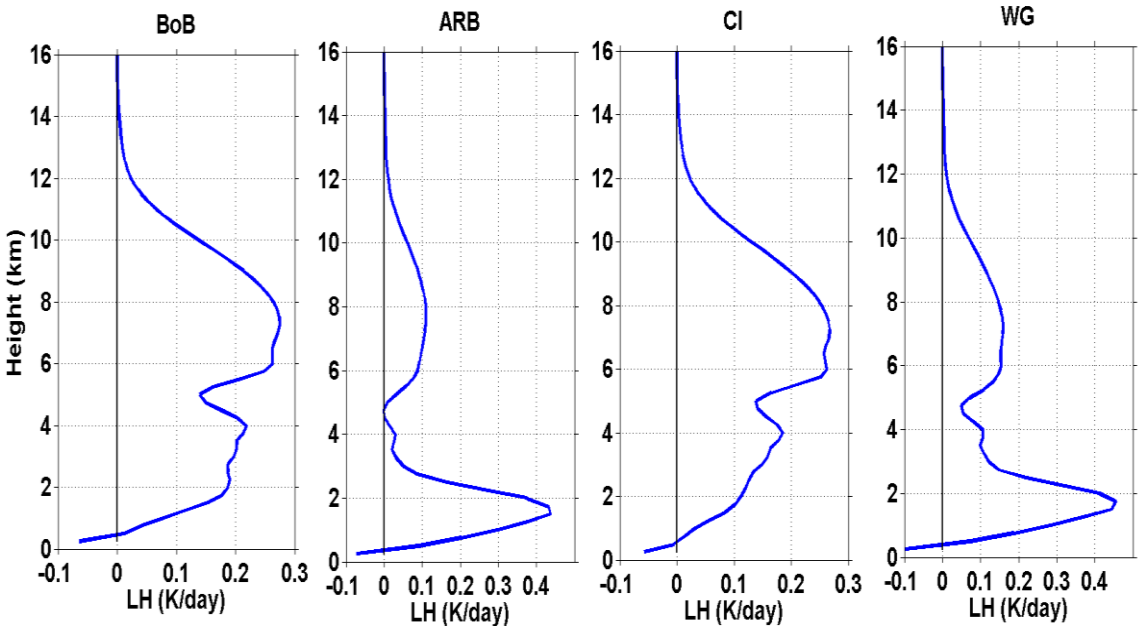

Figure 6.2: Mean vertical profiles of LH over the BoB, ARB, CI and WG.

6.4 Vertical structure of latent heating during Indian summer monsoon region

Figure 6.3 shows the zonally averaged (60^0-90^0 E) diurnal variability of vertical distribution of LH with latitude during ISM period. The increase in LH magnitude with latitude is clearly seen in figure 6.3 from 00 LT to 15 LT. These spatial and vertical structure evolutions of LH can be used as a proxy of convective organization. The observations shown in figure 6.3 suggest the northward propagation of convective activity over these latitudes (*Raut et al*., 2009). The largest amount of latent heating is found during 12 and 15 LT at 20-25^0 N latitude, which corresponds to CI region. It is reported in the past that the convective activity over the land region during ISM peaks during late afternoon hours (*Wallace*, 1975; *Gray and Jacobson*, 1977; *Dai and Desser*, 1999; *Dai and Trenberth*, 2004; *Dai*, 2006; *Subrahmanyam and Kumar*, 2013). Most of the LH is confined within the mid troposphere. However, there are few vertical structures, which show significant LH up to 15 km altitude. These structures are appearing as vertical streaks in figure 6.3. Thus this figure captures the salient features of LH at diurnal scales over the ISM region. Further, to study the sub-regional characteristics of diurnal evolution of latent heating over the four study regions, the temporal and vertical distribution of latent heating are examined. Figure 6.4

(a-d) shows the diurnal evolution of vertical structure of LH over the BoB, ARB, CI and WG regions, respectively. This representation provides better insights into the diurnal evolution of vertical structure of LH over the study regions. From figure 6.4, it can be readily noted that the diurnal variability of LH over land and oceanic regions is different [*Subrahmanyam and Kumar*, 206].

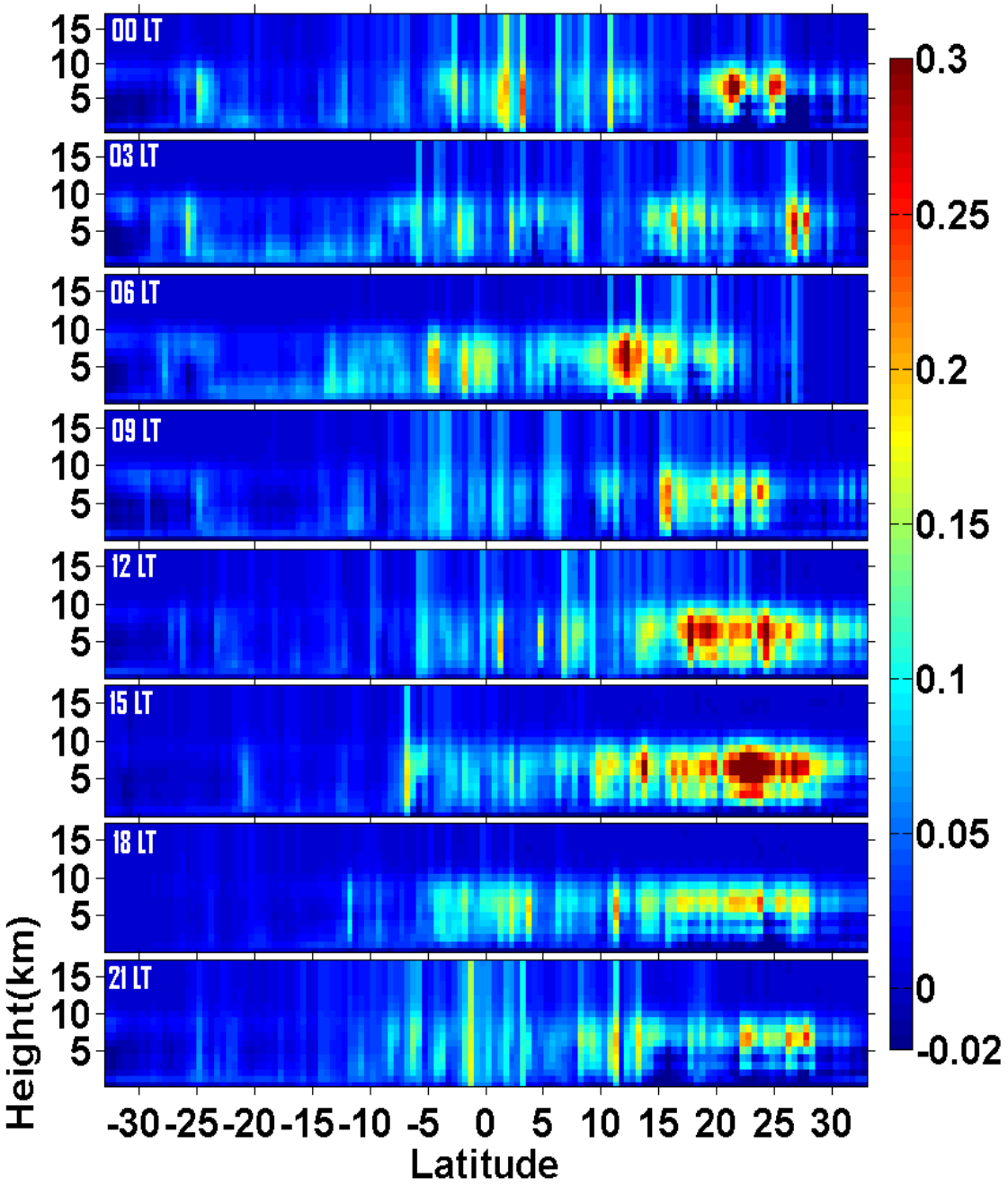

Figure 6.3: Zonally averaged (60-90^{0}E) diurnal variability of vertical distribution of LH (in K/hr) during JJA.

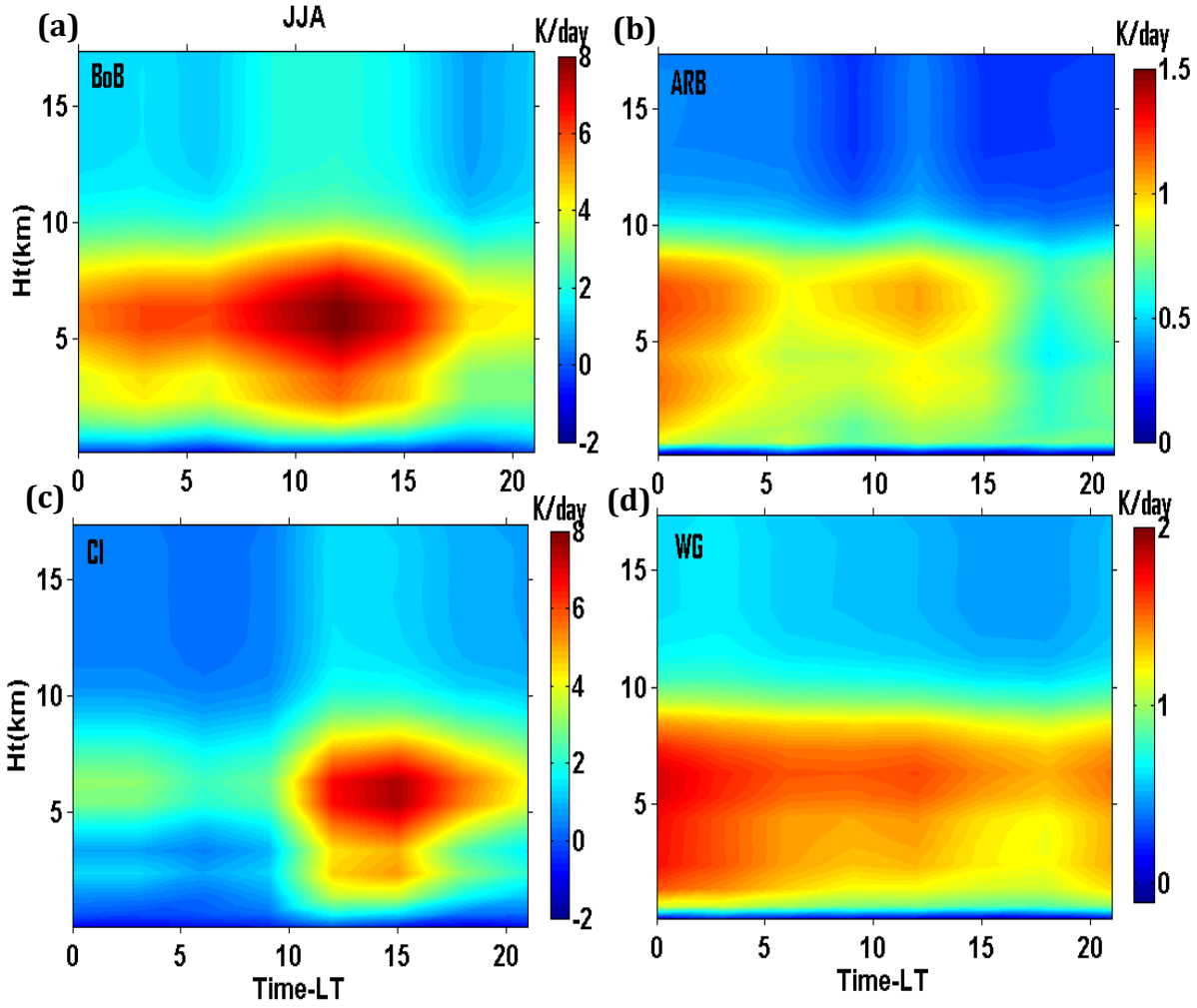

Figure 6.4: Diurnal variability of vertical structure of LH over BoB, ARB, CI and WG regions respectively during JJA.

The LH exhibits a broad peak during afternoon to late- afternoon over BOB with secondary peak during mid-night to early morning hours. Over the ARB, LH peaks during mid-night to early morning hours with a secondary peak during afternoon hours. However, the LH magnitudes are relatively lower over AEB as compared to the BoB region. The LH release over land regions are of specific interest to many previous studies because of their large magnitudes. Over CI, the LH peaks during the late afternoon hours and the large amount of latent heating occurs at an altitude of ~ 7 km. The maximum latent heating over CI is as strong as that of the BoB. The WG region has unique latent heating feature compared to other regions. Over the WG, LH peaks at mid-night hours and there seems to be uniform

secondary peak during other local times of the day. The LH magnitudes over WG are relatively lower as compared to all other study regions. Being a coastal region, WG exhibits a different LH structure as compared to other regions. The maximum magnitude of LH occurs at ~00-01 LT at 5 km height level over WG. Over all, shallow convection dominates over the ARB and WG region, which results in lower magnitudes of LH. Over BoB and CI, deep convection dominates and releases large amount of LH. The peak time of these regions are associated with the development of convective systems and prevailing dynamics. The diurnal evolution of LH over different parts of ISM plays a vital role in controlling the background dynamics and thus the advancement of the monsoon itself.

6.5 Vertical Structure of latent heating and their association with various cloud types

As discussed earlier, the latent hating of the atmosphere depends on the cloud type. In this regard, an attempt is made to associate the observed LH structure to various cloud types in the present study. Figure 6.5 shows the CloudSat cloud classification and corresponding TRMM reflectivity as well as vertical profile of LH on 8th September 2006. These observations of CloudSat and TRMM are near simultaneous. From figure 6.5 (a), it is evident that the deep convective clouds are present in the CloudSat observations with cirrus and altostratus clouds as anvils. The cloud top of the observed deep convective system is extending beyond 14 km, The TRMM-PR observations shows the reflectivity values corresponding deep convective cloud. As discussed in Chapter2, the CloudSat signal are attenuated in heavy precipitation conditions, whereas TRMM-PR signals are not sensitive to non-precipitating clouds. Figure 6.5 clearly demonstrates this aspect. The LH profile correspond to deep convective cloud is shown in figure 6.5 (c), which corresponds to solid black line in figure 6.5 (a). The LH is positive throughout the troposphere and negative at below 1 km, which results due to the evaporative cooling. The LH profile is peaking at ~5 km with a peak magnitude of ~4.2 (K/hr). This LH profile is thus corresponds to the deep convective clouds and similarly, it is envisaged that the various cloud types will be having different shape of LH profiles. However, it will be a difficult task to segregate the near-

simultaneous profiles of TRMM and CloudSat to quantify the observed LH profiles in terms of cloud types. In the present study, results obtained in chapter 3 are used to accomplish this task. In chapter 3, we have identified regions, where consistently particular type of clouds forms. For example, over Arabian Sea, there is a region where consistently Stratocumulus clouds from. Over BOB and CI region the deep convective clouds dominate along with Cirrus clouds. The regions where particular type of clouds predominantly formed is thus identified and the LH released over these regions are attributed to that cloud type.

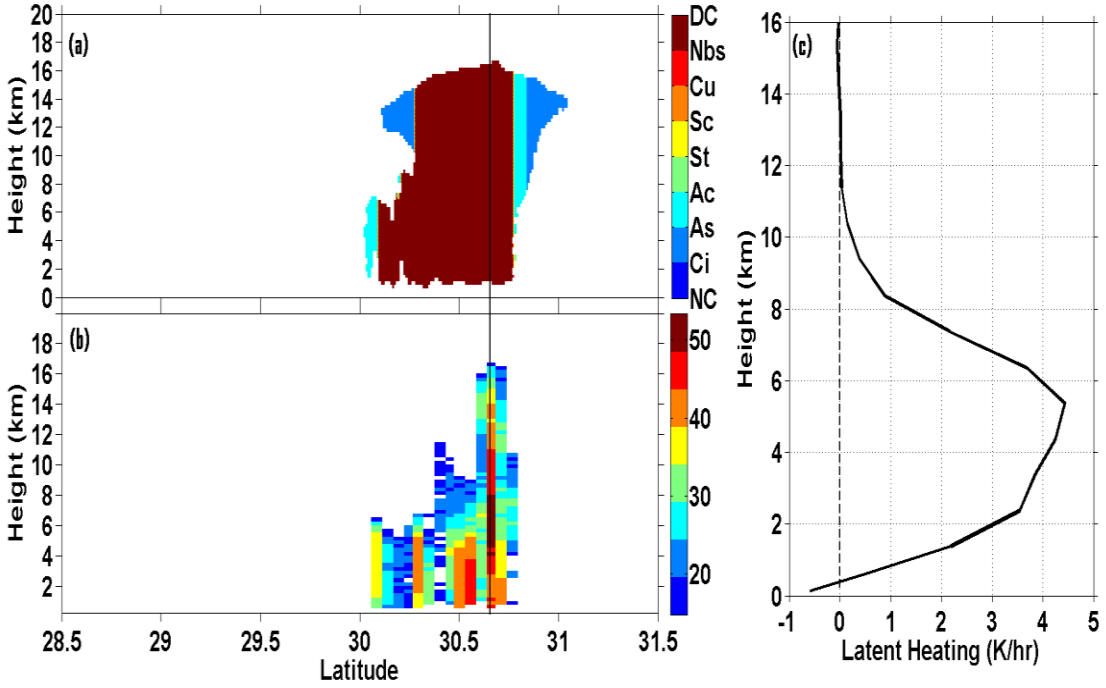

Figure 6.5 (a): CloudSat cloud classification (b) Co-located TRMM reflectivity and (c) corresponding vertical profile of latent heating on 8th September 2006.

Figure 6.6 shows the percentage of occurrence of various cloud types over the study regions of BOB, ARB and CI. The dominant cloud types are highlighted in the figure. It is to be noted that, over most part of the Indian region during summer monsoon, the Cirrus clouds will be dominating as discussed in chapter 3. In figure 6.6, though Cirrus cloud is most dominating over CI, the DC is highlighted as the LH released in DC is relatively larger than that of Ci. Thus the vertical profiles of LH observed over BOB and CI can be attributed to DC clouds whereas those observed over the ARB can be attributed to Stratocumulus clouds.

This is consistent with the LH profile shown in figure 6.2 over the study region. Over ARB Sea owing to the shallowness of the Stratocumulus clouds, the LH profile peak in the lower atmosphere whereas over CI and BOB, where DC cloud are dominant, the profiles peak in the mid-troposphere. Thus by identifying the dominant cloud types over a given region, the vertical structure of LH over that region can be attributed to particular type of clouds. This is for the first time that an attempt is made to investigate the vertical structure of LH with respect to cloud types using CloudSat and TRMM observations.

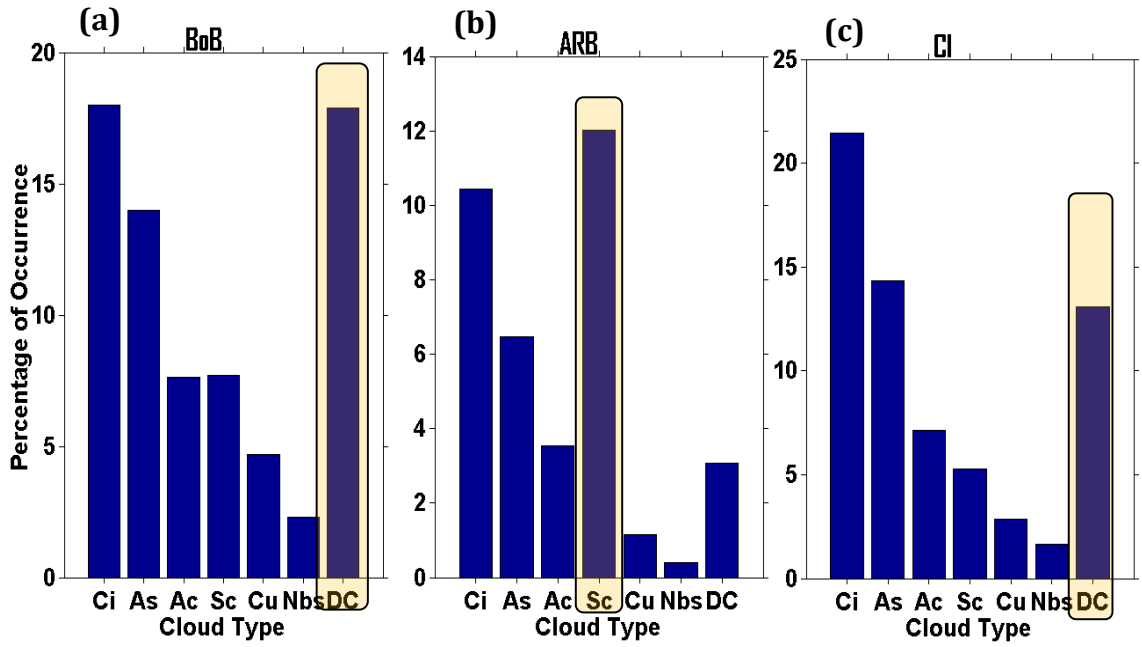

Figure 6.6: The percentage of occurrence of various cloud types over the BoB, ARB, and CI regions, respectively.

After investigating the vertical structure of LH and their association with various cloud types, an attempt is made to study their interannual variations. Figure 6.7 (a-b) shows the interannual variation of LH associated with DC cloud over BoB and CI, respectively. From this figure, it is evident that over both the regions the LH peaks around ~ 7km with a broad peak extending from 6-9 km. Over the BOB, a secondary peak can be observed in the lower troposphere between 2-4 km, which shows large interannual variability. Over the CI, though there is a secondary peak in the lower troposphere, it is not very consistently observed as in the case of BOB. Over both the study regions, LH magnitudes are relatively low in the 4-5 km altitude region which corresponds to melting layer. At melting layer

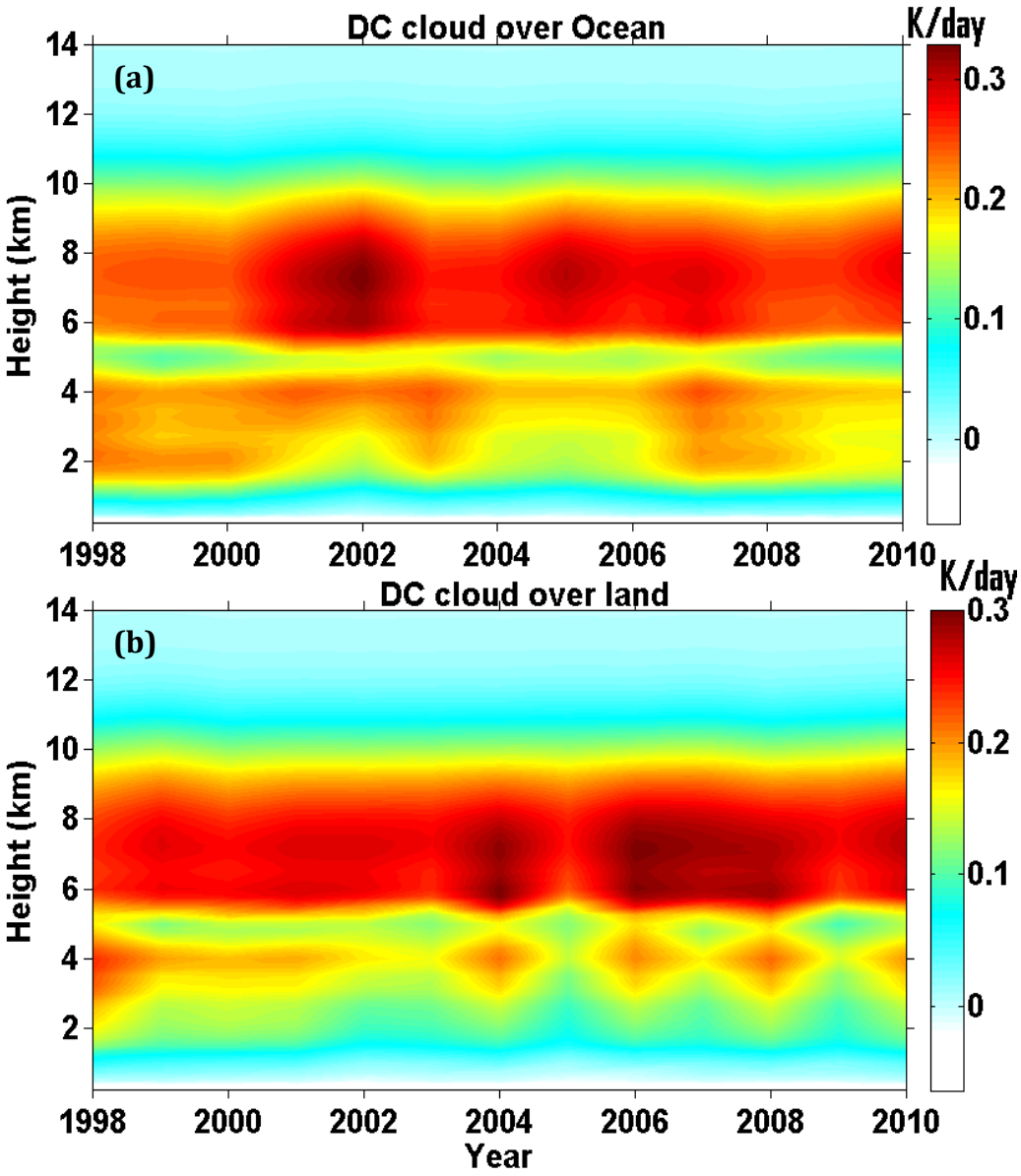

Figure 6.7: The interannual variation of vertical structure of LH associated with DC over (a) BoB and (b) CI.

which occurs at 0^0 isotherms, the ice melts in to water and thus absorbs the latent heat from the atmosphere and thus provides cooling effect. The melting of ice at 4-5 km lowers the magnitude of LH as shown in figure 6.7. One more interesting feature that can be observed from figure 6.7 is the lack of co-variation of LH over the two regions. For example, the peak LH occurs during the year 2002 over the BOB, whereas peak occurs during 2006 over CI. As discussed earlier, large amount of LH released in DC clouds are very important to understand the advancement of ISM and prevailing dynamics.

Figure 6.8 shows the interannual variability of vertical structure of LH associated with Stratocumulus clouds over the Arabian Sea. The relatively large LH is confined to lower troposphere below 2 km and there is considerably interannual variability. The peak LH is observed during the years 1999 and 2000.

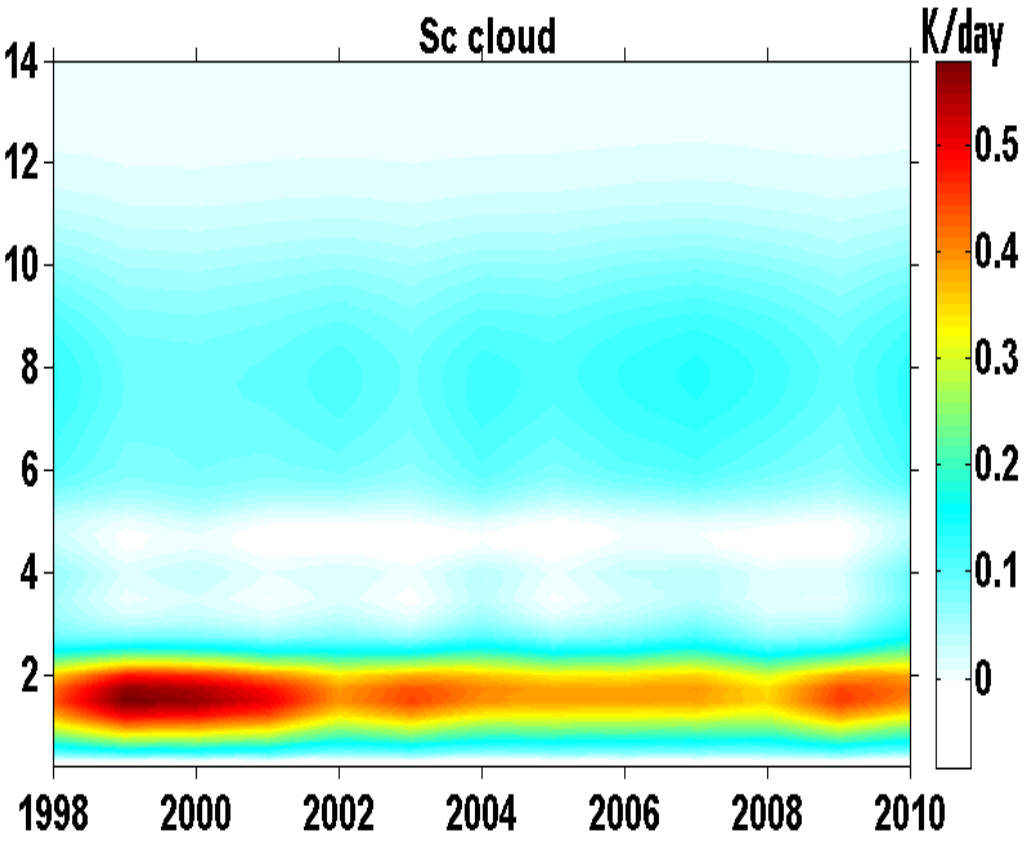

Figure 6.8: Same as figure 6.7 but for Stratocumulus clouds over ARB.

The interannual variability of LH associated with other clouds is also studied. However, as there are no distinct regions dominated by these clouds as in the case of DC and Sc, the observed LH couldn't be associated with the particular cloud type. The present study thus brought out the overall LH during the ISM region and attempted to associate the observed LH to particular cloud type. The significance of the present study lies in establishing the vertical structure of LH associated with various type of clouds, which will be helpful in better understanding and predicting the climate variability in GCMs and also important to elicit the different dynamical response of LH in climate models.

6.6 Summary

The spatial and temporal variability of latent heating distribution over the ISM region using 13 years of TRMM observations is investigated. The spatial and temporal distribution shows large amount of LH over specific regions such as the foot hills of Himalayas, the IGP and the BoB regions during ISM period. The vertical structure of LH over the ISM is also investigated. The LH variability at four regions of ISM Viz., BoB, ARB, CI and WG regions are further studied. Over the BoB and CI regions, vertical structure of LH is associated with the strong presence of deep convection which releases large amount of latent heat in the atmosphere, whereas over the ARB and WG the observed LH is attributed to the shallow convection. The observed profiles of latent heating over the ISM region showed large spatial and temporal variability in the magnitude reflecting the presence of organization of convection on mesoscale. The temporal variability of vertical structure of LH showed northward propagation of convective activity over the ISM during JJA period at diurnal scales. It is observed that the diurnal cycle of LH is more pronounced over CI (land) compared to the BoB and ARB regions. It is also observed that the LH peaks during mid-night to early morning over oceanic region (BoB and ARB) and during late afternoon over land region (CI). An attempt is made to associate the observed vertical structure of LH to the particular cloud type. Thus the present study brought out the 13 year mean spatial and vertical distribution of LH over the ISM region. The LH distribution and its role in driving the circulation will be carried out in near future.

Chapter 7

Summary and Future scope

This chapter presents the summary of the major results and conclusions derived from the present study and the scope for future research based on them. The present thesis focused on the major gap areas in the realm of cloud research *viz.,* three-dimensional distribution of various cloud types including multi-layered clouds and associated dynamics over the Indian and surrounding Oceanic region with emphasis on the following objectives,

1. To investigate the role of dynamics in three dimensional distribution of cloud types during the Indian summer monsoon
2. To study the composite distribution of cloud types in Tropical Cyclones formed in the North Indian Ocean surrounding the Indian region
3. To study the vertically resolved multi-layered clouds and associated dynamics
4. To study the spatial distribution of latent heating in precipitating clouds and to associate their vertical structure with various cloud types during the Indian summer monsoon

7.1 Summary of the major results and conclusions:

Overview to Earth's atmosphere with an emphasis on clouds and their myriad role in weather and climate are presented in **Chapter 1**. The classification of various cloud types, characteristics, measurement techniques, importance of cloud distribution over the globe with emphasis on Indian subcontinent and the major gap areas in realms of cloud studies are provided in this Chapter. Details of the various satellite observations and the methods used for the data analysis are presented in **Chapter 2**. The primacy satellite data used in the present thesis is 5

years (2006-2010) of CloudSat-CPR observations for investigating the three-dimensional distribution of various cloud types over the ISM region. The CloudSat 2B GEOPROF-LIDAR data are used to study the distribution of multi-layered clouds and TRMM-SLH observations were used to study the spatial and vertical structure of latent heating over the ISM region. The ERA-Interim reanalysis data fields are used to study the background dynamics over the ISM region. A detailed description of CloudSat, TRMM and ERA-Interim reanalysis datasets along with their limitations are also provided in this Chapter.

Chapter 3 brought out the three-dimensional distribution of various cloud types in terms of their frequency of occurrence for the first time using five years (2006–2010) of CloudSat observations over the ISM region. The mean distribution of cirrus (Ci) clouds emphatically showed the role of Tropical Easterly Jet in spreading the anvils of deep convective (DC) clouds forming over the Head Bay of Bengal (BoB). These clouds are most frequently observed over the Indian peninsula, south BoB and Indian Ocean. It is observed that the stratocumulus (Sc) clouds form most frequently over the north Arabian Sea and are confined to a narrow region. The confinement of Sc clouds over the Arabian Sea is attributed to the presence of thermal inversion in the lower troposphere, which inhibits the vertical development of clouds. Besides this, strong mixing of dry air coming from the Arabian Desert further limits the vertical development of clouds over the Arabian Sea. The prevailing dynamical features during the ISM period seem to be playing a key role in the formation of these clouds over the Arabian Sea. It is also observed that altocumulus (Ac) clouds form preferentially over Indian landmass and altostratus (As) clouds over BoB. The mean distribution of cumulus clouds showed three distinct peaks over the Tibetan Plateau, western coast and equatorial Indian Ocean. The distribution of DC clouds, which are very important from a hydrological standpoint, showed a pronounced peak in their occurrence frequency over Head BoB and secondary peaks over Western Ghats, south BoB and central India. The diurnal variations in frequency of occurrence of all these clouds are also studied using day- and night-time observations of CloudSat. The interannual variations of all these clouds are discussed, and it is observed that the

region over which a particular cloud occurs is consistent from one year to another. The mean vertical distribution of all the cloud types over the ISM region is also constructed using all the observations. The vertical structure of DC clouds showed interannual variations, which are consistent with the India summer monsoon rainfall observations during the study period. The present results thus brought out the three dimensional distribution of various cloud types over ISM region and identified the preferential regions for the formation of particular cloud type and associated dynamics. It is envisaged that the results discussed in this chapter will be helpful in quantifying the feedback of an individual cloud type to the ISM.

The three dimensional cloud type distributions over the tropical cyclones are investigated using CloudSat observations during the years 2006 to 2014 are presented in **Chapter 4**. A total number of 25 tropical cyclones (8 in Arabian Sea and 17 in Bay of Bengal) observed by CloudSat are analysed to construct the composite vertical structure of cloud type distribution. The cloud type distribution reproduced many of the known tropical cyclone features such as the DC clouds at the eye walls, Ci cloud anvils and cloud free zones between the inner and the outer rain bands known as Moat in the lower troposphere. It is found that the DC clouds are always accompanied by As and Ci clouds and their peak frequency of occurrence is ~ 50 % at ~50-100 km radial distance from the cyclone's eye. It is also observed that the DC clouds extend up to ~ 16 km near to the eye and their top altitudes decrease gradually as a function of radial distance from the eye of cyclone. The Ci cloud distribution showed a peak frequency of occurrence of 30% (at ~14-15 km altitude) at around ~200 km radially from the eye. The peak in Ci clouds is observed right next to the peak in the DC clouds indicating that Ci clouds form from the outflows of the DC clouds. However, the distribution of As clouds showed some discrepancy with respect to the present understanding of these clouds. This is probably due to CloudSat classifying the upper portion of the slanted DC cloud as As clouds. One more envisaged possibility is that the transition region between the DC and their outflows may also be classified as As clouds by the CloudSat algorithm. The Sc clouds are

observed in the center of cyclone as their vertical growth is inhibited by the downdrafts induced by the adjacent DC clouds, which limit their cloud top height to ~ 2.5 km. The Cu clouds are observed in the shadows of the DC cloud outflows and the significant amounts of these clouds are seen as far as ~ 600 km radially from the center of the eye. Most frequently, the Sc and Cu clouds are observed adjacent to each other in the present study. It is found that there are distant regions showing the peak in frequency of occurrence of various clouds embedded in the cyclone. The present study thus brought out the three-dimensional distribution of cloud types and associated dynamics in and around tropical cyclones.

Chapter 5 examined the frequency of occurrence of vertically resolved multilayer clouds across the globe for the first time using CloudSat observations. Four years (2007-2010) mean global distribution of one, two, three, four and five layered clouds are constructed and discussed in details in this Chapter. Interesting features such as very high frequency of occurrence of single layer clouds over Southern Ocean, midlatitude storm tracks, west coast of South America and South Africa and their association with large-scale circulations are discussed. The signature of descending branches of Hadley cell is very clear in multilayered cloud distribution maps as compared to that of single layered cloud distribution. Three regions over the equator (South America, Central Africa and Indonesia) are identified where more frequently multilayer clouds occurs. These regions coincide with the ascending limbs of Walker circulation. It is also observed that the maximum occurrence of multilayer clouds migrates along with the movement of ITCZ. Apart from the equatorial region, multilayer clouds are observed more frequently over Indian summer monsoon region. On an average, over the Indian region single-, double-, triple-, four- and five-layered cloud occur ~ 46%, ~ 26%, ~ 10%, ~ 4% and ~ 2%, respectively. The prevailing dynamics over the Indian region during ISM period play a crucial role in the formation of multi-layered clouds. After constructing the frequency distribution, further, the occurrence of top and base of multi-layered clouds is quantified in terms of zonal mean frequency of occurrence. Thus, the global distribution of multilayered clouds and

their association with large scale circulation are brought out using four years of CloudSat and CALIPSO observations. Further zonal mean frequency of occurrence of cloud base and top is constructed for multi-layer clouds. The cloud top altitude distribution of various clouds exhibited the signature of latitudinal structure of tropopause as expected. These are the first latitudinal distribution of vertically resolved multilayer cloud base and top altitudes estimated using space based active remote sensing observations, which can be used to verify the outputs of climate models as well as can be used to quantify the role of vertically resolved clouds in earth's radiation budget and global circulation.

Chapter 6 investigated the spatial and temporal variability of Latent Heating (LH) distribution over the ISM region using 13(1998-2013) years of TRMM observations. The spatial distribution of LH showed large amount of LH during ISM period over specific regions such as the foothills of Himalayas, the Indo Gangetic Plane (IGP) and the BoB regions. The temporal variability of vertical structure of LH showed northward propagation of convective activity over the ISM during JJA period at diurnal scales. The diurnal cycle of LH is more pronounced over Central India (CI) (land) as compared to the BoB and Arabian Sea (ARB) regions. It is observed that the LH peaks during mid-night to early morning hours over oceanic region (BoB and ARB) and during afternoon over land region (CI). However, it is observed that the diurnal cycle of LH over the BoB shows two peaks, one during the midnight-early morning hours and another during the late afternoon. Further, the observed vertical structure of LH is associated with various cloud types using the results obtained from CloudSat observations. The LH profile over the DC dominant regions shows a broad distribution with bimodal structure over the BoB & CI regions with peak value around 7 km. The LH profile associated with Sc and Cu dominant regions show peaks at lower levels over ARB and WG regions. The significance of the present study lies in constructing the vertical structure of LH in the regions dominated by DC, Sc and Cu cloud types over the ISM region.

7.2 Future Scope

The significance of the present study lies in establishing the thee-dimensional distributions of various types of cloud over the Indian region and the distribution of multi-layered clouds. The dynamics associated with formation of various types of cloud and multi-layered clouds are discussed in the present thesis. Further, the vertical distribution of latent heating also investigated over the Indian region. Based on the present results, the following studies will be taken up in near future to strengthen our understanding on cloud types and associated dynamics. Emphasis will also be given on the modelling aspects of clouds and their role in driving the mesoscale circulation. Listed below are the topics for future investigations:

1. The present study brought out the distribution of various types of cloud over the Indian region. However, simultaneous occurrences of various types of clouds are not explored, which will have different radiative impact on the atmosphere. Therefore the information on the preferential co-occurrence of various cloud types and their associated dynamics are required for complete understanding of cloud type feedback mechanisms in totality. This study will be taken up in near future using CloudSat observations.
2. The present thesis studied the vertical distribution of precipitating latent heating and its association with various types of cloud over the Indian region. But its impact on the background atmosphere is not addressed in the present thesis. It is important to study the role of latent heating, especially, in driving the circulation at mesoscales. This study will be taken up using Doppler Weather Radar observations along with reanalysis wind fields.
3. The present study brought out the vertical distribution of various cloud types in the Tropical cyclones. Once the cyclone is formed, further intensification and its movement depend on the latent heat released in the clouds embedded in them. The latent heat released in clouds modifies the internal dynamics of the cyclone and the dynamics in turn dictates the cloud distribution within the cyclone. So, it becomes important to study the latent heating and their role

in modifying the dynamics of Tropical Cyclones. The objective of this study can be achieved using TRMM observations and reanalysis datasets.

4. All the results presented in this thesis are contributing to better understanding of the cloud types, which in turn aids in better representation of clouds in climate models, which predicts the future of the earth's climate. However, the capabilities of climate model outputs in simulating the vertical structure of clouds and their feedback to the background atmosphere should be evaluated. The results obtained from the present analysis can be used to evaluate the climate model outputs on clouds and be taken up in future.

References

Adler, R. F. and E. B. Rodgers (1977), Satellite-observed latent heat release in a tropical cyclone, *Mon. Wea. Rev., 105,* 956–963.

Ahn, M. H., D. Han, H. Y. Won and V. Morris (2015), A cloud detection algorithm using the downwelling infrared radiance measured by an infrared pyrometer of the ground-based microwave radiometer, *Atmos. Meas. Tech*., *8*, 553–566, doi:10.5194/amt-8-553-2015

Anagnostou, E. N. (2004), Overview of Overland Satellite Rainfall Estimation for Hydro-Meteorological Applications, *Surveys in Geophysics*, *25*, 511-537, doi: 10.1007/s10712-004-5724-6

Baum and Co-authors (1995), Satellite remote sensing of multiple cloud layers, *J. Atmos. Sci., 52*, 4210–4230.

Behrangi, A., Sean P. F. Casey and Bjorn H. Lambrigtsen (2012), Three-dimensional distribution of cloud types over the USA and surrounding areas observed by CloudSat, *Int. J. Rem. Sen.*, *33 (*16), 4856-4870.

Bender, F. A. M., V. Ramanathan and G. Tselioudis (2011), Changes in extra tropical storm track cloudiness 1983–2008: observational support for a pole ward shift, *Clim. Dyn.,* doi:10.1007/s0038201110656.

Bengtsson, L., K. I. Hodges and E. Roeckner (2006), Storm tracks and climate change, *J. Clim., 19*, 3518–3543.

Bergman, J.W. and M. L. Salby (1997), The role of Cloud diurnal variations in the time-mean energy budget, *J. Clim.*, *10*, 1114-1124.

Bhat, G. S., A. Chakraborty, R. S. Nanjundiah and J. Srinivasan (2002), Vertical thermal structure of the atmosphere during active and weak phases of convection over the north Bay of Bengal: observation and model results, *Curr. Sci., 83*(3), 296–302.

Bu, Y.P., R. G. Fovell, and K. L. Corbosiero (2014), Influence of Cloud–Radiative Forcing on Tropical Cyclone Structure, *J. Atmos. Sci.*, *71*, 1644-1662, doi: 10.1175/JAS-D-13-0265.1.

Cess R. D. and Co-authors (1996), Cloud feedback in atmospheric general circulation models: an update, *J. Geophys. Res., 101*, 12791-12794.

Chen, T., W. B. Rossow, W. B. and Y. Zhang (2000a), Radiative effects of cloud-type variations, *J. Clim., 13*, 264–286.

Chen, T., Y. Zhang and W. B. Rossow (2000b), Sensitivity of atmospheric radiative heating rate profiles to variations of cloud layer overlap, *J. Clim., 13*, 2941–2959.

Cetrone, J. and R. A. Houze (2009), Anvil clouds of tropical mesoscale convective systems in monsoon regions, *Quart. J. Roy. Meteor. Soc., 135*, 305-317.

Dai, A. (2006), Precipitation characteristics in eighteen coupled climate models, *J. Clim., 19*, 4605–4630.

Dai, A. and C. Desser (1999), Diurnal and semidiurnal variations in global surface wind and divergence fields, *J. Geophys. Res., 104*, 31109– 31125.

Dai, A. and K. E. Trenberth (2004), The diurnal cycle and its depiction in the community climate system model, *J. Clim., 17*, 930–951.

Dee D. P. and Co-authors (2011), The ERA-Interim reanalysis: configuration and performance of the data assimilation system, *Q. J. R. Meteorol. Soc., 137,* 553–597. DOI:10.1002/qj.828

Devasthale, A and H. Grassal, (2009), A daytime climatological distribution of high opaque ice cloud classes over the Indian summer monsoon region observed from 25-year AVHRR data, *Atmos. Chem. Phys*.,*9*,4185-4196.

Dimri, A. P., D. Niyogi, A. P. Barros, J. Ridley, U. C. Mohanty, T. Yasunari and D. R. Sikka (2015), Western disturbances: a review, *Rev. Geophys*., doi:10.1002/2014RG000460.

Dong, B., R. T. Sutton, T. Woollings and K. Hodges (2013), Variability of the North Atlantic summer storm track: mechanisms and impacts on European climate, *Environ. Res. Lett., 8*, 034037.

Durden, S. L., S. Tanelli and G. Dobrowalski (2009), CloudSat and A-Train Observations of Tropical Cyclones, *The Open Atmospheric Science Journal,* 80-92.

Dvorak, V. F. (1984), Tropical cyclone intensity analysis using satellite data, NOAA Tech Rep. 11, pp. 45.

Emanuel, K. A. (2001), The contribution of tropical cyclones to the oceans' meridional heat transport, *J. Geophys. Res*., *106*, 14771–14782.

Frank, W. M. (1973), The structure and energetics of the tropical cyclone storm structure, *Mon. Wea. Rev.*, *105*(9), 1119-1135.

Frisinger, H. H. (1977), The History of Meteorology to 1800, Historical monograph Series, *American Meteorological Society History Publications*, New York, 148 pp.

Fudeyasu, H., Y. Wang, M. Satoh, T. Nasuno, H. Miura and W. Yanase (2010), Multiscale Interactions in the Lifecycle of a Tropical Cyclone Simulated in a Global Cloud-System- Resolving Model Part II: System-Scale and Mesoscale Processes, *Mon. Wea. Rev.*, *138*, 4305-4327.

Gadgil, S. (2003), The Indian Monsoon and its variability, *Annu. Rev. Earth Planet. Sci., 31*, 429–467.

Gambheer, A. V. and G. S. Bhat (2000), Life Cycle Characteristics of Deep Cloud Systems over the Indian Region Using INSAT-1B Pixel Data, *Mon. Wea. Rev., 128*(12), 4071-4083, doi:10.1175/1520-0493(2000)129h4071:LCCODCi2.0.CO;2.

Gambheer, A. V. and G. S. Bhat (2001), Diurnal variation of deep cloud systems over the Indian region using INSAT-1B pixel data, *Meteorol. Atmos. Phys.*, *78*, 215-225, doi: 10.1007/s703-001-8175-4.

Gill, A. E. (1980), Some simple solutions for heat-induced tropical circulation, *Quart. J. Roy. Meteor. Soc*., *106,* 447–462.

Goswami, B. N. and P. K. Xavier (2005), Dynamics of ‘‘internal’’ interannual variability of the Indian summer monsoon in a GCM, *J. Geophys. Res., 110*, D24104. doi:10.1029/2005JD006042.

Gray, W. M. and R. W. Jacobson (1977), Diurnal variation of deep cumulus convection, *Mon. Wea. Rev., 105*, 1171–1188.

Grossman, R. and O. Garcia (1990), The distribution of deep convection over ocean and land during the Asian summer monsoon, *J. Clim., 3,* 1032–1044.

Gupta, S. K., W. L. Darnell and A. C. Wilber, (1992), A parameterization for longwave surface radiation from satellite data: Recent improvements, *J. Appl. Meteorol*., *31*, 1361–1367.

Hartmann, D. L., L. A. Moy, and Q. Fu (2001), Tropical convection and the energy balance at the top of the atmosphere, *J. Clim., 14*, 4495–4511.

Hartmann, D. L., H. H. Hendon and R. A. Houze Jr. (1984), Some implications of the mesoscale circulations in tropical cloud clusers for large-scale dynamics and climate, *J. Atmos. Sci*., *41*, 113–121.

Haynes, J. M., C. Jakob, W. B. Rossow, G. Tselioudis and J. Brown (2011), Major characteristics of Southern Ocean cloud regimes and their effects on the energy budget, *J. Clim., 24*, 5061–5080.

Hazra, A., H. S. Chaudhari, S. Pokhrel, S. K. Saha (2015), Indian summer monsoon precipitating clouds: role of microphysical process rates, *Clim. Dyn.*, doi: 10.1007/s00382-015-2717-8.

Haynes, J. and G.L. Stephens (2007), Tropical oceanic cloudiness and the incidence of precipitation: Early results from CloudSat, *Geophys. Res. Lett., DOI: http://dx.doi.org/10.1029/2007GL029335.*

Hemsfiled, G. M. and R. Fulton (1994), Passive Microwave and Infrared Structure of Mesoscale Convective Systems, *Meteorol. Atmos. Phys*., *54*, 123-139.

Hence, D. A. and R. A. Houze (2011), Vertical structure of hurricane eyewalls as seen by the TRMM Precipitation Radar, *J. Atmos. Sci., 68*, 1637-1652.

Hence, D. A. and R. A. Houze (2012), Vertical structure of tropical cyclone rainbands as seen by the TRMM Precipitation Radar. *J. Atmos. Sci., 69*, 2644–2661.

Hence, D. A. and R. A. Houze (2008), Kinematic structure of convective-scale elements in the rainbands of Hurricanes Katrina and Rita [2005], *J. Geophys. Res.*, *113*, D15108, doi:10.1029/2007JD009429.

Hoskins, B. J. and K. Hodges (2005), A new perspective on Southern Hemisphere storm tracks, *J. Clim., 18*, 4108–4129.

Houghton, J. T. (1979a), The future role of observations from meteorological satellites, *Quart. J. Roy. Met. Soc*., *105*, 1-28.

Houghton, J.T. (1979b), The role of satellites in the tropical observing system, In Meteorology over the Tropical Oceans, *Roy. Met. Soc.*, 261-274.

Houze, R. A. (1982), Cloud clusters and large-scale vertical motions in the tropics, *J. Meteor. Soc. Japan, 60*, 396–410.

Houze, R. A. (2010), Clouds in Tropical Cyclones, *Mon. Wea. Rev.*, *138*, 293–344. doi**:** 10.1175/2009MWR2989.1.

Houze, R. A., D. C. Wilton and B. F. Smull (2007), Monsoon convection in the Himalayan region as seen by the TRMM Precipitation Radar, *Quart. J. Roy. Meteorol. Soc., 133*, 389–1411.

Howell, W. E. (1951), The classification of cloud forms. Clouds, fogs and aircraft icing, In "Compendium of Meteorology" (T. F. Malone, ed.), pp. 1162-1166. *Am. Meteorol. SOC*., Boston, Massachusetts.

Huang, J. and Co-authors (2005), Advanced retrievals of multilayered cloud properties using multispectral measurements, *J. Geophys. Res.*, doi:10.1029/2004JD005101

Iguchi, T., T. Kozu, R. Meneghini, J. Awaka, and K. Okamoto (2000), Rain-profiling algorithm for the TRMM precipitation radar, *J. Appl. Meteor., 39***,** 2038–2052.

Im, E., S. L. Durden, S. Tanelli and K. Pak (2006), Early Results on Cloud Profiling Radar Post-launch Calibration and Operations, *Proceedings of IGARSS 2006* and 27th Canadian Symposium on Remote Sensing, Denver, USA.

Im, E., S. Tanelli, S. L. Durden and K. Pak (2007), Cloud Profiling Radar Performance, *Proceedings of IGARSS 2007* (International Geoscience and Remote Sensing Symposium), Barcelona, Spain, July 23-27.

Im, E., W. Chialin S. L. Durden (2005), Cloud Profiling Radar for the CloudSat Mission, *IEEE Aerospace and Electronic Systems Magazine*, *20* (10), 15-18, http://trs-new.jpl.nasa.gov/dspace/bitstream/2014/37690/1/042971.pdf

Joseph, P. V. and S. Sijikumar (2004), Intraseasonal variability of the low level jet stream of the Asian summer monsoon, *J. Clim., 17***,** 1449–1458.

Khrgian, A. Kh. (1970), Meteorology, A Historical Survey, Vol. 1, 2nd revised Ed. pp. 38.

Kidd C. and E. C. Barrett (1990), The use of passive microwave imagery in rainfall monitoring, *Remote Sensing Reviews, 4*, 415–450.

Kidd, C. (2001), Satellite Rainfall Climatology: A Review, *Int. J. Clim., 21*, 1041–1066, DOI: 10.1002/joc.635

Kidder, S. Q., W. M. Gary and T. H. Vonder Haar (1978), Estimating tropical cyclone central pressure and outer winds from satellite microwave data, *Mon. Wea. Rev*., *106(*10), 1458–1464.

Klein, S. A., D. L. Hartmann and J. R. Norris (1995), On the relationship among low cloud structure, sea surface temperature, and atmospheric circulation in the summertime northeast Pacific, *J. Clim., 8*, 1140–1155

Kumar, S., A. Hazra, and B. N. Goswami, (2014), Role of interaction between dynamics, thermodynamics and cloud microphysics on summer monsoon precipitating clouds over the Myanmar coast and the western ghats, *Clim. Dyn.*, *43*, 911–924. doi:10.1007/s00382-013-909-3

Kummerow, C. and Co-authors (2001), The evolution of the Goddard Profiling Algorithm (GPROF) for rainfall estimation from passive microwave sensors, *J. Appl. Meteor., 40,* 1801–1820.

Kummerow, C., W. Barnes, T. Kozu, J. Shiue, and J. Simpson (1998), The Tropical Rainfall Measuring Mission (TRMM) sensor package, *J. Atmos. Oceanic Technol., 15*, 809–817.

Kunzi, KLAUS, P. Bauer, R. Eresmaa, P. Eriksson, B. Healy, M. Sean, L. Alberto, P. Nathaniel, A. S. Catherine, and G. Stephens, (2011), Microwave Absorption, Emission and Scattering: Trace Gases and Meteorological Parameters, 153-230. 10.1007/978-3-642-14791-3_4.

Laing, A. G. and J. M. Fritsch (1993), Mesoscale convective complexes over the Indian monsoon region, *J. Climate, 6*, 911–919.

L'Ecuyer, T. and Co-authors (2015), The observed state of the energy budget in the early 21st century, *J. Clim., 28*(21), 8319-8346.

L'Ecuyer, T. S., N. B. Wood, T. Haladay, G. L. Stephens and P. W. Stackhouse Jr. (2008), Impact of clouds on atmospheric heating based on the R04 CloudSat fluxes and heating rates data set, *J. Geophys. Res.*, *113*, D00A15, doi:10.1029/2008JD009951.

Li, J., J. Huang, K. Stamnes, T. Wang, Q. Lv and H. Jin (2015),A global survey of cloud overlap based on CALIPSO and CloudSat measurements, *Atmos. Chem. Phys*., 15, 519–536, doi:10.5194/acp-15-519-2015

Li, J., Y. Yi, P. Minnis, J. Huang, H. Yan, Y. Ma, W. Wang and J. Kirk Ayers (2011), Radiative effect differences between multilayered and single layer clouds derived from CERES, CALIPSO, and CloudSat data, *J. Quant. Spectrosc. Radiat. Transf., 11,* 361–375.

Li, Y., D. W. J. Thompson, G. L. Stephens and S. Bony (2014), A global survey of the instantaneous linkages between cloud vertical structure and large-scale climate, *J. Geophys. Res. Atmos.*, *119*, doi:10.1002/2013JD020669.

Liu, C. and E. J. Zipser (2005), Global distribution of convection penetrating the tropical tropopause, *J. Geophys. Res., 110*, doi:10.1029/2005JD006063.

Luo, Y., R. Zhang, and H. Wang (2009), Comparing Occurrences and Vertical Structures of Hydrometeors between Eastern China and the Indian Monsoon Region Using /CALIPSO Data, *J. Clim., 22*(4), 10521064.

Mace, G. G. (2010), Cloud properties and radiative forcing over the maritime storm tracks of the Southern Ocean and North Atlantic derived from A-Train, *J. Geophys. Res.*, *115*, D10201, doi:10.1029/2009JD012517.

Mace, G. G., Q. Zhang, M. Vaughan, R. Marchand, G. L. Stephens, C. Trepte and D. Winker (2009), A description of hydrometeor layer occurrence statistics derived from the first year of merged CloudSat and CALIPSO data, *J. Geophys. Res., 114*, doi:10.1029/2007JD009755

Mace, G. G., R. Marchand, Q. Zhang and G. L. Stephens (2007), Global hydrometeor occurrence as observed by CloudSat: initial observations from summer 2006, *Geophys. Res. Lett., 34*, doi:10.1029/2006GL029017

Mace, G. G., D. Vane, G. Stephens and D. Reinke (2007), Level Radar-Lidar Geoprof Product Process Description and Interface Control Document, Version 1.

Marchand, R. T., G. G. Mace, T. Ackerman and G. L. Stephens (2008), Hydrometeor Detection using CloudSat - an Earth Orbiting 94 GHz Cloud Radar, *J. Atmos. Ocean. Tech.*, *25* (4), 519-533.

Masunaga, H., M. Satoh and H. Miura (2008), A Joint Satellite and Global Cloud-Resolving Model Analysis of a Madden-Julian Oscillation event: Model Diagnosis, *J. Geophys. Res.*, *113*, D17210, doi:10.1029/2008JD009986.

Meenu, S., K. Rajeev, and K. Parameswaran (2011), Regional and vertical distribution of semitransparent cirrus clouds over the tropical Indian region derived from CALIPSO data, *J. Atmos. Sol. Terr. Phys., 73*, 1967-1979, doi:10.1016/j.jastp.2011.06.007.

Meenu, S., K. Rajeev, K. Parameswaran, and A. K. M. Nair (2010), Regional distribution of deep clouds and cloud top altitudes over the Indian subcontinent and the surrounding oceans*, J. Geophys. Res., 115 (* D05), 205, doi:10.1029/2009JD011802.

Middleton, W. E. K. (1965), *A history of the theories of rain,* Old Bourne, London.

Nair, A. K. M., K. Rajeev, S. Sijikumar, and S. Meenu (2011), Characteristics of a persistent "pool of inhibited cloudiness" and its genesis over the Bay of Bengal associated with the Asian summer monsoon, *Ann. Geophys., 29*(7), 1247-1252, doi: 10.5194/angeo-29-1247-2011.

Nakazawa, N. (1988), Tropical Super Clusters within Intraseasonal Variations over the Western Pacific, *J. Met. Soc. of Japan.*, *66*, No. 6823-838.

Narayanan, M. S. and B. M. Rao (1981), Detection of monsoon inversion by TIROS-N satellite, *Nature, 294,* 546–548.

Narendra Babu, A. N., J. B. Nee and K. K. Kumar (2010), Seasonal and diurnal variation of convective available potential energy [CAPE] using COSMIC/FORMOSAT3 observations over the tropics, *J. Geophys. Res., 115*, D04102, doi:10.1029/2009JD012535.

Nigam, S., C. Chung and E. DeWeaver (2000), ENSO diabatic heating in ECMWF and NCEP–NCAR reanalyses, and NCAR CCM3 simulation, *J. Clim., 13*, 3152–3171.

Norris, J. R. (1998), Low cloud type over the ocean from surface observations. Part II: Geographical and seasonal variations, *J. Clim.*, *11*, 383–403.

Norris, J. R. (1999), On trends and possible artifacts in global ocean cloud cover between 1952 and 1995, *J. Clim., 12*, 1864-1870.

Norris, J. R. (2000), Interannual and interdecadal variability in the storm track, cloudiness, and sea surface temperature over the summertime North Pacific, *J. Clim.*, *13*, 422–430.

Olson, W. S and Co-authors (2006), Precipitation and latent heating distributions from satellite passive microwave radiometry. Part I: Method and uncertainties, *J. Appl. Meteor. Clim., 45,* 702–720.

Olson, W. S., C. D. Kummerow, Y. Hong and W. K. Tao (1999), Atmospheric latent heating distributions in the Tropics derived from passive microwave radiometer measurements, *J. Appl. Meteor., 38,* 633–664.

Peng, J., H. Zhang, and Z. Li (2014), Temporal and spatial variations of global deep cloud systems based on CloudSat and CALIPSO satellite observations, *Adv. Atmos. Sci*., *31*(3), 593–603, doi:10.1007/s00376-013-3055-6.

Pokhrel, S. and D. R. Sikka (2013), Variability of the TRMM-PR total and convective and stratiform rain fractions over the Indian region during the summer monsoon, *Clim. Dyn., 41,* 21–44. doi:10.1007/s00382-012-1502-1.

Pruppacher, H. R. and J. D. Klett (1978), Microphysics of Clouds and Precipitation, D. Reidel, Hingham, Massachusetts

Pruppacher, H. R. and J. D. Klett, (1997), Microphysics of clouds and precipitation, *Kluwer Academic*, Norwell, Massachusetts, pp. 659, ISBN 0-7923-4211-9.

Quante, M. (2004), The role of clouds in the climate system, *Journal De Physique Iv*, *121*, 61–86.

Rajeev, K. and Co-authors (2008), Observational assessment of the potential of satellite-based water vapor and thermal IR brightness temperatures in detecting semitransparent cirrus, *Geophys. Res. Lett., 35*(L08808), doi:10.1029/2008GL033393.

Rajeevan, M., P. Rohini, K. Niranjan Kumar, J. Srinivasan, and C. K. Unnikrishnan (2012), A study of vertical cloud structure of the Indian summer monsoon using CloudSat data, *Clim. Dyn., 40*(3-4), 637-650, doi:10.1007/s00382-012-1374-4.

Ramanathan, V. and Co-authors (1989), Cloud-radiative forcing and climate: results from the earth radiation budget experiment, *Science, 24*, 357-363.

Randall, D. A. and Co-authors (2007), Climate models and their evaluation. In: Solomon S et al [eds] Climate Change 2007: the physical sciences basis, contribution of Working Group I to the Fourth Assessment Report of the Intergovernmental Panel on Climate Change, chap 4. Cambridge University Press, Cambridge, pp 589–662.

Randall, D. A., D. Harshvardhan and T. G. Corsetti (1989), Interactions among radiation, convection, and largescale dynamics in a general circulation model, *J. Atmos. Sci., 46*, 1943–1970.

Rappaport, E. N., J. L. Franklin, L. A. Avila, S. R. Baig, J. L. Beven, E. S. Blake, C. A. Burr, J. G. Jiing, C. A. Juckins, R. D. Knabb, C. W. Landsea, M. Mainelli, M. Mayeld, C. J. McAdie, R. J. Pasch, C. Sisko, S. R. Stewart and A. N. Tribble (2009), Advances and challenges at the national hurricane center, *Weather and Forecasting*, *24*(2), 395-419.

Reihl, H. and J. Malkus J. (1958), On the heat balance in the equatorial trough zone, 503–537, http://snow.atm.ncu.edu.tw/TC/RiehlMalkus1958.pdf.

Rienecker, M. M. and Co-authors (2011), MERRA: NASA's ModernEra Retrospective Analysis for Research and Applications, *J. Clim., 24*, 3624–3648. doi:10.1175/JCLID1100015.1

Roca, R. and V. Ramanathan (2000), Scale Dependence of Monsoonal Convective Systems over the Indian Ocean, *J. Clim., 13*(7), 1286-1298, doi:10.1175/ 1520-0442(2000)013h1286:SDOMCSi2.0.CO;2.

Roca, R., M. Viollier, L. Picon, and M. Desbois (2002), A multisatellite analysis of deep convection and its moist environment over the Indian Ocean during the winter monsoon, *J. Geophys. Res., 107*(D19), doi:10.1029/2000JD000040

Roca, R., S. Louvet, L. Picon, and M. Desbois (2005), A study of convective systems, water vapor and top of the atmosphere cloud radiative forcing over the Indian Ocean using INSAT-1B and ERBE data, *Meteorol. Atmos. Phys., 90*, 49-65, doi:10.1007/ s00703-004-0098-3.

Rogers, M. and D. Vane (2010), The CloudSat Education Network: Scientifically significant collaborative research between students and scientists, *Geoscience and Remote Sensing Symposium (IGARSS)-IEEE International*. 978-1-4244-9566-5/10

Rossow, W. and Co-authors (1985), ISCCP cloud analysis algorithm intercomparison, *Adv. Space Res., 5*(6), 185, doi:10.1016/0273-1177(85)90319-9.

Rossow, W. B. (1989), Measuring Cloud Properties from Space: A Review, *J. Clim*., *2*(3), 201-213, doi:10.1175/1520-0442(1989)002h0201:MCPFSAi2.0.CO;2.

Rossow, W. B., R. A. Schiffer (1999), Advances in understanding clouds from ISCCP. *Bull. Amer. Meteorol. Soc., 80***,** 2261–2288.

Rossow, W., Y. Zhang and J. Wang (2005), A statistical model of cloud vertical structure based on reconciling cloud layer amounts inferred from satellites and radiosonde humidity profiles, *J. Clim., 18*, 3587–3605.

Sassen, K. and Z. Wang (2008), Classifying clouds around the globe with the CloudSat radar: 1-year of results, *Geophys. Res. Lett.*, *35*, L04805, doi:10.1029/2007GL032591.

Sassen, K. and Z. Wang (2008), Level 2 Cloud Scenario Classification Producr Process Description and Interface Control Document, version 4.0.

Sathiyamoorthy, V. P. K. Pal and P. C. Joshi (2004), Influence of the upper tropospheric wind shear upon cloud radiative forcing in the Asian Monsoon Region, *J. Clim., 17*(14), 2725–2735.

Sathiyamoorthy, V., C. Mahesh, G. Kaushik, Satya Prakash, Bipasha P. Shukla and A. K. Mathur (2013), Characteristics of low clouds over the Arabian Sea. *J. Geophys. Res., 118,* 13489–13503, doi: 10.1002/2013JD020553.

Sathiyamoorthy, V., Shukla and Bipasha (2011), A study on radiative properties of Indian summer monsoon clouds, *Met. and Atmos. Phys., 113*, 55-66.

Satoh, S. and A. Noda (2001), Retrieval of latent heating profiles from TRMM radar data. *Proc. of the 30th Int. Conf. on Radar Meteorology*, Munich, Germany, *Amer. Meteor. Soc*., 340–342.

Schneider-Carius, K. (1955), *Wetterkunde und Wetterforschung,* Kari Alber Verlag, Munchen, 423 pp.Schumacher, C., R. A. Houze and I. Kraucunas (2004), The tropical dynamical response to latent heating estimates derived from the TRMM precipitation radar, *J. Atmos. Sci., 61,* 1341–1358.

Schumacher, C., R.A. Houze and I. Kraucunas (2004), The Tropical Dynamical Response to Latent Heating Estimates Derived from the TRMM Precipitation Radar, *J. Atmos. Sci.,* 61, 1341–1358, https://doi.org/10.1175/1520-0469(2004)061<1341:TTDRTL>2.0.CO;2

Schumacher, C. and R. A. Houze (2003), The TRMM precipitation radar's view of shallow, isolated rain, *J. Appl. Meteorol*., 42, 1519–1524.

Scorer, R. S. (1963), Cloud nomenclature, *Q. J. R. Meteorof. Sac., 89*, 248-253.

Senior, C. A. and J. F. B. Mitchell (1993), Carbon dioxide and climate: the impact of cloud parameterization, *J. Clim.*, *6*, 393-418.

Shige, S., Y. N. Takayabu, W. K. Tao and D. E. Johnson (2004), Spectral retrieval of latent heating profiles from TRMM PR data. Part I: Development of a model-based algorithm, *J. Appl. Meteor., 43*, 1095-1113.

Shige, S., Y. Takayabu, W. Tao and C. Shie (2007), Spectral retrieval of latent heating profiles from TRMM PR data. PART ii: Algorithm improvement and heating estimates over tropical ocean regions, *J. App. Met.*, *46,* 1098–1124, doi: http://dx.doi.org/10.1175/JAM2510.1

Simpson, J., C. Kummerow, W.-K. Tao, and R. Adler (1996), On the Tropical Rainfall Measuring Mission (TRMM), *Meteor. Atmos. Phys., 60,* 19–36.

Simpson, J., R. F. Adler and G. R. North (1988), A Proposed tropical rainfall measuring mission (TRMM) satellite, *Bull. Amer. Meteorol. Soc.*, *69*, 278-295.

Slingo, A. (1990), Sensitivity of the Earth's radiation budget to changes in low clouds, *Nature*, *343*, 49–51.

Slingo, A. and J. M. Slingo (1988), The response of a general circulation model to cloud longwave radiative forcing. I. Introduction and initial experiments, *Q. J. R. Meteorol. Soc., 114*, 1027–1062

Stephens, G. L. (2005), Cloud feedback in the climate system: a critical review, *J. Clim., 18*, 237–273.

Stephens, G. L. and C. D. Kummerow (2007), The Remote Sensing of Clouds and Precipitation from Space: A Review, *J. Atmos. Sci., 64*, 3742-3765, DOI: 10.1175/2006JAS2375.1

Stephens, G. L. and Co-authors (2002), The Cloudsat Mission And The A-Train, *Bull. Am. Meteorol. Soc*., *83*, 1771-1790.

Stephens, G. L. and Co-authors (2008), CloudSat mission: Performance and early science after the first year of operation, *J. Geophys. Res., 113*, D00A18. doi:10.1029/2008JD009982.

Stephens, G. L. and T. L'Ecuyer (2015), The Earth's energy balance, *Atmos. Res.*, *166*, 195–203, doi.org/10.1016/j.atmosres.2015.06.024

Su, H., J. H. Jiang, D. G. Vane and G. L. Stephens (2008), Observed vertical structure of tropical oceanic clouds sorted in large-scale regimes, *Geophys. Res. Lett.*, *35*, doi:10.1029/2008GL035888.

Su, H., J. H. Jiang, J. Teixeira, A. Gettelman, X. Huang, G. L. Stephens, D. Vane and V. S. Perun (2011), Comparison of regime-sorted tropical cloud profiles observed by CloudSat with GEOS5 analyses and two general circulation model simulations, *J. Geophys. Res., 116,* doi:10.1029/2010JD014971.

Subbaramayya, I. and R. Ramanadham (1981), On the onset of the Indian southwest monsoon and the monsoon general circulation, *Monsoon Dynamics*, J. Lighthill and R. P. Pearce, Eds., Cambridge University Press, 213–220.

Subrahmanyam, K. V. and K. K. Kumar (2013), CloudSat observations of cloudtype distribution over the Indian summer monsoon region, *Ann. Geophys., 31*, 1155–1162. doi:10.5194/angeo3111552013.

Subrahmanyam, K.V. and K. K. Kumar (2016), TRMM observations of Latent heat distribution over the Indian summer monsoon region and associated dynamics, *Proc. of SPIE* Vol. 9876, 98762W, doi: 10.1117/12.2223905.

Subrahmanyam, K. V. and K. K. Kumar (2017), CloudSat observations of multi layered clouds across the globe, *Clim. Dyn., 49*, 327-341, doi:10.1007/s00382-016-3345-7.

Subrahmanyam, K.V and K. K. Kumar (2018a), Vertical structure of stratocumulus clouds and associated dynamics over the Arabian Sea during Indian summer monsoon season, *J. Appl. Remote Sens.* 12(1), 016018 (2018), doi: 10.1117/1.JRS.12.016018.

Subrahmanyam, K.V. and K. K. Kumar (2018b), Cloud type distribution in Tropical Cyclones formed in the North Indian Ocean using CloudSat observations, *IEEE Journal of Selected Topics in Applied Earth Observations and Remote Sensing, 11(2), 339-344, doi: 10.1109/JSTARS.2017.2786666*.

Subrahmanyam, K. V., K. K. Kumar and A. N. Babu (2015), Phase relation between CAPE and precipitation at diurnal scales over the Indian summer monsoon region, *Atmos. Sci. Let.,* doi: 10.1002/asl2.566.

Tang, X. and B. Chen (2006), Cloud type associated with the Asian summer monsoons as determined from MODIS/TERRA measurements and a comparison with surface observations, *Geophys. Res. Lett., 33,* L07814. doi:10.1029/2006GL026004.

Tao, W. -K. and Co-authors (2016), TRMM Latent Heating Retrieval: Applications and Comparisons with Field Campaigns and Large-Scale Analyses, *Meteor. Monogr*., No.*56*, Amer. Meteor. Soc., DOI: 10.1175/AMSMONOGRAPHS-D- 15-0013.1

Tao, W. -K. And Co-authors (2006), Retrieval of Latent Heating from TRMM measurements, *Bull. Amer. Meteorol. Soc.*, 1555-1572.

Tao, W.-K. (2003), Goddard Cumulus Ensemble (GCE) model: Application for understanding precipitation processes. Cloud Systems, Hurricanes, and the Tropical Rainfall Measuring Mission (TRMM), *Meteor. Monogr*., No. *51*, Amer. Meteor. Soc., 107–138.

Tao, W.-K., S. Lang, J. Simpson, and R. Adler (1993), Retrieval algorithms for estimating the vertical profiles of latent heat release: Their applications for TRMM, *J. Meteor. Soc. Japan*, *71*, 685–700.

The Cloud Profiling Radar (CPR), http://cloudsat.atmos.colostate.edu/instrument

Tourville, N., G. L. Stephens, M. DeMaria and D. Vane (2015), Remote Sensing of Tropical Cylcones: Observations from CloudSat and A-Train Profilers, *Bull. Amer. Meteorol. Soc*., 609-622, doi:10.1175/BAMS-D-13-00282.1

Trenberth, K. E. and J. T. Fasullo (2010), Tracking earth's energy, *Science*, *328*, 316–317

Trenberth, K.E., J. T. Fasullo, and M. A. Balmaseda (2014), Earth's energy imbalance, *J. Clim.*, *27*, 3129–3144.

Velden, C. and W. Smith (1983), Monitoring tropical cyclone evolution with NOAA satellite microwave observations, *J. Appl. Meteor.*, *22,* 714-724.

Wallace, J. M. (1975), Diurnal variations in precipitation and thunderstorm frequency over the conterminous United States, *Mon. Wea. Rev.,* 103, 406–419.

Wallace, J. M. and P. V. Hobbs (1977), Atmospheric Science: An Introductory Survey, 483 pp., Academic Press, San Diego, Orlando, FL, USA.

Wallace, J. M. and P. V. Hobbs (2006), Atmospheric Science 2nd Edition: An Introductory Survey, 483 pp., Academic Press, San Diego, Orlando, FL, USA.

Wang, J. and W. B. Rossow (1995), Determination of cloud vertical structure from upper-air observations, *J. Appl. Meteor., 34*, 2243–2258.

Wang, J. and W. B. Rossow (1998), Effects of Cloud Vertical Structure on Atmospheric Circulation in the GISS GCM, *J. Clim., 11* (11), 3010-3029, doi:10.1175/1520-0442(1998)011h3010:EOCVSOi2.0.CO;2.

Wang, J., W. B. Rossow and Y. Zhang (2000), Cloud vertical Structure and Its Variations from a 20-Yr Global Rawinsonde Dataset, *J. Climate., 13*, 3041-3056.

Wang, Z. and K. Sassen (2001), Cloud type and macrophysical property retrieval using multiple remote sensors, Journal of Applied Meteorology, 40, 1665–1682.

Waters, W. J., Kunzi, KLAUS, L. Pettyjohn, R., K. L. Poon, R., H. Staelin, D. (1975), Remote Sensing of Atmospheric Temperature Profiles with the Nimbus 5 Microwave Spectrometer, *J. Atmos. Sci., 32*, 10.1175/1520-0469(1975)032<1953:RSOATP>2.0.CO;2.

Webster, P. J. and Co-authors (1998), Monsoons: Processes, predictability, and the prospects for prediction, *J. Geophys. Res., 103*, 14451-14510.

Webster, P. J. and G. L. Stephens (1984), Cloud–radiation interaction and the climate problem, In: Houghton J [ed] The global climate. Cambridge University Press, Cambridge, pp 63–78

Webster, P.J. (1972), Response of tropical atmosphere to local, steady forcing, *Mon, Wea. Rev., 100*(7), 518-541.

Wielicki, B. A., R. D. Cess, M. D. King, D. A. Randall and E. F. Harrison (1995), Mission to Planet Earth: Role of clouds and radiation in climate, *Bull. Am. Meteorol. Soc*., *76*, 2125–2153.

Winker, D. M., W. H. Hunt and M. J. McGil (2007), Initial performance assessment of CALIOP, *Geophys. Res. Lett., 34*, L19803. doi:10.1029/2007GL030135, 2007.

WMO (1974), Manual on Codes, *WMO* Publ. 306, Vol. 1

Wonsick, M. M., R. T. Pinker and Y. Govaerts (2009), Cloud Variability over the Indian Monsoon Region as Observed from Satellites, *J. Appl. Meteorol. Clim., 48*, 1803-1821.

World Meteorological Society (1956), International Cloud Atlas, Vol. 1. Geneva.

Wu, D. L. and Co-authors (2009), Vertical distributions and relationships of cloud occurrence frequency as observed by MISR, AIRS, MODIS, OMI, CALIPSO, and CloudSat, *Geophys. Res. Lett., 36*, L09821. doi:10.1029/2009GL037464

Yan, Y., Y. Liu, and J. Lu (2016), Cloud vertical structure, precipitation, and cloud radiative effects over Tibetan Plateau and its neighbouring regions, *J. Geophys. Res. Atmos*., *121*, 5864–5877, doi:10.1002/2015JD024591.

Yanai, M., S. Esbensen and J. H. Chu (1973), Determination of bulk properties of tropical cloud clusters from large-scale heat and moisture budgets, *J. Atmos. Sci., 30*, 611–627.

Yang, Y. J., D. R. Lu, Y. F. Fu, F. J. Chen, Y. Wang (2015), Spectral Characteristics of Tropical Anvils Obtained by Combining TRMM Precipitation Radar with Visible and Infrared Scanner Data, *Pure Appl. Geophys.*, *172*, 1717–1733, DOI 10.1007/s00024-014-0965-x.

Yang, S. and E. A. Smith (1999), Moisture budget analysis of TOGA COARE area using SSM/I retrieved latent heating and large-scale Q2 estimates, *J. Atmos. Oceanic Technol.*, *16*, 633–655, doi:10.1175/1520-0426(1999)016,0633:MBAOTC.2.0.CO;2.

Yang, S., W. S. Olson, J.-J. Wang, T. L. Bell, E. A. Smith, and C. D. Kummerow (2006), Precipitation and latent heating distributions from satellite passive microwave radiometry. Part II: Evaluation of estimates using

independent data, *J. Appl. Meteor.*, *45*, 721–739, doi:10.1175/JAM2370.1.

Yuan, X., J. Patoux and C. Li (2009), Satellite based midlatitude cyclone statistics over the Southern Ocean: 2. Tracks and surface fluxes, *J. Geophys. Res., 114*, D04106. doi:10.1029/2008JD010874

Yuan, J. and R. A. Houze, Jr. (2011), Vertical Structures of Anvil Clouds of Tropical Mesoscale Convective Systems Observed by CloudSat, *J. Atmos. Sci.,* 68, 1653-1674, DOI: 10.1175/2011JAS3687.1

Zhang, Y., H. Chen, and R. Yu (2014), Vertical structures and physical properties of the cold-season stratus clouds downstream of the Tibetan Plateau: Differences between daytime and night time, *J. Clim*., *27*(18), 6857–6876, doi:10.1175/jcli-d-14-00063.1.

Zhang, J., H. Chen, Z. Li, X. Fan, L. Peng, Y. Yu, and M. Cribb (2010), Analysis of cloud layer structure in Shouxian, China using RS92 radiosonde aided by 95 GHz cloud radar, *J. Geophys. Res*., *115*, D00K30, doi:10.1029/2010JD014030.

Zipser, E. J., D. Cecil, C. Liu, S. Nesbitt and D. Yorty (2006), Where are the most intense thunderstorms on earth?, *Bull. Am. Meteorol. Soc., 87*, 1057–1071.

Zuidema, P. (2003), Convective Clouds over the Bay of Bengal, *Mon. Wea. Rev., 131*(5), 780-798, doi:10.1175/1520-0493(2003)131h0780: CCOTBOi2.0.CO;2.

Ann. Geophys., 31, 1155–1162, 2013
www.ann-geophys.net/31/1155/2013/
doi:10.5194/angeo-31-1155-2013

Annales Geophysicae
Open Access

CloudSat observations of cloud-type distribution over the Indian summer monsoon region

K. V. Subrahmanyam and K. K. Kumar

Space Physics Laboratory, Vikram Sarabhai Space Centre, Thiruvananthapuram, Kerala, India

Correspondence to: K. K. Kumar (kishore_nmrf@yahoo.com)

Received: 26 February 2013 – Revised: 22 May 2013 – Accepted: 24 May 2013 – Published: 3 July 2013

Abstract. The three-dimensional distribution of various cloud types over the Indian summer monsoon (ISM) region using five years (2006–2010) of CloudSat observations during June-July-August-September months is discussed for the first time. As the radiative properties, latent heat released and microphysical properties of clouds differ largely depending on the cloud type, it becomes important to know what types of clouds occur over which region. In this regard, the present analysis establishes the three-dimensional distribution of frequency of occurrence of stratus (St), stratocumulus (Sc), nimbostratus (Ns), cumulus (Cu), altocumulus (Ac), altostratus (As), cirrus (Ci) and deep convective (DC) clouds over the ISM region. The results show that the various cloud types preferentially occur over some regions of the ISM, which are consistent during all the years of observations. It is found that the DC clouds frequently occur over northeast of Bay of Bengal (BoB), Ci clouds over a wide region of south BoB–Indian peninsula–equatorial Indian Ocean, and Sc clouds over the north Arabian Sea. Ac clouds preferentially occur over land, and a large amount of As clouds are found over BoB. The occurrence of both St and Ns clouds over the study region is much lower than all other cloud types.The interannual variability of all these clouds including their vertical distribution is discussed. It is envisaged that the present study opens up possibilities to quantify the feedback of individual cloud type in the maintenance of the ISM through radiative forcing and latent heat release.

Keywords. Meteorology and atmospheric dynamics (tropical meteorology)

1 Introduction

Owing to its socioeconomic impacts, the Indian summer monsoon (ISM) is one of the most investigated topics in the realms of meteorology. Many studies on the ISM by several researchers across the globe contributed constructively to the present understanding of this enigmatic large-scale system (Webster et al., 1998; Gadgil, 2003). Generally, it is believed that the continental-scale land–sea thermal contrast is the origin of large-scale monsoon circulation (Wallace and Hobbs, 1977). However, once the monsoon is set, its advancement, maintenance and withdrawal depends not only on the large-scale dynamics but also on the internal dynamics initiated by the cloud systems embedded within the monsoon system. These cloud systems over the ISM region modify the thermal structure and moisture budget of the troposphere by releasing latent heat, modifying the radiative heat, and through precipitation. Thus the clouds are an important integral part of the monsoon system, and any attempt to understand the latter should include the detailed investigations on the former. Realizing its importance, many attempts were made in the past to study the cloud distribution over the ISM region (Grossman and Garcia, 1990; Laing and Fritch, 1993). Most of these studies used passive remote sensing techniques and are thus limited to fraction of cloud cover over the ISM region. However, Wonsick et al. (2009) focused on detailed study on cloud variability over the monsoon region in terms of total, low, high and convective cloud amounts throughout the different phases of the monsoon. Very recently, Li et al. (2011) accessed the radiative impacts of single- and multi-layered clouds using A-Train observations. These results indicated that the multi-layer clouds have a significant impact on radiation budget and differ with that of single-layered clouds. Thus it is important to know not only the amount of cloud

Published by Copernicus Publications on behalf of the European Geosciences Union.

cover but also its vertical distribution. For example, high-level clouds tend to warm the climate, while low-level clouds lead to a cooling effect (Ramananthan et al., 1989). Recently, Tang and Chen (2006), using the MODIS/Terra measured cloud properties dataset, investigated the characteristics of clouds associated with the Asian summer monsoon. These authors emphasized the distribution of low-, mid- and high-level clouds and found that a large amount of high clouds exist in the Indian monsoon region. Thus it becomes important to know the three-dimensional distribution of the clouds.

Apart from the total cloud amount and its vertical distribution, one more important aspect of clouds is the cloud type. It is known that depending upon the cloud type, the radiative properties, the latent heat released and microphysical properties of clouds largely differ. Chen et al. (2000) investigated the radiative flux changes induced by the occurrence of different cloud types using International Satellite Cloud Climatology Project cloud data and a radiative transfer model. These authors emphatically showed that the cloud-type variations are as important as cloud cover in modifying the radiation field of the earth–atmosphere system and further showed that the largest annual mean changes of the global top-of-atmosphere and surface shortwave radiative fluxes are produced by stratocumulus, altostratus, and cirrostratus clouds; whereas cirrus, cirrostratus, and deep convective clouds cause most of the annual mean changes in the global top-of atmosphere longwave radiative fluxes. Thus it becomes clear that, apart from the three-dimensional distribution of cloud cover, it is important to have cloud type distribution to quantify the feedback provided by the clouds in totality.

Even though there are studies on cloud distribution over the ISM region, there are no studies focusing on cloud type distribution. Sufficient knowledge of the spatial distribution of individual cloud types would aid the accurate radiation and latent heat calculations, which in turn would help in accessing the role of clouds in the maintenance and advancement of the ISM. So it becomes important to know which types of clouds occur over which region. In this regard, a study is carried out using five years (2006–2010) of CloudSat observations during June-July-August-September (JJAS) months to establish the three-dimensional distribution of individual cloud types over the ISM region for the first time. Section 2 provides the data and methodology. Results are discussed in Sect. 3, and Sect. 4 provides the summary.

2 Data and methodology

Five years of CloudSat observations during June-July-August-September months over the ISM region form the basis for the present study. The cloud profiling radar (CPR) onboard CloudSat operates at 94 GHz with cross- and along-track resolution of 1.4 and 1.7 km respectively, which is a part of the A-Train constellation. With $\sim$ 240 m vertical resolution, CPR can probe optically thick large-particle layers. However, CPR is not sensitive to optically thin clouds such as high-altitude cirrus clouds. More details on CloudSat can be found in Stephens et al. (2008). For the present study, we use the 2B-CLDCLASS data product of version 5 over the ISM region (10° S to 30° N, 50° to 100° E). In the following section, we briefly discuss the cloud classification algorithm, which was implemented in deriving the 2B-CLDCLASS product.

Wang and Sassen (2001) developed an algorithm to classify clouds by combining the measurements of ground-based multiple remote sensors. Further, Sassen and Wang (2008) described the cloud cluster analysis for classifying clouds by using vertical and horizontal cloud properties, the presence or absence of precipitation from both CloudSat and MODIS observations along with ECMWF temperature profiles. The present data product uses this algorithm for cloud type classification. The cloud cluster analysis converts the vertical profiles of reflectivity from CloudSat into meaningful microphysical data quantities and identifies the clouds based on the cloud mask algorithm. The cloud clustering analysis provides cloud horizontal and vertical extent features and cloud layer structure with significant CPR cloud mask values ($\geq$ 30). Further, classification of the cloud type is done based on microphysical properties, maximum reflectivity and corresponding temperature at that level, cloud vertical and horizontal extent and the precipitating properties. Complete details on the cloud classification algorithm can be found in the 2B-CLDCLASS product description document at http://www.cloudsat.cira.colostate.edu/dataHome.php. The maximum number of cloud types provided by this product is eight: cirrus (Ci), altostratus (As), altocumulus (Ac), stratus (St), stratocumulus (Sc), cumulus (Cu), nimbostratus (Ns) and deep convective (DC) clouds (i.e., cumulonimbus). Out of the eight clouds, Ns, St, Sc, Cu, Ac and Dc are categorized as precipitating clouds, and remaining clouds are non-precipitating clouds. Further these clouds are classified into high-, middle- and low-level clouds. This product is available as a function of latitude, longitude and altitude with the same resolution as that of CPR. There have been attempts in the recent past to validate this product. The CloudSat Educational Network (CEN), a primary education and public outreach component of the CloudSat mission, collected visual observations of cloud type during the period of 2007–2008 and compared the observed cloud types to those retrieved using the CloudSat 2B-CLDCLASS product. There were 227 coincidental measurements of CEN and CloudSat within $\sim$ 100 km radius. The preliminary comparison has shown 66 % agreement between the surface observers and CloudSat observations (Rogers and Vane, 2010). Very recently, Behrangi et al. (2012) used the 2B-CLDCLASS product to study the vertical and horizontal distributions of the cloud types across different seasons over the contiguous USA and surrounding areas. In this study, the authors describe the 2B-CLDCLASS product in detail including their limitations:

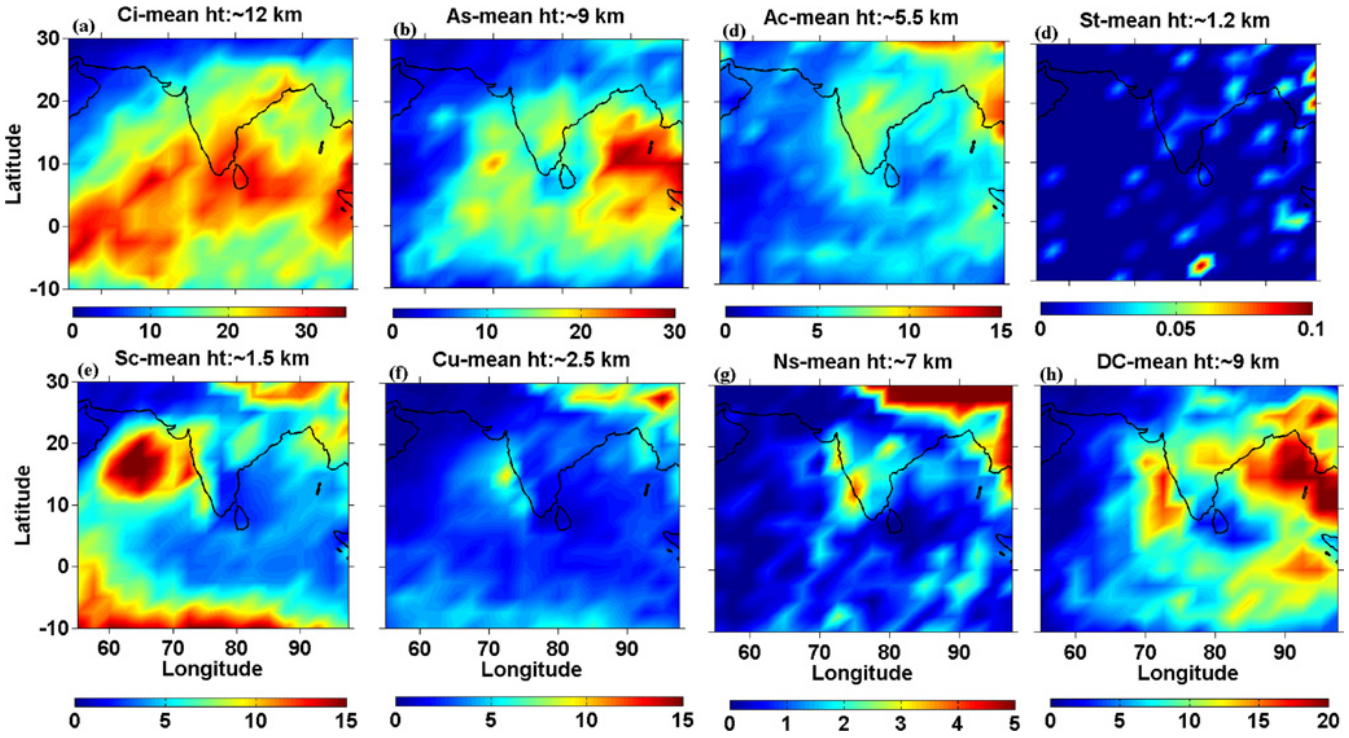

Fig. 1. Five-year (2006–2010) mean distribution of frequency of occurrence during JJAS of **(a)** Ci, **(b)** As, **(c)** Ac, **(d)** St, **(e)** Sc, **(f)** Cu, **(g)** Ns and **(h)** DC clouds over the ISM region. Both day- and nighttime observations of CloudSat are used for the analysis. The mean altitude provided at the top of the maps corresponds to the average of peak altitudes at which maximum frequency of occurrence is observed over the study region (see text for more details).

(1) surface contaminations in the lower 3 to 4 range bins of CPR vertical reflectivity profiles will have implications in classifying St and Sc clouds, and (2) the CPR is not sensitive to high-altitude thin clouds, which will have implications in detecting the Ci clouds. Thus both these limitations will result in fewer detections of St, Sc and Ci clouds than actually present. One should keep these things in mind while interpreting the observations. The second limitation can be overcome by combining the CALIPSO observations. However, it will be done in near future.

We have followed the following procedure to calculate the frequency of occurrence of each cloud type. (1) The observations over the study region are grouped into 2.5×2.5 grid boxes. (2) The number of occurrences of each cloud type as a function of altitude is estimated in each grid box. (3) The number of occurrences of each cloud type is then divided by the number of occurrences of all cloud types at each altitude. (4) Step 3 yielded the height profile of frequency of occurrence of each cloud type within each grid box. (5) From these height profiles, the altitude at which the maximum frequency of occurrence takes place is found for each cloud type for a given grid box. (6) The maximum frequency of occurrence at the altitude (provided by step 5) is then used to create the maps over the ISM region, which will be discussed in the next section. The height profiles of frequency of occurrence in each grid box provided the 3-D distribution of cloud types over the ISM region.

3 Results and discussion

By adopting the method described in Sect. 2, we quantified the frequency of occurrence of various cloud types, and Fig. 1a–h show the five-year (2006–2010) mean distribution of frequency of occurrence of Ci, As, Ac, St, Sc, Cu, Ns and DC clouds over the ISM region during JJAS. Figure 1 contains both daytime and nighttime observations of CloudSat. It has to be remembered that we have estimated the frequency of occurrence at each altitude bin and Fig. 1 corresponds to the altitude where maximum frequency of occurrence of corresponding cloud is observed. As the altitude at which maximum frequency of occurrence takes place differs from one grid box to another, we have taken the mean of these altitudes over the study region, and the same is provided in Fig. 1 as mean altitude. From Fig. 1a it is evident that the distribution of Ci is highly concentrated over south Bay of Bengal (BoB), Indian peninsula and Indian Ocean. During the ISM, the convective storms over most northern parts of BoB (known as head BoB) produce copious amounts of Ci clouds (formed from the anvil of deep convective clouds), which are spread over the ISM region by the strong Tropical Easterly Jet (TEJ)

(Sathiyamoorthy et al., 2004). The maximum percentage of occurrence of Ci cloud is ∼ 30–35 %. As discussed in Sect. 2, the CloudSat underestimates the occurrence of Ci clouds as it is not sensitive to optically thin cirrus clouds. CloudSat observations over the ISM region are limited to two local times per day. If there are any diurnal variations in particular cloud occurrence, it may bias the frequency of occurrence estimations discussed here (however, an attempt is made to bring out the differences between the frequencies of occurrence of each cloud during day- and nighttime over the ISM region, which will be discussed later in this section). The Ci clouds are known for their role in radiative forcing, and thus their unambiguous spatial distribution assumes its importance. Figure 1b shows the distribution of frequency of occurrence of As clouds, which seem to occur preferentially over BoB compared to over the Arabian Sea. Interestingly, occurrence frequency of As cloud is higher over oceans than over land in contrast to Ac cloud distribution shown in Fig. 1c, which frequently occur over land. The frequency of occurrence of Ac is found to be high over Bangladesh, Tibetan Plateau region and uniformly distributed over the Indian landmass. The preferential occurrence of Ac over land is a relatively new observation and needs to be further investigated in terms of microphysical processes associated with Ac clouds. Frequency of occurrence of St and Ns clouds is shown in Fig. 1e and g, respectively. From these maps it is evident that occurrence of these two clouds is very low compared to other cloud types over the study region. Especially the occurrence of St clouds is almost non-existent over the ISM region. This can be to some extent attributed to the surface contamination of CPR in the lower heights up to ∼ 1 km. But, in the case of Ns cloud distribution, there is considerable amount of occurrences over the Tibetan Plateau region.

Frequency of occurrence of Sc cloud is shown in Fig. 1e, which readily reveals its maximum occurrence over the Arabian Sea region and also over equatorial Indian Ocean. It is interesting to note that the Sc clouds form scarcely over the BoB. The spatial distribution of Sc clouds is also very crucial as it plays an important role in shortwave radiative forcing resulting in cooling of the surface. The confinement of Sc clouds over the Arabian Sea can be attributed to the descending motion from monsoon convection apart from lower tropospheric thermal inversion that occurs during the ISM period over this region (Sathiyamoorthy et al., 2011). The weak descending motions over the Arabian Sea during the ISM period can suppress the vertical development of clouds. The strong winds over the Arabian Sea during the ISM period can cool the sea surface by upwelling, which also can play a role in suppressing the convection. Besides these reasons, there is a strong mixing of dry air from Arabian Desert at around 650–500 hpa (figure not shown), which further dilutes the vertical development of the convection over the Arabian Sea. Thus there are strong dynamical processes that prevail over the Arabian Sea, which results in limiting the convection growth and seems to be the prime reason for formation of Sc clouds as observed in the present study.

Figure 1f shows the frequency of occurrence of Cu clouds, which are relatively high over Tibetan Plateau region and the western coast of southern India. A secondary peak can also be observed in Cu occurrence over equatorial Indian Ocean. Other than these regions, Cu occurrence frequency is very low over the study region. The distribution of DC clouds, which are very important in both radiative and latent heat estimations as well as in precipitation over the ISM region, is shown in Fig. 1h. Compared to other cloud types, the distribution of DC clouds has been well documented over the ISM region (Grossman and Garcia, 1990; Laing and Fritsch, 1993; Houze et al., 2007). From Fig. 1h, it can be noted that the DC clouds are highly concentrated in the northeast of BoB, a consistent feature reported by earlier studies (Zuidema, 2003). A secondary peak in frequency of occurrence of DC can be noted over the western coast of India and central India. These DC clouds produce large amounts of precipitation, and good or bad monsoon mostly depends on the distribution and frequency of occurrence of these clouds. It is also known that the highest mean precipitation over the ISM region takes place over BoB, and thus the distribution of DC clouds becomes very important not only from a hydrological standpoint but also from a dynamical standpoint as large amounts of latent heat released in these system maintain the monsoon circulation (Zuidema, 2003). The continental tropical convergence zone, which extends from the Indo-Gangetic Plain into the BoB, plays a key role in the development of DC clouds by pumping the sufficient moisture into the atmosphere over the north BoB. Thus Fig. 1a–h depict the five-year mean distribution of various cloud types associated with the ISM, and it is observed that dynamics plays a vital role in this distribution. As mentioned earlier, it is important to know what type of cloud forms over which region to assess the feedback provided by the clouds to the large-scale ISM. Figure 1 provides these details for the first time.

It is important to know the diurnal variation in occurrence of cloud types, if any, as CloudSat observations cover only two local times over the ISM region. These satellites cross the Equator at approximately 13:30 and 01:30 local times. Over the ISM region CloudSat observations are made at ∼ 06:00–09:00 UTC (local day) and 18:00–21:00 UTC (local night). The results depicted in Fig. 1 correspond to the mean of all the observations regardless of day or night. As the observations from CloudSat are available during both day and night, an attempt is made to evaluate the difference between the day and night distribution of frequency of occurrence of various cloud types, and the same is shown in Fig. 2. We have generated the distribution maps similar to Fig. 1 for both day- and nighttime separately. The nighttime maps are then subtracted from the daytime maps to obtain the difference between the two. The positive values in Fig. 2 indicate that the particular cloud type occurrence is higher during the daytime than during the nighttime. The first impression from

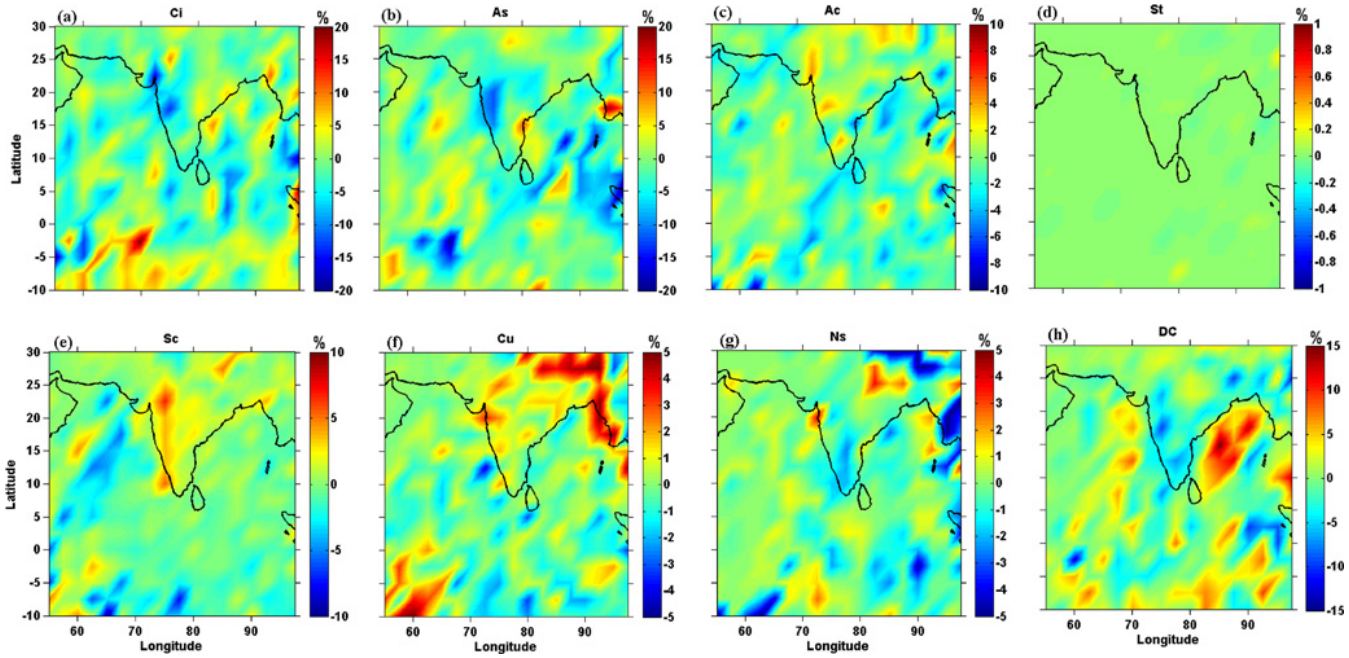

Fig. 2. Same as Fig. 1 but for differences in frequency of occurrence during day- and nighttime.

this figure is that there is no coherent diurnal variation in occurrence of various cloud type except for DC clouds over BoB. Again, the St cloud is underrepresented here. Most of the clouds show a diurnal variation of $\sim 5\,\%$ in their occurrence. However, there are pockets of isolated highs in diurnal variations as in the case of Ci clouds over the Indian Ocean, which show diurnal variation as high as 20 %. The DC clouds show $\sim 15\,\%$ diurnal variations especially over BoB. With these few exceptions, there is no notable diurnal variation in the occurrence of particular cloud types over the ISM region. Thus the five-year JJAS mean distribution of frequency of occurrence of cloud types shown in Fig. 1 is not much affected by the diurnal variations in cloud occurrence frequency as CloudSat observations are available during both local day- and nighttime as confirmed from Fig. 2.

One of the most complex problems associated with the ISM is its interannual variability (Goswami and Xavier, 2005). A part of the interannual variability of the ISM can be attributed to the interannual variability of the various cloud distribution and the feedback provided by these clouds. In order to investigate the interannual variability of the frequency of occurrence of various cloud types, we have established the same for individual years from 2006 to 2010. Figure 3a–f show the interannual variations in frequency of occurrence of the various cloud types Ci, As, Ac, Sc, Cu and DC clouds respectively from 2006 to 2010. The interannual variability of St and Ns is not included here as their frequency of occurrence is lower than other cloud types, as mentioned earlier. The frequency of occurrence of Ci clouds is relatively higher over the south Arabian Sea and equatorial Indian Ocean in 2006, 2007 and 2010, whereas the distribution of Ci is higher over south BoB in 2008 and 2009. However, during all the years, one can notice the signature of TEJ in the distribution of Ci clouds. Further, the distribution of Ci clouds depends on the distribution of DC clouds over head BoB, as a majority of Ci clouds over the ISM are formed from the outflow of DC clouds. The interannual variation of As clouds is shown in Fig. 3b, which readily reveals that the distribution of these clouds is limited to BoB during the years 2006, 2008 and 2009, whereas it is observed over the Arabian Sea also during the years 2007 and 2010. With an exception during the year 2009, the distribution of As over the Arabian Sea seems to exhibit the biennial oscillation. Figure 3c depicts the interannual variation of Ac clouds; as discussed earlier, these clouds preferentially form over land. There is a little interannual variation in the Ac cloud distribution over the ISM region. The interannual variation of Sc clouds is shown in Fig. 3d. It is very interesting to note the consistency of these cloud occurrences over the Arabian Sea as well as over the equatorial Indian Ocean during all the years. Except during the 2009, the frequency of occurrence of these clouds over the Arabian Sea is coherent and limited to a narrow region, and the interannual variation is not very prominent. Figure 3e shows the interannual variation of Cu clouds. There are two prominent peaks in the occurrence of these clouds: one over the Tibetan Plateau and the other over the west coast of India. There is a little interannual variation in their occurrence over these regions. Finally, the interannual variation of DC cloud occurrence is shown in Fig. 3f. From this figure, it is evident that the DC clouds spread over the entire BoB and

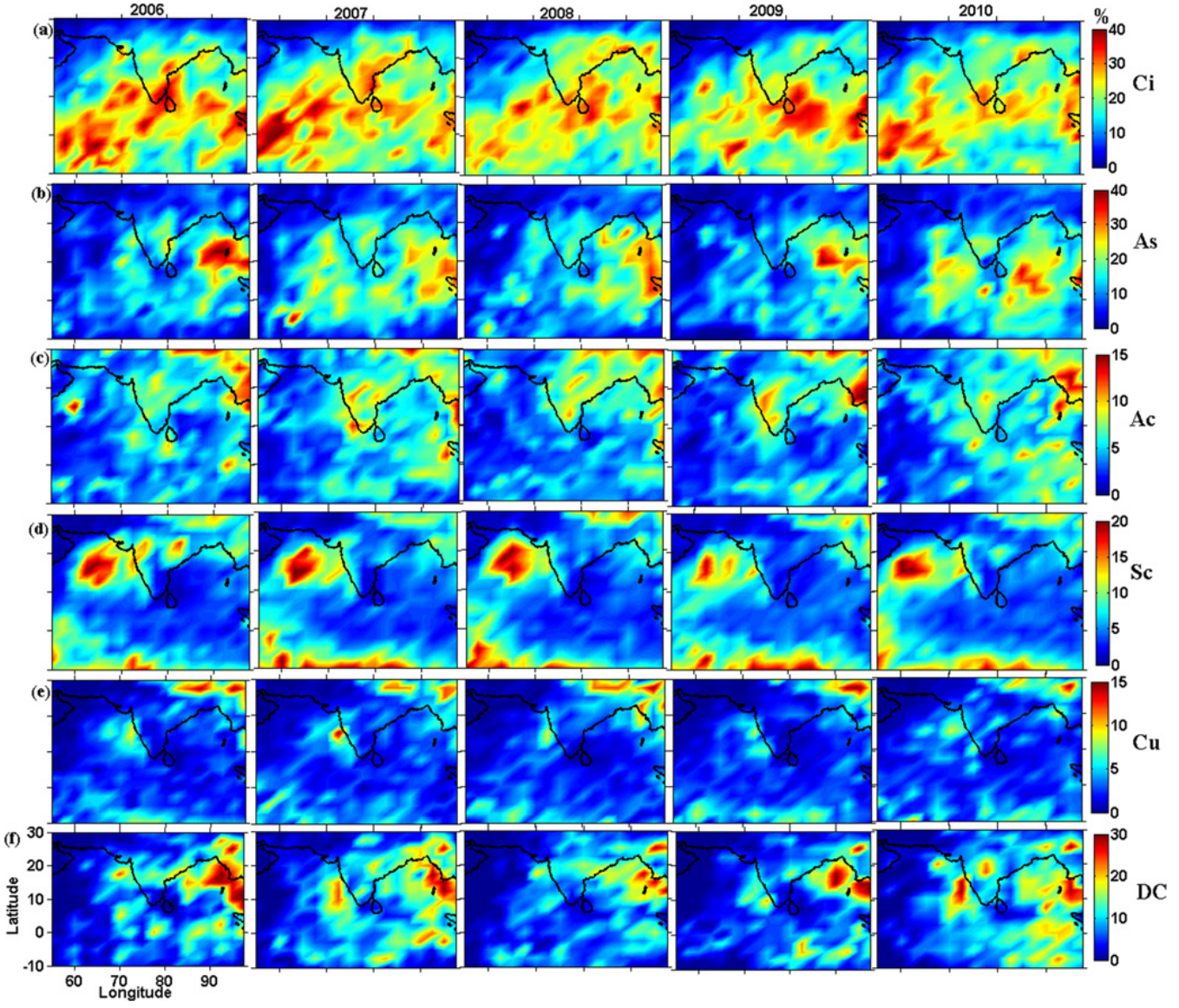

Fig. 3. Distribution of frequency of occurrence of **(a)** Ci, **(b)** As, **(c)** Ac, **(d)** Sc, **(e)** Cu and **(f)** DC clouds during the years 2006–2010.

the Arabian Sea region in 2007 and 2010, whereas in 2006, 2008 and 2009 they are highly concentrated in the north-east BoB. One more noteworthy observation is the lack of DC clouds over the Indian landmass during the year 2009 as compared to other years. The year 2009 was a drought year with 22 % deficiency in all India monsoon rainfall as compared to the long-term monsoon rainfall over the region. Thus Fig. 3a–f describe the interannual variation in distribution of frequency of various cloud types occurring over the ISM region. The dynamical, thermal and moisture structure of the background atmosphere during these years could be the principal reason for the observed interannual variability of these clouds, which have to be further investigated.

As mentioned earlier, the distributions shown in Figs. 1 and 3 correspond to the height at which maximum occurrence of that particular cloud is found. However, it will be useful to have the height distribution of various cloud types over the ISM region. In this regard, we have averaged the frequency of occurrence of individual cloud types in each range bin over the entire ISM region, and Fig. 4a–f show the vertical distribution of frequency of occurrence of Ci, As, Ac, Sc, Cu and DC clouds, respectively. The vertical distribution of Ci, As, Ac, Sc, Cu and DC clouds peaks at 12, 7.5, 6, 1.1, 2 and 5 km height, respectively. The deviations of all India monsoon rainfall from the long-term mean during the individual years 2006–2010 are given in Fig. 4f. This information has been taken from the India Meteorological Department. From these rainfall deviations, it can be noted that the year 2009 is a drought, and all other years are near-normal (2006 and 2008) to excess years (2007 and 2010). During

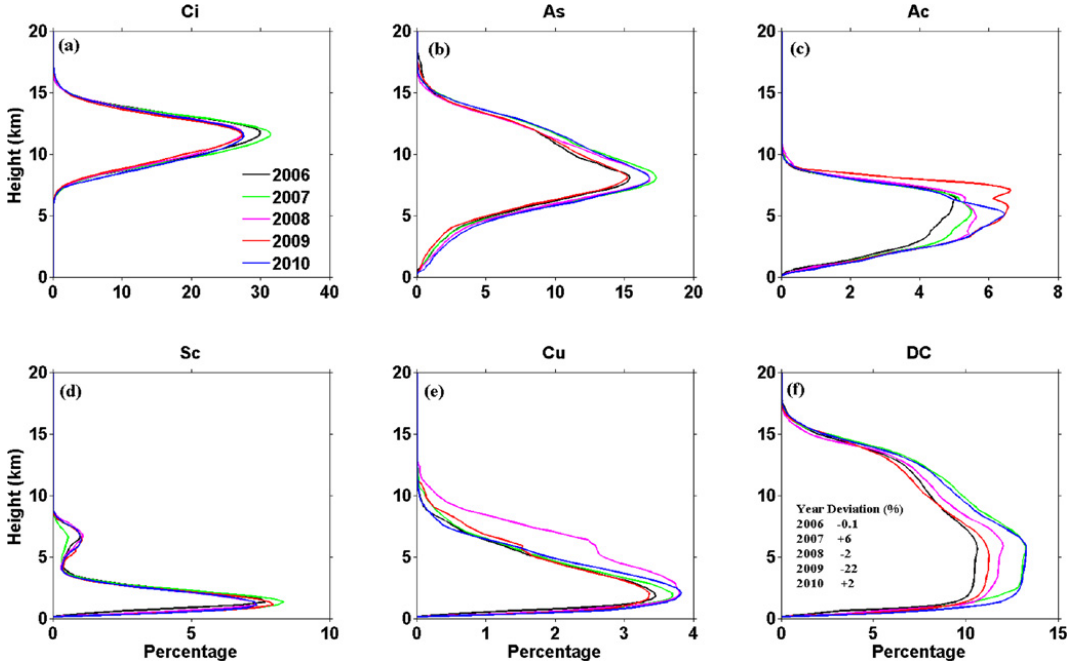

Fig. 4. Vertical distribution of frequency of occurrence of **(a)** Ci, **(b)** As, **(c)** Ac, **(d)** St, **(e)** Cu and **(f)** DC clouds averaged over the ISM region during 2006–2010.

the drought year of 2009, it can be noticed that the frequencies of occurrence of all cloud types are reduced compared to other years, and it is very interesting to note that the vertical distribution of DC clouds reflects the monsoon rainfall (i.e., their frequency of occurrence is higher in excess years than in near-normal and drought years). Thus the present study established the three-dimensional distribution of various cloud types occurring over the ISM region for the first time, which are very vital for understanding the feedback provided by the clouds to the monsoon system. The present study also opens up the possibility to assess the role of individual cloud types in modifying the background thermal structure of the troposphere through radiative and latent heat.

4 Conclusions

Five years (2006–2010) of CloudSat observations over the ISM region are used to establish the three-dimensional distribution of various cloud types in terms of their frequency of occurrence for the first time. The mean distribution of Ci clouds emphatically showed the role of TEJ in spreading the anvils of DC clouds forming over the head BoB. These clouds are most frequently observed over the Indian peninsula, south BoB and Indian Ocean. It is observed that the Sc clouds form most frequently over the north Arabian Sea and are confined to a narrow region. The prevailing dynamical features during the ISM period seem to be responsible for the formation of these clouds over the Arabian Sea. It is also observed that Ac clouds form preferentially over land and As clouds over BoB. The mean distribution of Cu clouds showed three distinct peaks over the Tibetan Plateau, western coast and equatorial Indian Ocean. The distribution of DC clouds, which are very important from a hydrological standpoint, showed a pronounced peak in their occurrence frequency over head BoB and secondary peaks over western coast, south BoB and central India. The frequencies of occurrence of St and Ns clouds are found to be much lower than other cloud types over study region. The diurnal variations in frequency of occurrence of all these clouds are also established using day- and nighttime observations of CloudSat. The interannual variations of all these clouds are discussed, and it is observed that the region over which a particular cloud occurs is consistent from one year to another. The mean vertical distribution of all the cloud types over the ISM region is also established. The vertical structure of DC showed year-to-year variations, which is consistent with the India summer monsoon rainfall observations during that study period. It is envisaged that the present study will be helpful in quantifying the feedback of an individual cloud type to the ISM. Even though the present study discussed the prevailing dynamical features during the ISM period to some extent, further investigations are needed to look into the dynamical aspects associated with the ISM and their role in dictating the observed distribution of a particular cloud type, which will be our immediate priority.

Acknowledgements. The authors are greatly thankful to the CloudSat team for the 2B-CLDCLASS data, which were obtained from

the CloudSat website http://www.cloudsat.cira.colostate.edu.

Topical Editor P. Drobinski thanks one anonymous referee for her/his help in evaluating this paper.

References

Behrangi, A., Casey, S. P. F., and Lambrigtsen, B. H.: Three-dimensional distribution of cloud types over the USA and surrounding areas observed by CloudSat, Int. J. Remote Sens., 33, 4856–4870, 2012.

Chen, T., Rossow, W. B., and Zhang, Y.: Radiative effects of cloud-type variations, J. Climate, 13, 264–286, 2000.

Gadgil, S.: The Indian Monsoon and its variability, Annu. Rev. Earth Planet. Sci., 31, 429–467, 2003.

Goswami, B. N. and Xavier, P. K.: Dynamics of "internal" interannual variability of the Indian summer monsoon in a GCM, J. Geophys. Res., 110, D24104, doi:10.1029/2005JD006042, 2005.

Grossman, R. and Garcia, O.: The distribution of deep convection over ocean and land during the Asian summer monsoon, J. Climate, 3, 1032–1044, 1990.

Houze, R. A., Wilton, D. C., and Smull, B. F.: Monsoon convection in the Himalayan region as seen by the TRMM Precipitation Radar, Q. J. Roy. Meteorol. Soc., 133, 389–1411, 2007.

Laing, A. G. and Fritsch, J. M.: Mesoscale convective complexes over the Indian monsoon region, J. Climate, 6, 911–919, 1993.

Li, J., Yi, Y., Minnis, P., Huang, J., Yan, H., Ma, Y., Wang, W., J., and Ayers, K.: Radiative effect differences between multi-layered and single-layer clouds derived from CERES, CALIPSO, and CloudSat data, J. Quant. Spectr. Radiat. T., 112, 361–375, 2011.

Ramanathan, V., Cess, R. D., Harrison, E. F., Minnis, P., Barkstrom, B. R., Ahmad, E., and Hartmann, D.: Cloud-radiative forcing and climate: results from the earth radiation budget experiment, Science, 24, 357–363, 1989.

Rogers, M. and Vane, D.: The Cloudsat Education Network: Scientifically significant collaborative research between students and scientists," Geoscience and Remote Sensing Symposium (IGARSS), 2010 IEEE International, 84, 25–30, doi:10.1109/IGARSS.2010.5651427, 2010.

Sassen, K. and Wang, Z.: Classifying clouds around the globe with the CloudSat radar: 1- year of results,Geophys. Res. Lett., 35, L04805, doi:10.1029/2007GL032591, 2008.

Sathiyamoorthy, V., Pal, P. K., and Joshi, P. C.: Influence of the upper tropospheric wind shear upon cloud radiative forcing in the Asian monsoon region, J. Climate, 17, 2725–2735, 2004.

Sathiyamoorthy, V., Shukla, B. P., and Pal, P. K.: A study on radiative properties of Indian summer monsoon clouds, Meteorol. Atmos. Phys., 113, 55–66, 2011.

Stephens, G. L., Vane, D. G., Tanelli, S., Im, E., Durden, S., Rokey, M., Reinke, D., Partain, P., Mace, G. G., Austin, R., L'Ecuyer, T., Haynes, J., Lebsock, M., Suzuki, K., Waliser, D., Wu, D., Kay, J., Gettelman, A., Wang, Z., and Marchand, R.: CloudSat mission: Performance and early science after the first year of operation. J. Geophys. Res., 113, D00A18, doi:10.1029/2008JD009982, 2008.

Tang, X. and Chen, B.: Cloud type associated with the Asian summer monsoons as determined from MODIS/TERRA measurements and a comparison with surface observations, Geophys. Res. Lett., 33, L07814, doi:10.1029/2006GL026004, 2006.

Wallace, J. M. and Hobbs, P. V.: Atmospheric Science: An Introductory Survey, Academic Press: Orlando, FL, USA, 1977.

Wang, Z. and Sassen, K.: Cloud type and macrophysical property retrieval using multiple remote sensors, J. Appl. Meteorol., 40, 1665–1682, 2001.

Webster, P. J., Magaña,V. O., Palmer, T. N., Shukla, J., Tomas, R. A., Yanai, M., and Yasunari, T.: Monsoons: Processes, predictability, and the prospects for prediction, J. Geophys. Res., 103, 14451–14510, 1998.

Wonsick, M. M., Pinker, R. T., and Govaerts, Y.: Cloud Variability over the Indian Monsoon Region as Observed from Satellites, J. Appl. Meteorol. Clim., 48, 1803–1821, 2009.

Zuidema, P.: Convective clouds over the Bay of Bengal, Mon. Weather Rev., 131, 780–798, 2003.

Journal of
Applied Remote Sensing

RemoteSensing.SPIEDigitalLibrary.org

Vertical structure of stratocumulus clouds and associated dynamics over the Arabian Sea during Indian summer monsoon season

Kandula Venkata Subrahmanyam
Karanam Kishore Kumar

SPIE.

Kandula Venkata Subrahmanyam, Karanam Kishore Kumar, "Vertical structure of stratocumulus clouds and associated dynamics over the Arabian Sea during Indian summer monsoon season," *J. Appl. Remote Sens.* **12**(1), 016018 (2018), doi: 10.1117/1.JRS.12.016018.

Vertical structure of stratocumulus clouds and associated dynamics over the Arabian Sea during Indian summer monsoon season

Kandula Venkata Subrahmanyam and Karanam Kishore Kumar*
Indian Space Research Organization, Vikram Sarabhai Space Centre, Space Physics Laboratory, Trivandrum, Kerala, India

Abstract. Five years of CloudSat observations during the Indian summer monsoon (ISM) season are used to investigate the vertical structure of stratocumulus (Sc) clouds and associated dynamics over the western part of Arabian Sea. The amount of Sc clouds formed over these regions are quantified in terms of their frequency of occurrence (FOC) and the same is used to study their vertical structure, which is very important from their radiative impact standpoint. The analysis revealed that Sc clouds predominantly form in the 0.5- to 3-km altitude region with mean thickness of 2.5 km over the study region. However, the maximum FOC of Sc clouds is found at ~1.2-km altitude. The prevailing meteorological conditions over the study region are also investigated using ERA-Interim reanalysis datasets, to figure out why the Sc clouds persistently form over this region during ISM period. The analysis revealed that the presence of strong thermal inversion at 850-hPa level formed due to large-scale subsidence, presence of a low-level jet at 850-hPa level, and the advection of dry air at 650-hPa level from the Arabian Desert lead to the inhibition of vertical development of Sc clouds over the Arabian Sea. The significance of the present study lies in characterizing the vertical structure of Sc clouds formed persistently over the Arabian Sea during ISM and divulging the prevailing dynamics and thermal structure responsible for the formation of the Sc clouds over the study region. [DOI: 10.1117/1.JRS.12.016018]

Keywords: vertical structure; dynamics; stratocumulus.

Paper 170673 received Jul. 28, 2017; accepted for publication Jan. 5, 2018; published online Jan. 26, 2018.

1 Introduction

In general, clouds are classified as low [cumulus (Cu), stratocumulus (Sc), and stratus (St)], middle [altostratus (As), nimbostratus (Ns), and altocumulus (Ac)], high [cirrus (Ci), cirrostratus, and cirrocumulus] level, and vertical (cumulonimbus) clouds. These clouds altogether contribute ~50% to the Earth's albedo by effectively reflecting the sunlight back to space.[1,2] Apart from the Earth's radiation budget, the clouds play an important role in diabatic heating of the atmosphere by releasing a large amount of latent heat and in the hydrological process. Owing to their transiency and large range of sizes, the clouds remain as one of the large contributors to the uncertainty in climate models. Among these various cloud types, Sc clouds cover more of Earth's surface (23% of the ocean surface and 12% of the land surface) than any other clouds.[3] The shortwave forcing of Sc clouds is more than their long-wave forcing and thus effectively cools the Earth's surface.[4] Earlier studies show that a 4% increase in the presence of the Sc cloud would be sufficient to offset the radiative forcing produced by doubling of CO_2 concentrations in the Earth's atmosphere.[4–8] There were many studies on Sc clouds with special emphasis on their microphysical properties and their interaction with radiation. The global mean thickness of Sc is about 300 to 400 m,[9] and their horizontal extent is around 1000 km or more. These clouds exhibit a variety of structures, especially over the oceans.[4] Owing to their very thin vertical

*Address all correspondence to: Karanam Kishore Kumar, E-mail: kishore_nmrf@yahoo.com

1931-3195/2018/$25.00 © 2018 SPIE

structure, these clouds are difficult to simulate using global models as they are thinner than the vertical grid resolution of the models.[10] Due to inadequate representation of vertical structure of Sc clouds in the climate models, their effects on shortwave radiation are under-predicted in models.[11] Thus, even though there is a plethora of observations of Sc clouds, their representation in global models is not improved.

A capping temperature inversion and the supply of moisture are essential ingredients for the formations of Sc clouds. It has been observed that Sc clouds preferentially form under the descending branches of large-scale circulations, such as Hadley and Walker circulations, over the ocean surfaces.[7,4,12] The descending branches of large-scale circulation will be relatively warmer due to adiabatic compression of the air and thus triggers the formation of temperature inversion in the lower troposphere. The relatively cool moist air in the marine boundary layer is trapped by these inversion layers and thus aids in the formation of the Sc cloud. The radiative cooling at the top of the cloud will ensure the maintenance of marine boundary layer convection and hence the maintenance of Sc clouds. Thus, mechanism for the formation and maintenance of Sc clouds and their interaction with the solar radiation over the oceans are relatively well understood. Recently, Wood[4] provided a comprehensive review on the Sc clouds, which included their climatology, spatiotemporal variability at different scales, and microphysical structure and processes.

The space-based passive infrared radiometers on-board geostationary satellites are providing much of the spatial and temporal information of Sc clouds. However, the much-needed vertical structure of these clouds is being provided by the active remote sensing instruments, such as Cloud Profiling Radar (CPR) on-board CloudSat[13] and lidar on-board CALIPSO. The cloud radar operating at 35 and 94 GHz provides microphysical properties of these clouds, which are very useful in assessing their radiative properties. Even though there are many studies on Sc clouds across the globe, the studies on their vertical structure and associated dynamics are relatively less. Further, studies on persistent Sc clouds formed over certain regions of the globe are less explored. For example, during the Indian summer monsoon (ISM) (June to September), a persistent layer of Sc clouds forms over the northern Arabian Sea.[14,15] The vertical structure of these clouds, their spatiotemporal variability, and associated dynamics are yet to be investigated in detail. Sathiyamoorthy et al.[14] reported the characteristics of low clouds over the Arabian Sea using Kalpana-1 satellite data and International Satellite Cloud Climatology Project cloud data. These authors also discussed the radiative impacts of the low-level clouds over this region. However, one of the missing elements of this particular study is the vertical structure of the Sc clouds observed over the Arabian Sea. Subrahmanyam and Kumar[12] reported the spatial distribution of various cloud types, including Sc clouds, during ISM season using CloudSat/CALIPSO observations. This study did not focus on the Sc clouds and discussed the various cloud types in general. Thus, it is clear from the aforementioned discussion that even though there are studies on Sc cloud distribution over the Arabian Sea during ISM period, there are no studies on their vertical distribution. Owing to the importance of vertical structure of Sc clouds in Earth's radiation budget, this study aims at characterizing the spatiotemporal variability of vertical structure of Sc clouds and associated dynamics over the Arabian Sea during the ISM period of 2006 to 2010 using CloudSat observations. We adopt the dynamical mechanism proposed by Sathiyamoorthy et al.[14] to explain the role of dynamics in the formation of Sc clouds over the Arabian Sea. Section 2 provides the data used and the methodology followed in this study. Results are discussed in Sec. 3, and Sec. 4 provides the summary.

2 Datasets and Methodology

Five years (2006 to 2010) of CloudSat/CALIPSO observations over the ISM region are used for this study. The CPR on-board CloudSat satellite is the first space-borne millimeter wavelength radar launched in June 2006 as a part of A-Train constellation.[13] The transmitting frequency of the CPR is 94 GHz and is a nadir-looking radar, which measures the backscattered power returned from water droplets in clouds. The ground footprint of CPR is ~1.4 km along-track and ~1.7 km across-track direction. The vertical resolution of CPR is 500 m; however, the radar oversamples the backscattered signals to provide a vertical resolution of ~240 m

at 125 vertical bins. The revisit of CPR on same location is ~16 days, and the ground separation distance between the two successive CloudSat orbits is ~1.8° in longitude. The CPR is able to penetrate the optically thick clouds but cannot detect the thin clouds, such as semitransparent Ci clouds. On the other hand, CALIPSO, which is also a part of A-Train constellation of satellites, carries a lidar on-board to detect optically thin clouds, which are not detected by CPR. At the same time, CALIPSO cannot provide information on thick clouds. Thus, the combination of CloudSat and CALIPSO complements each other in providing the wealth of information on vertical structure of clouds from the space. For this study, five years of CloudSat 2B-CLDCLASS data during June to September over the ISM region are used, which provide vertically resolved cloud type classification. The cloud type classification is done based on the microphysical (liquid water content and precipitation) and macrophysical (cloud vertical and horizontal length) properties of cloud along with the European Centre for Medium-Range Weather Forecasts temperature fields. The 2B-CLDCLASS data provide eight cloud types viz., Ci, As, Ac, St, Sc, Cu, Ns, and deep convective (DC) clouds. A complete description of the cloud classification algorithm can be found in 2B-CLDCLASS product data sheet in CloudSat website.[16] Subrahmanyam and Kumar[12] reported the frequency of occurrence (FOC) of various cloud types and their associated dynamics over the ISM region. A similar procedure as described by Subrahmanyam and Kumar[12] is adopted in this study to quantify the FOC of Sc clouds over the Arabian Sea during ISM period. In brief, CloudSat observations are grouped in $2.5° \times 2.5°$ grids, and then the vertical distribution of FOC of Sc cloud is calculated within each grid and then monthly mean FOC are estimated. Apart from the space-based observations, the ERA-Interim (ERA-I) reanalysis datasets of temperature and wind fields are used for this study.[17] ERA-I data provide the global atmospheric reanalysis fields from January 1, 1979, with a sequential data assimilation scheme using available observations. Currently, ERA-I reanalysis contains six-hourly gridded estimates of meteorological variables (temperature, wind, humidity, ozone, and surface pressure) in three dimensions, and it also estimates the large number of three-hourly surface parameters.

3 Results and Discussion

Five years of CloudSat observations of Sc clouds during 2006 to 2010 over ISM region (June to August) are grouped into $2.5° \times 2.5°$ grids. The FOC of Sc clouds is then estimated. Figure 1(a) shows the five-year mean spatial distribution of FOC of Sc clouds during ISM. The FOC of Sc cloud at each height bin has been estimated, and Fig. 1(a) corresponds to the height where the maximum FOC of Sc cloud is observed in each grid. From this figure, it is evident that the maximum FOC of Sc cloud is found to be over the western part of Arabian Sea, which is consistent with the previous studies.[14,15] The maximum FOC of Sc clouds is observed to be at 15°N, 65°E. However, there is a drastic contrast in the FOC of Sc clouds over the Arabian Sea and Bay of Bengal (BoB) regions, which is more abundant over the Arabian Sea. The reasons for confinement of Sc cloud over the Arabian Sea will be discussed in the subsequent paragraphs. From Fig. 1(a), it can also be noted that considerable amount of Sc cloud forms over the Western Ghats region. Previous studies reported the maximum FOC of Cu clouds over the Westland Ghats region.[12] There is a possibility that thinning out of shallow Cu clouds can lead to formation of Sc clouds.[4] Thus, Fig. 1(a) shows the spatial distribution of Sc clouds over ISM region in terms of their FOC. Further to construct the mean climatology of vertical distribution of these clouds over the ISM region, CloudSat observations are averaged over 55°E to 70°E longitudinal band, where the maximum FOC of Sc clouds is observed. Figure 1(b) shows the five-year mean height–latitude section of FOC of Sc clouds corresponding to aforementioned longitudinal band. From this figure, it can be noted that the vertical extent of the observed Sc is limited to ~3 km, above which the FOC is <1%. The peak in FOC is observed around 1.2 km. From this figure, it can also be noted that the high occurrence of Sc clouds takes place between 10°N and 22.5°N latitudes over the ISM region. The mean altitude of base of Sc cloud is found to be around 0.5 km and mean top altitude around ~3 km. Therefore, the mean thickness of Sc clouds occurring over the Arabian Sea during the ISM period is ~2.5 km. The dynamical factors associated for the controlling the vertical development of Sc cloud are discussed later in this section.

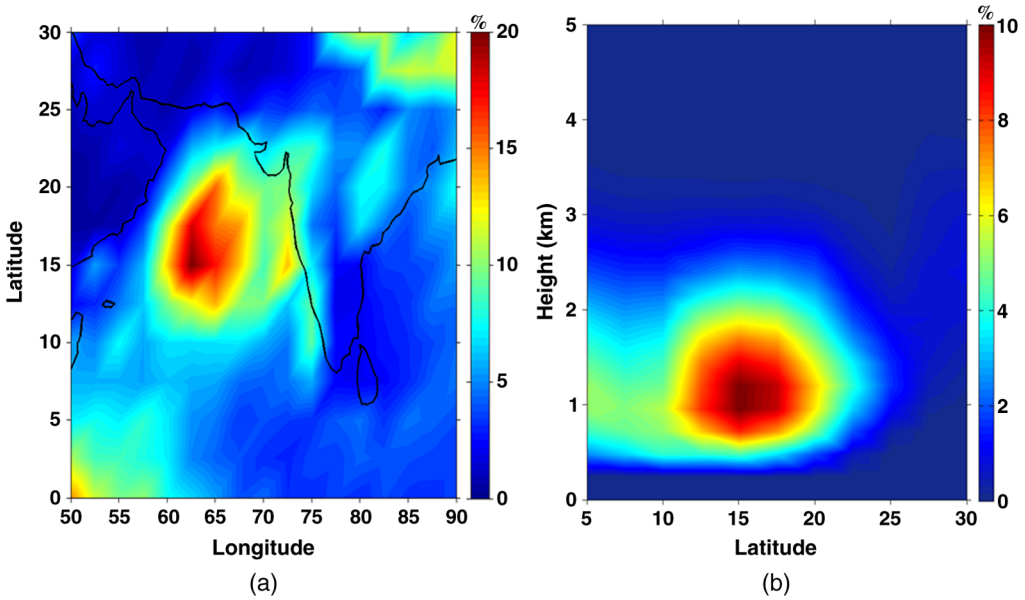

Fig. 1 Five-year (2006 to 2010) mean spatial distribution of FOC of Sc clouds averaged during the months of June, July, August, and September in each year using CloudSat observations over the ISM region in terms of (a) longitude–latitude section (corresponds to the height where the maximum FOC of Sc cloud is observed in each 2.5 × 2.5 grid) and (b) latitude–height section (the FOC of Sc clouds is averaged in the 55°E to 70°E longitude sector).

Figure 2 shows the monthly mean vertical structure of FOC of Sc clouds, which is constructed by estimating their monthly mean vertical structure in the 10°N to 20°N latitudinal and 60°E to 75°E longitudinal belt. From this figure, it is evident that the Sc clouds preferential occur over the Arabian Sea during ISM monsoon and their occurrence is negligible during other seasons. Thus, the FOC of Sc clouds is significant during June, July, August, and September months with maximum during the month of August. Further, to investigate the interannual variability, FOC of Sc clouds is derived during the years 2006 to 2010 and is shown in Fig. 3. From this figure, it is evident that Sc clouds persistently form over the Western Arabian Sea year after year during the ISM with more or less same FOC. However, during the year 2009, the FOC of Sc cloud is found to be relatively less as compared to other years over the Arabian Sea. The year

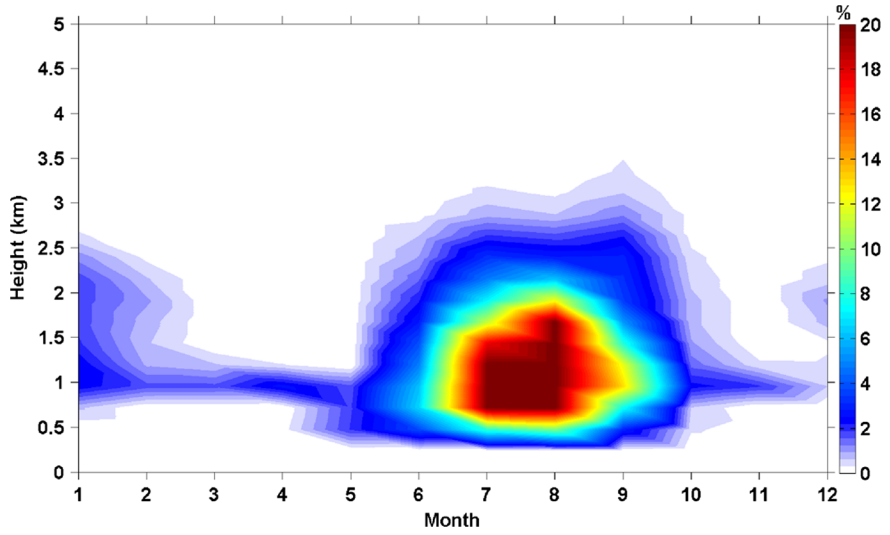

Fig. 2 Five-year mean height–month section of FOC of Sc clouds averaged in the 10°N to 20°N latitudinal and 60°E to 75°E longitudinal belt.

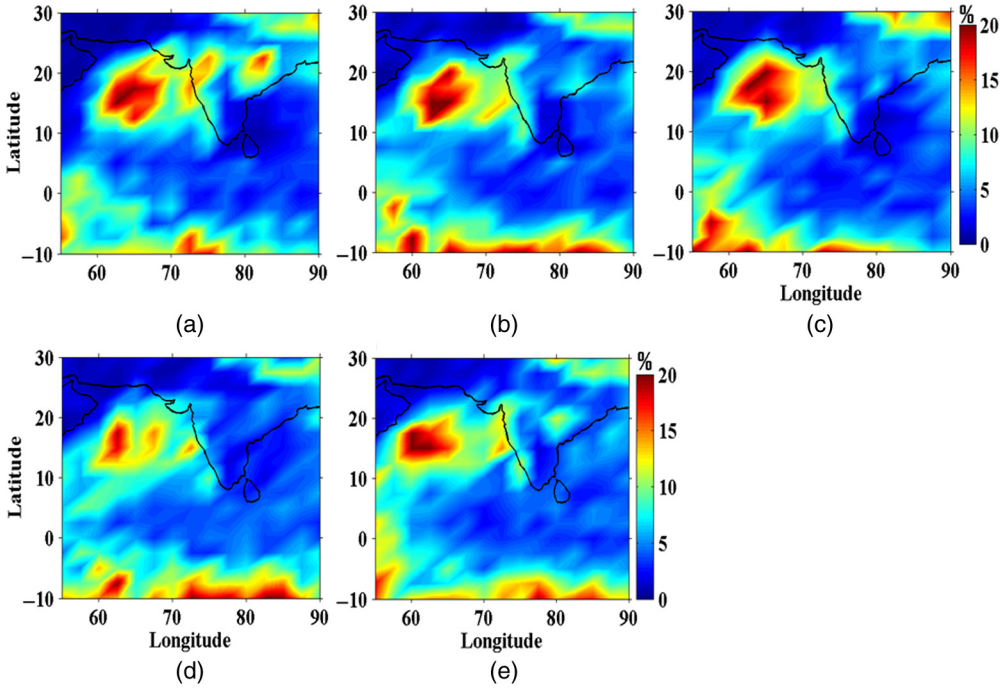

Fig. 3 Longitude–latitude section of FOC of Sc clouds during the years (a) 2006, (b) 2007, (c) 2008, (d) 2009, and (e) 2010 depicting the interannual variability.

2009 was a drought year with ISM rainfall deviation of −22% from the climatological mean. The years 2006 and 2008 were near normal, where the rainfall deviations were −0.1% and −2%, respectively. The years 2007 and 2010 were excess years with +6% and +22% departures, respectively. This information has been taken from India Meteorological Department records. It seems that the strength of the monsoon has a role in the formation of Sc clouds over the Arabian Sea. This will be discussed in detail while discussing the dynamical factors influencing the formation of Sc clouds. Thus, Fig. 2 shows the interannual variability in FOC of Sc clouds over the ISM region, which consistently shows the formation of Sc clouds over the Arabian Sea. The preferentially occurrence of Sc clouds during ISM over the Arabian Sea and the prevailing dynamics and thermal structure aiding in their formation is further investigated using reanalysis datasets.

Figures 4(a) and 4(b) show the climatological mean winds and corresponding divergence field at 850-hPa level, respectively, during ISM period constructed using ERA-I reanalysis winds. As mentioned earlier, we adopt the mechanism proposed by Sathiyamoorthy et al.[14] to demonstrate the role of dynamics in the formation of Sc clouds over the Arabian Sea. Among many atmospheric circulation features during ISM, the low-level jet (LLJ) occurring at 850 hPa is one of the prominent factors, which is shown in Fig. 4(a). The thermal gradient between the Indian Ocean and Asian landmass is the primary driver for the LLJ. The core of the ISM LLJ lies around 850-hPa level. The LLJ plays a vital role in transporting the moisture from oceanic to land region resulting in widespread rainfall over the Indian subcontinent.[18] From Fig. 4(a), it can be noted that the winds accelerate in the 5°N to 10°N region (entrance) and decelerate in the 15°N to 20°N region (exit).[14] Thus, the moisture carried by the LLJ from the entrance region (with accelerating winds) converges at the exit region (with decelerating winds). This low-level convergence as shown in Fig. 4(b) may be conducive for moisture convergence to form clouds over this region.[14] Figure 4(b) shows the mean divergence over the study region derived from the ERA-I reanalysis. Negative (positive) values indicate the presence of convergence (divergence) over the Arabian Sea. However, the upper-level winds, sea surface temperature (SST), and the background thermal structure dictate the vertical development of the clouds. Figure 4(c) shows the vector winds over the ISM region at 650-hPa level. From this figure, it is evident that there are strong southward winds from the Arabian land mass toward the Arabian Sea during this season. These winds are supposed to be very dry as they pass through

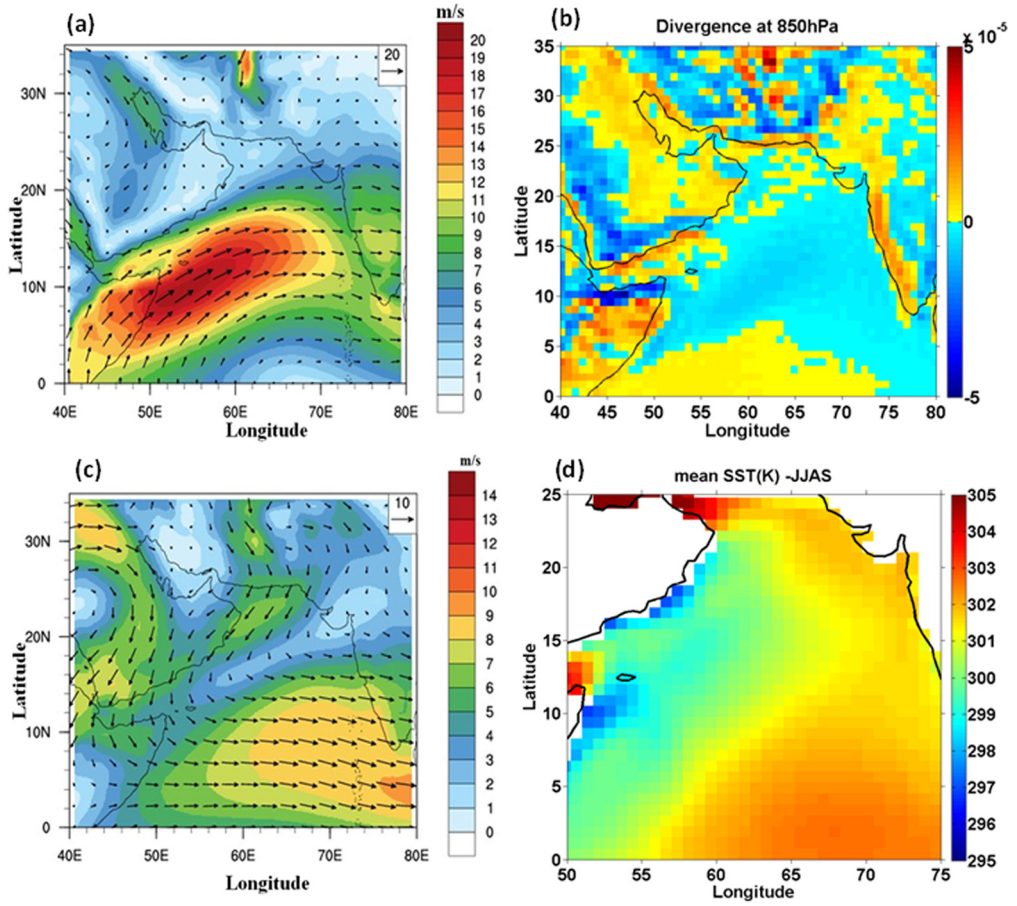

Fig. 4 Five-year mean climatology of (a) winds at 850 hPa, (b) divergence at 850 hPa, (c) winds at 650 hPa, and (d) SST derived from ERA-I reanalysis datasets during the ISM period.

the desert region and, thus, can affect the vertical development of the clouds through entrainment. Thus, from Figs. 4(a) and 4(c), it can be noticed that the lower tropospheric winds by transporting moist air are conducive for formation of the clouds whereas midtropospheric winds by transporting dry air inhibits their vertical development over the study region. Figure 4(d) shows the five-year mean climatology of SST over the Arabian Sea, which shows the relatively lower temperature in the most parts of Arabian Sea as compared to Indian Ocean. Further, as mentioned earlier, the background thermal structure also plays a vital role in the vertical development of the clouds. To investigate this aspect, the temperature profiles from ERA-I reanalysis datasets are examined over the study region. Figure 5 shows the monthly mean profiles of temperature over the study region for June, July, August, and September months. From this figure, it can be noted that there exists a strong thermal inversion in the 950- to 850-hPa level over the Arabian Sea. As mentioned earlier, the thermal inversions inhabit the vertical development of clouds, and thus, these regions are favorable for formation of low-level clouds, such as Sc clouds. However, depending on the strength of the inversion, the vertical growth of the clouds will be varying. If the thermal inversion is week or the updraft is very strong, the clouds can overshoot the inversion layer and, thus, can reach higher altitudes. These thermal inversions together with advection of dry air at 650-hPa level from the Arabian Desert lead to inhibition of vertical development of clouds over the west Arabian Sea. The formation of thermal inversions over the Arabian Sea was reported in the past.[19] One of the important factors contributing to the formation of these inversion layers is the subsidence associated with monsoon convection over the Indian land mass and BoB. To examine, whether such subsidence is present over the study region, the vertical velocity dataset from ERA-I reanalysis data is used. Figure 6 shows the mean pressure–longitude section of Omega and winds at 15°N (where FOC of Sc clouds is maximum) during the month of August over the study region. The negative velocity

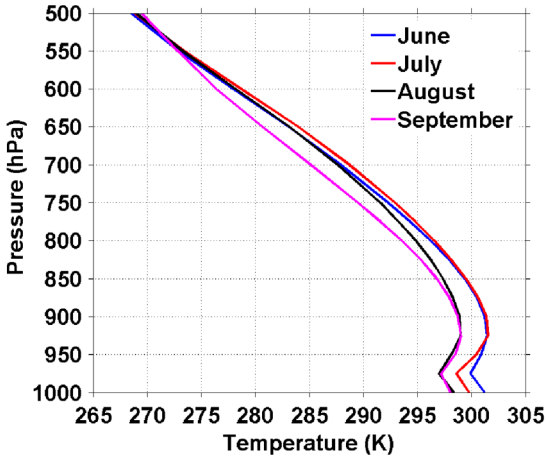

Fig. 5 Monthly mean temperature profiles at 60°E and 17.5°N temperature observed over the Arabian Sea during ISM period.

shows the upward motion and positive velocities show the downward motions. It is known that the magnitudes of vertical velocities provided by reanalysis are not validated. However, the reanalysis datasets are able to identify the large-scale up and downdrafts, for example, the Walker circulation can be readily identified using the vertical velocities derived from reanalysis datasets.[12] From Fig. 6, it is evident that the strong subsidence takes place over the study region, which can result in thermal inversion through adiabatic compression. The dry and hot air advected from the Arabian Desert may also play a role in development of the observed inversion layers. Also, the downdrafts over the study region can directly suppress the vertical development of clouds as shown in Fig. 6. Descending motion of monsoon circulation can be seen in Fig. 6 during the month of August, in which the DC activity is high over Indian region as well as over BoB. The negative (positive) Omega values indicate the upward (downward) motion of monsoon convection shown by solid arrow symbol in Fig. 6 over the longitude sector around 90°E to 100° E. The associated downward motion can be found around the 55°E to 60°E, where the maximum FOC of Sc cloud forms [Fig. 1(a)]. Thus, the thermal inversions formed over the Arabian Sea due to descending motion induced by monsoon convection play a key role in the formation of observed Sc clouds. A strong convection can overcome the thermal inversion layers and can develop into deep convection. However, the strength of the convection has dependency

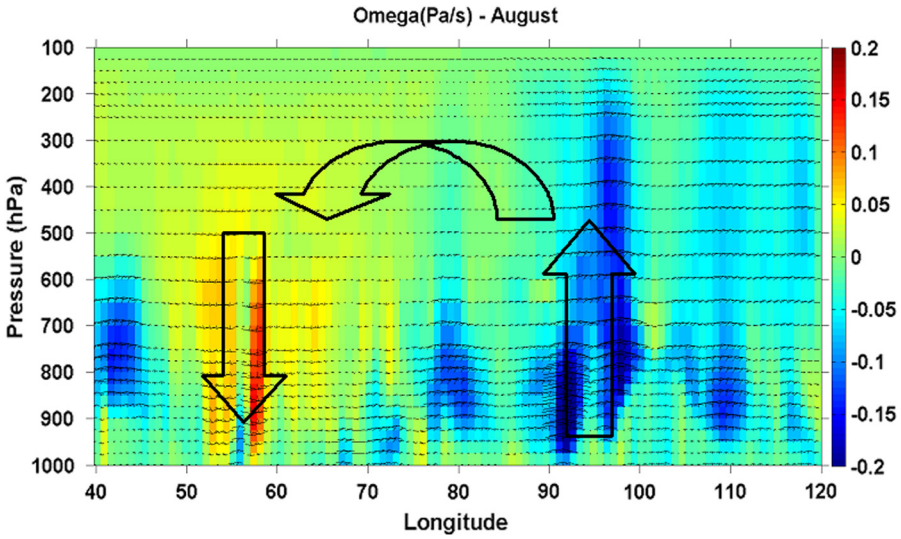

Fig. 6 Five-year mean climatology pressure–longitude section of Omega and winds derived from ERA-I reanalysis datasets.

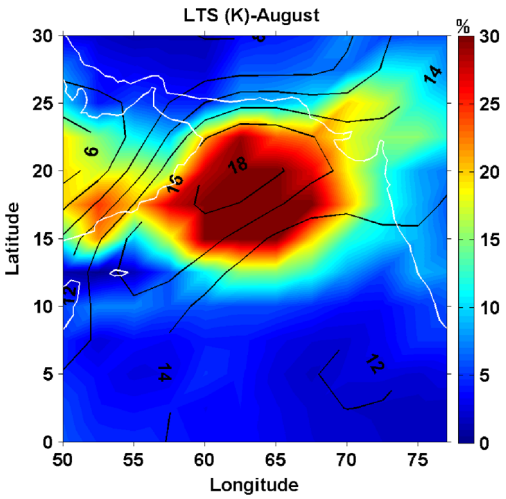

Fig. 7 Five-year mean spatial distribution of FOC of Sc clouds along with contours of LTS over the study region observed during the month of August.

on the SST, which is relatively low over the study region as shown in Fig. 4(c). The strong winds over the Arabian Sea during the ISM period can cause upwelling of the sea and, thus, cooling the sea surface, which in turn weakens the convection. Thus, there are three factors, viz., low SST, large-scale subsidence-induced thermal inversion, and dry air intrusion in midtroposphere, that influence the vertical development of clouds over the study region and favor the formation of Sc clouds.

In general, Sc clouds tend to form under large-scale subsidence associated with the Hadley as well as Walker circulations. One of the important parameters used in the earlier studies to identity the potential locations for the formation of Sc clouds is the lower tropospheric stability (LTS). The LTS is an indicator of the atmospheric stability at lower levels, which is defined as the difference of potential temperature at 700- and 1000-hPa levels.[20] If the observed LTS is higher, then there is less chance for the vertical development of clouds. Figure 7 shows the mean distribution of Sc clouds in terms of FOC along with LTS in contours during the month of August. From this figure, it is evident that the region of maximum in FOC coincides with the regions of larger LTS. This observation suggests that the areas of high LTS are not favorable for development of clouds vertically as discussed earlier. However, the larger LTS magnitudes are consequence of the thermal inversion as shown in Fig. 5. Thus, this study brought out the important dynamical and thermal structure aspects over the Arabian Sea, which explains the selective formation of Sc clouds over the study region.

4 Summary and Concluding Remarks

Using five years of CloudSat observations over the ISM region, the three-dimensional structure of Sc clouds and associated dynamics are characterized. Large amount of Sc clouds, which is quantified in terms of FOC, have been observed over the Arabian Sea during ISM period. The maximum FOC of Sc cloud is found to be over the western part of Arabian Sea, especially at 15° N, 65°E. The analysis revealed that the vertical extent of Sc clouds is limited to ~3 km and the peak in FOC located at 1.2 km over the study region. The vertical structure of Sc clouds further revealed that the mean thickness of Sc clouds occurring over the Arabian Sea during the ISM period is ~2.5 km. The maximum FOC of Sc clouds over the study region is found during the month of August. A detailed analysis is carried out to investigate why the Sc clouds preferentially form over the study region during ISM period using reanalysis datasets. Two distinct wind systems one at 850 hPa and another at 650 hPa are observed over the study region. A strong low-level south-westerly jet is observed at 850 hPa over the study region, which is instrumental in bringing the moisture over ISM region whereas dry northerly winds from Arabian Desert regions are observed over the study region at 650 hPa, which can inhibit the vertical development of

clouds by advecting the dry air. The strong low-level winds over the Arabian Sea can also lower the SST through upwelling and, thus, weakening the convection. Moreover, the vertical profiles of temperature have shown the sharp inversion layers associated with large-scale subsidence induced by monsoon convection over the Indian land mass as well as BoB. These thermal inversion layers inhibit the air parcel to move vertically and thus prohibiting the vertical development of the clouds. The regions of large LTS, which represents the stability of the lower troposphere, are found to be coinciding with the regions of large FOC of Sc clouds. Similarly, Sc clouds can form under the descending branches of large-scale circulations, such as Walker and Hadley circulations. For example, the large fraction of Sc clouds form over the Peruvian as well as over the west coast of California. The formation of Sc clouds over these regions also can be explained on the basis of large-scale subsidence and LTS as discussed in this study. The large-scale subsidence over the west coast of California is provided by the descending branch of Hadley cell whereas over the Peruvian coast it is provided by descending branch of Walker cell. Over the Arabian Sea, as discussed in this study, the subsidence is provided by the Monsoon convection. Thus, this study for the first time divulges the vertical structure of Sc clouds over the Arabian Sea during ISM period and brings out the dynamical and thermal structure aspects associated with the Sc cloud formation over the study region. It is envisaged that the results will have implications in identifying the potential regions of persistent Sc cloud formation other than descending branches of large-scale circulations as well as in understanding the vertical structure of Sc clouds and associated dynamics.

Acknowledgments

The authors are greatly thankful to CloudSat team and ISCCP team and the data were obtained from the CloudSat websites,[16,21] respectively. Authors are also thankful to reanalysis data team for providing the rich information on the background wind and other ancillary information.

References

1. E. F. Harrison et al., "Seasonal variation of cloud radiative forcing derived from the earth radiation budget experiment," *J. Geophys. Res.* **95**, 18687–18703 (1990).
2. L. V. Leahy et al., "On the nature and extent of optically thin marine low clouds," *J. Geophys. Res.* **117**, D22201 (2012).
3. C. J. Hahn and S. G. Warren, "A gridded climatology of clouds over land (1971–96) and ocean (1954–97) from surface observations worldwide," Numeric Data Package NDP-026EORNL/CDIAC-153, CDIAC, Department of Energy, Oak Ridge, Tennessee (2007).
4. R. Wood, "Stratocumulus clouds," *Mon. Weather Rev.* **140**, 2373–2423 (2012).
5. A. Slingo, "Sensitivity of the Earth's radiation budget to changes in low clouds," *Nature* **343**, 49–51 (1990).
6. H. P. Hanson, "Marine stratocumulus climatologies," *Int. J. Climatol.* **11**(2), 147–164 (1991).
7. D. Randall et al., "Outlook for research on subtropical marine stratification clouds," *Bull. Am. Meteorol. Soc.* **65**, 1290–1301 (1984).
8. C. S. Bretherton et al., "The EPIC 2001 stratocumulus study," *Bull. Am. Meteorol. Soc.* **85**, 967–977 (2004).
9. R. F. Challan et al. "The albedo of fractal stratocumulus clouds," *J. Atoms. Sci.* **51**, 2434–2455 (1994).
10. P. M. Caldwell, Y. Zhnag, and A. K. Stephen, "CMIP3 subtropical stratocumulus cloud feedback interpreted through a mixed-layer model," *J. Clim.* **26**, 1607–1625 (2013).
11. J. Richter, "Climate model biases in the eastern tropical oceans: causes, impacts and ways forward," *WIREs Clim. Change* **6**, 345–358 (2015).
12. K. V. Subrahmanyam and K. K. Kumar, "CloudSat observations of cloud-type distribution over the Indian summer monsoon region," *Ann. Geophys.* **31**, 1155–1162 (2013).
13. G. L. Stephens et al., "The CloudSat mission and the A-Train," *Bull. Am. Meteorol. Soc.* **83**, 1771–1790 (2002).

14. V. Sathiyamoorthy et al., "Characteristics of low clouds over the Arabian Sea," *J. Geophys. Res.* **118**, 13489–13503 (2013).
15. K. V. Subrahmanyam and K. K. Kumar, "CloudSat observations of multi layered clouds across the globe," *Clim. Dyn.* **49**, 327–341 (2017).
16. Z. Wang and K. Sassen, "Level 2 cloud scenario classification product process description and interface control document," Version 5.0, http://www.cloudsat.cira.colostate.edu/dataHome.php (24 July 2007).
17. D. P. Dee et al., "The ERA-Interim reanalysis: configuration and performance of the data assimilation system," *Q. J. R. Meteorol. Soc.* **137**, 553–597 (2011).
18. P. V. Joseph and S. Sijikumar, "Intraseasonal variability of the low-level jet stream of the Asian summer monsoon," *J. Clim.* **17**, 1449–1458 (2004).
19. M. S. Narayanan and B. M. Rao, "Detection of monsoon inversion by TIROS-N satellite," *Nature* **294**, 546–548 (1981).
20. S. A. Klein, D. L. Hartmann, and J. R. Norris, "On the relationship among low-cloud structure, sea surface temperature, and atmospheric circulation in the summertime northeast Pacific," *J. Clim.* **8**, 1140–1155 (1995).
21. W. B. Rossow and R. A. Schiffer, "Advances in understanding clouds from ISCCP," *Bull. Am. Meteorol. Soc.* **80**, 2261–2288 (1999).

Kandula Venkata Subrahmanyam received his BSc degree in 2003 and his master's degree in physics in 2005 from Nagrajuna University, Guntur, India. His field of interest includes remote sensing of clouds using space and ground-based radars. He is working as scientist at Vikram Sarabhai Space Centre, Thiruvananthapuram, India, and also pursuing his PhD.

Karanam Kishore Kumar received his BSc degree with mathematics, physics, and electronics as electives in 1995, his MScTech degree in engineering physics with university gold medal in 1998, and his PhD in physics in 2004, all from Sri Venkateswara University, Tirupati, India. His research interests include radar remote sensing of the Earth's atmosphere and atmospheric dynamics. Currently, he is working as a scientist at Vikram Sarabhai Space Centre, Thiruvananthapuram, India.

CloudSat Observations of Three-Dimensional Distribution of Cloud Types in Tropical Cyclones

K. V. Subrahmanyam, Karanam Kishore Kumar, and Natalie D. Tourville

***Abstract*—The present study investigates the three-dimensional distribution of various cloud types in tropical cyclones formed in the North Indian Ocean surrounding the Indian subcontinent using CloudSat observations of 25 cyclones occurred during 2006–2014. A composite cloud type distribution of cirrus (Ci), altostratus (As), altocumulus, stratocumulus, cumulus, nimbostratus and deep convective (DC) is constructed by combining all the observations as a function of the radial distance from the eye of a cyclone for the first time. The present analysis shows that the peak frequency of occurrence of the DC clouds is 50% at ∼50–100 km radial distance from the cyclone's eye. The Ci clouds are found at altitudes around 13–15 km with a maximum frequency of occurrence of 30% at ∼200 km from the center of the cyclone's eye. The present results suggest that there could be a possible discrepancy in classifying the observed clouds into DC and As clouds using CloudSat observations. All the observations during the study period led to the construction of composite cloud type distribution in the tropical cyclones, which aids in visualizing what type of clouds dominates in which part of the cyclone. Thus, the present study provides a three-dimensional distribution of various clouds embedded in tropical cyclones and associated dynamics, which is very important in better representation of tropical cyclones in numerical weather models and can be used to evaluate the tropical cyclone simulations.**

***Index Terms*—Cloud types, CloudSat, tropical cyclones.**

I. Introduction

OWING to their socioeconomic impacts, tropical cyclones are cynosure for meteorologists as well as common men. The devastation caused by tropical cyclones makes them one of the important topics of research in the realms of meteorology. The prediction of intensity and movement of tropical cyclones is one of the important topics addressed by several researchers across the globe to understand these complex atmospheric–oceanic systems. There have been numerous studies on preconditioning of tropical cyclogenesis [1]–[3], its internal structure, frequency of occurrence, and dynamics [4]–[6]. Among many atmospheric processes associated with tropical cyclones, the clouds embedded in these systems play an important role in their sustenance and intensification [6]. The intensification and movement of the tropical cyclones, among other factors, depend on the latent heat released in the clouds embedded in them [6]. The latent heat released in clouds modifies the internal dynamics of a cyclone, and the dynamics, in turn, dictate the cloud distribution within in the cyclone. However, the amount of latent heat released by various cloud types is different and there is no direct measurement of this quantity. By knowing the cloud type, it may be possible to infer the latent heat released indirectly. So it becomes important to study the cloud-type distribution within a cyclone for having better insights into its internal dynamics and vice versa.

Understanding about the structure and dynamics of tropical cyclones is improved tremendously with the TRMM-PR observations [6], [7]. Information on three-dimensional distributions of nonprecipitating clouds and their types was very limited until the launch of CloudSat [8] and CALIPSO [9] satellites. The combined observations from CloudSat/CALIPSO provide three-dimensional distributions of various cloud types [10]–[12]. Apart from observational studies on tropical cyclones, numerical model based studies were also carried out [13]–[15]. In recent times, using cumuli parameterization schemes, atmospheric modelers are able to investigate the development of tropical cyclones using climate models [15], [16]. However, most of the climate models are not able to simulate the vertical structure of clouds in tropical cyclones [17], [18]. L'Ecuyer *et al.* [19] showed the composite structure of a tropical cyclone observed by CloudSat in connection with background wind shear and further showed that environmental wind shear plays a vital role in the dynamics and formation of the tropical cyclone. One of the missing elements in observations of tropical cyclones is the three-dimensional distribution of cloud types embedded in these systems. In this regard, the present study aims at constructing the vertically resolved composite cloud type distribution embedded in tropical cyclones as a function of radial distance from the eye of the cyclones formed in the North Indian Ocean using CloudSat observations. The results discussed in the present study are envisaged to shed light on which type of clouds form in which part of a cyclone, which will have potential implications in understanding the energy budget of a tropical cyclone system. Section II describes data and methodology, results are discussed in Section III, and Section IV provides the summary of the present study.

II. Data and Methodology

For the present study, observations of a cloud profiling radar (CPR) (onboard CloudSat) over tropical cyclones formed in the

Manuscript received July 13, 2017; revised September 11, 2017 and October 9, 2017; accepted December 20, 2017. *(Corresponding author: K. V. Subrahmanyam.)*

K. V. Subrahmanyam and K. K. Kumar are with the Space Physics Laboratory, Vikram Sarabhai Space Centre, Indian Space Research Organisation, Trivandrum 695022, India (e-mail: kvsm2k@gmail.com; kishore_nmrf@yahoo.com).

N. D. Tourville is with the Cooperative Institute for Research in the Atmosphere, Colorado State University, Fort Collins, CO 80523 USA (e-mail: Natalie.Tourville@colostate.edu).

Color versions of one or more of the figures in this paper are available online at http://ieeexplore.ieee.org.

Digital Object Identifier 10.1109/JSTARS.2017.2786666

Arabian Sea (ARB) and the Bay of Bengal (BoB) surrounding the Indian subcontinent during the years 2006–2014 are used. The operating frequency of the CPR is 94 GHz and it provides observations with 240 m vertical resolution and 1.4 and 1.7 km cross- and along-track resolution, respectively [8]. Recently, Tourville *et al*. [12] compiled A-Train observations over tropical cyclones, which is a unique dataset to investigate the different aspects of clouds embedded in tropical cyclones. This dataset provides information on the vertical structure of clouds, precipitation, cloud properties, environmental storm conditions, and tracks of the cyclone [8]. Among these datasets, the 2B-CLDCLASS product of CloudSat, which provides the cloud-type information, is used for the present study [20]. CloudSat algorithm classifies clouds into eight types viz., cirrus (Ci), altostratus (As), altocumulus (Ac), stratus (St), stratocumulus (Sc), cumulus (Cu), nimbostratus (Ns), and deep convective (DC). The classification is based on different aspects of vertical and horizontal scales of hydrometeors using the CPR measured reflectivity and ancillary data including ECMWF temperature profiles and surface topography [20].

The 2B-CLDCLASS data product employs a cloud cluster algorithm for cloud-type classification. The cloud cluster algorithm derives various cloud types using the reflectivities from the CPR along with other additional information from ECMWF re-analysis data. The algorithm considers only the significant CPR cloud mask values 30 and above, which is provided by a cloud mask algorithm. Furthermore, classification of the cloud type is done based on microphysical properties, maximum reflectivity and corresponding temperature at that level, cloud vertical and horizontal extent, and the precipitating properties. However, the CPR is not sensitive to optically thin clouds such as high-altitude thin Ci clouds [10], [11], [21]. The limitations of 2B-CLDCLASS product are 1) surface contaminations in the lower 3–4 range bins of CPR vertical reflectivity profiles, which will have implications in classifying St/Sc clouds and 2) the CPR is not sensitive to high altitude thin clouds, which will have implications in detecting the Ci clouds [21], [22], [11], [12]. Both these limitations will result in fewer detection of St, Sc, and Ci clouds than actually present. One should keep these limitations in view while interpreting the observations. Despite these limitations, cloud-type classification is derived, which is very useful for assessing the role of clouds in energetics and dynamics of the atmosphere as a function of cloud type. More details on CloudSat can be found in [21]. In the present study, we have adopted the following steps discussed by [12] to calculate the frequency of occurrence of each cloud type as a function of distance from the eye of the cyclone. Step 1: The CloudSat observations are gridded with respect to the distance from the center of the tropical cyclone. Step 2: The number of occurrences of each cloud type such as Ci, As, Ac, St, Sc, Cu, Ns, and DC is estimated at each height interval (240 m) of CPR observations. Step 3: The number of occurrence of each cloud type is divided by the number of occurrence of all cloud types at each height interval, which provides frequency of occurrence of each cloud type. This quantity is used to construct the composite cloud type distribution in tropical cyclones as a function of distance from the eye of the cyclone. More details on the methodology of estimating frequency of occurrence of cloud types can be found in [11].

TABLE I
LIST OF TROPICAL CYCLONES OCCURRED IN NORTH INDIAN OCEAN DURING 2006 TO 2014

S. No.	Cyclone name	Period	Basin
1	MUKDA	Sep. 21–24, 2006	ARB
2	AKASH	May 12–15, 2007	BoB
3	GONU	Jun. 1–7, 2007	ARB
4	SIDR	Nov. 11–16, 2007	BoB
5	NARGIS	Apr. 27 to May 7, 2008	BoB
6	RASHMI	Oct. 25–27, 2008	BoB
7	KHAIMUK	Nov. 13–16, 2008	BoB
8	NISHA	Nov. 25–29, 2008	BoB
9	BIJILI	Apr. 14–17, 2009	BoB
10	AILA	May 23–26, 2009	BoB
11	PHYAN	Nov. 4–11, 2009	ARB
12	LAILA	May 17–21, 2010	BoB
13	BANDU	May 19–23, 2010	ARB
14	PHET	May 30 to Jun. 7, 2010	ARB
15	GIRI	Oct. 20–23, 2010	BoB
16	JAL	Nov. 1–8, 2010	BoB
17	THANE	Dec. 25–30, 2011	BoB
18	MURJAN	Oct. 22–26, 2012	ARB
19	NILAM	Oct. 28 to Nov. 1, 2012	BoB
20	MAHASEN	May 10–17, 2013	BoB
21	LEHAR	Nov. 23–28, 2013	BoB
22	MADI	Dec. 6–13, 2013	BoB
23	NANAUK	Jun. 10–14, 2014	ARB
24	HUDHUD	Oct. 7–14, 2014	BoB
25	NILOFAR	Oct. 25–31, 2014	ARB

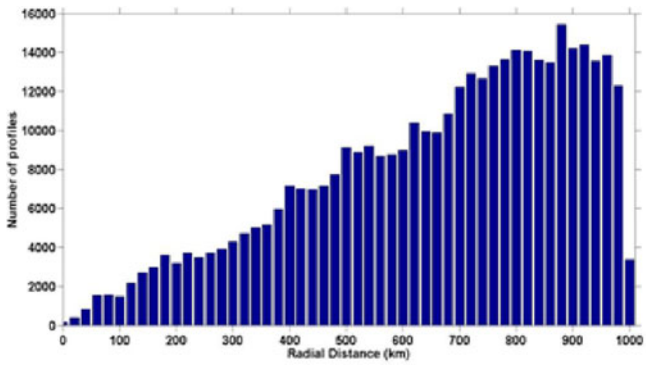

Fig. 1. Number of CPR profiles as a function of radial distance from the eye of the cyclone.

A total number of 25 tropical cyclone (8 in the ARB and 17 in the BoB) passages during 2006–2014 are investigated for the present study and Table I shows the list of tropical cyclones along with their time of occurrence. Fig. 1 shows the number of profiles as a function of radial distance from the eye of cyclones that are used to construct the composite cloud type distribution. From this figure, it is clear that there are relatively few observations over the eye of a cyclone as compared to other parts of the system. However, the cloud-type distribution is normalized with the total number of observations to estimate the frequency of occurrence of each cloud as a function of radial distance from the eye of the cyclone. Furthermore, we have separated these observations into two subsets, one set having observations during the developing stage and other during the mature stage. The

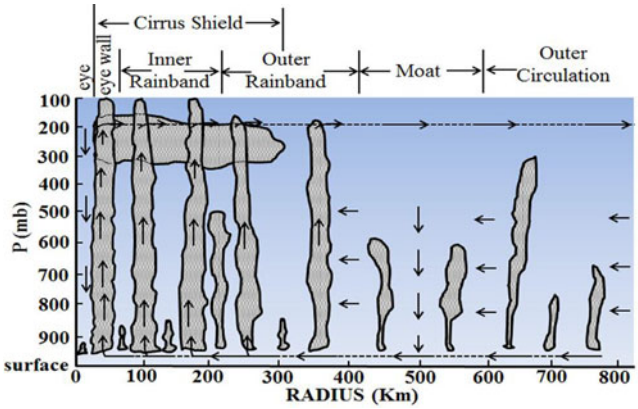

Fig. 2. Schematic view of vertical cross section of a tropical cyclone (adapted from [22]).

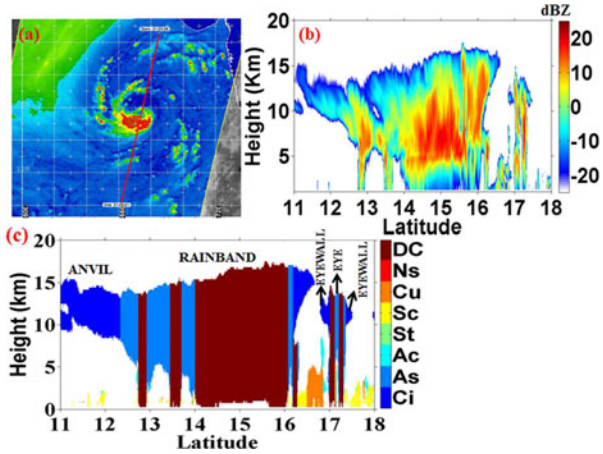

Fig. 3. CloudSat track through the GONU cyclone's (a) eye on Jun. 2, 2007. (b) The CloudSat reflectivity corresponding to CloudSat tracks shown in (a), and (c) the cloud-type distribution corresponding to CloudSat tracks shown in (a).

developing and mature stages are identified using the formation of a well-defined eye and the information provided by the India Meteorological Department. However, identifying the eye during formative and dissipating stage is very difficult and thus we focused on the mature stage of the cyclone alone in the present study.

III. Results and Discussion

Fig. 2 depicts the schematic of the vertical cross section of the tropical cyclone (redrawn from [22]) highlighting the vertically resolved cloud distribution and internal circulation. The basic anatomy of the cyclone consists of an eye, eye-wall, moat, and inner and outer rainbands. However, the nomenclature slightly differs among the meteorologists. From this illustration, it is clear that the eye-wall, and the inner and the outer rainbands of cyclones consist of DC systems reaching up to the tropopause and the presence of Ci clouds resulting from outflows of these DC systems. This is a simplified cloud distribution of a tropical cyclone and there are other clouds embedded within these systems. From this schematic, it can be observed that the top of the DC clouds decreases with distance from the eye. This is attributed to the inhibition of vertical development of clouds by the outflows of deep convection from the eye-wall region of a cyclone. The dynamics responsible for the formation of DC clouds as well as Ci clouds in various regions of the tropical cyclone is reported by [4]–[7]. A complete description of cloud distribution, especially cloud types in tropical cyclones, is yet to be generalized and the present study is an attempt toward this end using CPR observations on board CloudSat.

Fig. 3(a) shows CloudSat track through the GONU cyclone's eye on Jun. 2, 2007. The GONU cyclone was developed on Jun. 1, 2007 in the eastern ARB and it developed into the matured stage on 4th June. It started weakening on 6th June and then dissipated on 7th June after making the landfall. The CloudSat reflectivity observations along its track over the GONU cyclone provided valuable information on the vertical structure of clouds, as shown in Fig. 3(b), which corresponds to the CloudSat ground tracks indicated by the red line in Fig. 3(a). Fig. 3(b) depicts the vertical cross section of cloud reflectivity as observed by the CPR along the CloudSat track. From this figure, echo tops reaching as high as 15–16 km corresponding to DC clouds can be observed. In conventional geostationary satellite observations, it is difficult to discern the high cloud and deep clouds and the active remote sensing observations used in the present study resolve this paradox. The horizontal distribution of radar reflectivity along the CloudSat track also reflects the circulation pattern within a tropical cyclone. The regions that are void of clouds represent the regions of down drafts, regions with reflectivity spread through ∼2–15 km represent the updraft region, and the regions where the reflectivity is confined in 10–15 km region represent the convective outflow regions. Thus, using the reflectivity structure, one can infer some of the dynamical aspects of the cyclone structure. Furthermore, the cloud-type distribution is constructed and is depicted in Fig. 3(c) corresponding to CloudSat track shown in Fig. 3(a). In Fig. 3(c), the various sectors of the tropical cyclone viz., eye, eye wall, rainbands, and anvils are labeled. Only small portion of the eye of the GONU cyclone is captured by the CPR in one direction. However, it provides valuable information on the vertical structure of cloud types embedded in the observed cyclone. One can observe the clouds such as Sc, Ac, and As within the eye. This region is void of any DC clouds as this region is dominated by the downdrafts from surrounding DC systems [2], [4], [6], [7]. On either side of the eye, DC systems representing the eye wall can be noticed in Fig. 3(c). The outflows from the eye walls can be noticed in the form of Ci clouds below which there are Cu and Sc clouds. The rainband is dominated by the DC clouds, which occupy the latitude band between 14° and 16° followed by the thick As and Ci clouds.

The vertical cross section shown in Fig. 3(c) along the cyclone eye represents the typical cloud-type distribution, which is consistent with the present understanding. The cloud-type distribution depicted in Fig. 3(c) is from instantaneous observations of CloudSat over the GONU cyclone, and as mentioned in Section II, a total number of 25 cyclone observations are used to construct a composite cloud type distribution. It is known that the cloud distribution varies largely from one cyclone system to another and also depends on the category and stage of a

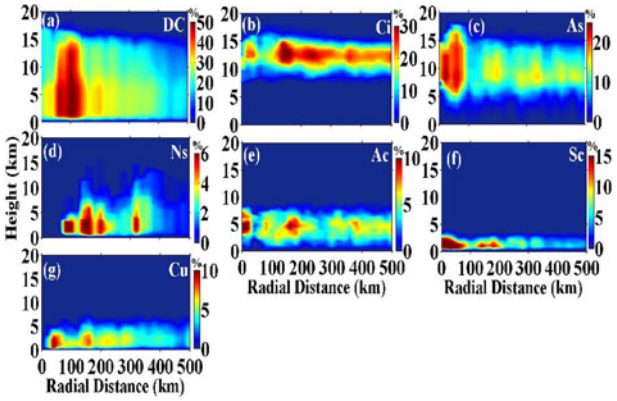

Fig. 4. (a)–(g) The composite frequency of occurrence of deep convective clouds (DC), cirrus (Ci), altostratus (As), nimbostratus (Ns), altocumulus (Ac), stratocumulus (Sc), cumulus (Cu), respectively, as a function of height and radial distance from the eye of the cyclone.

cyclone. In the present study, we have segregated the CloudSat observations based on the various stages of the cyclone viz., developing, mature, and dissipating stages. It is observed that there are very few CloudSat observations during the dissipating stage of the cyclone, which are not sufficient to construct the composite cloud type distribution. The cloud-type distribution constructed during the developing stages of the cyclone (figure not shown) is not very coherent as the system was still evolving. Due to these reasons, the present study focuses on the cloud-type distribution during the mature stage of the cyclone alone. So, by making use of multiple observations of CloudSat over different parts of the mature stage of tropical cyclones, a composite cloud type distribution is constructed as a function of height and the radial distance from the cyclone's eye.

Fig. 4(a)–(g) shows the frequency of occurrence of DC, Ci, As, Ns, Ac, Sc, Cu, respectively, as a function of height and radial distance from the eye of a cyclone. The DC clouds distribution depicted in Fig. 4(a) shows its peak frequency of occurrence of 50% at ∼50–100 km radial distance from the eye with a vertical extent of ∼16 km. The tallest DC clouds form very near the eye of a cyclone and the tops of these clouds gradually decrease thereafter as a function of radial distance. Most of the previous studies have shown the DC clouds very near to the eye of the cyclones and the present results show that even though these clouds are present near to the eye, the maximum frequency of their occurrence is slightly away from the eye, as shown in Fig. 4(a). From this figure, it is evident that the DC clouds distribution shows a band structure representing their preferential regions for formation such as the inner and the outer rainbands. The frequency of occurrence of DC clouds drastically decreases beyond 500 km from the eye. The warm sea surface temperature and low-level convergence of moisture are the prime driving force for the DC cloud formation in cyclones. The latent heat released in these clouds forms the basis for further intensification of the cyclone [6]. Both the latent heating of condensation and freezing contributes to the heating apart from cloud radiative heating. The DC clouds formed in the cyclones are different from the DC clouds that form in another convective system. The main difference between these two types of DC clouds being the swirling updrafts and cloud bases in the cyclones [4], [6], [7].

By now, it is well known that the outflows in the DC clouds in cyclones are responsible for the generation of Ci clouds. The Ci cloud distribution in tropical cyclones is depicted in Fig. 4(b), which shows that these clouds occur at around 13–15 km height region with a maximum frequency of 30% (at 14–15 km altitude) at around ∼200 km radially from the eye of cyclones. It is interesting to note that the peak in Ci clouds is observed just after the peak in the DC clouds shown in Fig. 4(a), which further strengthens the assertion that the principal source for Ci clouds is the outflows from the DC clouds. This observation also vouches for the present approach for constructing the composite cloud distributions using multiple cyclone observations. Significant amounts of Ci clouds are observed up to 1000 km radial distance from the eye, which is well known from earlier observations [5], [6]. From this figure, it is also clear that the Ci cloud tops are gradually decreasing as a function of radial distance as in the case of DC clouds. The outflow from the DC clouds, which forms the Ci clouds, plays a vital role in radiative forcing as well as in limiting the vertical growth of the DC clouds. Apart from the outflows of the DC clouds, there is a possibility of *in situ* generated Ci clouds. However, in cyclones, the majority of Ci clouds are formed from the DC cloud outflows. With time, Ci clouds transform into the large and deeper St and cirrostratus clouds. Furthermore, the cirrostratus clouds can seed the As cloud formation.

Fig. 4(c) shows the distribution of As clouds in tropical cyclones. The As cloud distribution shown in this figure is not consistent with the present understanding of characteristics of these clouds. In general, As clouds occur in the height region of ∼3–10 km in the tropics and are classified as the midlevel clouds. But Fig. 4(c) shows tops of As clouds as high as 16 km near the eye of the cyclone with a peak frequency of occurrence of ∼25%. There seems to be an issue in distinguishing DC and As clouds in the cloud classification algorithm, especially in cyclones. It can be explained on the basis of the tilted DC clouds in tropical cyclones. As mentioned earlier, the DC clouds in the tropical cyclones swirl and thus will be tilted with respect to its base. The CPR, which observes the clouds in nadir view, may be classifying the upper portion of the tilted DC as As cloud. This scenario is illustrated in Fig. 5, which shows the possibility of the CPR classifying the upper portion of the DC clouds as As. The rectangular box shown in Fig. 5, which is a part of eye-wall DC clouds, may be classified as As cloud in the present algorithm. This type of slanting eye-wall clouds is discussed by [6]. One more possibility is that the transition region between the DC clouds and their outflows may also be classified as As clouds. This assertion is substantiated by the cloud classification observations depicted in Fig. 3(c), which shows that the DC clouds are accompanied by As clouds in most of the cases. Furthermore, from Fig. 4(a), it can be noted that near to the eye of the cyclone, the frequency of occurrence of DC clouds is limited to ∼7 km. Above this altitude, a peak in the frequency of occurrence of As clouds is observed over this region.

Thus, it seems that the cloud classification algorithm identifies the upper portions of the DC clouds and the transition

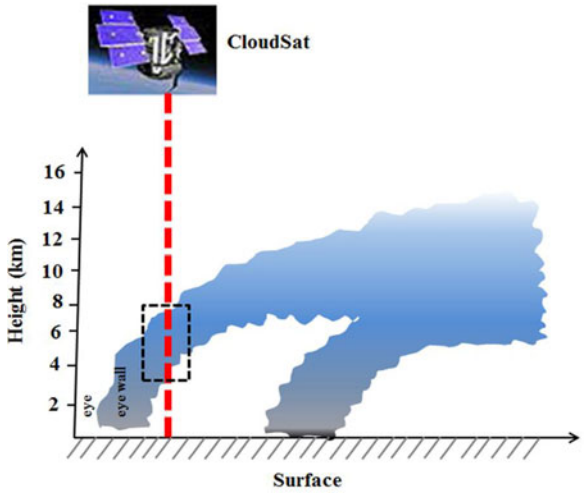

Fig. 5. Illustration of CloudSat nadir view over the upper portion of the tilted DC cloud.

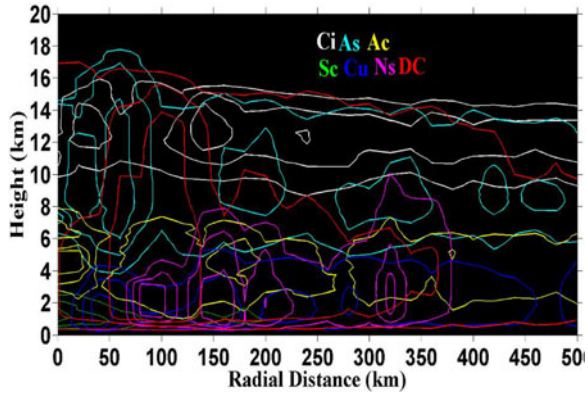

Fig. 6. Comprehensive view of the frequency of occurrence of various cloud types embedded in the tropical cyclones. The contour intervals are not the same for all the clouds. White, cyan, yellow, green, blue, magenta, and red colors for Ci, As, Ac, Sc, Cu, Ns, and DC clouds, respectively.

region between these clouds and their outflows as As clouds. So while estimating the frequency of occurrence of DC clouds and As clouds in the tropical cyclones, these aspects have to be considered. However, this will not have any consequence on the overall frequency of occurrence of the DC clouds as it will only affect the vertical distribution, as shown in Fig. 4(a). In the present study, we have not implemented any corrections to existing cloud-type identification and retained the original classification provided by the CloudSat product. The As clouds descend to lower heights with time and can evolve as Ns clouds. However, apart from As clouds, Ns clouds can form directly also. Fig. 4(d) shows the composite height distribution of Ns clouds as a function of the radial distance from the cyclone's eye. From this figure, it can be noted that the frequency of occurrence of Ns clouds is relatively low (∼6%) as compared to the other clouds discussed so far. Ns are rain-bearing clouds and dominate in contributing to the precipitation production. These clouds are limited in their occurrence within ∼400 km from the eye of the cyclones with their tops reaching ∼10 km. Thus, the outflows from the DC clouds can trigger the formation of Ci, As, and Ns clouds and influence their frequency of occurrence in tropical cyclones.

Fig. 4(e) shows the composite height distribution of frequency of occurrence of Ac clouds as a function of the radial distance from the eye of the cyclone. The figure shows a peak frequency of occurrence of 10% near to the eye. The horizontal extent of these clouds is very large and comparable to that of Ci clouds. Even though the Ac clouds are not important for their contribution to the precipitation production, these clouds play a significant role in radiative forcing. Fig. 4(f) shows the composite distribution of frequency of occurrence of Sc clouds as a function of the radial distance from the eye of the cyclone. From this figure, it evident that the Sc clouds most frequently occur near the eye of the cyclone with a peak frequency of occurrence of ∼15%. The tops of Sc clouds are confined to ∼2.5 km and these clouds can form up to a horizontal distance of 600 km region around the cyclone. It is well known that the dynamical response of ascending air in the DC clouds near the eye wall of the cyclone will induce descending motion in the eye of the cyclone and the descending air is responsible for the cloud-free zone in the eye. However, the low-level convergence of moisture in the eye results in the formation of Sc clouds, whose vertical development is inhibited by the downdrafts initiated by the adjacent DC clouds. The downdrafts in the eye give rise to an inversion layer in the lower troposphere that acts as a lid to the raising air, thus limiting the vertical development of the clouds. Apart from Sc clouds, it is also common to observe the Cu clouds in the eye. Fig. 4(g) shows the composite height distribution of frequency of occurrence of Cu clouds as a function of radial distance from the eye. The frequency of occurrence of these clouds shows a peak of ∼10% with their tops reaching up to ∼5 km. Reasonable amount of these clouds can be seen as far as ∼500 km from the eye. Most of these clouds are formed in the shadows of the DC cloud outflows and under the downdraft regions of cyclones. Most often Sc and Cu clouds are formed adjacent to each other in cyclones. Thus, Fig. 4 depicts the composite height distributions of various clouds as a function of radial distance from the eye of a cyclone, which is consistent with the conceptual models of tropical cyclones. An attempt is also made to construct the composite cloud type distributions separately for the ARB and BOB. The analysis revealed that there are not many changes in the cloud-type distributions over the ARB and BOB (figure not shown).

Furthermore, to have a comprehensive view of the cloud-type distribution embedded in tropical cyclones, a contour map of frequency of occurrence of all clouds is generated, as shown in Fig. 6. This type of representation aids in visualizing what type of clouds dominates in which part of the cyclone. The contour intervals are not the same for all the clouds. The decrease of cloud tops as a function of the radial distance from the eye is more clearly seen in this figure. The peak in frequency of occurrence of the DC clouds is followed by the Ci cloud peak. There are distinct regions showing the peak in the frequency of occurrence of various clouds embedded in the cyclone. For example, the Ns clouds show their frequency of occurrence at distant bands from the cyclone's eye in Fig. 6 with decreasing

frequency of occurrence from one band to another. Overall, the mean cloud-type distribution (mean over 0–1000 km horizontal extent of cyclones) is investigated. The consistency of the cloud distribution discussed in the present study with that of the conceptual models is very encouraging. Thus, the present study brought out the composite vertical structure of cloud types in the tropical cyclones for the first time using CloudSat observations.

IV. Conclusion

CloudSat observations of tropical cyclones formed in the North Indian Ocean during the years 2006–2014 are investigated to construct the composite cloud type distribution embedded within tropical cyclones. It is found that the DC clouds are always accompanied by As and Ci clouds and their peak frequency of occurrence is ∼50% at ∼50–100 km radial distance from the cyclone's eye. The Ci cloud distribution showed a peak frequency of occurrence of 30% (at ∼14–15 km altitude) at around ∼200 km radially from the eye. The distribution of As clouds showed some discrepancy with respect to the present understanding of these clouds. The Sc clouds are observed in the center of the cyclone as their vertical growth is inhibited by the downdrafts induced by the adjacent DC clouds. The Cu clouds are observed in the shadows of the DC cloud outflows and the significant amounts of these clouds are seen as far as ∼500 km radially from the center of the eye. Overall, the present study shows that on an average, the tropical cyclone consists of following distribution of clouds: Ci ∼ 20%, As ∼ 15%, Sc ∼ 5%, Cu ∼ 5%, Ns ∼ 15%, and DC ∼ 15%. The composite cloud type distribution discussed in the present study can be employed to understand the latent and radiative heating of the cyclone environment, which depend on the type of the clouds and play a major role in cyclone dynamics. This will be the topic of our research in near future. Thus, the present study brought out the three-dimensional distribution of cloud types and associated dynamics in and around tropical cyclones using the CloudSat observations for the first time. It is envisaged that the results discussed in the present study will have implications in understanding the role of clouds and their associated dynamics in intensifying and sustenance of the cyclones.

Acknowledgment

The authors are greatly thankful to CloudSat team for providing the observations.

References

[1] W. M. Gray, "Global view of the origin of tropical disturbances and storms," *Monthly Weather Rev.*, vol. 96, pp. 669–700, 1968.
[2] W. M. Gray, "The formation of tropical cyclones," *Meteorol. Atmos. Phys.*, vol. 67, pp. 37–69, 1998.
[3] DeMaria, J. A. Knaff, and B. H. Connell, "A tropical cyclone genesis parameter for the tropical Atlantic," *Weather Forecasting*, vol. 16, pp. 219–233, 2001.
[4] M. Yanai, "Dynamical aspects of typhoon formation," *J. Meteorol. Soc. Jpn.*, vol. 39, no. 4, pp. 282–309, 1961.
[5] G. J. Holland and R. T. Merrill, "On the dynamics of tropical cyclone structure changes," *Quart. J. Roy. Meteorol. Soc.*, vol. 110, pp. 723–745, 1984.
[6] R. A. Houze, "Clouds in tropical cyclones," *Monthly Weather Rev.*, vol. 138, pp. 293–344, 2010.
[7] D. A. Hence and R. A. Houze, "Kinematic structure of convective-scale elements in the rainbands of Hurricanes Katrina and Rita (2005)," *J. Geophys. Res.*, vol. 113, 2008, Art. no. D15108.
[8] G. L. Stephens *et al.*, "The CloudSat mission and the A-train," *Bull. Amer. Meterorol. Soc.*, vol. 83, pp. 1771–1790, 2002.
[9] D. M. Winker, W. H. Hunt, and M. J. McGill, "Initial performance assessment of CALIOP," *Geophys. Res. Lett.*, vol. 34, 2007, Art. no. L19803.
[10] A. Behrangi, P. F. Sean Casey, and H. L. Bjorn, "Three-dimensional distribution of cloud types over the USA and surrounding areas observed by CloudSat," *Int. J. Remote Sens.*, vol. 33, no. 16, pp. 4856–4870, 2012.
[11] K. V. Subrahmanyam, and K. K. Kumar, "CloudSat observations of cloud-type distribution over the Indian summer monsoon region," *Ann. Geophys.*, vol. 31, pp. 1155–1162, 2013.
[12] N. Tourville *et al.*, "Remote sensing of tropical cylcones: Observations from CloudSat and A-train profiliers," *Bull. Amer. Meteor. Soc.*, vol. 96, pp. 609–622, 2015.
[13] K. V. Ooyama, "Numerical simulation of the life cycle of tropical cyclones," *J. Atmos. Sci.*, vol. 26, pp. 3–40, 1969.
[14] S. S. Chen and W. M. Frank, "A numerical study of the genesis of extratropical convective meso-vortices. Part I: Evolution and dynamics," *J. Atmos. Sci.*, vol. 50, pp. 2401–2426, 1993.
[15] H. Fudeyasu *et al.*, "Multiscale interactions in the life cycle of a tropical cyclone simulated in a global cloud-system-resolving model Part II: System-scale and mesoscale processes," *Monthly Weather Rev.*, vol. 138, pp. 4305–4327, 2010.
[16] Y. P. Bu, R. G. Fovell, and K. L. Corbosiero, "Influence of cloud–radiative forcing on tropical cyclone structure," *J. Atmos. Sci.*, vol. 71, pp. 1644–1662, 2014.
[17] H. Su *et al.*, "Comparison of regime-sorted tropical cloud profiles observed by CloudSat with GEOS5 analyses and two general circulation model simulations," *J. Geophys. Res.*, vol. 116, 2011, Art. no. D09104.
[18] H. Masunaga, M. Satoh, and H. Miura, "A joint satellite and global cloud-resolving model analysis of a Madden-Julian oscillation event: Model diagnosis," *J. Geophys. Res.*, vol. 113, 2008, Art. no. D17210.
[19] T. S. L'Ecuyer, N. B. Wood, T. Haladay, G. L. Stephens, and P. W. Stackhouse Jr., "Impact of clouds on atmospheric heating based on the R04 CloudSat fluxes and heating rates data set," *J. Geophys. Res.*, vol. 113, 2008, Art. no. D00A15.
[20] K. Sassen and Z. Wang, "Classifying clouds around the globe with the CloudSat radar: 1-year of results," *Geophys. Res. Lett.*, vol. 35, 2008, Art. no. L04805, Doi: 10.1029/2007GL032591.
[21] R. T. Marchand, G. Mace, T. Ackerman, and G. Stephens, "Hydrometeor detection using CloudSat—An earth orbiting 94 GHz cloud radar," *J. Atmos. Ocean. Technol.*, vol. 25, no. 4, pp. 519–533, 2008.
[22] W. M. Frank, "The structure and energetics of the tropical cyclone storm structure," *Monthly Weather Rev.*, vol. 105, no. 9, pp. 1119–1135, 1973.

K. V. Subrahmanyam was born in India, in 1983. He recevied the B.Sc. degree in mathematics, physics and chemistry as electives, in 2003 and the Master's degree in physics in 2005 from Nagrajuna University, Guntur, India.

His research interest focuses on remote sensing of clouds using space- and ground-based radars.

Karanam Kishore Kumar received the B.Sc. degree in mathematics, physics and electronics as electives, the M.Sc.Tech. degree in engineering physics with the University Gold medal, and the Ph.D. degree in physics from Sri Venkateswara University, Tirupati, India, in 1995, 1998, and 2004, respectively.

His research interests include radar remote sensing of the Earth's atmosphere and atmospheric dynamics.

Natalie D. Tourville received the B.S. degree in chemical engineering and the M.S. degree in atmospheric science from Colorado State University, Fort Collins, CO, USA, in 1998 and 2010, respectively.

She currently supports CIRA research projects CloudSat and Orbital Carbon Observatory-2 and is a Linux System Administrator with the CIRA Fort Collins office. She also supports projects such as GOES satellite imagery and ingest, GOES-R, CloudSat, and several Regional Atmospheric Mesoscale Modeling Branch projects.

CloudSat observations of multi layered clouds across the globe

K. Venkata Subrahmanyam & Karanam Kishore Kumar

Climate Dynamics
Observational, Theoretical and Computational Research on the Climate System

ISSN 0930-7575
Volume 49
Combined 1-2

Clim Dyn (2017) 49:327-341
DOI 10.1007/s00382-016-3345-7

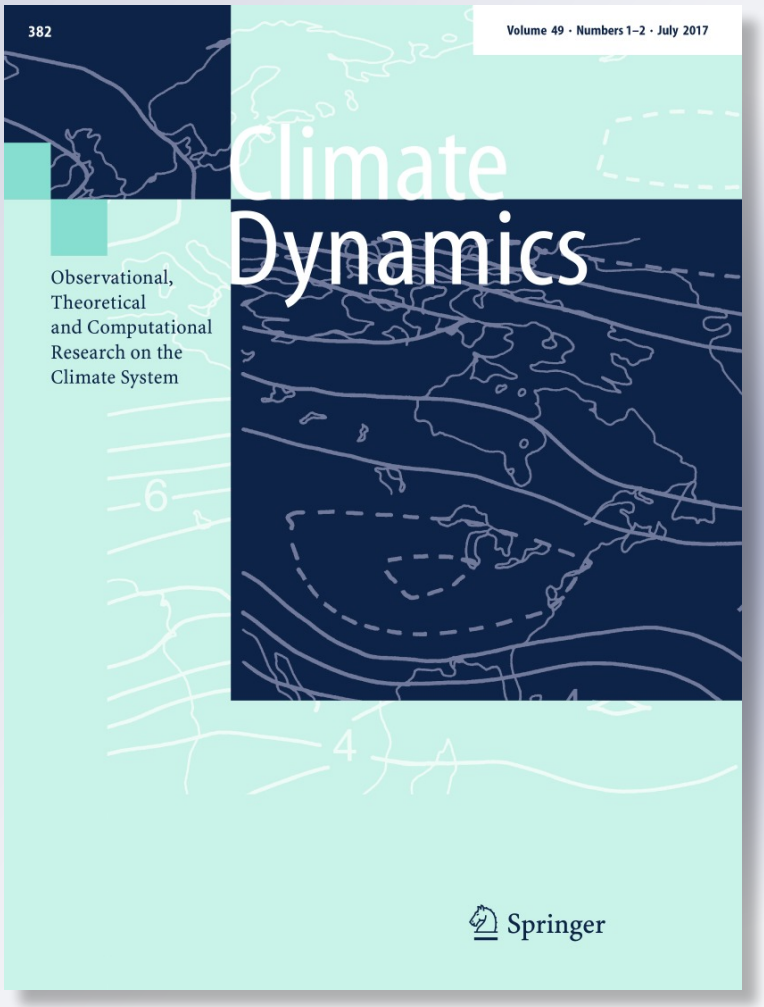

Springer

Clim Dyn (2017) 49:327–341
DOI 10.1007/s00382-016-3345-7

CloudSat observations of multi layered clouds across the globe

K. Venkata Subrahmanyam[1] · **Karanam Kishore Kumar**[1]

Received: 12 November 2015 / Accepted: 6 September 2016 / Published online: 10 September 2016

Abstract Vertically resolved multi-layer cloud distributions over the globe using 4 years of CloudSat/CALIPSO observations during 2007–2010 are discussed. The quantitative information on the frequency of occurrence of one- to five-layered clouds across the globe is established, which are of immense importance from the global climate standpoint. After segregating the CloudSat observations into different seasons, the 4 years of mean global maps of frequency of occurrence of one to five-layered clouds are discussed in details. These global maps provide much needed quantification of vertically resolved multi-layer clouds by revealing when and where the frequency of occurrence of multi-layer clouds are maximum including the number of layers. On an average, it is observed that over the globe one-, two-, three-, four- and five-layer clouds occur 53, 20, 3.5, 0.4 and 0.04 % of the time respectively. High fraction of single layer clouds is observed over the descending limbs of Hadley cell where relatively large lower tropospheric stability is found. The regions where multi-layer clouds are more frequent are identified and discussed along with large scale circulation. Apart from quantifying the frequency of occurrence of multi-layer clouds, the latitudinal distribution of zonal mean occurrence of cloud base and top altitudes of each cloud layer is constructed for boreal winter and summer. These analyses provide the cloud base and top altitudes of one to five-layered clouds, which are important to understand the vertical structure of the multi-layered clouds. The significance of the present study lies in establishing the global distribution of vertically resolved multi-layer clouds and the role of large-scale dynamics in controlling their distribution for the first time.

Keywords Multi-layered clouds · Large-scale circulation · CloudSat

1 Introduction

Owing to its importance in hydrological cycle, general circulation and radiative forcing, any aspect of clouds is a cynosure to meteorologists as well as common men across the globe. As the accurate representation of cloud processes and their feedback in the general circulation models are the need of the hour, cloud studies have been placed at a high pedestal by the meteorological community. By now, it is well established that the clouds remain the largest uncertainty in climate model forecasts (Stephens 2005; Randall et al. 2007). By interacting with both short- and long-wave radiation, clouds play crucial role in the radiative budget at the surface, within and at the top of the atmosphere. Understanding of the atmospheric radiative heating and latent heat release associated with clouds are central to any study dealing with general circulation as well as precipitation. Realizing the importance of clouds in Earth's radiation budget and hydrological cycle, a host of studies carried out in the past to divulge this ubiquitous feature of the earth's atmosphere. Most of these studies emphasized the importance of cloud vertical structure on atmospheric circulations, including the effects of variations of cloud top and base heights, cloud-layer thicknesses, and the vertical distribution of multilayered clouds as they significantly modify vertical and horizontal gradients in radiative and latent heat fluxes (Webster and Stephens 1984). The unanimous view of many of the atmospheric researchers is that the

✉ K. Venkata Subrahmanyam
kvsm2k@gmail.com

[1] Space Physics Laboratory, Vikram Sarabhai Space Centre, Thiruvananthapuram 695022, India

detection of multi-layered clouds is important from climate standpoint and any attempt to quantify the global warming should include the radiative impacts of clouds (Gupta et al. 1992; Wielicki et al. 1995; Wang et al. 2000; Chen et al. 2000). Thus it is important to have quantitative measurements of the geographic distribution and variations of cloud vertical layers.

There were studies in the past, which emphatically showed the cloud effects on the general circulation (Slingo and Slingo 1988; Randall et al. 1989; Wang and Rossow 1998). Especially, Randall et al. (1989) examined the response of the atmospheric circulation by varying the cloud vertical distributions in the models. These authors confirmed that the circulation is sensitive to the vertical distribution of clouds, which modifies the vertical radiative heating of the atmosphere. Wang and Rossow (1998) performed a series of experiments using the NASA Goddard Institute for Space Studies General Circulation Model (GCM) to study the effects of vertical distribution of clouds on atmospheric circulations. These authors focused on the importance of the vertical structure by exploring quantitatively the different effects between single- and multi-layered clouds. One of the important findings of this study was that the vertical gradients in the cloud distribution were more important to the circulation strength than horizontal gradients. Rossow et al. (2005) pointed out that the key to understand the cloud–dynamical feedback is determining the nature of the relation of radiative and latent heating rate profiles induced by cloud vertical structure. Mace et al. (2007) reported that the vertical distribution of zonally averaged hydrometeor occurrence and showed the relationship of clouds with components of the atmospheric general circulation. So, it becomes inevitable to establish the vertical distribution of clouds and to study their role in modifying the atmospheric circulation for better understanding of cloud feedback mechanisms in totality.

The ground based observations using Radars, Lidars and radiosondes provided much needed microphysical properties of clouds, which lead to better understanding of precipitation and radiative properties of the clouds. Even though the ground based techniques provide a wealth of information on clouds, they are not capable of providing the spatial distribution of clouds and their properties on large scale. On the other hand, the regional as well as global distribution of clouds is provided by space based observations. Most of the space based passive remote sensing techniques provide the two-dimensional distribution/properties of clouds. Most available satellite measurements from nadir pointing passive remote sensing instruments are limited to retrieval of information about the uppermost cloud layer or column-integrated properties whereas active remote sensing techniques provide the vertically resolved cloud properties thus providing three-dimensional perspective of the clouds (Simpson et al. 1988).

The spaced based active remote sensing instruments are providing extensive observations on vertical distribution of clouds. The importance of having multi-layer cloud information has been realized very early and many attempts were made in the past to retrieve the same. Baum et al. (1995) proposed a method to retrieve the multi-layer cloud properties from AVHRR observations using a modified multispectral, multiresolution method. Using this method these authors discriminated the single- and multi-layer clouds. Wang and Rossow (1995) established a method that uses the rawinsonde observations to determine cloud vertical structure. In a seminal study, Wang et al. (2000) reported climatology of cloud vertical structure using 20-years of global rawinsonde observations of humidity profiles. This climatology provided much needed information about single layer and multi-layer clouds including top and base heights along with thickness of each layer. However, this study was limited to the rawinsonde stations spread over the globe and could not provide the complete picture of multi-layer cloud distribution across the globe. Later, Huang et al. (2005) proposed a multi-layer cloud retrieval system by combining satellite visible and infrared radiances and surface microwave radiometer measurements. However, this detection method works only in non-precipitating conditions. On the other hand, recent cloud radar and lidar observations onboard CloudSat and CALIPSO respectively as a part of the A-Train mission providing a wealth of information on the three-dimensional distribution of clouds on a global scale (Stephens et al. 2002). The combination of passive and active remote sensing instruments operating in the A-Train mission providing unprecedented information on cloud vertical structure, aerosol climate effects, and more accurate estimates of surface long-wave fluxes and atmospheric heating rate profiles. Luo et al. (2009) documented the seasonal variations in occurrence frequency and location of single- and multi-layer hydrometeors. Wu et al. (2009) investigated the differences/similarities of vertical distributions of cloud occurrence frequency from various passive and active sensors. Recently, Li et al. (2011) accessed the radiative impacts of single and multi-layered clouds using A-Train observations. The results indicated that the multi-layer clouds have a significant impact on radiation budget due to their high frequency of occurrence globally and obvious radiative effect differences with that of single layered clouds. However, this study didn't distinguish how many layers are there in the multi-layer clouds.

The above discussion thus emphasizes the importance of cloud vertical structure for climate related studies. However, there are very few studies in the past focusing on this issue, especially using satellite based active remote sensing techniques. In this regard, a study is carried out with

a central objective of addressing the multi-layer cloud structures across the globe using 4 years of (2007–2010) CloudSat and CALIPSO observations. The present study describes the geographical distribution and frequency of occurrence of multi-layered clouds, which are resolved into one-, two-, three-, four- and five-layer clouds across the globe. As most of the earlier studies did not further classify the multi-layered clouds into two-, three-, four- and five-layer clouds, the present study focus on this issue, which is a relatively new component in the ongoing studies of vertical structure of clouds. An attempt is also made to discuss the manifestation of large-scale circulations in geographical distribution of multi-layer clouds. Section 2 describes the data and methodology. Results are discussed in Sect. 3 and Sect. 4 summarizes the findings.

2 Data and methodology

With the launch of Cloud Profiling Radar (CPR) on-board CloudSat in early June 2006 and Cloud-Aerosol Lidar with Orthogonal Polarization (CALIOP) on-board CALIPSO in late April 2006, unprecedented information on vertical distribution of hydrometeors are available for the atmospheric research community. CloudSat and CALIPSO observations have been extensively used in the recent past to study the cloud vertical structure. For the present study, we use 2B-GEOPROF-LIDAR, a combined auxiliary product of CloudSat and CALIPSO observations. This product is produced by extracting the maximum information from the combined potentially spatial overlap region by radar and lidar sensors. This product provides information on the parameters related to vertical structure of clouds, which includes the location of cloud layers in the vertical column, cloud base, cloud top and number of cloud layers. The cloud profiling radar onboard CloudSat operates at 94 GHz with cross- and along-track resolution of 1.4 and 1.7 km respectively. With ~240 m vertical resolution, this radar can probe optically thick large-particle layers. However, CloudSat is not sensitive to optically thin clouds. On the other hand, the Lidar on board CALIPSO owing to its shorter operating wavelength (532 nm) has ability to sense optically thin layers and tenuous cloud tops with vertical resolution as high as 30 m. Details of CloudSat and CALIPSO can be found in Stephens et al. (2008) and Winker et al. (2007) respectively. The synergy between these two instruments can nearly provide a complete picture of cloud distribution across the globe. Mace et al. (2009) suggest that greater than 90 % of cloud layers are correctly identified as cloud, by making use of the combination of the CloudSat and CALIPSO observations.

The 2B-GEOPROF-LIDAR product contains the combined cloud mask information, which indicates the confidence level in detection of clouds, ranging from 0 to 40. A cloud mask of 30–40 indicates the high-confidence detections and less false detections (i.e., less than 2 % for 30 and less than 0.2 % for values of 40). More details on CloudSat products can be found in the CloudSat Data Products Handbook (http://www.cloudsat.cira.colostate.edu).

Four years (2007–2010) of 2B-GEOPROF-LIDAR data product have been used for the present study with cloud mask of 30–40. The maximum number of cloud layers provided by this product is five. From this product, seasonal variations in frequency of occurrence of one-, two-, three-, four-, and five-layered hydrometeors are determined over the globe. First, the observations are gridded into 2.5° × 2.5° (longitude × latitude) for each season and then frequency of occurrence of each cloud layer are determined within the grid. Table 1 illustrates the method followed to determine the frequency of occurrence of each layer. In each grid, the number of occurrence of each layer is counted and the same is normalized by the total number of CloudSat observations in each grid. Following this procedure, the seasonal variation in frequency of occurrence of each cloud layer is determined across the globe. For interpreting the observed geographical distribution of multi-layered clouds in terms of large-scale circulation, Modern Era Retrospective analysis for Research Application (MERRA) data during the present observational period are used to estimate the meridional mass stream function (MSF) and vertical velocities. The details of MERRA reanalysis can be found in Rienecker et al. (2011).

3 Results and discussion

By adopting the method described in Sect. 2, we quantified the frequency of occurrence of various cloud layers ranging from one- to five-layers. The observations are categorized into four seasons viz., December–January–February (DJF), March–April–May (MAM), June–July–August (JJA) and September–October–November (SON). For each season, 4 years of observations during 2007–2010 are averaged to obtain the mean global distribution of each cloud layer. Figure 1a–d shows the mean seasonal variation of frequency of occurrence of single layer clouds during DJF, MAM, JJA and SON over the globe respectively. The striking feature of this figure is, the high frequency of occurrence of single layer clouds during all the seasons over the Southern Ocean. The single layer clouds more or less uniformly distributed over the entire longitudinal belt over 60°–70°S. The frequency of occurrence of single layer clouds over this region ranges from 60 to 70 % with minimal seasonal variations. However, a close look at Fig. 1a, c reveal that the frequency of occurrence of single layered clouds over Southern ocean is relatively high during Austral summer as

Table 1 Illustration of the method followed to determine the frequency of occurrence of multi-layer clouds

1	1	1	1	2	2	2	3	4	4
1	1	1	1	2	2	2	3	4	4
1	1	1	1	1	2	3	3	4	4
1	1	2	2	2	2	3	3	4	5
1	1	0	2	2	2	3	3	4	5
1	1	1	2	2	3	3	3	4	5
1	0	1	2	2	3	3	4	4	5
0	0	1	2	0	3	3	4	5	0
1	1	0	0	2	3	3	4	5	5
1	1	1	2	2	3	3	4	5	5

2.5 degree

2.5 degree

One-layer cloud occurrence—28; two—22; three—19; four—14; five—9

Total no. of observations—100

Percentage for one-layer clouds = (28/100) × 100 = 28 %

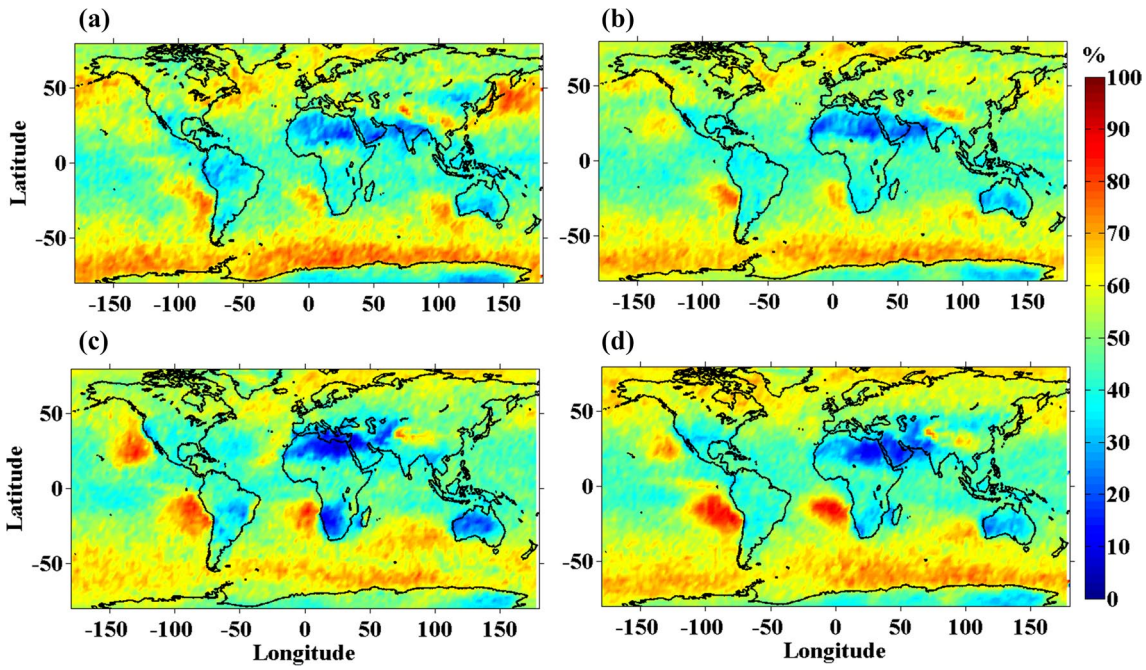

Fig. 1 Four years mean seasonal variation of frequency of occurrence of single layer clouds during **a** DJF, **b** MAM, **c** JJA and **d** SON across the globe

compared to winter. From International Satellite Cloud Climatology Project (ISCCP), it is known that the mean cloud fraction over the Southern Ocean is about ~0.79 (Rossow and Schiffer 1999). Trenberth and Fasullo (2010) reported that the climate model errors in simulating top of atmosphere fluxes over the Southern ocean are among the largest

anywhere in the world. In this regard, any information on these cloud regimes becomes very important to accurately represent them in climate models. These recent model simulations emphasized the importance of having quantitative information on these cloud regimes. Recently, Haynes et al. (2011) using multiple datasets of ISCCP and CloudSat–CALIPSO observations investigated the characteristics of Southern ocean cloud regimes and their effects on the energy budget. These authors reported the vertical structure of the clouds as well as the occurrence of precipitation over the Southern Oceanic region. The present study also emphatically bring out the seasonal variations in distribution of single-layered cloud over the Southern Ocean and further discussion on vertically resolved multi-layer clouds over this region, which is relatively new compared to earlier studies, will be presented later in this section.

Apart from Southern and Northern hemispheric high latitudes, high fraction of single layer clouds also occur over the South Pacific Ocean near west coast of the South America (~ at 20°–30°S latitudinal belt) and over the South Atlantic Ocean near west coast of South Africa. These two cloud regimes show pronounced seasonal variation with maximum occurrence during SON (~80 %) and minimum during MAM (~60 %). An additional patch of high fraction of single layered clouds occurs over the North Pacific Ocean near west coast of the North America (~ at 20°–30°N latitudinal belt), which shows maximum during JJA and minimum during DJF. On the other hand, very low frequency of occurrence of one-layered clouds can be noticed from Fig. 1a–d over the North and South Africa, the Middle-East and Australia over the 20°–30° latitude belt in both the NH and SH. Even though the low frequency of occurrence of one-layered clouds is observed over the same geographical locations during all the seasons, they exhibit pronounced seasonal variation in magnitude with very low fractions during JJA in both the hemispheres. However, it is very interesting to note the couplet of low and high fraction of one-layer clouds over the descending branch of the Hadley cell, which is more prominently seen during JJA over the west coast of South Africa and South America. It is expected to be cloud free zone over the descending branch of the Hadley cell. Over the land, the driest regions are found over the descending branches of Hadley Cell. However, over the oceanic regions of Hadley Cell descending branch, due to availability of moisture in the lower levels, single layer clouds can form as observed in Fig. 1. A detailed discussion on Hadley cell circulation and their relation to single layer clouds will be discussed later in this section. Apart from above-mentioned regions, relatively high fraction of single layer clouds are observed over the Himalayan mounts in the 30°–35°N latitudes. The occurrences of single layered clouds are observed during all most all the seasons with occurrence frequency of 50–60 %. During the DJF i.e. boreal winter, the weather over these regions is dominated by Western disturbances (Dimri et al. 2015) and during JJA i.e., boreal summer by Asian summer monsoon. The topographical features of this region plays vital role in observed cloudiness over these regions during winter and summer seasons. One more striking feature of Fig. 1a–d is the high occurrence (~60 %) of single layer cloud over Northern Hemisphere high-latitudes. Over this region, the frequency of occurrence of one-layered clouds is high over the oceans compared to land. One can notice the strong seasonal variation with winter maximum in single layered cloud occurrence over Pacific and Atlantic Ocean at latitudinal belt of 40°–60°N. It is also interesting to note the band of propagating clouds over the Atlantic Ocean sandwiched between Europe and Green Land, coinciding with the midlatitude storm tracks (Hoskins and Hodges 2005; Bengtsson et al. 2006; Yuan et al. 2009; Dong et al. 2013). Unlike over Southern ocean where single layered clouds uniformly distributed along the longitude, over Northern high latitudes, single layered-clouds are not uniformly distributed. Thus the seasonal variations in frequency of occurrence of single layered clouds are brought out using the 4 years of combined observations of CloudSat and CALIPSO. The distribution of single layered cloud occurrence and their association with large scale circulations will be discussed later in this section.

Figure 2a–d shows the distribution of two-layered clouds during the DJF, MAM, JJA and SON seasons. Most of the earlier studies, distinguished the single and multi-layer clouds. However, the multi-layer clouds were not further classified into two-, three-, four- and five-layered clouds. In the present study, the multi-layer clouds are further classified into different layers as mentioned earlier, which is relatively a new component of the present study. One more interesting inference that can be drawn from Figs. 1 and 2 is the frequency of occurrence of single layered cloud is high over oceans, whereas in the case of two-layered cloud it is high over land, especially over the low latitude-equatorial belt. One can notice the migration of Inter Tropical Convergence Zone (ITCZ) from South to North and back during DJF to SON. Over the equatorial region, the high frequency of occurrence of two–layer clouds (~40 %) is observed over South America, Central Africa and Indonesian regions during all the seasons with maximum during DJF and minimum during JJA over the 5°S–5°N latitudes. The locations of relatively high frequency of occurrence of two layered clouds over the equatorial regions more or less coincide with the ascending limbs of the Walker circulation. Walker circulation and its association with multi-layer clouds will be discussed later in this section. During the JJA, there is an increase in the frequency of occurrence of two-layered clouds over Indian sub-continent and surrounding oceans, which persist during SON also. This

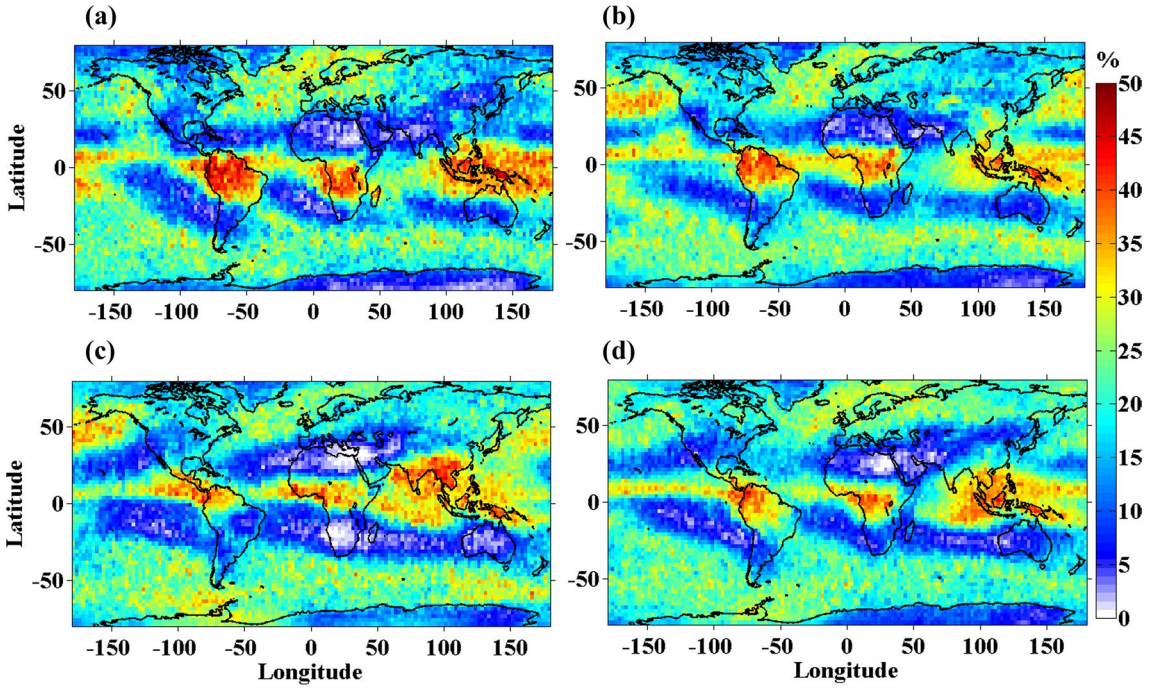

Fig. 2 Same as Fig. 1 but for two-layer clouds

observation can be readily attributed to the presence of Indian summer monsoon circulation over this region, which is dominated by the formation of various kinds of clouds such as cumulus, stratocumulus, cirrus etc. (Subrahmanyam and Kumar 2013). Over Southern Ocean also, there is relatively high frequency of occurrence of two-layered clouds, which are spread across the longitudes similar to single layer-clouds shown in Fig. 1. However two-layered clouds are relatively discrete as compared to one-layered clouds over this region. Apart from these regions, over Arctic and North Pacific oceanic regions also one can notice the relatively high frequency of occurrence of two-layered clouds. Thus the global distribution of two-layered clouds is quantified and the regions with high frequency of occurrence of these clouds are identified.

Figure 3a–d depicts the three-layered cloud distribution over the globe during the above-mentioned four seasons. The three-layered cloud distribution is more or less similar to two-layered cloud distribution shown in Fig. 2. The low frequency of occurrence of three-layered clouds is again observed over the descending branch of Hadley cell. The signature of descending branch of Hadley cell is more pronounced in three-layered clouds and the white patches in the Fig. 3 indicate that there were no three-layered clouds at all over that particular region during the observational period. Over the Southern Ocean, three-layered clouds are observed but very discrete in nature. Over this region, there is a seasonal variation in the occurrence of three layered clouds with maximum occurrence during Austral winter. Apart from Southern oceanic regions, a frequency of occurrence of 15–20 % in three layered cloud formation can be noticed over Indian sub-continent and surrounding oceanic regions during boreal summer season, which can be directly attributed to the Indian summer monsoon. Abundance of deep convective clouds are formed during the Indian summer monsoon period and produces a copious amount of cirrus clouds, which are formed form the anvil of deep convective clouds and spread by the tropical easterly jet. Moreover, during this season, the monsoon low level jet brings moisture from the adjacent oceans to the Indian sub-continent thus aiding the formation of clouds. The prevailing dynamics during this season is dominated by low level jet in the lower troposphere and tropical easterly jet in the upper troposphere. It is believed that the shears associated with these jets play a vital role in the formation of multi-layered clouds by smearing the clouds. During the Austral summer also relatively high frequency of occurrence in these clouds are observed over ITCZ, especially over land regions viz., South America, Central Africa and Indonesia. These regions again coincide with the ascending limbs of walker circulation as discussed in the case of two-layered clouds. Overall, many of the features of three-layered cloud distribution are similar to that of two-layered cloud distribution.

Figure 4a–d shows the frequency of occurrence of four-layered clouds over the globe during DJF, MAM, JJA and SON seasons. Even though the frequency of occurrence is very low compared to two- and three-layered clouds, the

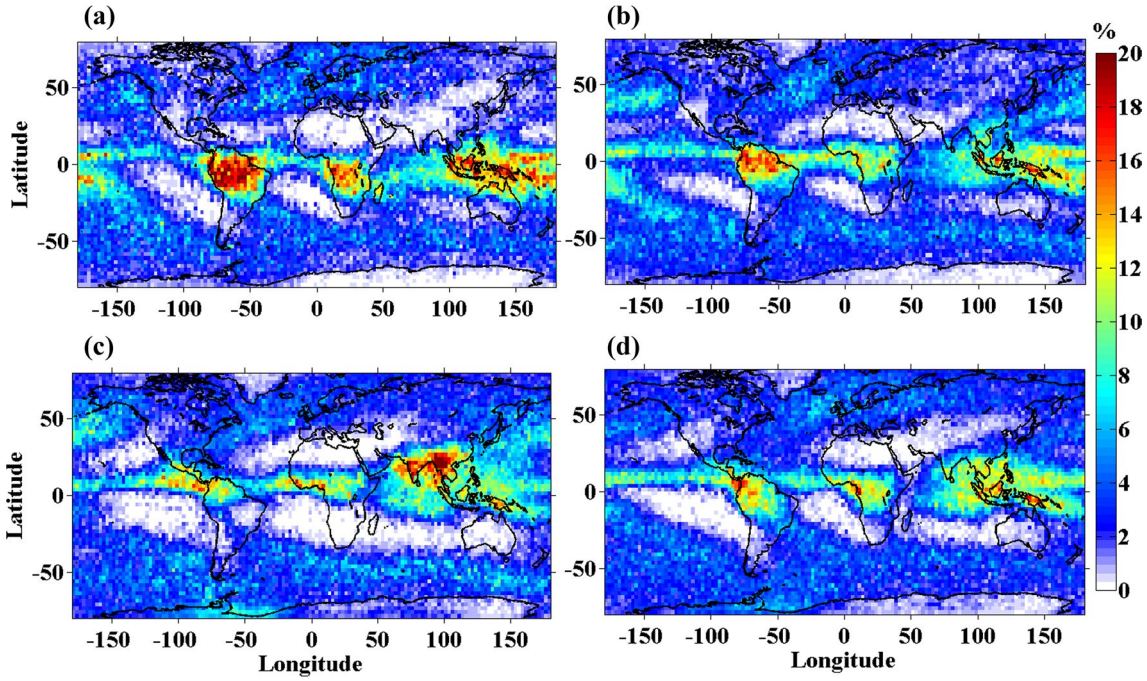

Fig. 3 Same as Fig. 1 but for three-layer clouds

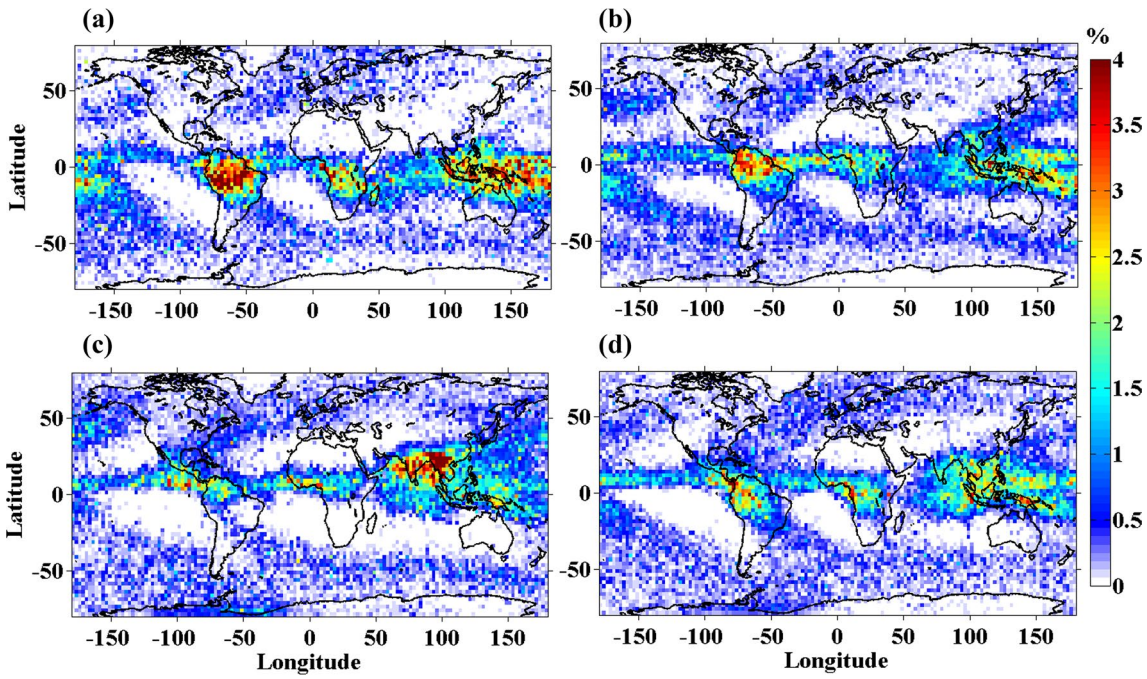

Fig. 4 Same as Fig. 1 but for four-layer clouds

geographical locations, where the maximum occurrence of four-layered clouds is found, are the same. The notable features very similar to Figs. 2 and 3 are the equatorial maxima during almost all the seasons and pronounced maxima during JJA over the Indian sub-continent. However, one can note ~5 % of four-layered clouds over isolated pockets of Southern Oceanic region, especially during Austral Summer. The distribution of five-layered clouds for all the four seasons is shown in Fig. 5a–d. From this figure, it is evident that the frequency of occurrence of five-layered clouds

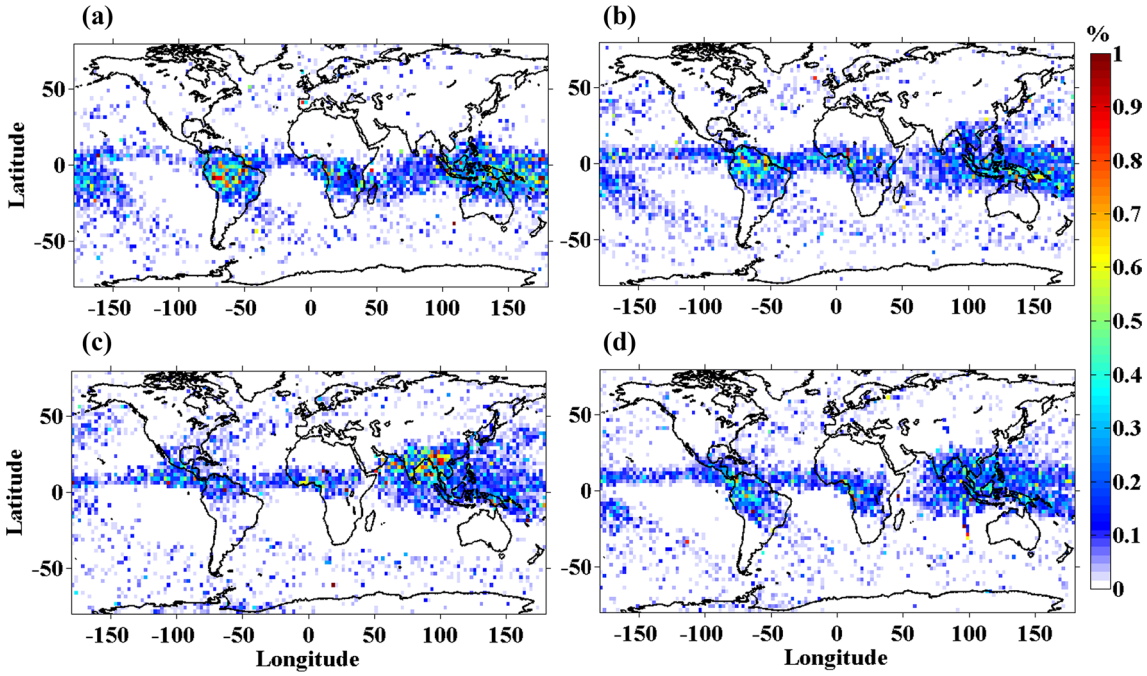

Fig. 5 Same as Fig. 1 but for five-layer clouds

is very low and limited to few geographical locations over the globe. The equatorial belt has the maximum occurrence of five-layered clouds during all the seasons compared to all other latitudinal belts, except during JJA, where maximum occurrence shifts to Indian sub-continent as in the case of other multi-layer clouds. During the JJA, as discussed earlier, Indian summer monsoon sets over the Indian subcontinent and the winds over this region is dominated by low level westerly jet in the 1–2 km region and tropical easterly jet in the 14–16 km region. The wind shears generated by these two jets in the lower and upper troposphere may play a crucial role in formation of multi-layer clouds (Sathiyamoorthy et al. 2004). Further, the latent heat released in the monsoon clouds over this region modifies the tropospheric thermal structure thus altering the vertical structure of static stability, which is important for the cloud formations and its vertical development (Houze 1982; Bhat et al. 2002). One more important observation from Fig. 5 is the occurrence of five-layered clouds over the midlatitude storm tracks, which are very prominently seen in the Southern Pacific and Atlantic Oceans during all the seasons. In the Northern Hemisphere also one can notice the occurrence of five-layered clouds over the Atlantic Ocean storm track. These observations of multi-layer cloud distribution over storm track assumes their importance as there are reports, which suggest that these storm tracks are shifting towards the poles and becoming narrower (Bender et al. 2011). To assess the consequence of this storm track shifting towards the poles and their effect on clouds and radiation budget, it becomes obvious to characterize the vertical structure of clouds over these regions.

In order to study the role of large scale circulation in the formation of one to five layered clouds depicted in Figs. 1, 2, 3, 4 and 5, we have analyzed global circulations viz., Hadley and Walker circulation along with the lower tropospheric stability (LTS). To examine the role of large-scale circulation in formation of persistent clouds over Southern Ocean, the annual mean meridional mass stream function (MSF) is estimated using MERRA reanalysis data. The MSF can be used to delineate the large-scale meridional circulation of the atmosphere. Figure 6 shows the annual mean MSF derived using monthly mean meridional winds during the observational period. The positive values of MSF indicate the clockwise circulation and negative values the anti-clockwise circulations. From this figure it can be noted that the annual mean ascending limb of the Hadley Cell is located slightly off the equator into the NH. However, the location of ascending limb of Hadley Cell show pronounced seasonal variation, which migrates from SH to NH during Austral Summer to boreal summer (figure not shown). From Fig. 6, it can be noted that at around 60°S there exists a rising limb of Polar cell. The vertical motions over these latitudes aid in transporting water vapor up in the atmosphere thus resulting in formation of clouds. The rising limb of Northern hemispheric Polar cell over 60°N as shown in Fig. 6, plays a key role in the formation of clouds observed over Northern Hemisphere (NH) high latitudes as in the case of their Southern Hemispheric (SH)

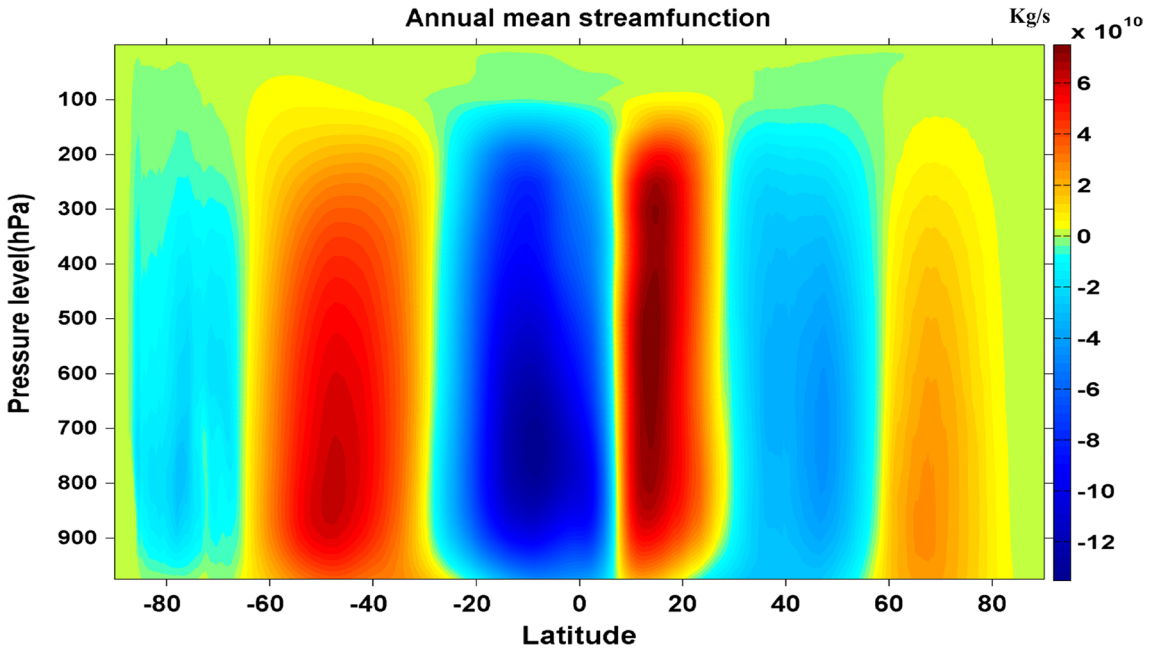

Fig. 6 Annual mean meridional mass stream function calculated using MERRA re analysis data during observational period

counter parts. However, over NH the maximum cloudiness is confined to oceans, which can be attributed to the availability of water vapor in the ascending limbs of Polar Cell. The high fraction of single layered cloud regimes observed over west coast of the South America, South Africa and North America (~ at 20°–30° latitudinal belt in respective hemisphere) coincide with the descending branches of Hadley cell as shown in Fig. 6 on either side of the equator. At the same time, the spatial distribution of multi layered clouds depicted in Figs. 2, 3, 4 and 5 show very low cloud amounts over above mentioned regions consistent with the descending branch of Hadley cell. Thus it is clear from Fig. 2 that unambiguous Hadley cell signature can be found in multi-layer cloud distribution rather than single-layered cloud distribution shown in Fig. 1. However, the pressure–latitude section of MSF shown in Fig. 6 is a zonal mean representation of Hadley cell where as the multi layered cloud distribution shown in Figs. 1, 2, 3, 4 and 5 is zonally resolved. To investigate the zonally resolved Hadley cell, the vertical velocity data from MERRA reanalysis is examined at 500 hPa level (figure not shown). This analysis clearly shown the subsidence over the regions of high fraction of single layered clouds observed in the 20°–30° latitude belt of both the hemisphere as shown in Fig. 1. As mentioned earlier, to study the lower atmospheric stability, we estimated LST. Figure 7a–d shows the 4 year (2007–2010) average LTS derived from monthly re-analysis data during DJF, MAM, JJA and SON respectively. LTS is derived using potential temperature difference between 700 and 1000 hPa levels (Klein et al. 1995). The physical significance of LTS is that it indicates the vertical growth of clouds. Cloud may not vertically grow, if LTS is high and thus they may be confined to the lower levels of the atmosphere. From Fig. 7, it is evident that LTS is high over the regions where the occurrence of single-layered cloud is more especially over descending branches of Hadley cell. We also investigated the seasonal variation of CAPE using COSMIC observations and their relation to occurrence of multi-layered clouds. The seasonal evolution of CAPE using COSMIC was reported by Narendra Babu et al. (2010). It is observed that the locations of high CAPE magnitude are coincident with the region of multi-layered cloud during all seasons.

Figure 8 shows the annual mean pressure–longitude section of vertical velocities (in Pa/s) averaged over 10°S–10°N latitudinal belt, which are obtained from MERRA reanalysis data. The positive values indicate the ascending motion and negative values the descending motion. From this figure, it is evident that there are three distinct regions of ascending motion over the South America, Central Africa and Indonesia reaching up to 200 hPa level (~14 km). The ascending limb over Indonesia is wide spread as compared to that of other two regions. These ascending limbs show pronounced seasonal variability in both, locations and intensities of ascending limbs. These ascending limbs play a vital role in formation of clouds and the background horizontal winds and thermal structure are also important in formation of multi-layered clouds. The studies on the formation of multi-layered clouds associated with ascending limbs of Hadley cell and Walker cell are not

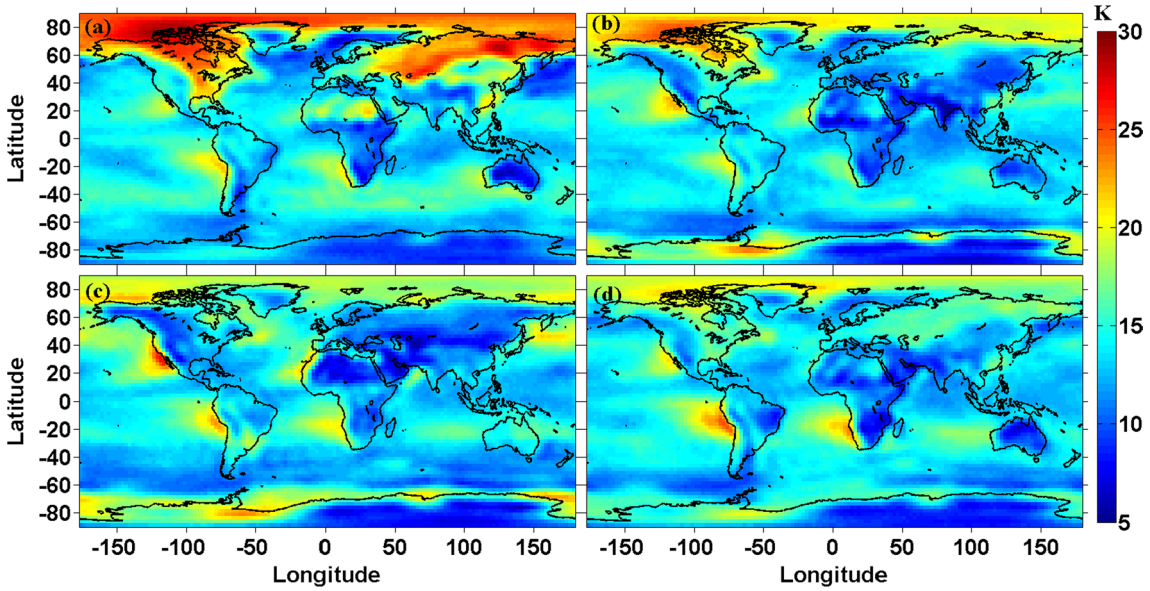

Fig. 7 The 4 year (2007–2010) mean lower tropospheric stability for **a** DJF, **b** MAM, **c** JJA and **d** SON

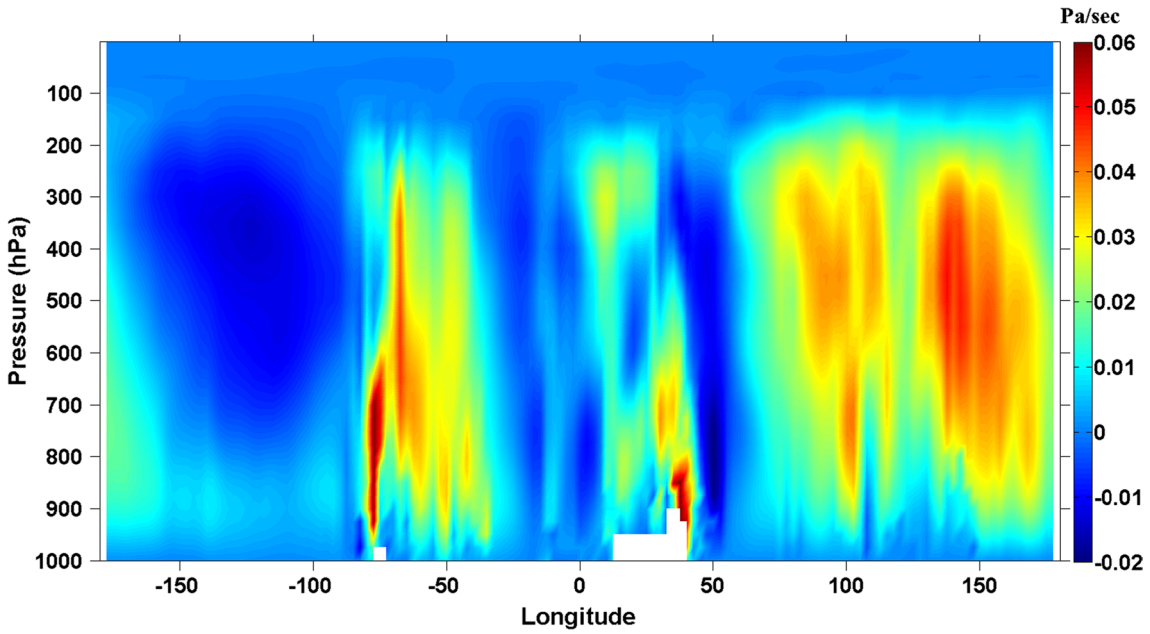

Fig. 8 Pressure-longitudinal section of climatological mean vertical velocities averaged over 10°S–10°N latitudinal belts

readily available in the literature. However, there are studies on occurrence of deep convective systems over these regions (Zipser et al. 2006). Deep convective clouds over these regions transport the moisture into the upper troposphere there by facilitating the formation of cirrus clouds. The detachment of anvils from the deep convective systems also contributes to the formation of cirrus clouds. Thus the geographical location of ascending limbs of Walker circulation coincides with the peaks of frequency of occurrence of multi layered clouds over low latitude and equatorial regions.

After constructing the climatology of one-, two-, three-, four- and five-layered clouds across the globe, an effort is made to further quantify the occurrence of multi-layer clouds in terms zonal mean frequency of occurrence. Figure 9a–d shows the zonal mean frequency of occurrence of one-, two-, three- and four-layered clouds respectively. The each latitudinal distribution curve shown in Fig. 9 is

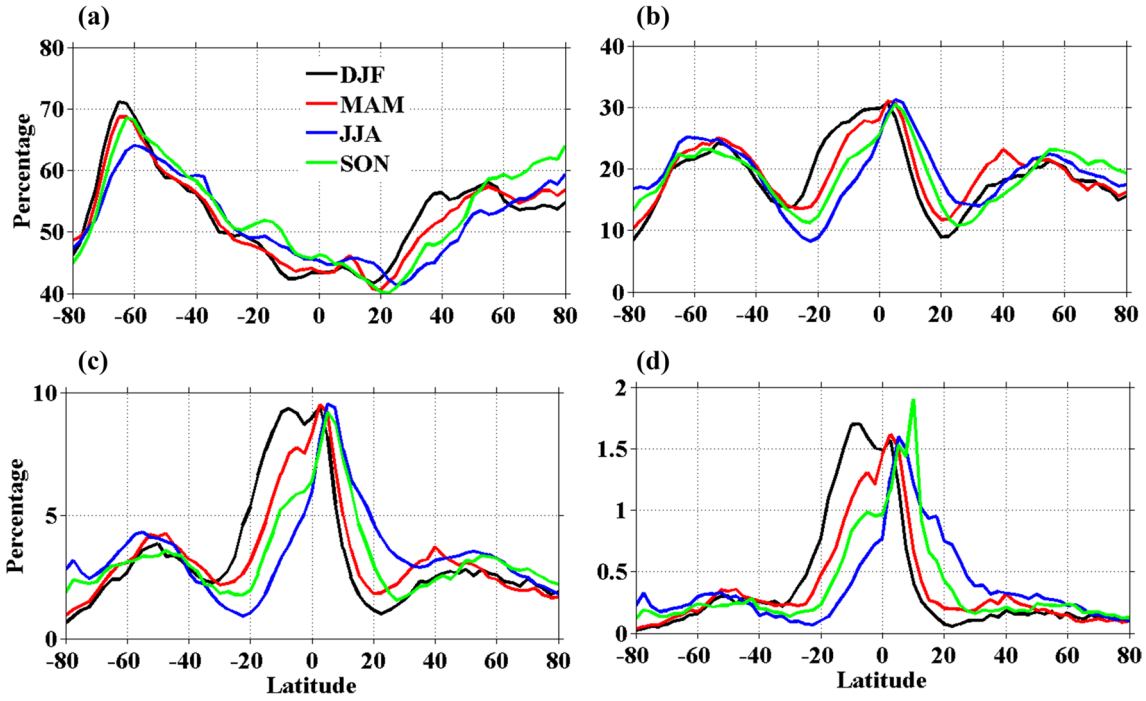

Fig. 9 The latitudinal and seasonal distribution of zonal mean frequency of occurrence of **a** single, **b** double, **c** triple and **d** four-layer clouds

the 4 years mean. Form this figure, it can be noted that the single layer cloud distribution exhibits two peaks, one over Southern Hemispheric high latitudes and another over Northern Hemispheric high latitude coinciding with the ascending limb of Polar Cell. The minimum in frequency of occurrence of one-layered clouds is observed over the Tropics as shown in Fig. 9a during all the seasons. As mentioned earlier, there is very little seasonal variation in frequency of occurrence of single layered clouds. However, over Southern Oceanic region occurrence of single layer clouds are relatively more during Austral summer as compared to Austral winter. The zonal mean latitudinal distribution of two-layered clouds depicted in Fig. 9b reveals three peaks. Two peaks are found over the same region as in the case of single layered cloud distribution shown in Fig. 9a. However, there is an additional peak over the equator in the two-layered cloud distribution, which can be attributed to the presence of ascending limbs of Walker circulation over these regions. Over the ascending limb of Walker circulation, the moist air is pumped up into the atmosphere resulting in the formation of clouds (Liu and Zipser 2005; Zipser et al. 2006). Depending on the stability of the atmosphere cumulus or deep convective systems form over these regions. Further the anvils of deep convective systems may detach to form cirrus clouds, which on descending to lower heights can form mid-level clouds such as alto stratus clouds. So it is envisaged that the regions over the Walker circulation are conducive for formation of multi-layered clouds. The minimum in frequency of occurrence of two-layered clouds observed over 20°–30° latitude belt over both the hemispheres in Fig. 9b correspond to the descending branch of Hadley cell. The presence of downdrafts over these regions will not be favorable for formations of multi-layered clouds. It can also be noticed from the Fig. 9b that during JJA two-layered cloud occurrence is maximum over tropical latitudes, where the occurrence of single-layered cloud is less. It can be also noted that the Southern Hemispheric high latitudes show maximum two-layered cloud occurrence during winter and minimum during summer whereas the low-latitudes show the exactly the opposite i.e., maximum during summer and minimum during winter. There is no systematic seasonal variation over Northern Hemispheric high latitude in the occurrence of two-layered clouds, which show maximum during SON. However, the Northern Hemispheric low-latitude follows the expected pattern showing maximum during summer and minimum during winter. The 4-year zonal mean latitudinal distributions of three-layered clouds are shown in Fig. 9c, which is very similar to Fig. 9b except for magnitudes. The SH exhibits pronounced seasonal variation in three-layered cloud distribution as compared to the NH. Figure 9d depicts the zonal mean four-layered cloud distribution, which also exhibits similar variations as two and three cloud layers. The zonal mean five-layered cloud distribution was also estimated (not shown), which shows preferential peak over the tropical latitude. The occurrence of five-layered cloud is

more over 0°–20°S latitude during DJF and MAM seasons, while it is more over 0°–20°N latitudes during JJA and SON periods. Thus Fig. 9 shows the zonal mean latitudinal distribution of various cloud layers. We have evaluated the interannual variation of all the cloud-layers and found that there is no significant variation except for maximum occurrence of all the cloud layers. From this figure, it is evident that the occurrence of three- and four-layered clouds are more over the tropical latitudes compared to other latitudes. Over all, it is observed that on an average over the globe one-, two-, three-, four- and five-layered clouds occur at 53, 20, 3.5, 0.4 and 0.04 % frequency respectively. Thus the present study brought out the preferential locations for multi-layered cloud formations and the role of large-scale dynamics in controlling their distribution.

After establishing the distribution of multi-layer clouds, an attempt is made to establish the vertical distribution of cloud top and base of single as well as multi-layer clouds across globe. However, it is difficult task to present the above-mentioned parameters across the globe as it is not practical to average the cloud parameters in a grid. For example, in a given grid of 2.5° × 2.5°, if we estimate the mean cloud base or top of one-layer cloud, it can be misleading as there can be a cirrus cloud with high base/top or a cumulus cloud with low base/top. By averaging these two different cloud bases one can end up with misleading values. Thus the mean cloud top and base height in a grid cannot be representative of a given region. The alternative is to have a number of occurrences of various cloud top and bases ranging from 0.25 to 18 km height with 0.25 km interval. Considering the volume of the data to be processed and the number of illustrations to be made, the analysis is restricted to the summer and winter of the year 2007. First, the number of occurrences are estimated over the entire globe in 2.5° × 2.5° and the same is averaged across the longitudinal belt to provide zonal mean occurrences of particular cloud base and top as function of latitude as shown in Figs. 10a–j and 11a–j for winter and summer respectively. It is to be remembered that only the number of occurrences is averaged but not the cloud base and top. Left panel of Fig. 10 depicts the latitudinal distribution of zonal mean occurrences of cloud bases of one-, two-, three-, four- and five-layered clouds and the right panel shows the respective tops for the winter season of 2007. The striking feature of the one-layered cloud base latitudinal distribution shown in Fig. 10a is the high occurrence of very low level clouds with base ranging from 0.25 to 1 km over both Southern and Northern mid and polar latitudes. However, the high occurrence of low level cloud base is spread over several latitudes in the Southern hemisphere as compared to its Northern counterpart. Over the Northern hemisphere midlatitude region around 40°–50°N, one can notice the secondary maximum in the occurrence

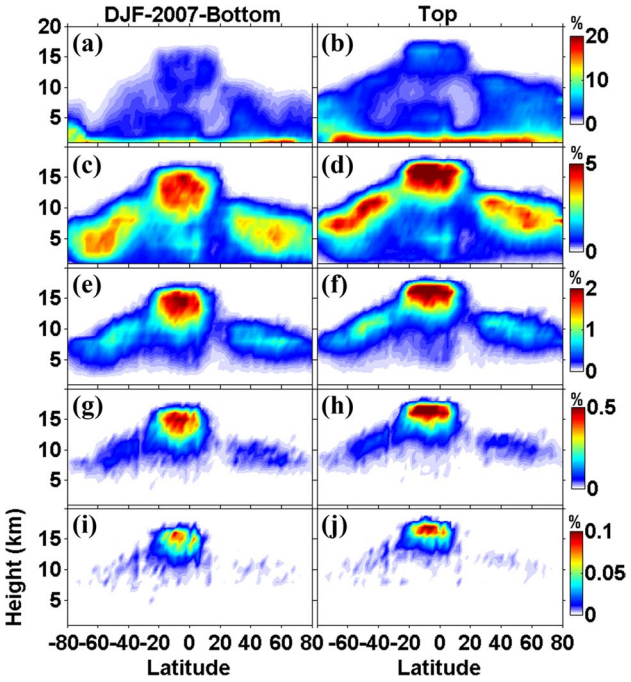

Fig. 10 *Left* the latitudinal distribution of zonal mean occurrences of cloud base altitudes of one-, two-, three-, four- and five-layered clouds for the winter season of 2007. *Right* same as left panel but for cloud top altitudes

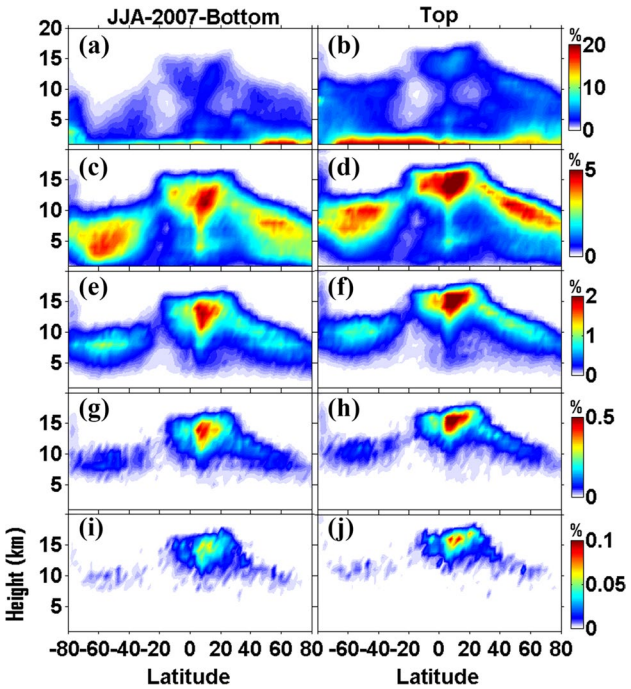

Fig. 11 Same as Fig. 10 but for boreal summer of 2007

of cloud base altitudes ranging from 3 to 6 km, which is not observed in the Southern hemisphere. Over the tropics, the maximum occurrence of single layer cloud base takes place

primarily in three bands, 0.5–2, 4–5 and 10–15 km in the Southern hemisphere, where ITCZ prevails during boreal winter and in the Northern hemisphere it is in the 0.5–2 and 12–15 km range. The cloud top occurrence corresponding to the single-layered clouds is shown in the Fig. 10b, which confirms that the most of the clouds observed over southern ocean and North Atlantic are indeed shallow clouds. However, over Northern mid and polar latitudes the cloud tops occur over a very wide band ranging from 1 to 10 km as compared to their southern hemispheric counterparts. One can notice the latitudinal structure of the tropopause, which limits the cloud top altitudes. The cloud tops occur in two bands (3–7 and 14–17 km) over the tropics in Southern hemisphere and in one band in the Northern hemisphere (14–17 km). Even though, we can roughly infer the cloud type using their base and top altitudes, we restrict our discussion to their base and top altitudes.

Figure 10c, d shows the latitudinal distribution of zonal mean occurrence of base and top altitude of two-layered cloud for the boreal winter of 2007. It is to be remembered that here we considered the base and top of all the two-layered clouds, which is present in all the multi-layer cloud regimes namely two-, three-, four- and five-layered clouds. From this figure it can be noted that the two-layered cloud bases exhibit similar distribution over mid and polar latitudes of both the hemispheres, which ranges from ~3 to 10 km. Over the tropical latitudes, the Southern hemisphere shows relatively more number of occurrence of two-layered cloud base in the 9–15 km band and spread over 0°–20°S latitudinal band whereas in Northern hemisphere it is limited to 0°–5°N. The latitudinal distribution of cloud top altitude shown in Fig. 10d also exhibit similar features as cloud base altitudes except that their altitudes are higher. It is interesting to note that the cloud top altitudes reach as high as 17 km in the tropics. Again, one can notice the latitudinal structure of tropopause pronounced in the latitudinal distribution of cloud top altitudes. The latitudinal distribution of base and top altitudes of three-, four- and five-layered clouds also shows the similar structure of two-layered cloud and are shown in the Fig. 10e–j. The base altitudes of three-layered cloud are in the range of 5–12 km over the mid and polar latitude of both the hemisphere and it is in the range of 12–16 km in the Tropics. The cloud top altitudes of three-layer clouds is also in slightly higher range as compared to their bottoms as shown in Fig. 10f as expected. However, the four-layered cloud occurrences are limited to tropical and midlatitudes and the five-layered cloud occurrence is limited to tropical latitudes only. As mentioned earlier the occurrence of multi-layer clouds are relatively more and spread over wider latitudinal band in the southern hemispheric tropical latitudes as compared to the Northern hemisphere, which can be attributed to the position of ITCZ during the boreal winter. Similar latitudinal distributions during the boreal summer of 2007 were carried out and are shown in Fig. 11a–j. The summer time latitudinal distribution of base and top altitudes of various clouds exhibit similar features as that of winter time distribution except that the maximum occurrence shifts to Northern hemisphere from Southern hemisphere along with the position of ITCZ. Thus for the first time, the cloud base and top altitudes of multi-layer clouds segregated into different layers are brought out using CloudSat and CALIPSO observations. The frequency distribution of vertically resolved multi-layered clouds and their base and top altitudes discussed in the present study will have profound implications in investigating the role of clouds in radiative forcing of the atmosphere as well as in the general circulation. At this juncture, where one of the largest uncertainties in the present day climate models is thought to be the representation of vertically resolved clouds and their feedback, the results presented here assumes its significance.

4 Summary

For the first time, the frequency of occurrence vertically resolved multi-layer clouds across the globe has been established using 4 years of CloudSat Auxiliary product 2B-GEPOROF-LIDAR. This merged CloudSat and CALIPSO product can resolve cloud layers up to five. After gridding the observations into 2.5° × 2.5°, they were segregated into four seasons. Four years mean global distribution of one-, two-, three-, four- and five-layered clouds are constructed and discussed in details. Interesting features such as very high frequency of occurrence of single layer clouds over Southern Ocean, midlatitude storm tracks, west coast of South America and South Africa and their association with large-scale circulations are discussed. The signature of descending branches of Hadley cell is very clear in multi-layered cloud distribution maps as compared to that of single-layered cloud distribution. Three regions over the equator (South America, Central Africa and Indonesia) are identified where more frequently multi-layer clouds occurs. These regions coincide with the ascending limbs of Walker circulation. It is also observed that the maximum occurrence of multilayer clouds migrates along with the movement of ITCZ. Apart from the equatorial region, multi-layer clouds are observed more frequently over Indian summer monsoon region and mid-latitude storm tracks. On an average over the globe it is observed that one-, two-, three-, four- and five-layered cloud occur at 53, 20, 3.5, 0.4 and 0.04 % frequency respectively. These global maps of frequency distribution of various cloud layers provide much needed information on where and when the multi-layer clouds are observed more frequently including the number of layers. After constructing the frequency distribution,

further the occurrence of multi-layered clouds is quantified in terms of zonal mean frequency of occurrence. It is noted that the zonal mean latitudinal distribution of single-layer cloud exhibits two peaks, whereas two-, three- and four-layered clouds show three peaks. Thus, for the first time the global distribution of multi-layered clouds and their association with large-scales circulation are brought out using 4 years of CloudSat and CALIPSO observations. Further zonal mean frequency of occurrence of cloud as and top is constructed. The cloud top altitude distribution of various clouds exhibited the signature of latitudinal structure of tropopause as expected. These are the first latitudinal distribution of vertically resolved multi-layer cloud base and top altitudes estimated using space based active remote sensing observations, which can be used to verify the outputs of climate models as well as can be used to quantify the role of vertically resolved clouds in earth's radiation budget and global circulation.

Acknowledgments The authors are greatly thankful to CloudSat and CALIPSO team for 2B-GEPROF LIDAR product, which was obtained from the website http://www.cloudsat.cira.colostate.edu.

References

Baum et al (1995) Satellite remote sensing of multiple cloud layers. J Atmos Sci 52:4210–4230

Bender FAM, Ramanathan V, Tselioudis G (2011) Changes in extratropical storm track cloudiness 1983–2008: observational support for a poleward shift. Clim Dyn. doi:10.1007/s00382-011-1065-6

Bengtsson L, Hodges KI, Roeckner E (2006) Storm tracks and climate change. J Clim 19:3518–3543

Bhat GS, Chakraborty A, Nanjundiah RS, Srinivasan J (2002) Vertical thermal structure of the atmosphere during active and weak phases of convection over the north Bay of Bengal: observation and model results. Curr Sci 83(3):296–302

Chen T, Zhang Y, Rossow WB (2000) Sensitivity of atmospheric radiative heating rate profiles to variations of cloud layer overlap. J Clim 13:2941–2959

Dimri AP, Niyogi D, Barros AP, Ridley J, Mohanty UC, Yasunari T, Sikka DR (2015) Western disturbances: a review. Rev Geophys. doi:10.1002/2014RG000460

Dong B, Sutton RT, Woollings T, Hodges K (2013) Variability of the North Atlantic summer storm track: mechanisms and impacts on European climate. Environ Res Lett 8:034037

Gupta SK, Darnell WL, Wilber AC (1992) A parameterization for longwave surface radiation from satellite data: recent improvements. J Appl Meteorol 31:1361–1367

Haynes JM, Jakob C, Rossow WB, Tselioudis G, Brown J (2011) Major characteristics of Southern Ocean cloud regimes and their effects on the energy budget. J Clim 24:5061–5080

Hoskins BJ, Hodges K (2005) A new perspective on Southern Hemisphere storm tracks. J Clim 18:4108–4129

Houze RA Jr (1982) Cloud clusters and large-scale vertical motions in the tropics. J Meteorol Soc Jpn 60:396–410

Huang J et al (2005) Advanced retrievals of multilayered cloud properties using multispectral measurements. J Geophys Res. doi:10.1029/2004JD005101

Klein SA, Hartmann DL, Norris JR (1995) On the relationship among low-cloud structure, sea surface temperature, and atmospheric circulation in the summertime northeast Pacific. J Clim 8:1140–1155

Li J, Yi Y, Minnis P, Huang J, Yan H, Ma Y, Wang W, Kirk Ayers J (2011) Radiative effect differences between multi-layered and single-layer clouds derived from CERES, CALIPSO, and CloudSat data. J Quant Spectrosc Radiat Transf 112:361–375

Liu C, Zipser EJ (2005) Global distribution of convection penetrating the tropical tropopause. J Geophys Res 110:D23104. doi:10.1029/2005JD006063

Luo Y, Zhang R, Wang H (2009) Comparing occurrences and vertical structures of hydrometeors between Eastern China and the Indian Monsoon Region Using CloudSat/CALIPSO Data. J Clim 22(4):1052–1064

Mace GG, Marchand R, Zhang Q, Stephens G (2007) Global hydrometeor occurrence as observed by CloudSat: initial observations from summer 2006. Geophys Res Lett 34:L09808. doi:10.1029/2006GL029017

Mace GG, Zhang Q, Vaughan M, Marchand R, Stephens G, Trepte C, Winker D (2009) A description of hydrometeor layer occurrence statistics derived from the first year of merged CloudSat and CALIPSO data. J Geophys Res 114:D00A26. doi:10.1029/2007JD009755

Narendra Babu AN, Nee JB, Kumar KK (2010) Seasonal and diurnal variation of convective available potential energy (CAPE) using COSMIC/FORMOSAT-3 observations over the tropics. J Geophys Res 115:D04102. doi:10.1029/2009JD012535

Randall DA, DA Harshvardhan D, Corsetti TG (1989) Interactions among radiation, convection, and large-scale dynamics in a general circulation model. J Atmos Sci 46:1943–1970

Randall DA et al (2007) Climate models and their evaluation. In: Solomon S et al (eds) Climate Change 2007: the physical sciences basis, contribution of Working Group I to the Fourth Assessment Report of the Intergovernmental Panel on Climate Change, chap 4. Cambridge University Press, Cambridge, pp 589–662

Rienecker MM, Suarez MJ, Gelaro R, Todling R, Bacmeister J, Liu E, Bosilovich MG, Schubert SD, Takacs L, Kim GK, Bloom S, Chen J, Collins D, Conaty A, Da Silva A et al (2011) MERRA: NASA's Modern-Era Retrospective Analysis for Research and Applications. J Clim 24:3624–3648. doi:10.1175/JCLI-D-11-00015.1

Rossow WB, Schiffer RA (1999) Advances in understanding clouds from ISCCP. Bull Am Meteorol Soc 80:2261–2287

Rossow W, Zhang Y, Wang J (2005) A statistical model of cloud vertical structure based on reconciling cloud layer amounts inferred from satellites and radiosonde humidity profiles. J Clim 18:3587–3605

Sathiyamoorthy V, Pal PK, Joshi PC (2004) Influence of the upper-tropospheric wind shear upon cloud radiative forcing in the Asian Monsoon Region. J Clim 17(14):2725–2735

Simpson J, Robert FA, Gerald RN (1988) A proposed Tropical Rainfall Measuring Mission (TRMM) Satellite. Bull Am Meteorol Soc 69:278–295

Slingo A, Slingo JM (1988) The response of a general circulation model to cloud longwave radiative forcing. I. Introduction and initial experiments. Q J R Meteorol Soc 114:1027–1062

Stephens GL (2005) Cloud feedback in the climate system: a critical review. J Clim 18:237–273

Stephens GL, Vane DG, Boain RJ, Mace GG, Sassen K, Wang Z, Illingworth AJ, O'Connor EJ, Rossow WB, Durden SL, Miller SD, Austin RT, Benedetti A, Mitrescu C (2002) The CloudSat mission and the A-Train. Bull Am Meterorol Soc 83:1771–1790

Stephens GL, Vane DG, Taneli S (2008) CloudSat mission: performance and early science after the first year of operation. J Geophys Res 113:D00A18. doi:10.1029/2008JD009982

Subrahmanyam KV, Kumar KK (2013) CloudSat observations of cloud-type distribution over the Indian summer monsoon region. Ann Geophys 31:1155–1162. doi:10.5194/angeo-31-1155-2013

Trenberth KE, Fasullo JT (2010) Tracking earth's energy. Science 328:316–317

Wang J, Rossow WB (1995) Determination of cloud vertical structure from upper-air observations. J Appl Meteorol 34:2243–2258

Wang J, Rossow WB (1998) Effects of cloud vertical structure on atmospheric circulation in the GISS GCM. J Clim 11:3010–3029

Wang J, Rossow WB, Zhang Y (2000) Cloud vertical structure and its variations from a 20-yr global rawinsonde dataset. J Clim 13:3041–3056

Webster PJ, Stephens GL (1984) Cloud–radiation interaction and the climate problem. In: Houghton J (ed) The global climate. Cambridge University Press, Cambridge, pp 63–78

Wielicki BA, Cess RD, King MD, Randall DA, Harrison EF (1995) Mission to Planet Earth: role of clouds and radiation in climate. Bull Am Meteorol Soc 76:2125–2153

Winker DM, Hunt WH, McGill MJ (2007) Initial performance assessment of CALIOP. Geophys Res Lett 34:L19803. doi:10.1029/2007GL030135

Wu DL, Ackerman SA, Davies R, Diner DJ, Garay MJ, Kahn BH, Maddux BC, Moroney CM, Stephens GL, Veefkind JP, Vaughan A (2009) Vertical distributions and relationships of cloud occurrence frequency as observed by MISR, AIRS, MODIS, OMI, CALIPSO, and CloudSat. Geophys Res Lett 36:L09821. doi:10.1029/2009GL037464

Yuan X, Patoux J, Li C (2009) Satellite-based midlatitude cyclone statistics over the Southern Ocean: 2. Tracks and surface fluxes. J Geophys Res 114:D04106. doi:10.1029/2008JD010874

Zipser EJ, Cecil D, Liu C, Nesbitt S, Yorty D (2006) Where are the most intense thunderstorms on earth? Bull Am Meteorol Soc 87:1057–1071

TRMM observations of Latent heat distribution over the Indian summer monsoon region and associated dynamics

Kandula Venkata Subrahmanyam and Karanam Kishore Kumar
Space Physics Laboratory, Vikram Sarabhai Space Centre, Thiruvananthapuram-695022, India
E-mail:kvsm2k@gmail.com

ABSTRACT

The latent heat released/absorbed in the Earth's atmosphere due to phase change of water molecule plays a vital role in various atmospheric processes. It is now well established that the latent heat released in the clouds is the secondary source of energy for driving the atmosphere, the Sun being the primary. In this context, studies on latent heat released in the atmosphere become important to understand the some of the physical processes taking place in the atmosphere. One of the important implications of latent heat release is its role in driving the circulations on various temporal and spatial scales. Realizing the importance of latent heat released in the clouds, a comprehensive study is carried out to understand its role in driving the mesoscale circulation. As Indian summer monsoon (ISM) serves as natural laboratory for studying the clouds and their microphysics, an attempt is made to explore the latent heat distribution over this region using 13 years of Tropical Rainfall Measuring Mission (TRMM) observations. The observed profiles of latent heating over ISM region showed large spatial and temporal variability in the magnitude thus reflecting the presence of organization of convection on mesoscale. The latent profiles in convective and stratiform regions are segregated to study the differences in their interaction with large-scale environment. Various re-analysis dataset were used to examine the role of latent heating distribution on the mesoscale circulation. The significance of the present study lies in establishing the vertical distribution of latent heating and their impact on the background circulation.

Key words: TRMM, Latent heating, Indian summer monsoon (ISM)

1. INTRODUCTION

The latent heat released in tropical clouds in the atmosphere accounts for ~ 75 % of the total diabatic heating in the Earth's atmosphere (e.g., [5]). The latent heat released/absorbed in the Earth's atmosphere due to phase change of water molecule plays a vital role in various atmospheric processes. Latent heat plays a major role in driving and modulating atmospheric circulation on various temporal and spatial scales that is from mesoscale to synoptic and planetary scales (e.g., [4]). It is now well established that the latent heat released in clouds is the secondary source of energy for driving the atmosphere, the Sun being the primary. The vertical distribution of latent heating in the atmosphere is also associated with vertical energy transport throughout the troposphere [3]. The dynamics of the tropical atmosphere strongly depends on the both vertical and horizontal distribution of latent heating (e.g., [10]). Variations in the height of the heating peak have significant implications for large-scale circulations in the atmosphere (e.g, [4]). For example, Schumacher et al. [6] show that geographical and temporal variability in convective and stratiform rain fractions, both of which have different vertical heating distributions, plays an important role in shaping the structure of the large-scale tropical circulation response, stressing the importance of accurate estimates of the temporal and three-dimensional variability of latent heating. Studies have shown that improved vertical distribution of latent heating allow a better representation of tropical east-west circulation (e.g., the walker circulation) by models other than those using simple heating functions, such as Webster [9] and Gill [1]. Thus, correct assessment of the vertical distribution of heating will lead to better simulations of the large-scale circulation structures. Determining this latent heating distribution is difficult because heating cannot be directly measured. Yanai et al [11] described atmospheric heating and the latent heating contribution involving Q1 and Q2, which are residuals of heat and moisture budgets of the resolvable motion, respectively. However, TRMM observations provide the distribution of latent heating in the tropical regions. As Indian summer monsoon (ISM) serves as natural laboratory for studying the clouds and their microphysics, an attempt is made to explore the latent heat distribution over this region using 13 years of Tropical Rainfall Measuring Mission (TRMM) observations. The main focus of the present study is vertical structure of latent heating derived from TRMM and its spatial and temporal distribution over the ISM region. Further, we studied the integrated vertical distribution of latent heating and their inter-annual variability. An attempt is also made to discuss the dynamical implication of latent heat distribution over the ISM region. The following section describes the data and methodology used for the present study. Section 3 presents the results and discussions and summary is provided in the section 4.

Remote Sensing of the Atmosphere, Clouds, and Precipitation VI, edited by
Eastwood Im, Raj Kumar, Song Yang, Proc. of SPIE Vol. 9876, 98762W
· © 2016 SPIE · CCC code: 0277-786X/16/$18 · doi: 10.1117/12.2223905

2. DATA AND METHODOLOGY

TRMM is the first space rain gauge launched in 1997 and it sweeps latitudes between 38S and 38N and was located above the Earth's surface at an altitude of 402.5 km with an inclination of 35 degree to earth's equatorial plane. The swath width of TRMM-PR is 215 km and a horizontal footprint of 4.3 km at nadir. The prime objective of TRMM is to study the variability in tropical precipitation in both space and time. In fact, understanding the nature of variability in precipitation has been increased tremendously with TRMM measurements. Another prime objective of this mission is to study the vertical structure of latent heating released in the earth's atmosphere. There are few algorithms (such as PRH and SLH) for retrieving the latent heating from TRMM observations. In the present study, we use 13 years of (1998 to 2010) Spectral Latent Heating (SLH) data (SLH-L3-V2) to investigative the vertical structure of latent heating. This dataset uses the TRMM-precipitation radar measurements and a cloud resolving model (CRM) generated look-up table for both land oceanic regions over the tropics [7]. The information taken from TRMM include convective and startiform classification, cloud height, surface rain rate and more. In addition, there are separate look-up tables for convective and shallow startiform regimes based on precipitation cloud top height. Time-mean spatial distribution of vertically integrated latent heating is estimated over the ISM region for the present study. Further, zonally averaged latitudinal height distribution of latent heating (LH) is estimated.

3. RESULTS AND DISCUSSION

Figure 1 (a & b) shows the 13 (1998-2010) year mean climatological distribution of rainfall over India during winter [December, January , February (DJF)] and summer [June, July, August(JJA)] respectively. From figure 1(a) it is evident that the Indian region is very dry during DJF and large amount of rainfall occurs over Western Ghats, Foot hills of the Himalayas and the Eastern Bay of Bengal during JJA, which is dominated by ISM. Thus, figure 1(a & b) depicts the typical climatological mean rainfall over the ISM region and shows its major features. Figure 1(c) & (d) shows the vertically integrated latent heating (K/hr) over the ISM region for the period 1998-2010 during DJF and JJA respectively. The most noticeable feature during JJA is higher LH values over the Bay of Bengal (BoB), the Indian Ocean and over Indo-Gangetic Plane (IGP) region. Another interesting feature is the LH pattern over monsoon trough region, which show relatively large magnitudes as shown in figure 1(d). During DJF, the higher LH values found to be over eastern Equatorial Indian Ocean, which is the location of Inter Tropical Convergence Zone (ITCZ), where the deep convection prevails during that season. The major difference in spatial distribution of LH during DJF and JJA is due to the migration of ITCZ. The ITCZ migrates northward from January to September and drifts back to equator ward between October and January. Thus primarily, movement of ITCZ is responsible for the observed latitudinal pattern in the intergraded LH distribution over the ISM region. The LH released within this zone drives large-scale circulation in the atmosphere. We also studied the vertically integrated latent heating anomalies from 1998 to 2010 over the ISM region (figure not shown). There is little inter-annual variability in the integrated LH over the study region. However there are interannual variability in the vertical profiles of LH over the study region, which can be associated with the inter-annual variability of monsoon precipitation. Moreover, the mean inter-annual variability of ISM is governed by the internal dynamics of the monsoon, which modifies the year-year precipitation and thus changes in LH variability (e.g., [2]). Figure 2 shows the 13 years mean vertical profiles of LH over the BoB, Arabian Sea (ARB), Central India (CI) and Western Ghats (WG) respectively. The observed vertical structure of LH is very similar over BoB and CI, which peaks at ~ 7km. But, the LH magnitudes are slightly larger in BoB than CI region, because BoB experience a strong presence of deep convection which releases large amount of latent heating in the atmosphere [8]. Over the ARB and WG regions, the LH vertical structure is mainly associated with shallow convective clouds and thus LH profiles peaks at ~ 2 km height over both the regions. it is also interesting to note that the vertical structure of LH exhibits a bi-modal distribution over BoB and CI regions. The latent heating associated with deep convection is positive thought out the troposphere and it peaks around mid-tropospheric level (~ 6-7 km height) as seen over the BoB and CI regions. The heating associated with shallow convection is positive and peaks at lower tropospheric heights as observed over the ARB and WG regions.

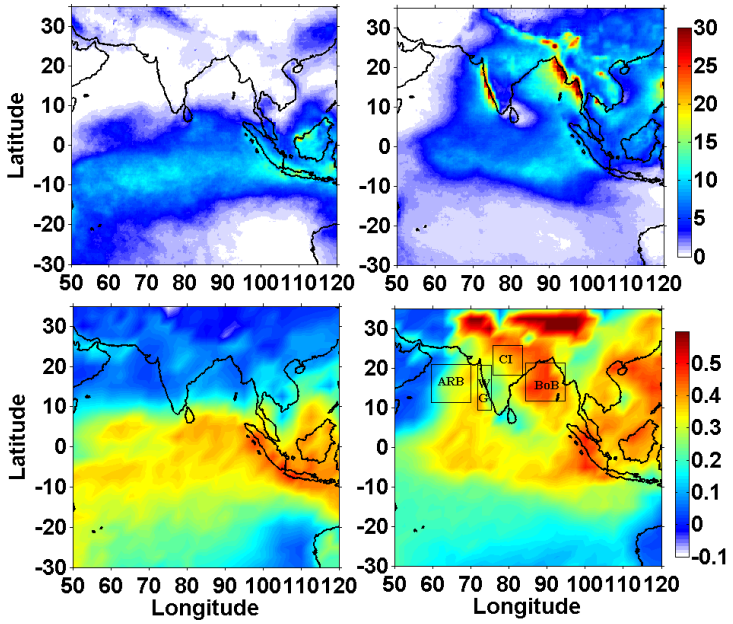

Figure 1: Thirteen year mean rainfall (mm) during (a) DJF and (b) JJA and vertical integrated LH (K/hr) for (c) DJF and (d) JJA over ISM region.

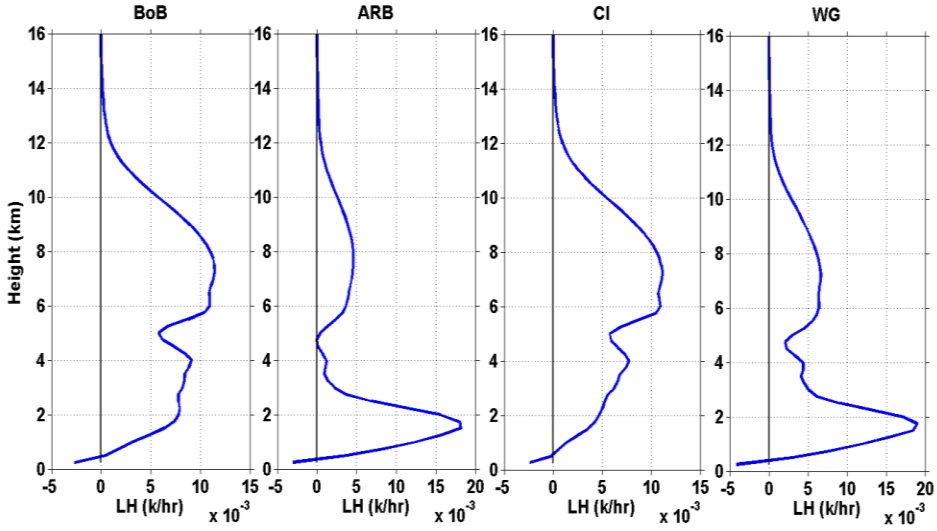

Figure 2: Mean vertical profiles of LH over the BoB, ARB, CI and WG.

Figure 3 shows the zonally averaged temporal variability of vertical distribution of LH with latitude during ISM period. The increase in LH magnitude with latitude is clearly seen in figure 3 from 00 LT to 15 LT as shown by red colour arrow. These spatial and vertical structure evolutions of LH can be used as a proxy of convective organization. The observations shown in figure 3 suggest the north-eastward propagation of convective activity over these latitudes (Raut et al., 2009). Further, to study the sub-regional characteristics of latent heating over the BoB, ARB, CI and WG regions, the temporal and vertical distribution of latent heating is examined. Figure 4(a-d) shows the temporal vertical structure of LH over the BoB, ARB, CI and WG regions respectively. This temporal vertical structure of LH gives a better knowledge about how LH varies in time both diurnally and vertically for different regions. The BoB and ARB are corresponds to oceanic regions and CI corresponds to land region. The LH exhibits different diurnal cycles over land and oceanic regions.

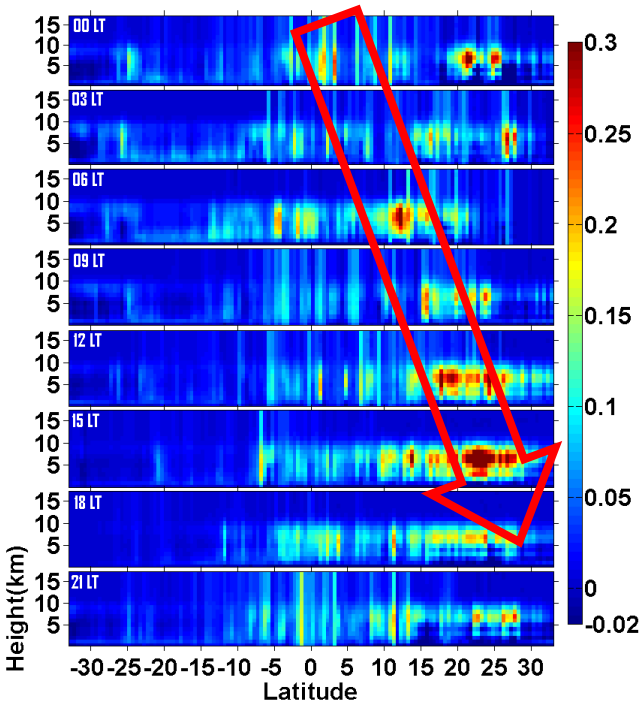

Figure 3: zonally averaged temporal variability of vertical distribution of LH (in K/hr) during JJA.

The LH peaks at around early morning/late-night over the BOB with a secondary broad peak ranging from pre-afternoon to late- afternoon. Over the ARB, it peaks at around early morning (~ 6hr LT) and a secondary peak can be noted at evening hours with relatively lower magnitudes as compared to the BoB region. The land regions are of specific interest to many previous studies because of their large magnitudes. The maximum latent heating over CI is as strong as that of the BoB. However, over CI, the LH peaks during the afternoon hours and the large amount of latent heating occurs at an altitude of ~ 7 km during. The WG region has unique latent heating feature compared to other regions. Over the WG, LH peaks at early morning and late-evening with relatively lower magnitudes as compared to all regions. Being a coastal region, WG exhibits a different LH structure as compared to other regions. The maximum magnitude of LH occurs at ~ 15 LT at 5 km height level over WG. Over all, shallow convection dominates over the ARB and WG region, which results in lower magnitudes of LH. Over BoB and CI, deep convection dominates and releases large amount of LH. The peak time of these regions are associated with the development of convective systems and prevailing dynamics.

4. SUMMARY

The spatial and temporal variability of latent heating distribution over the ISM region using 13 years of TRMM observations is investigated. The spatial and temporal distribution of LH shows specific regions such as the foot hills of Himalayas, the IGP and the BoB regions with large amount of LH during ISM period. The vertical structure of LH over the ISM is also investigated. The LH variability at three regions of ISM Viz., BoB, ARB, CI and WG regions are further studied. Over the BoB and CI regions, vertical structure of LH is associated with the strong presence of deep convection which releases large amount of latent heat in the atmosphere, whereas over the ARB and WG the observed LH is due to the shallow convection. The observed profiles of latent heating over the ISM region showed large spatial and temporal variability in the magnitude reflecting the presence of organization of convection on mesoscale. The temporal variability of vertical structure of LH showed northward propagation of convective activity over the ISM during JJA period at diurnal scales. The diurnal cycle of LH is more pronounced over CI (land) compared to the BoB and ARB regions. It is observed that the LH peaks during early morning over oceanic region (BoB and ARB) and during afternoon over land region (CI). Thus the present study brought out the 13 year mean spatial and vertical distribution of LH over the ISM region. The LH distribution and its role in driving the circulation will be carried out in near future.

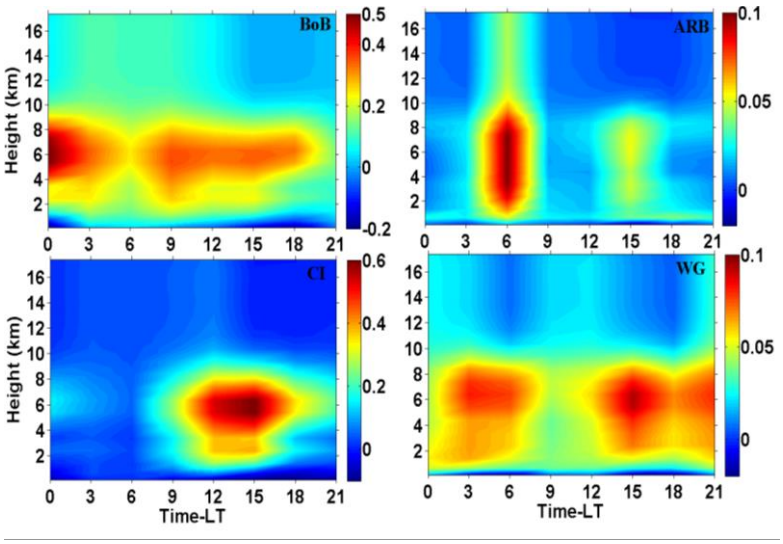

Figure 4: Temporal variability of vertical structure of LH (in K/hr) over BoB, ARB, CI and WG regions respectively during JJA.

REFERENCES

[1] Gill, A. E., "Some simple solutions for heat-induced tropical circulation", Quart. J. Roy. Meteor. Soc., 106, 447–462 (1980).

[2] Goswami B.N., "Interannual variations of Indian summer monsoon in GCM: External conditions versus internal feedbacks", J. Climate., 11:501-522 (1998).

[3] Houze, R. A., "Cloud clusters and large-scale vertical motions in the tropics", J. Meteor. Soc. Japan, 60, 396–410 (1982).

[4] Nigam, S., Chung C., and DeWeaver E., "ENSO diabatic heating in ECMWF and NCEP–NCAR reanalyses, and NCAR CCM3 simulation", J. Climate, 13, 3152– 3171(200).

[5] Reihl, H. and Malkus J., "On the heat balance in the equatorial trough zone", 503– 537(1958), http://snow.atm.ncu.edu.tw/TC/RiehlMalkus1958.pdf.

[6] Schumacher, C., Houze R., and Kraucunas I., "The tropical dynamical response to latent heating estimates derived from the trmm precipitation radar", Journal of Atmospheric Sciences, **61**, 1341–1358 (2004).

[7] Shige, S., Takayabu Y.N., Tao W.-K. and Johnson D.E., "Spectral retrieval of latent heating profiles from TRMM PR data. Part I: Development of a model-based algorithm", J. Appl. Meteor., 43,1095-1113(2004).

[8] Subrahmanyam, K.V. and Kumar, K. K., "CloudSat observations of cloud-type distribution over the Indian summer monsoon region", Ann. Geophys., 31, 1155-1162 (2013).

[9] Webster, P.J., "Response of tropical atmosphere to local, steady forcing", Mon, Wea. Rev., 100 (7), 518-541(1972).

[10] Yanai, M., Chen B., and Tung W.W., "The Madden–Julian oscillation observed during the TOGA COARE IOP: Global view", J. Atmos. Sci., 57, 2374–2396 (2000).

[11] Yanai, M., Esbensen S., and Chu J.H., "Determination of bulk properties of tropical cloud clusters from large-scale heat and moisture budgets", J. Atmos. Sci., 30, 611–627 (1973).